

# **Biofouling in membrane bioreactors: Nexus between polyacrylonitrile surface charge and community composition**

Biofouling in membraanbioreactoren:

Nexus tussen polyacrylonitrile oppervlaktelading en gemeenschapssamenstelling

Promotoren:

Prof. Ivo Vankelecom

Departement Microbiële en Moleculaire Systemen  
Centrum voor Oppervlaktechemie en Katalyse

Prof. Dirk Springael

Departement Aard- en Omgevingswetenschappen  
Afdeling Bodem- en Waterbeheer

Masterproef voorgedragen  
tot het behalen van het diploma van  
Master of science in de bio-ingenieurswetenschappen:  
milieutechnologie

**Marie-Aline Hernalsteens**

juni 2015

*"Dit proefschrift is een examendocument dat na de verdediging niet meer werd gecorrigeerd voor eventueel vastgestelde fouten. In publicaties mag naar dit proefwerk verwezen worden mits schriftelijke toelating van de promotor, vermeld op de titelpagina."*

# Acknowledgments

The very first person I have to sincerely thank is **Louise Vanysacker**, former Postdoc at the KU Leuven and currently working at *De Watergroep*: eventually she was not part of this adventure, but she convinced me to have a go with it and she could not be more right. Moreover Louise reviewed my work externally in the very end and gave me valuable advice on the content.

I thank my promotor, Prof. Dhr. **Ivo Vankelecom** (Centre for Surface Chemistry and Catalysis, COK), and my co-promotor, Prof. Dhr. **Dirk Springael** (Division of Soil and Water Management), for believing in me in the first place, as well as for their contribution to constructive insights during the whole year.

My supervisors, the PhD students **Shazia Ilyas** and **Lisendra Marbelia** (COK) and the Postdoc **Basak Ozturk** (Division of Soil and Water Management), have done a wonderful job. Shazia and Lisendra, thank you for your (technical) support when you took over the maintenance of the bioreactor in my absence and for the follow-up of the (external) membrane performance measurements. Basak, thank you for your support. But most important, thank you for being that passionate about all you do and demanding towards me. And you know, from the *Destiny's Child*, you are Beyoncé, without doubt 😊.

Thank you to the external evaluators Prof. Dr. ir. **Kristel Bernaerts** (Department of Chemical Engineering) and Prof. Dhr. **Koenraad Muylaert** (Faculteit Wetenschappen @ Campus Kulak Kortrijk) for assessing my work.

Next I would like to thank all people who helped or informed me on measurement techniques or gave me their support during experiments.

First I need to thank the **staff of Bonte Ateliers Leuven** for providing me in good quality PVC membrane frames.

I would like to thank **Pedro**, the cleaning man, for keeping our workspace tidy at every moment of the week and for the delicious sweets he baked.

From the COK group, I would like to thank warmly **Werner Wouters**, highly skilled technician, for helping me improving the bioreactor set-up. Thank you to **Matthias Mertens**, doctorate student, for his general good mood and ready-to-help behaviour (i.a., during my quest for glutaraldehyde). Next I want to thank **Maarten Bastin** for his unconditional devotion when it comes to SEM measurements in

the early morning. Finally I thank **Dirk Dom** for explaining me the functioning of the vacuum oven, **Nithya Joseph** for explaining me high-throughput and SEM equipment and **Hanne Mariën** for giving me her advice on the quality of my hand-made membranes.

From the Division of Soil and Water Management group, I would like to thank **Dries Grauwels**, marathon laboratory technician, for the numerous bump-into-you moments. I thank **Karla Moors**, laboratory technician, but in particular **Lynn Lemoine**, doctorate student, for their precious advice during DGGE measurements and support when I needed it most. Also **Benjamin Horemans** is part of this rather extended acknowledgments list for having performed remarkable CLSM measurements in my company and for his help showing me around in the laboratory. Finally I thank **Karliën Cassaert**, the secretary, for ordering the products most needed for the experiments, and for helping all master thesis students organizing the fantastic Jungle party in December 2014.

From the Department of Chemical Engineering, I would like to thank **Liesel Cluyts** for technical support during Hach Lange measurements and for guiding in the laboratories. I also need to thank Prof. Dr. ir. **Ilse Smets** for giving me advice concerning bulking problems of the bioreactor, as well as Prof. Dr. ir. **Kristel Bernaerts** for helping me in the completion of the Hach-Lange risk analysis forms. Finally I want to thank **Hassan Farrokhzad**, PhD student, for his support during CAM measurements.

From the Department of Physics and Astronomy, I sincerely thank Prof. Dhr. **Alexander Volodin** for the energy he has put into the countless AFM measurements.

From the Department of Materials Engineering I am grateful towards **Gregory Pyka** and **Oksana Shishkina** for the time they spent looking for potential porometry measurement improvements on my samples on an unselfish way.

From the *Institut des Sciences Chimiques de Rennes* I thank Prof. Dhr. **Anthony Szymczyk** for the zeta potential measurements he performed with tremendous rapidity.

I finally thank from my heart my friends, namely the master thesis students **Claudia Moens**, **Marieke Verbeke**, **Steffie Evers**, **Mathias Nijsen** and **Kris Dox**, without whom this adventure would not have taken place, as well as the radiant master thesis student **Marie Mulier**, with whom I had the most intense peptalks and data exchange. And in the very end I thank my lovely family for encouraging me on staying on track by means of delicious meals, comforting arms and positive conversations.

## Abstract

The membrane bioreactor (MBR) technology can now be considered a well-established alternative wastewater treatment system to conventional techniques (CASP). Advantages comprise the delivery of higher effluent quality as well as the smaller footprint requirement. However, aside from the high investment cost, one of the main drawbacks and research challenges of membrane technology is membrane fouling. Due to membrane fouling the performance of the filtration process decreases with time, which implies high energy demands and operational costs related to fouling prevention, mitigation and remediation. Example studies on membrane fouling in view of process optimization are manifold, but there still exists a lack of knowledge about the microorganisms taking part in the fouling process (i.e., biofouling) and their specific relation to the membrane surface chemistry and to the wastewater environment. Thus this slows down the development of more targeted anti-(bio)fouling strategies.

The purpose of this study was to elucidate the relationship between the specific surface charge (neutral, positive, negative) of polyacrylonitrile (PAN) membranes and the development and composition of the microbial community in the biofouling layer developed during 40 days in a submerged laboratory-scale aerobic membrane bioreactor (HT-MBR) operated on protamylasse feed. The work was performed using 13 wt% pure PAN membranes as well as 11 wt% PAN membranes having undergone surface modifications (hydrolysis, layer-by-layer deposition of poly(allyl amine hydrochloride) (PAH) and poly(acrylic acid) (PAA)). The synthesized membranes were analyzed thoroughly in term of their physico-chemical properties (via ATR-FTIR, SEM, AFM, CAM, volume porosity measurement, electrokinetic characterization) and their permeability/filterability (via CWP, critical flux). The membrane biofouling was characterized based on molecular techniques (PCR-DGGE) and physico-chemical techniques (via ATR-FTIR, SEM, CLSM).

The results revealed that the synthesized ultrafiltration (UF) membranes were only different in their charges and chemical composition (due to functionalization) but not in pore size, porosity, clean water permeability or surface roughness. This it allowed the fouling experiments to be solely determined by these differences. Fingerprinting analysis indicated selective enrichment of bacterial populations from the sludge suspension within the biofilms at any time point. Biofilm community composition seemed to change with time. But since no difference was observed between the biofilm community of different membranes at specific time points, it could be concluded that the local characteristics of the membrane (here: charge) do not play a decisive role on the long term selection of the key foulants. Enhanced knowledge on the specific relation between membrane and microorganisms as well as inter-microbial relations should allow for development of more targeted anti-fouling strategies.

**Keywords:** membrane bioreactor, polyacrylonitrile, surface charge, biofouling, PCR-DGGE fingerprinting.



## Abstract (Dutch)

Membraan bioreactor technologie (MBR) kan vandaag beschouwd worden als een waardevol alternatief voor afvalwaterbehandeling via conventionele technieken (CASP). Voordelen zijn onder meer de hoge effluentkwaliteit en de kleine voetafdruk. Nochtans nadelen gerelateerd aan de hoge investeringskost maar vooral membraanvervuiling verhinderen een uitgebreide toepassing van de MBR technologie. Membraanvervuiling beïnvloedt de performantie van de membranen tijdens het filtratieproces en veroorzaakt een toenemend energieverbruik en oplopende kosten gerelateerd aan preventie, mitigatie en remediatie van het fenomeen. Voorbeeldstudies over membraanvervuiling met het oog op procesoptimalisatie zijn talrijk, maar er is nog steeds een tekort aan kennis over de micro-organismen die deelnemen aan het proces, genaamd 'biofouling'. Ook is er gebrek aan kennis over hun specifieke relatie met de oppervlakte chemische eigenschappen van de membranen en het afvalwater milieu. Dit heeft tot gevolg dat de ontwikkeling van meer doelgerichte anti-(bio)fouling strategieën sterk wordt ondermijnd.

Dit werk had als doel de verduidelijking van de specifieke relatie tussen de membraan oppervlaktelading (neutraal, positief, negatief geladen) van polyacrylonitrile (PAN) membranen en de ontwikkeling en samenstelling van de microbiële gemeenschap in de biofilm dat gedurende 40 dagen ontwikkelde in een laboratorium aerobe membraan bioreactor (HT-MBR) gevoed met protamylasse. Membranen hiervoor gebruikt waren 13 w/w % zuivere PAN en 11 w/w % PAN gemodificeerd via hydrolyse of coating van de polymeren polyallylaminehydrochloride (PAH) en polyacrylzuur (PAA). De physico-chemische eigenschappen van de gesynthetiseerde membranen werden grondig bestudeerd (via ATR-FTIR, SEM, AFM, CAM, volume porosimetrie, electrokinetische metingen) evenals hun permeabiliteit/filterabiliteit (via CWP, kritische flux). De biofouling werd gekarakteriseerd via moleculaire technieken (PCR-DGGE) and physico-chemische technieken (ATR-FTIR, SEM, CLSM).

The resultaten duiden dat de gesynthetiseerde ultrafiltratie (UF) membranen enkel onderling verschilden in hun oppervlaktelading en chemische samenstelling (omwille van de modificatie), maar niet in poriegrootte, porositeit, water permeabiliteit of oppervlakte ruwheid. Deze bevindingen gaven aan dat de fouling experimenten uitsluitend bepaald werden door de aangehaalde verschillen. Fingerprinting toonde selectieve aanrijking aan van bacteriële populaties uit de slibsuspensie in de biofilm op elk tijdstip. De samenstelling van de microbiële biofilm gemeenschap leek met de tijd te veranderen. Maar aangezien geen verschillen merkbaar waren tussen de biofilm gemeenschappen van de verschillende membranen op de bestudeerde tijdstippen, kon geconcludeerd worden dat de lokale karakteristieken van de membranen (hier: lading) geen significante rol spelen in de selectie van sleutel foulants op lange termijn. Verhoogde kennis van de specifieke relaties tussen membraan en micro-organisme alsook van de inter-microbiële relaties moet op termijn de ontwikkeling van doelgerichte anti-fouling strategieën mogelijk maken.

**Sleutelwoorden:** membraan bioreactor, polyacrylonitrile, oppervlaktelading, biofouling, PCR-DGGE fingerprinting.





## List of abbreviations and symbols

2D	Two dimensional	HT-MBR	High throughput membrane bioreactor
3D	Three dimensional	i.a.	<i>inter alia</i> , among other things
A	Total surface area of the membrane (m <sup>2</sup> )	i.e.	<i>id est</i> , that is
AFM	Atomic Force Microscopy	iMBR	Immersed or submerged MBR
ANAMMOX	ANAerobic AMMonium OXidation	I <sub>s</sub>	Streaming current (A)
AnMBR	Anaerobic membrane bioreactor	J	Volumetric flux (LMH)
ATR-FTIR	Attenuated Total Reflectance Fourier Transform Infrared Spectroscopy	J <sub>c</sub>	Critical flux (LMH)
BOD	Biological/biochemical oxygen demand (g l <sup>-1</sup> )	J <sub>w</sub>	Pure water flux (LMH)
B <sub>v</sub>	Volumetric or organic loading rate (kg COD m <sup>-3</sup> d <sup>-1</sup> )	K	Permeance (LMH bar <sup>-1</sup> )
B <sub>x</sub>	Sludge loading rate (kg COD kg <sup>-1</sup> MLSS d <sup>-1</sup> )	L	Channel length (m)
CAM	Contact Angle Measurement	LMH	l m <sup>-2</sup> h <sup>-1</sup>
CANON	Completely Autotrophic Nitrogen removal Over Nitrite	LPM	l min <sup>-1</sup>
CASP	Conventional Activated Sludge Process	MBR	Membrane bioreactor
C <sub>e</sub>	Effluent concentration	m <sub>dry</sub>	Mass of air-dried membrane coupon (g)
CFU	Colony Forming Units	MF	Microfiltration
C <sub>i</sub>	Influent concentration	MLSS	Mixed liquor suspended solids (g l <sup>-1</sup> )
CLSM	Confocal Laser Scanning Microscopy	MLVSS	Mixed liquor volatile suspended solids (g l <sup>-1</sup> )
C-membranes	Cleaned membranes	MPN	Most Probable Number
COD	Chemical oxygen demand (g l <sup>-1</sup> )	mQ-H <sub>2</sub> O	MilliQ water
CTAB	Cetyltrimethylammonium bromide	m <sub>wet</sub>	Mass of wet membrane coupon (g)
CWP	Clean water permeance (LMH bar <sup>-1</sup> )	n	Sample size
DGGE	Denaturing Gradient Gel Electrophoresis	N	Nitrogen
d-H <sub>2</sub> O	Demineralised water	NC	Negative control
DMSO	Dimethyl sulfoxide	NF	Nanofiltration
DNA	Deoxyribonucleic acid	NH <sub>3</sub> -N	Ammonia
DO	Dissolved oxygen (mg l <sup>-1</sup> )	NH <sub>4</sub> <sup>+</sup> -N	Ammonia
DSVI	Diluted sludge volume index (ml g <sup>-1</sup> )	NO <sub>2</sub> <sup>-</sup> -N	Nitrite
dΔP/dt	Fouling rate (mbar h <sup>-1</sup> )	NO <sub>3</sub> <sup>-</sup> -N	Nitrate
e.g.	<i>exempli gratia</i> , for example	OTU	Operational Taxonomic Unit
eMBR	Side stream or external MBR	P	Phosphorus
EPS	Extracellular polymeric substance	P'	Permeability coefficient (l m <sup>-1</sup> h <sup>-1</sup> bar <sup>-1</sup> )
F:M	Food-to-microorganism ratio (kg COD kg <sup>-1</sup> MLSS d <sup>-1</sup> )	P(E)I	Poly(ether)imide
FI	Filament Index	P(E)S	Poly(ether)sulfone
h <sub>ch</sub>	Channel height (m)	PA	Polyamide
HRT	Hydraulic retention time (h)	PAA	Poly(acrylic acid)
PAH	Poly(allylamine hydrochloride)	sTN	Soluble total nitrogen (g l <sup>-1</sup> )

## VIII

PAN	Polyacrylonitrile	SEM	Scanning Electron Microscopy
PAN-H	Hydrolyzed PAN membrane	sP	Soluble phosphorus
PC	Polycarbonate	SRT	Sludge retention time (d)
PCR	Polymerase Chain Reaction	SVI	Sludge volume index ( $\text{ml g}^{-1}$ )
PE	Polyethylene	TMP	Transmembrane pressure (bar)
PEEK	Polyetheretherketon	TN	Total nitrogen ( $\text{g l}^{-1}$ )
P-membranes	Pristine membranes	TP	Total phosphorus ( $\text{g l}^{-1}$ )
$\text{PO}_4^{3-}\text{-P}$	Orthophosphate	T-RFLP	Terminal Restriction Length Polymorphism
PP	Polypropylene	TS	Total solids ( $\text{g l}^{-1}$ )
PTFE	Polytetrafluoroethylene	TSA	Tryptone Soy Agar
PVDF	Polyvinylidene fluoride	TSS	Total suspended solids ( $\text{g l}^{-1}$ )
qPCR	Quantitative Polymerase Chain Reaction	UASB	Upward-flow anaerobic sludge blanket reactor
r	Average pore radius (m)	UCT	University of Cape Town
$R_a$	Adsorption resistance ( $\text{m}^{-1}$ )	UF	Ultrafiltration
rcf	Relative centrifugal force	VSS	Volatile suspended solids ( $\text{g l}^{-1}$ )
$R_{\text{cleaning}}$	Resistance after cleaning ( $\text{m}^{-1}$ )	$V_{\text{total}}$	Total volume of membrane ( $\text{m}^3$ )
$R_{\text{cp}}$	Resistance due to concentration polarization ( $\text{m}^{-1}$ )	$V_{\text{voids}}$	Pore volume of membrane ( $\text{m}^3$ )
$R_f$	Total fouling resistance ( $\text{m}^{-1}$ )	W	Channel width (m)
$R_g$	Cake layer resistance ( $\text{m}^{-1}$ )	WU	Water uptake (%)
$R_{\text{irrec}}$	Long-term irrecoverable, irremovable or absolute fouling resistance ( $\text{m}^{-1}$ )	$\bar{X}$	Mean of sample data
$R_{\text{irrev}}$	Irreversible or permanent fouling resistance ( $\text{m}^{-1}$ )	$Z_i$	Height at location i (AFM) (nm)
$R_m$	Intrinsic clean or hydraulic membrane resistance ( $\text{m}^{-1}$ )	$\bar{Z}$	Average height over the locations (AFM) (nm)
$R_{\text{ms}}$	Root mean square height (nm)	$\Delta P$	Transmembrane pressure or hydrostatic pressure (bar)
RNA	Ribonucleic acid	$\Delta P/\Delta x$	Pressure gradient over the membrane cross-section ( $\text{bar m}^{-1}$ )
RO	Reverse osmosis	$\Delta x$	Membrane thickness (m)
$R_p$	Pore blocking resistance ( $\text{m}^{-1}$ )	$\epsilon$	Membrane surface porosity (-)
rpm	Rotations per minute	$\epsilon_0$	Vacuum permittivity ( $8.854\text{E-}12 \text{ F m}^{-1}$ )
$R_r$	Removable, reversible or temporary fouling resistance ( $\text{m}^{-1}$ )	$\epsilon_r$	Dielectric constant of the solution (-)
$R_t$	Total membrane resistance ( $\text{m}^{-1}$ )	$\eta$	Dynamic viscosity of the liquid permeating the membrane or of the electrolyte solution ( $\text{bar h}$ or $\text{kg m}^{-1} \text{ s}^{-1}$ )
s	Standard deviation of sample data	$\rho_w$	Water density ( $\text{g m}^{-3}$ )
SHARON	Single reactor system for High Ammonia Removal Over Nitrite	$\tau$	Pore tortuosity (-)
sCOD	Soluble chemical oxygen demand ( $\text{g l}^{-1}$ )	$\vartheta$	Contact angle (deg)
SE	Mean standard error	$\zeta$	Zeta potential (V)

## List of tables

<b>Table 1</b> Properties of the four pressure driven membrane processes (adapted from [36]–[38], [40]–[43]).	10
<b>Table 2</b> Comparison of the modules design and their characteristics (adapted from [5], [36], [38]).	13
<b>Table 3</b> Advantages of the MBR technology compared to the CASP.	18
<b>Table 4</b> Disadvantages of the MBR technology.	19
<b>Table 5</b> Comparison of the characteristics of iMBRs and eMBRs.	20
<b>Table 6</b> Comparison of aerobic and anaerobic conventional and membrane systems.	21
<b>Table 7</b> Example studies on the pioneer microbial community composition of the biofouling layer.	26
<b>Table 8</b> Most commonly used chemical cleaning agents for maintenance or intensive cleaning of membranes (based on [4], [38], [40], [48], [88]).	33
<b>Table 9</b> Average composition of the protamylasse residue (54% dry weight) (adapted from [132]).	41
<b>Table 10</b> Hach-Lange measurements performed on permeate, sludge and protamylasse feed solution samples.	44
<b>Table 11</b> Sequence and annealing temperature of the forward primer GC-63F and the reverse primer 518R [147].	56
<b>Table 12</b> Summary of the characteristics and operating parameters of the HT-MBR over both Transient Periods 1 and 2 and Fouling Periods 1 and 2. Values are given as (mean $\pm$ standard deviation).	61
<b>Table 13</b> COD, TN and phosphate concentrations in the feed solution, the sludge supernatant and/or the permeate as well as their nutrient ratio and the removal efficiencies (%). Values are given as (mean $\pm$ standard deviation). sCOD = soluble COD.	62
<b>Table 14</b> Critical flux values at the operating condition of the HT-MBR as well as corrected to a standard temperature of 20 °C, for the four membrane types. The values for the C-membranes were obtained via the flux-stepping experiments and based on a threshold fouling rate value of 6 mbar h <sup>-1</sup> , and used for extrapolation of the critical flux values of the P-membranes.	79
<b>Table 15</b> Approximate amount of bacteria in the sludge suspension, protamylasse feed solution from day 4 of the maintenance period, membrane surface and permeate, expressed as Most Probable Number (MPN) ml <sup>-1</sup> sample.	81
<b>Table 16</b> Overview of the membrane types synthesized and used in this work together with their physical properties determined via membrane performance measurements.	97



## List of figures

<b>Figure 1</b> Schematic of a typical three-stage wastewater treatment train, comprising a primary treatment, secondary treatment or Conventional Activated Sludge Process (CASP) and a tertiary treatment, after which the treated water is discharged in surface waters. The CASP detailed here, configured as the University of Cape Town (UCT-CASP) process, is the most commonly used configuration. VFA = volatile fatty acids. ....	4
<b>Figure 2</b> Illustration of the evolution with time of the microorganism community in .....	6
<b>Figure 3</b> Schematic of a membrane process (adapted from [38]).....	9
<b>Figure 4</b> Classification of membranes based on their morphology (adapted from [38]).....	11
<b>Figure 5</b> MBR membrane configurations: membrane, module and process train. ....	12
<b>Figure 6</b> Dead-end filtration (A) versus cross-flow filtration (B) (adapted from [37]). ....	13
<b>Figure 7</b> Flux decline over time caused by concentration polarization and membrane fouling (adapted from [37]). .....	14
<b>Figure 8</b> Internal or immersed MBR (A) versus side stream or external configuration (B).....	17
<b>Figure 9</b> Anaerobic membrane bioreactor in immersed configuration (based on [11]).....	21
<b>Figure 10</b> Evolution of the annual publications on MBR fouling, searched via Google Scholar until 2008 and via PubMed from 2009 to 2014 (adapted from [48]). ....	23
<b>Figure 11</b> Membrane fouling mechanisms. (A) surface fouling, (B) pore fouling, (C) cake layer formation .....	24
<b>Figure 12</b> Schematic of a biofilm formation process in an aerobic MBR system in cross-flow filtration mode on a porous membrane. (A) formation of a conditioning film, (B) initial bacterial attachment, (C) EPS production, (D) biofilm maturation, (E) bacterial detachment. Brown arrows represent decreasing permeability .....	26
<b>Figure 13</b> Typical fouling stages (adapted from [48]). ....	28
<b>Figure 14</b> Schematic of the factors affecting membrane fouling (adapted from [4], [7], [16], [42], [48], [52]).....	30
<b>Figure 15</b> Possible mechanism for the hydrolysis of PAN with NaOH (reproduced from [123]). ....	37
<b>Figure 16</b> Structure of the envelope-sized modules. (1) double folded membrane sheet, (2) spacer sheets, (3) permeate channel, (4) PVC frame. ....	38
<b>Figure 17</b> Final modules and their respective surface charges. (A) 13% PAN – neutral, (B) 11% PAN (-) – hydrolyzed, (C) 11% PAN (+) – 1 deposited layer PAH, (D) 11% PAN (-) – 2 deposited layers PAH & PAA. ....	38
<b>Figure 18</b> Schematic of the HT-MBR. (1) feed tanks, (2) feed pump and level controller, (3) bioreactor containing the 4x 4 replicate membrane modules immersed in activated sludge, (4) permeate pump, (5) air supply. The upper right figure represents the clustered arrangement of the membrane replicates inside the bioreactor.....	39
<b>Figure 19</b> Timeline of the fouling experiments.....	42
<b>Figure 20</b> High-throughput device for the CWP measurement of membrane coupons.....	49
<b>Figure 21</b> Set-up of the CWP measurement of the membrane modules. ....	50

<b>Figure 22</b> Membrane sampling. Each vertical line corresponds to a sampling moment. The same pattern is present at the back side of the module.....	54
<b>Figure 23</b> Flowdiagram applied for the culture-independent analysis of microbial communities .....	55
<b>Figure 24</b> ATR-FTIR spectra of the four membrane types (P-membranes).....	63
<b>Figure 25</b> SEM surface and cross-sectional visualization of the four membrane types (P-membranes). (A) 10 kV, magnification 1500x, (B) 10 kV, magnification 10 000x, (C) 12 kV, magnification 50 000x, (D) 10 kV, magnification 300x or 330x, (E) 10 kV, magnification 3000x. ....	65
<b>Figure 26</b> Atomic Force Microscopy observations (2D and 3D) of the four membrane types at 1x1 $\mu\text{m}$ and of only two membrane types at 10x10 $\mu\text{m}$ surface areas (P-membranes). The first and second row of images within each series (1x1 $\mu\text{m}$ or 10x10 $\mu\text{m}$ ) represent the three dimensional and the two dimensional surface structure respectively. The third row of images within each series represents the profile structure of the upper surface region of the membranes. ....	67
<b>Figure 27</b> Membrane surface roughness expressed as root mean square height (nm) for the four membrane types at 1x1 $\mu\text{m}$ and for two membrane types 10x10 $\mu\text{m}$ surface areas (P-membranes). Error bars represent standard deviations from the mean value ( $n = 3$ ). ....	68
<b>Figure 28</b> Contact angle images of the four membrane types (P-membranes) performed with d-H <sub>2</sub> O, and their respective contact angle $\vartheta$ . Values are given as (mean $\pm$ standard deviation) ( $n = 2 \times 3$ ).....	69
<b>Figure 29</b> Membrane volume porosity measurements (-) of the four membrane types (P-membranes) based on water uptake measurements. Error bars represent standard deviations from the mean value ( $n = 2$ ). ....	72
<b>Figure 30</b> Streaming current coefficient ( $\text{A bar}^{-1}$ ) versus $pH$ for the four membrane types (P-membranes). The intersection of the curves with the x-axis corresponds to the isoelectric point.....	73
<b>Figure 31</b> Clean water permeance ( $\text{LMH bar}^{-1}$ ) of coupons (pristine) ( $n = 3 \times 3$ ) and modules (P- and C-membranes) ( $n = 4 \times 2$ ) of the four membrane types, performed with mQ-H <sub>2</sub> O. Error bars represent standard deviations from the mean value.....	77
<b>Figure 32</b> Flux-stepping measurements on 13% PAN (neutral) modules (C-membranes). Error bars represent standard deviations from the mean value ( $n = 4$ ). ....	78
<b>Figure 33</b> Mean fouling rate ( $\text{mbar h}^{-1}$ ) versus average flux (LMH) as determined in the flux-stepping experiment on 13% PAN (neutral) modules (C-membranes) ( $n = 4$ ). The labels indicate the threshold limits for the critical flux determination. ....	78
<b>Figure 34</b> Dilution series in Tryptone Soy Agar of the sludge, protamylasse feed (maintenance day 4), permeate and random two randomly chosen membranes (Day 30 of the Fouling Period 2) ( $n = 3$ ). ....	81
<b>Figure 35</b> Microscopic image of the sludge sample after sonication (magnification 1000x, oil objective).....	82
<b>Figure 36</b> Evolution of the transmembrane pressure (mbar) of the module replicates of 13% PAN (neutral) during Fouling Period 1. Arrows indicate time points of biofilm sampling. ....	83
<b>Figure 37</b> Bacterial 16S rRNA gene community fingerprints (DGGE profile showing differences in community structure and respective dendrogram) derived from membrane biofilms, activated sludge and protamylasse feed solution at different sampling time points of the Fouling Period 1 performed in the HT-MBR. The scale bar represents the percentage similarity at the nodes. The standard markers were removed from the DGGE profile for the sake of clarity. ....	86

- Figure 38** Number of Operational Taxonomic Units derived from the number of band in the fingerprints of the membrane samples taken at different time points. Error bars represent standard deviations from the mean value based on the band number of the four membrane types ( $n = 4$ ). ..... 88
- Figure 39** Log-values of the Shannon diversity index for the membrane and activated sludge samples. Error bars represent standard deviations from the mean value calculated from the values homogenized over the different time points ( $n = 6$ ). ..... 89
- Figure 40** ATR-FTIR graph of the fouling layer of membrane 13% PAN (neutral). ..... 92
- Figure 41** SEM surface images of the fouling layer of membrane 13% PAN (neutral) at magnifications 250x (A), 1500x (B) and 10 000x (C) and 25 kV. .... 93
- Figure 42** CLSM images of the biofouling layer of membrane 13% PAN (neutral) at magnifications 40x and 320x320  $\mu\text{m}$  surface area (A) and magnification 100x and 125x125  $\mu\text{m}$  surface area (B). The QR code (C) gives access to a Youtube video highlighting the three dimensional structure of the biofilm (100x) by migration of the fluorescence signal over the cake depth. The images and the video were processed by means of the software evaluation version of Imaris Bitplane. .... 94





# Table of contents

Acknowledgments.....	I
Abstract.....	III
Abstract (Dutch).....	IV
List of abbreviations and symbols.....	VII
List of tables.....	IX
List of figures.....	XI
Table of contents.....	XIV
<b>Chapter 1: Context &amp; objectives.....</b>	<b>1</b>
1. Background and problem statement.....	1
2. Research objectives and research approach.....	2
<b>Chapter 2: Literature review.....</b>	<b>3</b>
1. CONVENTIONAL WASTEWATER TREATMENT.....	3
1.1. Wastewater treatment.....	3
1.1.1. Wastewater composition.....	3
1.1.2. Wastewater treatment train.....	4
1.2. Secondary wastewater treatment: CASP.....	4
1.2.1. Configuration: UCT-CASP.....	4
1.2.2. Sludge composition.....	6
1.3. Alternative technologies.....	7
1.3.1. Anaerobic digestion.....	7
1.3.2. Conventional anaerobic reactor.....	8
1.3.3. Membrane bioreactor.....	8
2. MEMBRANE BIOREACTOR FUNDAMENTALS.....	8
2.1. Definition.....	8
2.2. Membrane technology.....	9
2.2.1. Process classification.....	9
2.2.2. Membrane morphology and membrane materials.....	11
2.2.3. Membrane synthesis.....	12
2.2.4. Membrane modules.....	12
2.2.5. System design.....	13
2.2.6. Operating parameters.....	13
Volumetric flux and transmembrane pressure.....	13
Permeability coefficient.....	15
2.2.7. Critical flux concept.....	15
2.3. Membrane bioreactor technology.....	16
2.3.1. Historical market development.....	16
2.3.2. Prospects and constraints of the MBR technology.....	16
2.3.3. Process configurations.....	17
2.4. Current research trends.....	17
2.4.1. Anaerobic membrane bioreactors.....	17
2.4.2. Alternative membranes.....	22
2.4.3. Alternative configurations.....	22
3. FUNDAMENTALS OF MEMBRANE FOULING.....	22
3.1. Definition.....	23
3.2. Classification of membrane fouling.....	23
3.2.1. Classification based on the mechanism.....	23
3.2.2. Classification based on the permeability recovery.....	24
3.2.3. Classification based on the nature of the foulants.....	25
Organic and inorganic precipitates.....	25

	Biofouling and biofilm formation .....	25
3.3.	Fouling stages .....	28
3.4.	Fouling control strategies .....	29
3.4.1.	Improvement of the hydrodynamics .....	30
3.4.2.	Optimization of the membrane design .....	31
3.4.3.	Optimization of the process design .....	33
	Influence of operating conditions .....	33
<b>Chapter 3: Research methodology .....</b>		<b>35</b>
1.	MEMBRANE AND MODULE PREPARATION .....	35
1.1.	Membrane material .....	35
1.2.	Membrane casting .....	35
1.3.	Preparation of the hydrolyzed PAN membranes .....	36
1.4.	Layer-by-layer deposition: membrane functionalization .....	37
1.5.	Module potting .....	38
2.	OPERATING CONDITIONS OF THE LAB-SCALE MBR SYSTEM .....	39
2.1.	Membrane bioreactor design .....	39
2.1.1.	Laboratory-scale high-throughput membrane bioreactor .....	39
2.1.2.	Origin of activated sludge and feed .....	40
2.1.3.	Maintenance of the HT-MBR .....	41
2.2.	Quality measurements .....	42
2.2.1.	Operational parameters .....	42
2.2.2.	Physico-chemical analysis .....	43
2.2.3.	Microscopic analysis .....	44
3.	MEMBRANE PERFORMANCE MEASUREMENT .....	45
3.1.	Membrane sampling .....	45
3.2.	Physico-chemical related measurements .....	45
3.2.1.	Attenuated Total Reflectance Fourier Transform Infrared Spectroscopy .....	45
3.2.2.	Scanning Electron Microscopy .....	46
3.2.3.	Atomic Force Microscopy .....	46
3.2.4.	Contact Angle Measurement .....	47
3.2.5.	Volume porosity measurement .....	48
3.2.6.	Electrokinetic characterization .....	48
3.3.	Permeability related measurements .....	49
3.3.1.	Clean water permeance of membrane coupons .....	49
3.3.2.	Clean water permeance of membrane modules .....	50
3.3.3.	Critical flux determination .....	51
4.	BIOFOULING (COMMUNITY) CHARACTERIZATION .....	52
4.1.	Preliminary observations .....	52
4.1.1.	Bacterial enumeration .....	52
4.1.2.	Membrane fouling rate .....	53
4.2.	Microbiological identification .....	53
4.2.1.	Membrane sampling and sample storage .....	53
4.2.2.	Culture-independent analysis of microbial communities .....	54
	DNA extraction and purification .....	55
	Detection through Polymerase Chain Reaction .....	55
	Denaturing Gradient Gel Electrophoresis fingerprinting .....	56
4.3.	Physico-chemical analysis of the biofilm .....	57
4.3.1.	Attenuated Total Reflectance Fourier Transform Infrared Spectroscopy .....	57
4.3.2.	Scanning Electron Microscopy .....	57
4.3.3.	Confocal Laser Scanning Microscopy .....	58
5.	STATISTICAL ANALYSIS .....	58

<b>Chapter 4: Results &amp; discussion</b> .....	61
1. MEMBRANE BIOREACTOR AND QUALITY MEASUREMENTS.....	61
2. MEMBRANE PERFORMANCE MEASUREMENT.....	62
2.1. Physico-chemical related measurements.....	62
2.1.1. Attenuated Total Reflectance Fourier Transform Infrared Spectroscopy.....	62
2.1.2. Scanning Electron Microscopy.....	64
2.1.3. Atomic Force Microscopy.....	66
2.1.4. Contact Angle Measurement.....	69
2.1.5. Volume porosity measurement.....	71
2.1.6. Electrokinetic characterization.....	72
2.2. Permeability related measurements.....	76
2.2.1. Clean water permeance.....	76
2.2.2. Critical flux.....	77
3. BIOFOULING (COMMUNITY) CHARACTERIZATION.....	80
3.1. Preliminary observations.....	80
3.1.1. Bacterial enumeration.....	80
3.1.2. Membrane fouling rate.....	83
3.2. Microbiological identification.....	84
3.2.1. DGGE fingerprinting of PCR-amplified 16S rRNA gene fragments.....	84
3.3. Physico-chemical analysis of the biofilm.....	91
3.3.1. Attenuated Total Reflectance Fourier Transform Infrared Spectroscopy.....	91
3.3.2. Scanning Electron Microscopy.....	93
3.3.3. Confocal Laser Scanning Microscopy.....	93
<b>Chapter 5: Conclusion &amp; future prospects</b> .....	97
1. Conclusion.....	97
2. Future prospects.....	99
References.....	A-I
Appendix 1: Complementary results.....	A-XI
1. MEMBRANE BIOREACTOR AND QUALITY MEASUREMENTS.....	A-XI
1.1. Operation of the HT-MBR.....	A-XI
1.2. Physico-chemical analysis.....	A-XIV
1.3. Microscopic analysis.....	A-XV
2. MEMBRANE PERFORMANCE MEASUREMENT.....	A-XVIII
2.1. Physico-chemical related measurements.....	A-XVIII
2.1.1. Attenuated Total Reflectance Fourier Transform Infrared Spectroscopy.....	A-XVIII
2.1.2. Scanning Electron Microscopy.....	A-XX
2.2. Permeability related measurements.....	A-XXII
2.2.1. Clean water permeance.....	A-XXII
2.2.2. Critical flux.....	A-XXIII
3. BIOFOULING (COMMUNITY) CHARACTERIZATION.....	A-XXVI
3.1. Preliminary observations.....	A-XXVI
3.1.1. Membrane fouling rate.....	A-XXVI
3.2. Microbiological identification.....	A-XXVII
3.2.1. DGGE fingerprinting of PCR-amplified 16S rRNA gene fragments.....	A-XXVII
Appendix 2: Risk assessments.....	A-XXXI
Appendix 3: List of products.....	A-XXXIII
Appendix 4: CTAB protocol.....	A-XXXVII
Appendix 5: Polarized summary.....	A-XXXIX





# Chapter 1: Context & objectives

## 1. BACKGROUND AND PROBLEM STATEMENT

The growth of world populations, the increasing industrialization and the expansion of intensive agriculture from the 19<sup>th</sup> century pressurizes natural ecosystems in general and water bodies in particular [1]. Increased water consumption combined with an alarming deterioration of the water resource quality and the projections of climate change make water the most precious and important common good worldwide. Thus sanitation technology for the treatment of wastewaters produced by households or industrial activities is of strategic importance in order to provide the world populations with sufficient amounts of fresh water in the future and to ensure environmental protection.

The currently most commonly used wastewater treatment technology is the Conventional Activated Sludge Process (CASP), where pollutants and organics are removed from municipal and industrial wastewaters by biological degradation and subsequent separation of the cleaned water by sedimentation. Research aiming at improvement of this traditional approach started in the 1960s with alternative membrane based treatment technologies, which improve the separation efficiency by means of a filtration step through a membrane instead of sedimentation [2]–[6]. Driven by the increasing water scarcity and the more stringent regulations, Japan, South Korea, France and the UK have performed most of the pioneering research around membrane bioreactors (MBRs), so it's not surprising the first full-scale MBR plant for treatment of municipal wastewater has been installed in the UK in 1997. Yet MBR technology can now be considered an established wastewater treatment system delivering higher effluent quality as well as requiring a smaller footprint than the CASP [4].

The quantity and size of MBRs worldwide has increased exponentially with capacities ranging from  $< 1 \text{ m}^3 \text{ day}^{-1}$  to  $> 100\,000 \text{ m}^3 \text{ day}^{-1}$  [7]. However, aside from the high investment cost, one of the main drawbacks and research challenges of membrane technology is membrane fouling. Due to membrane fouling the performance of the filtration process decreases with time, which implies high energy demands and operational costs related to fouling prevention, mitigation and remediation. Example studies on membrane fouling in view of process optimization are manifold, but there still exists a lack of knowledge about the microorganisms taking part in the fouling process (i.e., biofouling) and their specific relation to the membrane surface chemistry and to the wastewater environment, thus slowing down the development of more targeted anti-(bio)fouling strategies.

## 2. RESEARCH OBJECTIVES AND RESEARCH APPROACH

The purpose of this study is to elucidate the relationship between the specific surface charge (neutral, positive, negative) of polyacrylonitrile (PAN) membranes and the development and composition of the microbial community in the biofouling layer developed during 40 days in a submerged laboratory-scale aerobic membrane bioreactor (HT-MBR) operated on protamylasse feed.

The effect of membrane composition on biofilm community structure and diversity is assessed by answering three questions:

- Does the bacterial biofouling community differ from the sludge community at a certain time point, i.e., are bacterial populations from the sludge specifically enriched within a biofilm?
- Does the bacterial biofouling community change with time, i.e., do temporal variations in local conditions favour or exclude specific bacterial populations?
- Does the bacterial biofouling community on a membrane differ from the one on another membrane type at a certain time point, i.e., does the membrane morphology, and more specifically do the membrane surface charges affect the biofilm community composition?

Two approaches are applied:

- Performance determination of the membranes based on physico-chemical related measurements (ATR-FTIR, SEM, AFM, CAM, volume porosity measurement, electrokinetic characterization) and permeability related measurements (CWP, critical flux);
- Biofouling characterization based on molecular techniques (PCR-DGGE) and physico-chemical techniques (ATR-FTIR, SEM, CLSM).

Chapter 2 of this work briefly explains conventional wastewater technology and reviews literature on membrane technology and membrane fouling as to introduce the reader on the topic and on the commonly used concepts and terminology. Chapter 3 presents the research plan comprising the methodology and planning of the experiments. Finally Chapter 4 gives an interpretation of the results, before concluding this work with some recommendations and future research perspectives.



# Chapter 2: Literature review

## 1. CONVENTIONAL WASTEWATER TREATMENT

The wastewater treatment principles, including an overview of the chemical and biological components of wastewater as well as a presentation of the conventional treatment train, are highlighted as springboard towards the introduction to alternative wastewater treatment technologies.

### 1.1. Wastewater treatment

#### 1.1.1. Wastewater composition

Wastewater is defined as “domestic sewage or liquid industrial waste that cannot be discarded in untreated form into lakes or streams due to public health, economic, environmental, and aesthetic considerations” [8]. Roughly spoken, untreated wastewater is a complex mixture of natural or man-made organic and inorganic compounds and potentially pathogenic microorganisms [1], [8], [9].

The composition of industrial wastewater varies according to the nature of the industrial process generating it. For instance, while wastewaters originating from the food processing industry (e.g., dairy, meat, sugar) are rich in dissolved and suspended organics (proteins, fats, sugars), wastewaters from the pharmaceutical or textile industry are enriched in surfactants and inorganic compounds [10].

On the contrary, municipal wastewater has a much more stable composition, but still depends on the weather variability (i.e., dilution with rainwater) and the life styles and technologies practiced in the producing society [1], [9]. The Flanders Environment Agency uses the ‘inhabitant equivalent’ to designate the amount and composition of wastewater produced daily per Flemish inhabitant [11]. It assumes an average Flemish wastewater composition of 90 g TS<sup>1</sup>, 54 g BOD<sup>2</sup>, 135 g COD<sup>3</sup>, 10 g TN<sup>4</sup> and 2 g TP<sup>5</sup> taking into account a daily wastewater flow of 150 l capita<sup>-1</sup> [9], [11]. The removal of

---

<sup>1</sup> The total solids (TS) (g l<sup>-1</sup>) represent the total amount of suspended and dissolved organic and inorganic solids in the sludge suspension [53].

<sup>2</sup> The biological/biochemical oxygen demand (BOD) (g l<sup>-1</sup>) represents the relative amount of dissolved oxygen (mg O<sub>2</sub> l<sup>-1</sup>) used by non-photosynthetic microorganisms to catalyze the biodegradation of dissolved and particulate compounds present in the wastewater [8], [11].

<sup>3</sup> The chemical oxygen demand (COD) (g l<sup>-1</sup>) represents the amount of BOD together with the amount of organic compounds that are chemically degradable. The COD does not comprise the oxygen necessary to oxidize nitrogen compounds but do comprise the oxygen needed to oxidize reduced sulfur compounds (SH<sup>-1</sup>, S<sup>2-</sup>) [11].

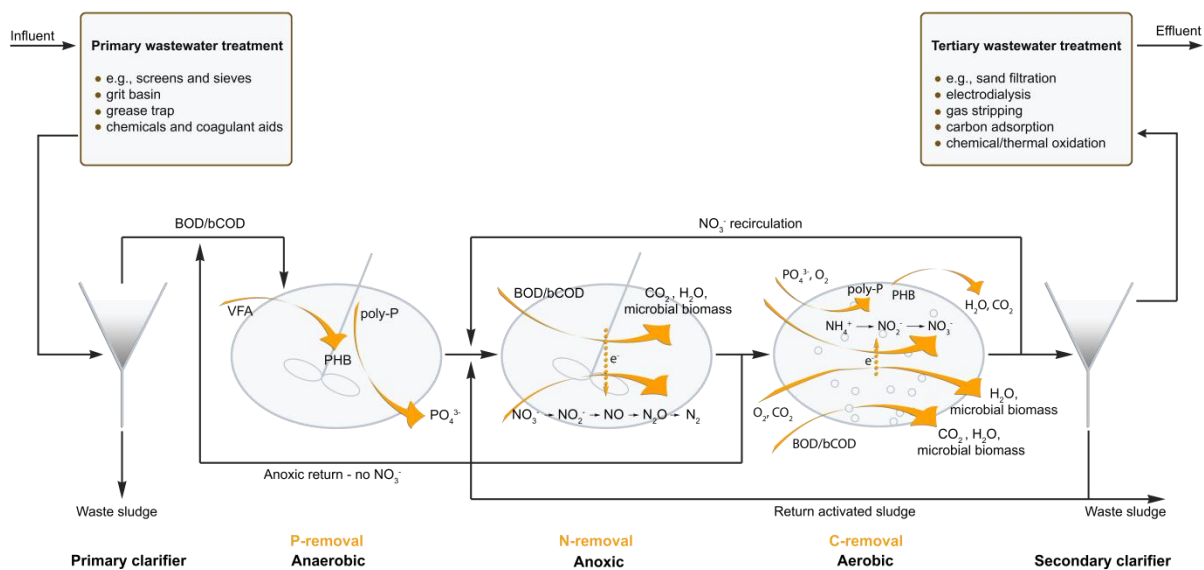
<sup>4</sup> Total nitrogen (TN) is a measure for the total amount of nitrogen compounds present in the wastewater, i.e., organic nitrogen (amino acids) but also inorganic nitrogen (ammonium (NH<sub>3</sub>-N and NH<sub>4</sub><sup>+</sup>-N), nitrite (NO<sub>2</sub><sup>-</sup>-N) and nitrate (NO<sub>3</sub><sup>-</sup>-N)) [11].

<sup>5</sup> Total phosphorus (TP) is a measure for the total amount of phosphate compounds present in the wastewater, i.e., organic phosphates (e.g., present in nucleic acids) but also inorganic phosphates (mainly orthophosphate PO<sub>4</sub><sup>3-</sup>) [11].

biodegradable substances (i.e., BOD), nitrogen and phosphorus species ( $\text{NO}_3^-$ -N,  $\text{NO}_2^-$ -N,  $\text{NH}_4^+$ -N and  $\text{PO}_4^{3-}$ -P) is crucial as to avoid eutrophication of the receiving water bodies and toxicity to aquatic organisms [1], [12]–[14]. Typical criteria for discharge of treated wastewater in surface waters depends on the type of wastewater (domestic versus industrial) and on the producing industrial sector, but are in the range of 30 mg TS  $\text{l}^{-1}$ , 20 mg BOD  $\text{l}^{-1}$ , 100 mg COD  $\text{l}^{-1}$ , 10 mg TN  $\text{l}^{-1}$  and 1 mg TP  $\text{l}^{-1}$  [11], [12], [15].

### 1.1.2. Wastewater treatment train

Treatment of wastewater dates from the late 1800s [11] and has as primary goal to eliminate toxic compounds and to reduce the amount of organic and inorganic compounds in the wastewater to a level where microbial growth becomes limited [8]. Today the most commonly used wastewater treatment technology for municipal and industrial sewage is a three-stage wastewater treatment train, consisting of primary, secondary and tertiary treatment technologies (Figure 1) [4], [6]. Mainly secondary or biological wastewater treatment has contributed largely to the improvement of the quality of water bodies worldwide for almost a century [13], [16].



**Figure 1** Schematic of a typical three-stage wastewater treatment train, comprising a primary treatment, secondary treatment or Conventional Activated Sludge Process (CASP) and a tertiary treatment, after which the treated water is discharged in surface waters. The CASP detailed here, configured as the University of Cape Town (UCT-CASP) process, is the most commonly used configuration. VFA = volatile fatty acids. (based on [9], [11], [12]).

## 1.2. Secondary wastewater treatment: CASP

### 1.2.1. Configuration: UCT-CASP

Different secondary wastewater treatment configurations exist aiming at the removal of the majority of the soluble and suspended organic matter (carbon (C)) and mineral nutrients (nitrogen (N) and



phosphorus (P), e.g.,  $\text{NH}_4^+$  -N,  $\text{NO}_3^-$  -N,  $\text{PO}_4^{3-}$  -P) from the wastewater, but the most commonly used Conventional Activated Sludge Process (CASP) for the treatment of wastewaters is the configuration of the University of Cape Town (UCT-CASP) [17]. The UCT-CASP is a continuously operated system consisting of a set of perfectly mixed basins connected by means of internal recirculation streams as showed in detail in **Figure 1**. In principle the UCT-CASP process could be optimized by incorporating multiple anoxic and aerobic zones in order to improve nutrient removal and lower energy costs [17].

Several microbially catalyzed reactions sequentially remove P, N and C compounds by conversion to  $\text{N}_2$ ,  $\text{CO}_2$  and  $\text{H}_2\text{O}$  and into a flocculent microbial suspension. P removal is typically achieved by the activity of Phosphate Accumulating Organisms, such as *Propionibacter* and *Acinetobacter*, which release  $\text{PO}_4^{3-}$  -P in anaerobic conditions but take up a larger amount of inorganic phosphate from the suspension under aerobic conditions. This results in a net accumulation of phosphate in their biomass (cells can accumulate up to 24% of their dry mass in the form of phosphate) [11], [12], [17]. N removal is typically based on a classical nitrification-denitrification process. The first step in N removal is achieved based on nitrification reactions catalyzed by autotrophic organisms, e.g., *Nitrosomonas*, *Nitrosococcus* and *Nitrospira* on the one hand ( $\text{NH}_3 \rightarrow \text{NO}_2^-$ ) and e.g., *Nitrobacter*, *Nitroeystis*, *Nitrococcus*, *Nitrospora* and *Nitrospira* on the other hand ( $\text{NO}_2^- \rightarrow \text{NO}_3^-$ ) under aerobic conditions [11]–[14]. Finally heterotrophic micro-organisms complete the N removal by denitrification under anoxic conditions ( $\text{NO}_3^- \rightarrow \text{N}_2$ ): *Pseudomonas*, but also *Acinetobacter*, *Flavobacterium*, *Agrobacterium*, *Chromobacterium*, *Achromobacter*, *Alcaligenes*, *Hyphomicrobium*, *Paracoccus*, *Thauera* sp. and *Bacillus* are reported to participate in the reactions [11]–[14]. Less energy-demanding novel nitrogen removal processes are under investigation for implementation at large scale [11]: the SHARON<sup>6</sup> process where the denitrification step starts from  $\text{NO}_2^-$  instead of  $\text{NO}_3^-$  [18], [19]; the ANAMMOX<sup>7</sup> process where  $\text{NO}_2^-$  and  $\text{NH}_4^+$  react together anaerobically to directly produce  $\text{N}_2$  [20], [21]; the CANON<sup>8</sup> process where  $\text{NH}_4^+$  is converted to  $\text{N}_2$  in a single oxygen-limited step [22], [23]; or a combination of these processes.

The series of perfectly mixed basins is followed by a secondary conventional gravity clarifier which separates the purified water from the microbial biomass. The sedimentation efficiency depends on the settling characteristics of the sludge, e.g., the size, shape and density of the particles, the composition and concentration of the suspension, but also on the hydrodynamic conditions in the sedimentation tank [9], [16]. The majority of the concentrated sludge is recirculated to ensure a high level of biodegradation, while the excess sludge may be processed for energy recovery or disposal [11].

---

<sup>6</sup> Single reactor system for High Ammonia Removal Over Nitrite

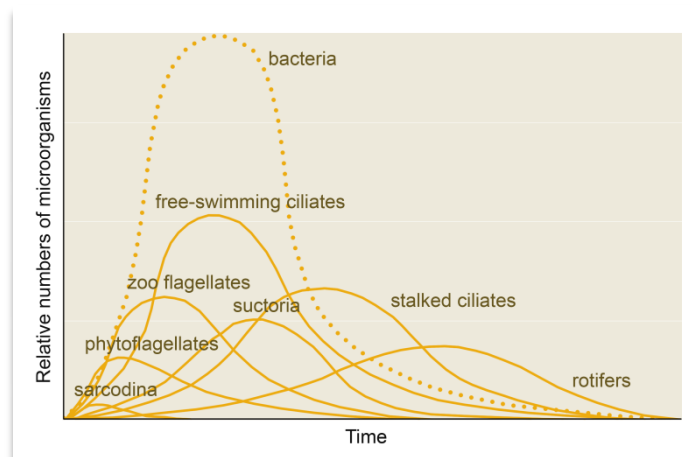
<sup>7</sup> ANaerobic AMMonium OXidation

<sup>8</sup> Completely Autotrophic Nitrogen removal Over Nitrite

### 1.2.2. Sludge composition

The mixture of water and microbes in the perfectly mixed basins is called mixed liquor and consists of suspended solids (i.e., microorganisms and inert material present as flocs typically at a size ranging between 10 and 600  $\mu\text{m}$  [24], [25]), dispersed microorganisms and organic and inorganic substances [2], [4], [11], [26], [27].

The secondary clarifier receives the mixed liquor and separates the microbial biomass from the purified water. Actually, the microbial biomass, also called activated sludge, is a diverse and uncontrolled consortium of dead cells and interacting organisms (average ratio 50%-50%) [11] including approximately 95% bacteria (cell length 1-5  $\mu\text{m}$  [28]) and 5% higher organisms which are mostly present free in the water phase, such as protozoa<sup>9</sup>, metazoans<sup>10</sup> and fungi (cell length 10-10 000  $\mu\text{m}$  [28]) (Figure 2) [5], [6], [11], [26], [29]. The dominance and balance of organisms present in the activated sludge determines the overall health of the system [26]. For an extensive discussion on the microorganisms and parameters affecting the activated sludge system, please refer to Eikelboom (2000) [28].



**Figure 2** Illustration of the evolution with time of the microorganism community in activated sludge (adapted from [30]).

Bacteria have the main role of removing the nutrients from the wastewater. Vanyacker et al. (2014) report the number of bacteria present in activated sludge to reach  $10^{13}$  bacteria  $\text{ml}^{-1}$  [16], which is higher than in natural environments (typically  $10^7$  bacteria  $\text{ml}^{-1}$  in freshwater habitats [8]). Bacteria living in activated sludge systems can be divided morphologically into floc-forming and filamentous

<sup>9</sup> Protozoa, consisting of ciliates, flagellates and amoebas, are unicellular microorganisms [28]. They make up to 3% of the activated sludge microorganisms and are considered to be the activated sludge cleaners by digestion of free-swimming bacteria and feeding on soluble organic nutrients [26].

<sup>10</sup> Metazoans are multicellular microorganisms consisting of i.a., rotifers and nematodes. They have little impact on wastewater treatment and mainly dominate old sludge [41].

bacteria [8]. The slow-growing filamentous bacteria are important for the development of well settled sludge in the secondary clarifier. Indeed, they form the backbone network or macrostructure of flocs by bridging behaviour [31], upon which a variety of small fast-growing floc-forming bacteria can adhere ('Filamentous Backbone Theory') as well as soluble, colloidal and suspended organics [6]. An excess of filamentous bacteria can cause sludge bulking in the clarifier and scum formation in the aeration basin [26], [29].

Sludge bulking is generally caused by e.g., *Sphaerotilus natans*, *Microthrix parvicella*, *Thiothrix* spp, Type 021N<sup>11</sup>, Type 0803/0914 or *Haliscomenobacter hydrossis* [28], [29], [32] and occurs when approximately  $10^7 \mu\text{m ml}^{-1}$  filaments are present in the activated sludge [11], [26]. Bulking sludge is a sludge characterized by slow compaction and poor settling [29], resulting in large, open and irregular floc structures due to excessive interfloc bridging [31].

Sludge foaming may be caused by fats or detergents present in the wastewater, but is more generally caused by the hydrophobic filamentous bacteria *Microthrix parvicella* and to a limited extent, *Nostocoida limicola* [28]. They produce high amounts of tensio-active biopolymers and induce scum formation, which results in odour and aesthetic problems, extra cleaning work and potential damage to the equipment [28].

### 1.3. Alternative technologies

The choice of wastewater treatment technology depends on physical and operational aspects, such as the wastewater origin, the volumetric flow or the pollutant concentration, as well as the objectives that have to be achieved (e.g., effluent standards) [9]. Although the CASP is the most widespread method to treat both municipal and industrial wastewater and typically has a lifespan of minimum 20 years [9], it has a series of disadvantages, as will be highlighted further in this chapter, **Section 2.3.2**. Therefore several authors have discussed alternative technologies to CASP.

#### 1.3.1. Anaerobic digestion

Smets (2012) reported the combination of aerobic wastewater treatment followed by anaerobic digestion of the produced excess sludge [11]. Hereby bacteria involved in anaerobic biodegradation of organic material – a four-step process at high temperatures (20-75°C) [33] involving acidification and methanogenesis – produce biogas, typically containing 70-90% CH<sub>4</sub>, 3-15% CO<sub>2</sub> and 0-15% N<sub>2</sub> gas [33]. The CH<sub>4</sub> gas may be recycled for fuel production or combusted to produce electricity and heat, generating approximately 380 kWh per 100 kg COD treated [5], [34], [35].

---

<sup>11</sup> Most filamentous microorganisms do not have a name but a number [28].

### 1.3.2. Conventional anaerobic reactor

Liao et al. (2006) and Smets (2012) discussed the use of an anaerobic reactor as a wastewater treatment technology on its own for the treatment of industrial (e.g., pulp & paper, textile, pharmaceutical, chemical industry), agricultural and food processing wastewaters (e.g., beverage industries) [11], [34]. These wastewaters typically contain large amounts of insoluble organic compounds [8] and thus are characterized by high organic strengths<sup>12</sup> (1000-85 000 mg COD l<sup>-1</sup>) [34]. For instance the Upward-flow Anaerobic Sludge Blanket Reactor (UASB) was discovered in the 1970s and consists of a sludge bed composed of microorganisms that form granules or pellets of 1-3 mm diameter. These pellets have sedimentation velocities up to 100 m h<sup>-1</sup> and are not washed out, in contrast to flocs. **Table 6** compares the characteristics of the UASB to the CASP. Anaerobic systems tend to achieve an effluent quality that is lower than in CASP due to the slow growth rates of the microorganisms. Anaerobic systems thus are mainly exclusively used for concentrated waste streams, while the CASP is used for more diluted waste streams (e.g., municipal water characterized by an organic strength between 250-800 mg COD l<sup>-1</sup> and suspended solids concentration between 120 and 400 mg l<sup>-1</sup>) [34]. Liao et al. (2006) reported the presence of almost 1600 anaerobic wastewater systems worldwide [34].

### 1.3.3. Membrane bioreactor

The most recent advances in wastewater treatment technology reside in the development of membrane bioreactors (MBRs). The pollutants from the wastewater undergo the same treatment as in the CASP but the sedimentation in the final clarifier is replaced by filtration through a membrane [11], [14]. For several years researchers have taken a closer look at both aerobic and anaerobic MBRs and their implementation in wastewater treatment. Next section gives a description of MBRs and their field of application.

## 2. MEMBRANE BIOREACTOR FUNDAMENTALS

Membrane bioreactor technology is presented starting from a general definition and focus on the main concepts and characteristics of membrane technology as core technology [2], including membrane synthesis, module configuration and operating parameters. Finally current research trends in the field are highlighted.

### 2.1. Definition

A MBR process is defined as the combination of two physical processes that aim at improving wastewater treatment efficiency: a biological treatment by suspended biomass, similar to the CASP, is

---

<sup>12</sup> The volumetric or organic loading rate ( $B_v$ ) (kg COD m<sup>-3</sup> d<sup>-1</sup>) represents the amount of substrate given daily to the microorganisms, expressed per reactor volume [11].

followed by liquid/solid separation by a porous membrane. Hereby the filtration through the membrane replaces the gravity sedimentation to clear the wastewater effluent [2]–[6].

## 2.2. Membrane technology

### 2.2.1. Process classification

A membrane process is a continuous unit operation consisting of a filter (porous or semi-permeable membrane) between two phases, the concentrated retentate, and the purified permeate (Figure 3). The membrane allows selective migration of compounds present in the influent depending on their size, shape and charge [36]. Migration through the membrane is the result of the presence of a driving force, either a temperature, pressure, concentration or electrical potential difference between the retentate and permeate side of the membrane [38]. Here only pressure driven membrane processes between two liquid phases are considered: a suction force is applied at the permeate side as to create a small vacuum, which adds to the static pressure of the water, resulting in migration through the membrane [36].

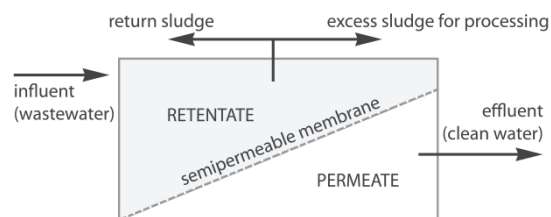


Figure 3 Schematic of a membrane process (adapted from [38]).

Four types of pressure driven membrane processes can be distinguished based on the properties of the membrane (mainly pore size), the size and chemical properties of the particles or molecules retained by the membrane, and the pressure applied [36]. An overview of these four types of processes is given in Table 1.

Microfiltration (MF) and ultrafiltration (UF) membranes are mainly implemented in traditional wastewater treatment plants. In general UF membranes result in better water quality and less obstruction of the pores since they are less accessible for particles [5], [36], [39]. Nanofiltration (NF) and reverse osmosis (RO) membranes have pores that may be hard to detect, called voids or free volume [16]. Migration through RO membranes can result in retention from 80% to 99%, depending on the specific compound [36]. The required effluent quality and the investment, treatment and replacement costs are intimately dependent of the choice of process type [36].



**Table 1** Properties of the four pressure driven membrane processes (adapted from [36]–[38], [40]–[43]).

Property	Membrane process <sup>13</sup>			
	Microfiltration	Ultrafiltration	Nanofiltration	Reverse osmosis
Pore size (nm)	50-10 000	1-100	0.1-5	0.05-1
Applied pressure (bar)	0.2-2	1-10	10-20	20-100
Permeability (l h <sup>-1</sup> m <sup>-2</sup> bar <sup>-1</sup> )	>> 50	10-50	1.5-15	0.05-1.5
Main separation principle	Sieving	Sieving	Sieving, diffusion/size exclusion, charge interactions	Diffusion/size exclusion
Membrane materials most frequently used	<ul style="list-style-type: none"> <li>▪ Polymeric: e.g., PC<sup>14</sup>, PEEK<sup>15</sup>, PA<sup>16</sup>, P(E)I<sup>17</sup>, P(E)S<sup>18</sup>, cellulose esters, PP<sup>19</sup>, PE<sup>20</sup>, PVDF<sup>21</sup>, PTFE<sup>22</sup>,</li> <li>▪ Inorganic: e.g., Al<sub>2</sub>O<sub>3</sub>, ZrO<sub>2</sub>, TiO<sub>2</sub>, SiC, SiO<sub>2</sub>, stainless steel</li> </ul>	<ul style="list-style-type: none"> <li>▪ Polymeric: e.g., PAN<sup>23</sup>, PVDF, PEEK, PA, P(E)I, PES, cellulose esters</li> <li>▪ Inorganic: e.g., Al<sub>2</sub>O<sub>3</sub>, ZrO<sub>2</sub></li> </ul>	Polymeric: e.g., cellulose esters, PES, P(E)I, PA	Polymeric : e.g., cellulose esters, PA
Most important applications	Wastewater treatment, food industry, metallurgy	Wastewater treatment, food industry	Food industry	Drinking water production, water desalination, wastewater treatment
Retained compounds	Suspended particles (fungi, bacteria, colloidal solids, oil emulsions)	Viruses	Macromolecules (proteins, polysaccharides)	Antibiotics, pesticides, small organic monomers (e.g., small sugars, vitamins), inorganic ions (e.g. Na <sup>+</sup> , K <sup>+</sup> , Cl <sup>-</sup> , Ca <sup>2+</sup> , Mg <sup>2+</sup> , SO <sub>4</sub> <sup>2-</sup> )

<sup>13</sup> No sharp boundaries exist between membrane processes, so values for pore size, applied pressure and permeability indicated in **Table 1** are guidelines rather than fixed values.

<sup>14</sup> Polycarbonate, a hydrophilic polymer.

<sup>15</sup> Polyetheretherketon, a hydrophilic polymer.

<sup>16</sup> Polyamide, a hydrophilic polymer

<sup>17</sup> Poly(ether)imide, a hydrophilic polymer.

<sup>18</sup> Poly(ether)sulfone, a hydrophilic polymer.

<sup>19</sup> Polypropylene, a hydrophobic polymer.

<sup>20</sup> Polyethylene, a hydrophobic polymer.

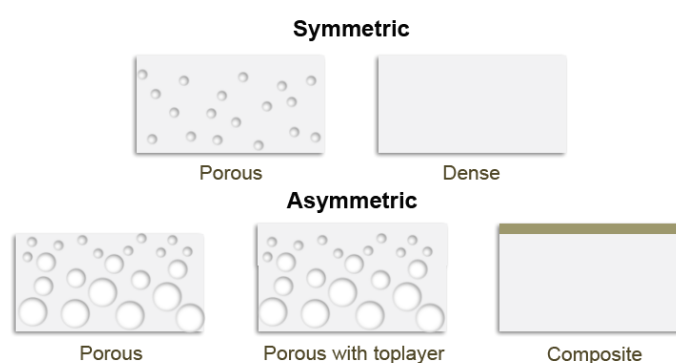
<sup>21</sup> Poly(vinylidene fluoride), a hydrophobic polymer.

<sup>22</sup> Polytetrafluoroethylene, a hydrophobic polymer.

<sup>23</sup> Polyacrylonitrile, a hydrophilic polymer.

### 2.2.2. Membrane morphology and membrane materials

Membranes are classified according to their morphology: symmetric membranes are distinguished from asymmetric membranes (Figure 4). Both are either porous or dense, but while the former exhibits the same structure along its cross-section, the latter does not and may even consist of several layers which can be optimized independently. These are so-called composite membranes. Symmetric membranes are self-supporting and have a working thickness of 10-200  $\mu\text{m}$ . In asymmetric membranes, it is the 0.1-0.5  $\mu\text{m}$  selective active skin layer that determines the flux, resistance and rejection characteristics. This skin layer is physically supported by a 50-150  $\mu\text{m}$  porous substructure [37], [38], [44].



**Figure 4** Classification of membranes based on their morphology (adapted from [38]).

While membrane morphology determines the efficiency of the membrane, membrane material determines the structural (thermal, chemical and mechanical) properties of the membrane [38]. In general membranes must exhibit a high permeability and selectivity, combined with sufficient chemical, thermal and mechanical stability [36].

Organic membranes are distinguished from inorganic membranes (Table 1). In pressure driven processes on aqueous systems, most membranes are constructed from organic or polymeric materials [45]. On the contrary, inorganic membranes may be applied for the purification of strongly alkaline or acid mixtures as well as in high temperature wastewaters. Some authors mention ceramic or metallic materials (e.g., [46], [47]). Inorganic membranes are generally hydraulically, thermally and chemically more stable than polymeric membranes, have a longer lifetime, are more fouling-resistant and their pore size can be better controlled to maintain high fluxes. However, their use is limited in large-scale applications since they are expensive and difficult to prepare [4], [36]–[38], [48]. Research is being performed in order to develop new membrane materials which are cost-attractive and highly efficient [48].

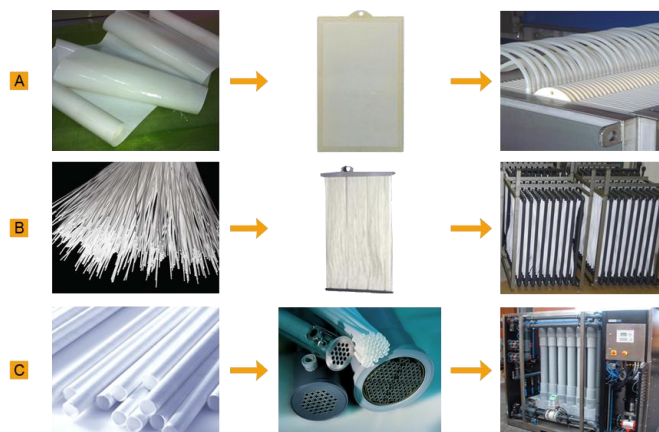
### 2.2.3. Membrane synthesis

As seen above, a lot of different membrane structures and materials exist, thus resulting in a large number of membrane synthesis methods. The majority of the commercially available membranes are polymeric and 90% of these are synthesized by the phase inversion process [38].

Phase inversion is a rapid process where a thermodynamically stable solution of a polymer and a solvent ('casting solution') is transformed from a liquid to a solid asymmetric membrane by controlled demixing by immersion in a coagulation bath containing a non-solvent. On the one hand, a continuous polymer-rich phase is formed that will become the membrane matrix of the solid porous membrane. On the other hand the open pore structure is obtained via the discrete polymer-lean phase [38].

### 2.2.4. Membrane modules

Membranes are generally mounted in separation units called modules, which are joined to form one large filtration unit, called a process train (Figure 5) [49].



**Figure 5** MBR membrane configurations: membrane, module and process train. (A) flat sheet, (B) hollow fibre, (C) multi-tubes (adapted from [4], [49]).

Depending on the type of separation to achieve, the maintenance requirements, the scale of the system and the costs, different module designs are on the market with their own application area (Table 2) [36], [38]. Based on geometry, modules made from flat-sheet membranes are distinguished from modules made from a large number of tube-like membranes (tubular, capillary or hollow fibre modules). Flat sheets are stacked either in vertically plate-and-frame modules or in spiral-wound modules. Both consist of two membrane sheets separated by an internal spacer, but in the latter configuration the system is wrapped around a central collection pipe and placed in a pressure tube. The spacer layer is a turbulence promoter aiming at reducing the risk of fouling [36], [38]. For a discussion on the appropriateness of flat sheet membranes versus tube-like membranes, please refer to Gunder et al. (1998) and Judd (2002) [50], [51].

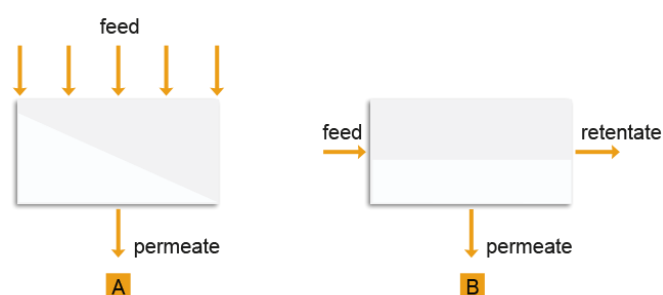


**Table 2** Comparison of the modules design and their characteristics (adapted from [5], [36], [38]).

Characteristic	Module design				
	Tubular ( $\phi > 10$ mm)	Plate and frame	Spiral wound	Capillary ( $0.5 < \phi < 10$ mm)	Hollow fibre ( $0.5$ mm $> \phi$ )
Packing density	Low (150-300 $\text{m}^2 \text{m}^{-3}$ )		→		High (200-500 $\text{m}^2$ $\text{m}^{-3}$ )
Investment	high		→		low
Fouling tendency	Low		→		Very high
Cleaning efficiency	Good		→		Poor
Membrane replacement	Yes/no	Yes	No	No	No
Application	MF, UF In-to-out filtration	MF, UF	MF, UF, (NF, RO)	MF, UF In-to-out filtration	NF, RO, (MF, UF) Out-to-in filtration

### 2.2.5. System design

In pressure driven membrane processes, the separation can be obtained in two ways: either by dead-end filtration, or by cross-flow filtration (Figure 6) [36]–[38]. During dead-end filtration the feed solution is applied perpendicular to the membrane surface. During cross-flow filtration the feed and permeate solution flow along the membrane, parallel with the surface in co-current or counter-current directions. Although dead-end filtration is energetically advantageous since it requires less pumping energy for filtration thanks to the hydraulic pressure built-up, the majority of the industrial applications is based on cross-flow filtration mode [36]. The main reason is the occurrence of fouling, whereby regularly cleaning of the membrane becomes necessary.



**Figure 6** Dead-end filtration (A) versus cross-flow filtration (B) (adapted from [37]).

### 2.2.6. Operating parameters

#### Volumetric flux and transmembrane pressure

According to Wang et al. (2009) the simplest model to describe ideal transport of liquids through a porous membrane is by considering a membrane as a number of uniformly distributed and evenly sized parallel cylindrical pores which cover the full membrane cross-section [45]. The volume flux may be described by the Hagen-Poiseuille equation:

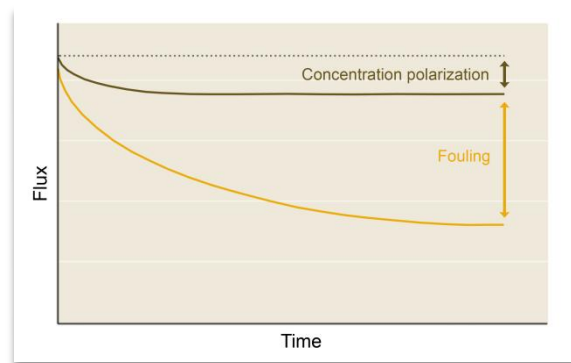
$$J = \frac{\varepsilon * r^2}{8 * \eta * \tau} * \frac{\Delta P}{\Delta x}$$
**Equation 1**

Where J (LMH, l m<sup>-2</sup> h<sup>-1</sup>) is the liquid flux through the membrane,  $\varepsilon$  (-) the surface porosity of the membrane (i.e., the volume fraction of pores),  $r$  (m) the average pore radius,  $\frac{\Delta P}{\Delta x}$  (bar m<sup>-1</sup>) the pressure gradient over the membrane cross-section,  $\eta$  (bar h) the apparent dynamic viscosity of the liquid permeating the membrane and  $\tau$  the pore tortuosity (-) ( $0 \leq \tau \leq 1$ ).

The flux (also called flow or permeation rate) describes how fast the membrane works and gives the volumetric flow rate per unit of membrane area. Working at higher fluxes allows in using smaller membrane surfaces thus decreasing investment costs. However higher fluxes have the tendency to increase the membrane fouling rate, thus makes it necessary to increase the shear stress along the membrane by increasing the operational costs related to aeration. Optimization of the system thus involves “making a choice between mutually counteractive variables”, as mentioned by Judd (2008) [4]. The surface porosity of the membrane is defined as:

$$\varepsilon (\%) = \frac{n * \pi * r^2}{A} * 100$$
**Equation 2**

Where  $n$  is the number of pores,  $\pi * r^2$  (m<sup>2</sup>) the average area of the pores and  $A$  (m<sup>2</sup>) the total area of the membrane. Surface porosity varies according to the membrane structure. MF membranes have a surface porosity between 5% and 70%, while the surface porosity of UF membranes generally only reaches 0.1% to 5% [38].



**Figure 7** Flux decline over time caused by concentration polarization and membrane fouling (adapted from [37]).

In pressure-driven membrane processes the pressure gradient over the membrane ( $\frac{\Delta P}{\Delta x}$ ) is the driving force of the filtration process. Theoretically, if this driving force is kept constant over time, a steady-state situation will establish with a constant flow over the membrane. Unfortunately this theory is only valid in ideal situations. In reality permeate flux will decline over time due to concentration

polarization<sup>24</sup> or fouling (Figure 7) [38], a phenomenon that will be explained in next section. The pressure difference over both permeate ( $P_{\text{permeate}}$ ) and retentate side ( $P_{\text{retentate}}$ ) of the membrane,  $\Delta P$ , is called the transmembrane pressure (TMP) [40], [52]:

$$\Delta P = P_{\text{retentate}} - P_{\text{permeate}} \quad \text{Equation 3}$$

Both the flux and TMP define the operating range of the MBR process [40].

### Permeability coefficient

Apart from the flux-concept described above, the efficiency of a membrane process can be expressed by several other parameters. One of these parameters is the permeability coefficient ( $\text{l m}^{-1} \text{h}^{-1} \text{bar}^{-1}$ ),  $P'$ , which is an intrinsic property of the membrane material and mainly affected by the operating temperature and the particle size distribution of the mixed liquor [40], [53]. It is defined as the permeance ( $\text{LMH bar}^{-1}$ ),  $K$ , multiplied by the membrane thickness,  $\Delta x$ , or also as the flux per unit TMP multiplied by the membrane thickness [4], [38]:

$$P' = K * \Delta x = \frac{\Delta V}{A * \Delta P * \Delta t} * \Delta x \quad \text{Equation 4}$$

#### 2.2.7. Critical flux concept

As already mentioned above, one of the major problems in pressure-driven membrane processes is the gradual reduction of the permeate flux below the theoretical capacity of the membrane during the filtration process, due to fouling. Field et al. (1995) introduced the concept of critical flux ( $J_c$ ) as quantitative parameter for the assessment of cross-flow MF membrane performance, which may enable identification of the appropriate operating conditions and optimization of the filtration process [54], [55].

A filtration process can be conducted in two ways, either constant-flux or constant-pressure filtration. The former involves the gradual increase in TMP in order to overcome the flux decline due to fouling phenomena [56]. The latter involves the gradual decrease in flux while keeping the TMP constant. Field et al. (1995) developed the hypothesis that on start-up of the filtration process, there exists a flux below which a decline of permeate flux with time does (almost) not occur, while above that flux fouling cannot be neglected and regularly cleaning becomes necessary [54]. This critical flux concept involves that it may be possible to operate a constant-flux filtration during up to one month [56]

---

<sup>24</sup> Concentration polarization is an increase of the concentration of retained substances near the membrane surface (from where water is selectively removed). It is inherent of membrane filtration but may induce membrane fouling. It can be decreased for instance by increasing turbulence in the mixed liquor [38].



without the obligation to gradually increase the TMP (i.e., operating at a sub-critical flux is theoretically characterized by a membrane fouling rate  $d\Delta P/dt = 0$  or a ratio  $dJ/d\Delta P = 0$ ). However this is almost never achieved. Even at low flux, marginal fouling does occur – mainly due to adsorption phenomena [57], [58] – and TMP values must be slightly increased in order to maintain a constant flux [56], [59]. When filtration progresses in long-term operations, more severe fouling becomes unavoidable leading to a roughly exponential TMP increase above the critical TMP value and flux decline [54], [59]. However van der Marel et al. (2009) reported that it is possible to operate at a flux higher than the critical flux, as long as no significant irreversible fouling occurs, i.e., at a flux between the critical flux and a flux of  $100 \text{ l m}^{-2} \text{ h}^{-1}$  [60].

The estimated critical flux value and fouling rate on the short-term also depends on the methodology used to assess it. The most widely used methodology is the TMP measurement in flux-stepping experiments during constant-flux filtration. However the short-term flux-stepping methodology used in laboratory- or pilot scale systems cannot be used to assess the long term fouling behaviour, nor in laboratory- or pilot scale systems, nor in full-scale systems [48], [61].

## 2.3. Membrane bioreactor technology

### 2.3.1. Historical market development

Yang et al. (2006) performed an extended study around the evolution and implementation of MBR technology in North-America [62], while Lesjean et al. (2008) surveyed the European MBR market [63]. Research on membrane bioreactors (MBRs) started in the 1960s. MBR technology is now implemented as 'Best Available Technology' for the treatment of industrial wastewaters from e.g., the food, pharmaceutical, textile or meat industry, which produce wastewaters with much more varying composition and organic loading than municipal wastewater. GE-Zenon Environmental Inc. (Canada), USFilter (USA), Kubota (Japan) and Mitsubishi-Rayon (Japan) are some of the largest European membrane suppliers, but are gradually expanding towards emerging economies such as Brazil or China [5]. It is expected that the technology will further develop as to respond to national and international environmental, economic and political expectations [3], [64]. Frost & Sullivan (2013), as cited by Royan (2014), estimated the global MBR market volume to be \$ 838.2 million in 2011 (i.e., € 716.2 million based on the actual conversion ratios) and is expected to increase up to \$ 3.44 billion by 2018 (i.e., € 2.63 billion) [65], [66].

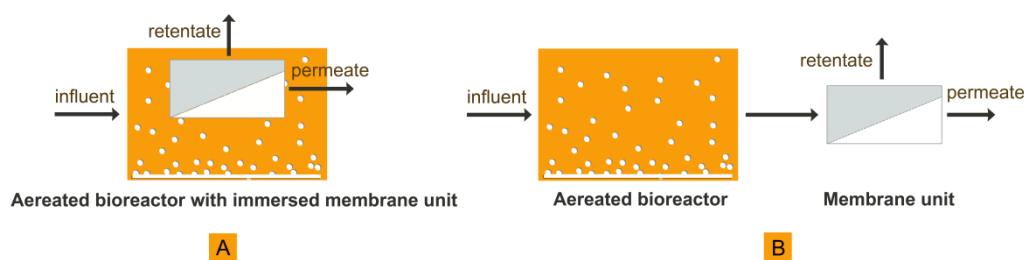
### 2.3.2. Prospects and constraints of the MBR technology

Several characteristics of MBRs make them advantageous compared to the CASP. However, many barriers still limit the faster and larger development of this technology, as depicted in **Table 3** and **Table 4** [5].

The most cited limitation of membrane filtration is membrane fouling. This phenomenon is related to interactions between the membrane surface and the soluble and particulate matter present in the activated sludge mixed liquor [16]. It mainly occurs in MF and UF filtration processes and is partly responsible for the retardation of faster commercialization of MBR technology since it has a large negative influence on the economics [38], [62], [67]. Membrane fouling is extensively discussed further in this chapter, **Section 3**.

### 2.3.3. Process configurations

At the beginning of MBR technology development, the majority of MBRs were based on a side-stream or external configuration (eMBR), where the membrane modules are located outside the reactor (**Figure 8**) [40]. In 1989 an internal or immersed MBR (iMBR) was used for the first time for the investigation of stable flux conditions and nutrient removal through hollow fibre membranes [68]. In this configuration the membrane module is immersed in the basin containing the active sludge. iMBRs now dominate the market [42]. **Table 5** compares iMBRs and eMBRs.



**Figure 8** Internal or immersed MBR (A) versus side stream or external configuration (B) (adapted from [4], [16], [40], [69]).

## 2.4. Current research trends

### 2.4.1. Anaerobic membrane bioreactors

One of the most widely explored trends in the last 10 years involves the development of immersed and external anaerobic membrane bioreactors (AnMBRs). This technology combines the membrane technology with anaerobic biological treatment (**Figure 9**) [4]. Actually, research around AnMBRs started in the late 1970s but the technology could only be successfully implemented at large scale in the 1990s [33], [34]. Nevertheless the process design still needs to be optimized further technically and economically in order to ensure greater large scale utilization of AnMBRs. Lin et al. (2013), Liao et al. (2006) and Stuckey (2012) reviewed extensively recent literature about AnMBRs [33], [34], [42]. For instance they reviewed the application of AnMBRs with different kinds of wastewater (synthetic, industrial, food processing, municipal) and at different scales (laboratory, pilot, full scale). They concluded that the AnMBR technology is mainly applicable to highly concentrated/high strength and particulate/high solids wastewater, such as sludge and wastewater from slaughterhouses.



**Table 3** Advantages of the MBR technology compared to the CASP.

Advantage compared to CASP	Additional notes	References
Space requirement and environmental footprint	Compact because of the absence of settling requirements which limits the sludge concentration to $5 \text{ g l}^{-1}$ and imposes large basins, thus applicable in space-limited locations. For instance, compare an average surface of $4452 \text{ m}^2$ (CASP) to $190 \text{ m}^2$ (MBR) for the treatment of $100\,000 \text{ kg COD day}^{-1}$ .	[4]–[6], [11], [16], [24], [25], [35], [36], [40], [56], [67], [69]–[74]
Easy up-scaling	Modular and compact design. Possible to assess technical and economical feasibility on a small-scale. Moreover possible to integrate in existing CASP.	[36]–[38], [48], [69]
Higher and constant effluent quality	The filtered effluent is nearly free of particles, bacteria and soluble organic substances, while in theory an infinite settling time is necessary in the CASP to obtain the same result. For instance, the presence of coliform bacteria <sup>25</sup> may be reduced to a factor $\log 7$ in the effluent compared to the original wastewater. Moreover e.g., bulking sludge or foaming phenomena ( <b>Section 1.2.2</b> ) do not affect the liquid-solid separation.	[3]–[6], [11], [16], [24], [25], [36], [40], [64], [67], [69]–[73], [75], [76]
Adjustable membrane properties	Membranes can be optimized independently from each other and from the reactor process, for instance in order to be compatible with the type of wastewater.	[6], [36]–[38]
Decoupling of hydraulic (HRT <sup>26</sup> ) and sludge retention time (SRT <sup>27</sup> )	HRT can be reduced to a minimum (4–6 h) independent of SRT, which can be increased (up to 30 days), thus offering great process control and increasing biomass concentration in the reactor.	[4]–[6], [25], [40], [71], [73]
Less excess sludge	Excess sludge, which needs to be processed (drying, handling, incineration), is minimized thus reducing overall costs. Moreover the produced excess sludge is more concentrated, thus making faster conversion of biodegradable material possible and easier post-treatment.	[4]–[6], [9], [11], [16], [24], [25], [35], [36], [56], [64], [67], [70]–[74], [76]

<sup>25</sup> Coliform bacteria are widely used as indicators for microbial water contamination [8]

<sup>26</sup> The hydraulic retention time (HRT) (h) represents the average time the microorganisms have been in contact with the biodegradable compounds in the wastewater [11].

<sup>27</sup> The sludge residence time (SRT) (d) represents the average time the microorganisms reside in the reactor. The more often sludge is removed from the reactor, the smaller the SRT [11].

**Table 4** Disadvantages of the MBR technology.

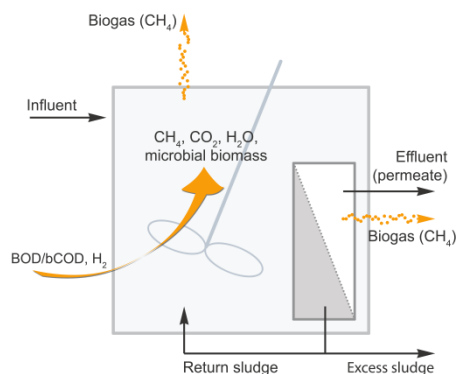
Disadvantages of the MBR	Additional notes	References
Flux decline (during constant-pressure filtration) or increase in TMP over time (during constant-flux filtration)	May be attributed to concentration polarization or fouling phenomena.	[5], [11], [16], [25], [36], [67], [69], [70], [76], [77]
High operational and maintenance costs	Costs related to wastewater pretreatment, membrane cleaning, membrane/module replacement and energy consumption (aeration, pumping). The latter reaches 0.2-1.5 kWh m <sup>-3</sup> produced water with a feed of 1 g COD l <sup>-1</sup> ). Membranes generally have a lifetime ranging from 3 to 8 years, depending on the membrane type, the operating conditions, the cleaning frequency and the characteristics of the influent.	[4], [5], [24], [36]–[38], [42], [69], [71], [75]
Complex design and operation	Operational protocols need to be executed well in order to assure a long lifetime of the system. Moreover MBR suppliers and users often lack knowledge about sludge properties and long-term performances of the system since it is a relatively new technology.	[4], [5], [70]
Aeration and oxygen transfer	Lower oxygen transfer due to i.a., higher biomass concentration. Thus a more intensive aeration is necessary in order to maintain a fast conversion of biodegradable material. On the other hand also floc size does influence oxygen transfer. Flocs in MBRs experience shear rates and on average tend to be 10 times smaller than flocs in CASP, resulting in higher oxygen transfer rates and removal rates.	[4], [5], [16], [24], [36], [69]
Variable investment costs	10-20% higher investment costs: large membrane surface area needed to maintain acceptable overall flux. Lower investment costs: no clarifier needed and compact installation. Moreover the cost of membrane modules decreases with the years.	[4], [5], [36], [71]



**Table 5** Comparison of the characteristics of iMBRs and eMBRs.

Characteristics	Immersed MBR system (iMBR)	Side-stream MBR system (eMBR)	References
Volumetric flux (LMH)	10-40	30-100	[49], [69]
Cross flow velocity ( $\text{m s}^{-1}$ )	0.5	1-6 Biomass subjected to high shear stress, resulting in small floc sizes (but without apparent impact on nutrient removals).	[42], [49]
TMP (bar)	0.2-0.5	2-6	[49]
Membrane type	Flat sheet, hollow fibre	Tubular	[49]
Space requirement	Small	High	[36]
Fouling tendency	Higher due to lower shear rates, thus need for larger membrane areas to maintain high fluxes. Cleaning by taking modules manually out of the reactor periodically.	Lower because of better controlled hydrodynamics. Modules are relatively easy to access and to disassemble for cleaning.	[36], [38], [42]
Peak flows	Additional modules which foul when not in use during normal flows.	Additional modules simple to disconnect when the flow is low.	[36]
Energy requirements	Compressor energy necessary for aeration (cleaning). This constitutes 30-50% of the total energy demand.	Recirculation pumps as well as compressor energy necessary for aeration (cleaning), thus higher energy costs than in iMBRs.	[4], [36], [42], [71]
Investment and operational costs	Variable capital costs (no external modules and pumps required but larger membrane areas necessary).	Higher investments and operational costs.	[38], [42]





**Figure 9** Anaerobic membrane bioreactor in immersed configuration (based on [11]).

**Table 6** compares aerobic and anaerobic conventional and membrane systems. The effect of lots of parameters on AnMBRs has been assessed recently but by using aerobic MBRs instead of AnMBRs and simply assuming to be similar thus extrapolated to AnMBRs [4], [42]. For instance, a large amount of work has been done concerning fouling in aerobic MBRs, as will be discussed later, but rather few information is available about anaerobic fouling and the best ways to control it [5]. However it is estimated that fouling control strategies in AnMBR are cheaper than in aerobic MBRs ( $0.80 \text{ kWh m}^{-3}$  treated water with a feed of  $1 \text{ g COD l}^{-1}$  compared to around  $2 \text{ kWh m}^{-3}$  treated water for the same feed) [42].

**Table 6** Comparison of aerobic and anaerobic conventional and membrane systems for the treatment of municipal wastewater (table based on [33] but extended with data from [4], [5], [34]–[36], [42], [43], [52], [56], [69]).

Parameter	CASP	UASB	Aerobic MBR	Anaerobic MBR
Start-up time	2-4 weeks	2-4 months	<1 week	<2 weeks
HRT (hour)	4-8	6-14	4-9	3-17
SRT (day)	3-15	30-100	5-20	>100
MLSS in bioreactor ( $\text{g l}^{-1}$ )	1-5	15-30	5-20	10-40
COD removal (%)	<95		95-99	94-98
Effluent COD ( $\text{mg l}^{-1}$ )	30-70	100-220	10-30	<100
Effluent TSS ( $\text{mg l}^{-1}$ )	<30 (5-8)	30-70	<1	<1
Effluent TN ( $\text{mg l}^{-1}$ )	8		5	
Effluent $\text{PO}_4^{3-} \text{-P}$ ( $\text{mg l}^{-1}$ )	1-3		0.3-3	
Organic loading rate ( $\text{kg COD m}^{-3} \text{ day}^{-1}$ )	<2	<30	<10	10-25

Anaerobic systems must be operated at higher temperatures than aerobic systems, thus consuming more electricity (compare on average  $0.45 \text{ kWh m}^{-3}$  for an aerobic MBR versus  $0.60 \text{ kWh m}^{-3}$  for an anaerobic MBR) [34]. This disadvantage could be balanced completely by recovery of the methane gas as explained previously in this chapter (**Section 1.3.1**) [33]. Moreover Stuckey (2012) reviewed recent literature demonstrating that anaerobic bioreactors could be operated stably at temperatures down



to 13°C [42]. However methane yield is strongly dependent on temperature, since methane is approximately 1.5 times more soluble at 15°C compared to 35°C, thus rendering methane recovery more difficult for lower temperature effluents [33]. Finally, although nutrient (N, P) removal in AnMBRs is limited compared to aerobic systems, this can be seen as an opportunity to recover and recycle these nutrients from the effluent of an AnMBR in view of reuse in agriculture [42].

#### 2.4.2. Alternative membranes

Another current research topic involves the development of alternative membranes including low-cost filters, dynamic membranes and membrane modifications [78], mainly in order to decrease the investment and operational costs of MBRs. Low-cost filters encompass non-wovens, meshes and filter cloths and may be used in applications that do not require high end-product quality [48]. Precoated or self-forming dynamic membranes are synthesized by filtering a solution of one or more membrane-forming materials such as hydrated oxides, polymers or colloidal materials through a porous support. This dynamic forming method is mainly used for the synthesis of NF and RO membranes [79]. Finally membrane surface modifications are mainly applied in order to increase the hydrophilic character of a hydrophobic membrane in order to limit its fouling tendency [78]. For an extensive review of these topics, please refer to Meng et al. (2009) [48].

#### 2.4.3. Alternative configurations

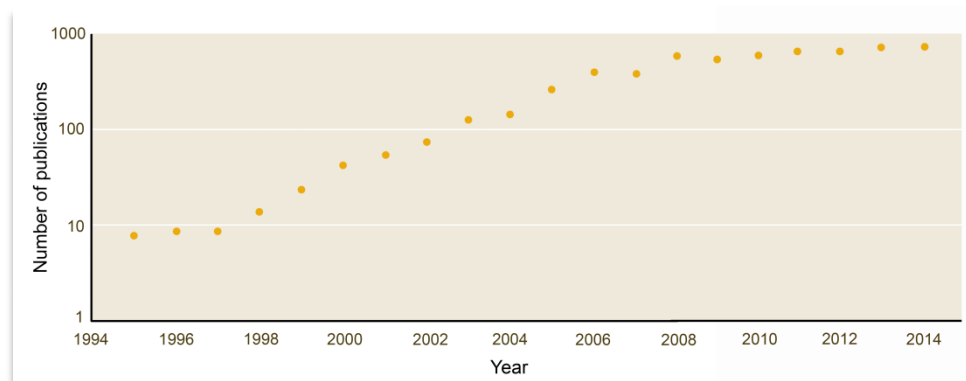
Li et al. (2005) studied the development of Aerobic Granular-Sludge Membrane Bioreactors which would be more effective for fouling control than normal aerobic MBRs [80]. These reactors contain large sized, dense, granular sludge as substitute for sludge flocs.

Finally research is being performed around extractive and diffusive MBRs in view of future commercialization [4], [52]. In 'normal' MBRs, the biomass is retained by the membrane while the permeate goes through it. In contrast, in diffusive MBRs the membrane is used to introduce a gas in its molecular form directly into the biofilm on the membrane surface in the bioreactor. This gas is then used for biotreatment. In extractive MBRs the membrane is used to extract specific (toxic) compounds from the reactor across the membrane in order to treat them biologically.

### 3. FUNDAMENTALS OF MEMBRANE FOULING

**Figure 10** emphasizes the growing importance of fouling in MBR filtration processes. Membrane fouling is one of the major problems concerning membrane filtration processes to be resolved, but because of the complexity of the fouling mechanisms and the variety of parameters influencing it, it is still unclear how to respond efficiently to that problem [16]. Moreover different researchers all

implement different operating conditions and module configurations during their investigations, thus making it difficult to draw uniform conclusions. For an intensive review on membrane fouling and fouling control actions, please refer to Wang et al. (2014) [81].



**Figure 10** Evolution of the annual publications on MBR fouling, searched via Google Scholar until 2008 and via PubMed from 2009 to 2014 (adapted from [48]).

### 3.1. Definition

Judd (2008) defined fouling as “the restriction, occlusion or blocking of membrane pores at the surface of the membrane, reducing the flow of permeate water through the membrane material” [4]. Membrane fouling is provoked by undesirable deposition and accumulation of salts, macromolecules, microorganisms, colloids, solutes and cell debris onto or within the membranes [75].

### 3.2. Classification of membrane fouling

Membrane fouling can be classified in three ways:

- based on the mechanism;
- based on the permeability recovery;
- based on the nature of the foulants.

#### 3.2.1. Classification based on the mechanism

Grelier et al. (2006) defined the fouling rate  $d\Delta P/dt$  as “the gradient of membrane resistance over time” [2] which can be written as [38], [52]:

$$R_t = R_m + R_f \quad \text{Equation 5}$$

Where  $R_t$  ( $m^{-1}$ ) is the total membrane resistance,  $R_m$  ( $m^{-1}$ ) is the intrinsic clean or hydraulic resistance of the membrane and  $R_f$  ( $m^{-1}$ ) is the time-dependent resistance due to fouling and concentration polarization ( $R_{cp}$ ).  $R_m$  is independent of mixed liquor characteristics or applied pressure and indicates the tolerance of the membrane against hydraulic pressure [78].

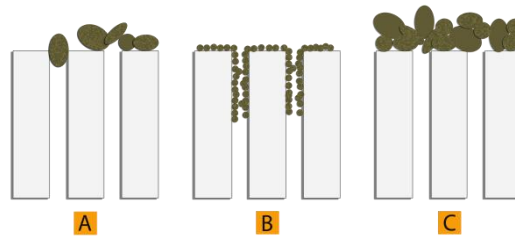
Ye et al. (2005) and Liang et al. (2005) defined the flux using the TMP and the concept of resistance ('Resistance-in-series model') [55], [71]:

$$J = \frac{\Delta P}{\eta * R_t} = \frac{\Delta P}{\eta * (R_m + R_f)} \quad \text{Equation 6}$$

With  $\eta$  (Pa h) the viscosity of the feed solution.  $R_f$  can be further divided into resistance due to surface, external or macro-fouling and resistance due to pore, internal or micro-fouling (Figure 11) [24], [40].

$$R_f = R_g + R_p + R_a + R_{cp} \quad \text{Equation 7}$$

The former includes resistance due to deposition and accumulation of particles on the membrane surface, eventually leading to a gel or cake layer ( $R_g$ ) (Figure 11). Cake layer formation is caused by particles with a size larger than the membrane pore size [49]. The cake layer is a porous structure on top of the membrane [48] that resembles the composition of the biomass flocs [82]. Lee et al. (2001) assumed the cake layer to contribute up to 80% to total membrane resistance [83].



**Figure 11** Membrane fouling mechanisms. (A) surface fouling, (B) pore fouling, (C) cake layer formation (adapted from [38]).

Pore or micro-fouling includes resistance due to pore blocking via soluble organic or microbiological material ( $R_p$ ) or resistance due to partial pore closure by adsorption of solutes or colloids on the walls on the pore channels ( $R_a$ ). Pore blocking is caused mainly by particles with a size comparable to the membrane pore size, while pore closure is caused by particles that are smaller than the pores [49].

### 3.2.2. Classification based on the permeability recovery

Ye et al. (2005) and Liang et al. (2005) wrote  $R_f$  in terms of the degree of fouling removability [55], [71]:

$$R_f = R_{irrev} + R_r + R_{irrec} \quad \text{Equation 8}$$

$R_{irrev}$  ( $m^{-1}$ ) is the irreversible or permanent fouling mainly caused by pore blocking by dissolved organic substances [71], [84] and is believed to be independent of filtration time [58]. Irreversible fouling is often insignificant compared to  $R_t$  or  $R_f$  [58] and can only be reduced to zero by using chemical cleaning methods [71].

$R_r$  ( $m^{-1}$ ) is the removable, reversible or temporary fouling and also includes the concentration polarization.  $R_r$  is mainly attributed to cake layer formation by mixed liquor suspended solids (MLSS) [48], [71] and can be removed by hydraulic cleaning methods [4], [71], [84].

Finally Judd (2008) also defined long-term irrecoverable, irremovable or absolute fouling,  $R_{irrec}$  ( $m^{-1}$ ) [4], which cannot be removed by any cleaning method and which defines membrane lifetime [48]. However, these three types of fouling are often defined differently in literature, often due to differences in measurement protocols, resulting in confusing situations where the meaning of the terms irreversible and irremovable fouling is interchanged [16], [48].

### 3.2.3. Classification based on the nature of the foulants

Recent reports [6], [16], [38], [48], [85] distinguished three types of foulants occurring simultaneously, based on their physical and chemical characteristics: organic precipitates, inorganic precipitates and biofouling.

#### Organic and inorganic precipitates

Organic precipitates are deposited biopolymers (proteins and carbohydrates) or humic substances (dissolved organic matter) resulting from non-covalent interactions between macromolecules or complexation reactions involving metal ions (e.g.,  $Ca^{2+}$ ,  $Mg^{2+}$ ) present in the feed solution and the mixed liquor [25], [76], [86].

Inorganic precipitates are inorganic salts (e.g.,  $CaSO_4$ ,  $CaCO_3$ ,  $SiO_2$ ,  $Fe(OH)_3$ ) present in the feed solution and the mixed liquor that precipitate ('scaling') onto the membrane surface due to concentration polarization or  $pH$  and temperature variations [85], [87].

#### Biofouling and biofilm formation

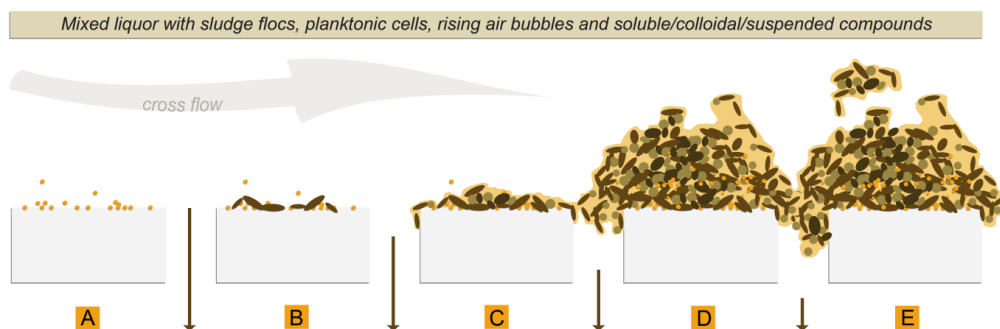
Biofouling refers to the undesirable gradual attachment on the wet membrane surface of individual cells, cell clusters or materials of biological origin present in the mixed liquor [88]. The bacteria present in the biofilm are believed to depend on the composition of the bulk solution, although it has been proven that biofilm composition differs largely from bulk composition, indicating the existence of specific biofilm-developing bacteria [3], [89]–[91]. **Table 7** gives some example studies that investigated the pioneer microbial composition of the membrane biofouling layer. The phylum of the *Proteobacteria*, which is characterized by the largest metabolic diversity among phyla [8], was reported to house the predominant pioneering bacteria. These pioneering bacteria attach to the membrane surface and influence the further attachment of other bacterial species during biofilm maturation [89]. All research groups use different operating conditions thus making generalizations very difficult.

**Table 7** Example studies on the pioneer microbial community composition of the biofouling layer.

Influent type	Membrane type	Dominant phylogenetic group	Reference
e.g., brackish water	RO for drinking water treatment	<i>Actinobacteria</i> , $\gamma$ - <i>Proteobacteria</i> , <i>Firmicutes</i> , <i>Flavobacteria</i>	[92]
Aerobic MBR fed with domestic wastewater	PE hollow fibre MF membrane	$\alpha$ - <i>Proteobacteria</i> , $\beta$ - <i>Proteobacteria</i> , $\gamma$ - <i>Proteobacteria</i> , $\delta$ - <i>Proteobacteria</i>	[90]
Aerobic MBR fed with domestic wastewater; potable water	MF membrane; spiral-wound RO membrane	$\alpha$ - <i>Proteobacteria</i> , $\gamma$ - <i>Proteobacteria</i>	[93]
Aerobic MBR fed with oligotrophic raw water	Polypiperazine flat sheet NF membrane and PES flat sheet UF membrane	$\gamma$ - <i>Proteobacteria</i>	[94]
Aerobic MBR fed with domestic wastewater	Flat sheet MF membranes	$\alpha$ - <i>Proteobacteria</i> , $\beta$ - <i>Proteobacteria</i> , <i>Bacteroidetes</i>	[3]
Aerobic MBR fed with domestic wastewater	PE hollow fibre MF membrane	$\gamma$ - <i>Proteobacteria</i>	[91]
Aerobic MBR fed with synthetic paper mill wastewater	PVDF flat sheet MF membrane	$\alpha$ - <i>Proteobacteria</i> , $\gamma$ - <i>Proteobacteria</i> , <i>Firmicutes</i>	[89]

Stoodley et al. (2002) and Vanysacker et al. (2014) discussed extensively five either sequential or simultaneous steps in the formation of a three-dimensional biofilm (**Figure 12**) [16], [95]:

- formation of a conditioning film;
- reversible and irreversible bacterial attachment;
- production of EPS;
- microcolony formation and biofilm maturation;
- bacterial detachment.



**Figure 12** Schematic of a biofilm formation process in an aerobic MBR system in cross-flow filtration mode on a porous membrane. (A) formation of a conditioning film, (B) initial bacterial attachment, (C) EPS production, (D) biofilm maturation, (E) bacterial detachment. Brown arrows represent decreasing permeability (adapted from [16]).

The first step in biofilm formation involves a physico-chemical change of the surface under consideration (e.g., change in roughness or degree of hydrophilicity) [96] due to adsorption/precipitation of particulate compounds or adhesion of dissolved substances onto the surface, such as humic acids, proteins and carbohydrates present in the mixed liquor [6], [16].

The second step in biofilm formation, the initial bacterial attachment, is provoked by random collisions of planktonic cells with the membrane surface [16] and an interplay between attractive van der Waals and hydrophobic forces and mostly repulsive electrostatic interactions between the membrane surface and the bacterial cell [97]. The bacterial attachment is then further promoted by interactions between bacterial cells and between the bacterial cell and the membrane (e.g., via cellular surface structures) [8].

The third step in biofilm formation is the production of extracellular polymeric substances (EPSs), triggered by intra- and intercellular communication [8] EPSs are composed of various macromolecular polyelectrolytes secreted by bacteria at or outside the cell surface. These biopolymers are mainly carbohydrates and proteins of various molecular weights (typically from a few thousand to several hundred thousand Daltons [98]) and at various ratios, but also lipids and nucleic acids are part of EPSs [4], [6], [36], [53], [55], [58]. The exact composition is yet not known [67], but Xuang et al. (2000) and Pollice et al. (2005) assumed it to be independent of the type of wastewater [61], [73]. These matrices thus provides mechanic strength and protection against environmental stress factors (e.g., antibiotics, *pH* changes) [16].

Vanysacker et al. (2014) reported that 400 articles were published between 1950 and 2014 on the role of EPSs in membrane fouling [16]. However there exists a lot of discussion around the question whether or not EPS have an influence on membrane fouling and at which extent [2], [25], [36], [48]. For instance Cho et al. (2002) stated that EPSs are important foulants [99] and Zhang et al. (2008) attributed irreversible fouling to EPS adsorption [100], but there is uncertainty whether the polysaccharides [7], [67] or the more hydrophobic proteins [27], [53] are the major contributors to fouling. Two example studies illustrate this disagreement: Metzger et al. (2007) and Chen et al. (2006) [82], [101].

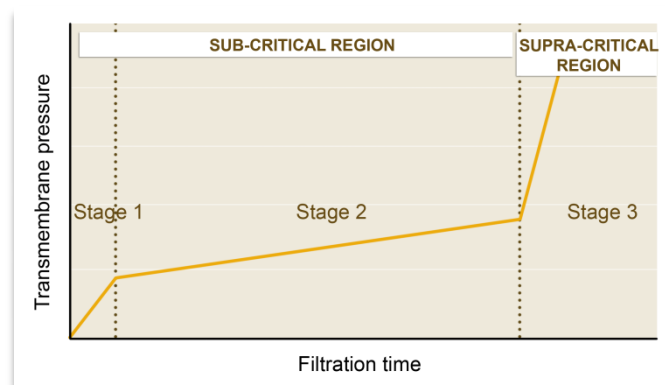
The fourth step in biofilm formation involves microcolony development, thus reducing the overall flux. A microcolony is defined as a cluster of cells on a surface, embedded in EPS, that has developed from a single colonizing bacterial cell [8]. As the biofilm continues to grow, anoxic or anaerobic conditions may develop in some parts of the biofilm and microniches may develop due to uneven spatial and temporal distribution of nutrients inside the biofilm [16], thus enhancing colonization of the surface by

new bacterial species that ultimately intimately cooperate with the well-established species [8]. The final architecture of the biofilm not only depends on the bacterial species, but also on the local flow environment and the nutrient availability [8].

Finally the last step in biofilm formation is bacterial detachment from the biofilm. Detachment occurs naturally (e.g., influenced by the physiology of the bacteria) or is provoked by human actions (e.g., membrane cleaning). Detached bacteria may start forming a biofilm elsewhere in the system [102].

### 3.3. Fouling stages

A long-term constant-flux filtration process seems to be characterized by a progressive increase of resistance to filtration, translated in a time-dependent TMP increase (or similarly by a time-dependent permeate flux decline) [85]. The time-dependency may be subdivided in two different regions (**Figure 13**), based on the critical flux concept as a central concept [56]. Pollice et al. (2005) considered the critical flux value to determine the transition between reversible and irreversible fouling [61].



**Figure 13** Typical fouling stages (adapted from [48]).

Field et al. (1995) distinguished Stage 1 and Stage 2 within the sub-critical region (i.e., when operating a constant-flux filtration at a flux below the critical flux) [54].

- **Stage 1**, also called 'conditioning' stage, consists of an initial short-term rapid linear rise in TMP occurring in just a few hours, probably due to adsorption and precipitation of colloids and solutes on the membrane surface and in the pores leading to pore blocking and closure [7], [48]. Stage 1 generally becomes less clear when membrane history becomes important (i.e., when the membrane is not virgin anymore but already has undergone fouling and subsequently cleaning) [7].
- **Stage 2**, also called 'sustainable stage', is characterized by a long and gradual linear or slightly exponential increase in TMP up to the critical flux value [99]. This stage is mainly due to organic precipitation and accumulation of EPSs present in the mixed liquor or produced by microorganisms in the biofilm on the membrane surface or into the membrane pores [7], [48], [99].



- Heterogeneous gradual pore closure and deposition of material at the membrane surface lead to spatial variations in local fluxes along the membrane which could exceed the critical flux of the suspension [61], [99]. At a certain point the supra-critical region is attained, the so-called **Stage 3** where operation cannot be maintained for an extended period of time without severe fouling to occur [7], [56], [61], [99]. Stage 3 is characterized by a sudden TMP jump. The cake layer gradually loses porosity by compression [76]. Transfer limitation inside de cake layer finally result in death of bacteria, thus more EPS release which further enhances fouling [39], [48], [53].

Zhang et al. (2006) reported that it may be desirable to limit the extent of Stage 1, to try to extend Stage 2 as much as possible and definitely to avoid Stage 3 [7]. Unfortunately Cho et al. (2002) reported that Stage 3 eventually occurs both in short-term filtration processes as in MBRs operated at long term, even if filtration was performed at a flux below the critical flux [99]. However Pollice et al. (2005) mentioned that Stage 3 arises more frequently in laboratory-scale set-ups [61]. Nevertheless Fan et al. (2000), as cited by Ognier et al. (2009), managed to run a MBR continuously during 70 days at a stable TMP that did equal four times the clear water TMP [58], [103].

#### 3.4. Fouling control strategies

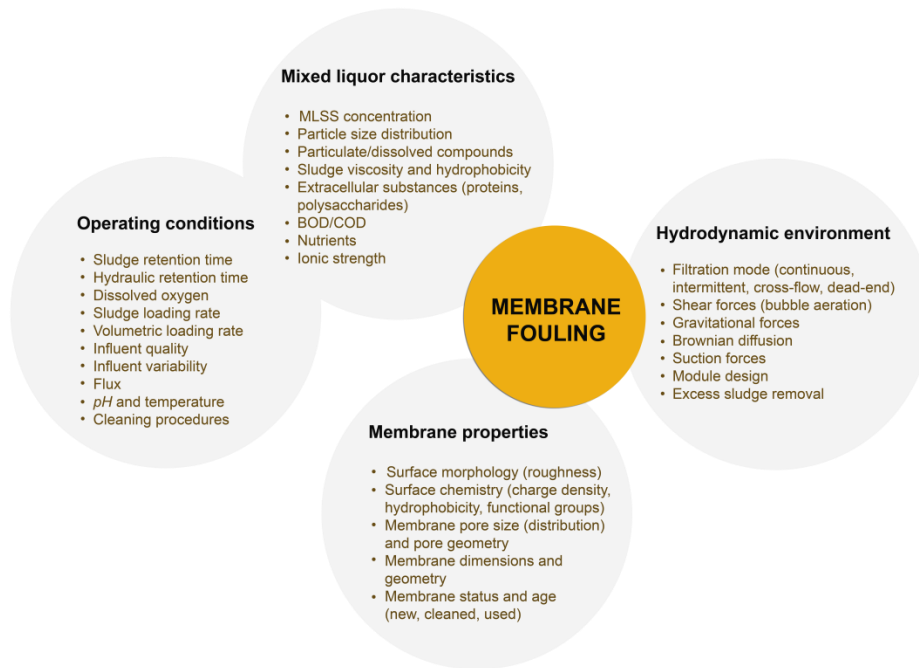
Zhang et al. (2006) discriminated between three interdependent parameters having an influence on membrane fouling and sludge filterability (**Figure 14**) [7]:

- the nature of the hydrodynamic environment;
- the membrane properties;
- the sludge characteristics, biopolymer concentration and microbial community structure, which in turn are affected by operating parameters impacting on biomass growth and decay.

Field et al. (1995) introduced three approaches for the avoidance and remediation of fouling [54]:

- the improvement of the hydrodynamics;
- optimization of the membrane and process design;
- periodic cleaning methods. Indeed, membrane fouling and biofilm formation are natural processes that cannot be avoided completely [104]. Cleaning technologies can be divided into mechanical, hydraulic, electrical and chemical methods [38], [105]. For an extensive review on membrane cleaning methods in membrane bioreactors, please refer to Wang et al. (2014) [81].

These approaches may be combined to efficiently counteract fouling. As a reference, Zhang et al. (2006) and Lee et al. (2007) reviewed studies focusing on specific fouling control strategies [7], [106]. The next sections highlight the effect of the hydrodynamic environment and the membrane and process design.



**Figure 14** Schematic of the factors affecting membrane fouling (adapted from [4], [7], [16], [42], [48], [52]).

### 3.4.1. Improvement of the hydrodynamics

Improvement of the hydrodynamics is inherently associated with decreasing the concentration polarization and enhancing back transport of the deposited particles on the membrane surface into the bulk mixed liquor [38]. This can be done in several ways.

Hydraulic cleaning methods involve intermittent operation modes such as back-flushing and/or relaxation [52], [62], [107]. Back-flushing means the flux is reversed by switching the pressure so that the permeate migrates in opposite direction through the membrane to the reactor for a limited amount of time [4], [40]. On the contrary during relaxation the pressure is switched off for a limited amount of time (i.e.,  $TMP = 0$ ), thus permitting the membrane and cake layer to relax, the latter becoming more open. In the latter case the layer is removed by the turbulent forces across the membrane surface and resuspended in the mixed liquor [4], [36], [38]. Back-flushing as well as relaxation mode are standard anti-fouling strategies used in most of the MBR processes [27]. However, since both methods reduce the overall flux through the membrane (since the filtration process is interrupted at discrete time moments, typically during 1-2 min every 8-10 min [4]), a relatively high instantaneous flux must be applied in order to compensate for this loss. Wu et al. (2008) and Metzger et al. (2007) reported the fouling behaviour to be more dependent on the instantaneous flux than the filtration mode (continuous or intermittent mode) [27], [82]. Also the duration, the interval and the strength of these hydraulic techniques were reported to influence the fouling rate [27]. Finally the efficiency of hydraulic cleaning tends to decline with filtration time [5], [27]. Thus a trade-off has to be made between permeation efficiency and fouling control [27].

Secondly hydrodynamic conditions can be improved by enhancing the shear forces along the membrane by sparging coarse oxygen or air bubbles (> 3 mm) from the bottom of the bioreactor or the membrane module (typically hollow fibres or flat sheets [4]) along the membrane surface, the so-called 'air-flush concept' [38]. Judd (2008) stated that on approximation the membrane permeability of submerged modules shows a linear increase with aeration rate [4]. Moreover this method has the supplementary advantages to provide extra oxygen in the reactor mixed liquor by diffusion of oxygen from the air bubble to the liquid [108] and to keep the biomass in suspension [5], [38]. It is however important to determine the optimal packing density and distance between the modules in order to optimize the air flow along the membrane surface [48], [62]. Finally it has been proven that there exists a maximal aeration rate, above which no further significant fouling reduction is observed [5].

### 3.4.2. Optimization of the membrane design

The membrane design involves the adjustment of the membrane properties as to reduce the affinity of the solutes with the membrane surface [54]. Stuckey (2012) distinguished three membrane surface modifications: increase in hydrophilicity, alteration of the surface charge and bacterial anti-adhesion modifications [42]. Liu et al. (2010) reported that a combination of these surface modifications yields the best results for control and minimization of membrane biofouling [109].

- Solute and bacteria in the mixed liquor tend to show a greater affinity towards hydrophobic membranes, as already mentioned previously in this chapter (**Section 2.4.2**). Thus it leads to more severe fouling than hydrophilic membranes [5], [48], [88], [96], where the bacteria-membrane interactions are mostly reversible [96]. Although research is being performed in order to increase the hydrophilicity of hydrophobic membranes (e.g., [110] [111] [112] [113] [114] ), it has been reported that the degree of hydrophilicity of a membrane is not a good indicator for biofouling tendency; on the contrary the membrane surface charge plays a very important role [96], [109]. Moreover the degree of hydrophobicity of bacteria may even increase when attached onto the membrane, as reported by Jinhua et al. (2006), thus enhancing further bacterial attachment [91].
- The electrical properties of membrane surfaces can be modified with polycations or polyanions [109]. Theoretically, electrostatic repulsion between the particles and the membrane surface will occur if they bear the same charge, thus reducing fouling tendency by counteraction of the attractive van der Waals forces [16], [78], [88]. However Pasmore et al. (2001) found that biofouling is minimized when membranes are electrically neutral and increases with increasing positive or negative charge [96]. This is most surprising since particles and bacteria must overcome the electrical double layer formed in electrolytes and adjacent to the charged membrane surface

as well as around their own cell membrane in order to attach onto the surface [115]. Most bacteria carry a net negative surface charge in aqueous environments due to the presence of phospholipids, (lipo)polysaccharides and proteins in their cell membrane [96], [97] Thus it is expected that negatively charged membrane surfaces will impede bacterial attachment. This theory is also known as the DLVO theory, named after its creators [16]. However Gottenbos et al. (2001) reported that although negatively charged surfaces reduce the chance of initial bacterial adhesion and thus delay the formation of a biofilm, the initially attached Gram-negative<sup>28</sup> bacteria did not develop further on positively charged surfaces. This is due to strong electrostatic attractions that impede bacterial elongation and division [116]. On the contrary Gram-negative as well as Gram-positive bacteria did grow exponentially on negatively charged surfaces after initial adhesion [117]. Thus charged surfaces do generally not exhibit one intuitive expectations.

- Bacterial anti-adhesion modifications involve the incorporation of biocides onto the membrane surface as to eliminate bacteria that eventually managed to attach to the surface [109]. Bazaka et al. (2012) reviewed surface modifications in clinical applications that may also be applicable in MBR applications, such as the incorporation of silver ions, bioactive antibodies, ZnO or TiO<sub>2</sub> [118]. Please refer to their work and to Li et al. (2008) for an extensive overview of all possible bacterial anti-adhesion modifications [118], [119].

Membrane morphology is important to consider as well. For instance membranes with a smooth surface will tend to foul less easily [36]. Indeed, increasing surface roughness has been reported to increase the potential attachment to surfaces as well as to disrupt the fluid flow thus reducing detachment of particles via shear forces [96].

When fouling prevention and mitigation mechanisms are insufficient, cleaning methods must be applied, implicitly implying that a proper choice of membrane material is of utmost importance.

- Mechanical cleaning can be translated in the use of e.g., rotating or vibrating modules [38] or ultrasonic treatment [48], [85], [105], which might result in membrane damage.
- Electrical cleaning by creation of an electrical field may be used to remove charged species from the cake layer.
- Chemical cleaning is a method to be used on longer timescales with a frequency from once per day ('maintenance cleaning') to once per year ('intensive cleaning') when other fouling control strategies are insufficient [36], [40]. **Table 8** gives most commonly used chemical cleaning methods.

---

<sup>28</sup> The distinction between Gram-negative and Gram-positive bacteria is based on differences in their cell wall structure. The cell wall of Gram-negative bacteria is made of a thin layer of peptidoglycan surrounding the cytoplasmic membrane and itself surrounded by an outer membrane bearing proteins, phospholipids and polysaccharides. On the other hand Gram-positive bacteria have a thick cell wall consisting of several peptidoglycan sheets stacked upon one another and no outer membrane [8].

**Table 8** Most commonly used chemical cleaning agents for maintenance or intensive cleaning of membranes (based on [4], [38], [40], [48], [88]).

Chemical cleaning agent	Example	Purpose
Strong acids	HCl, citric acid	To break metal-associated structures, e.g., inorganic precipitates and metal-organic complexes.
Enzymes	Amylase, protease	To destroy the cake layer.
Complexing agents	EDTA, polyacrylates	To remove organic and metal precipitates.
Disinfectants/oxidantia	H <sub>2</sub> O <sub>2</sub> , NaClO	To remove organic-based precipitation and microorganisms.
Bases	NaOH	To remove organic foulants.

### 3.4.3. Optimization of the process design

Pollice et al. (2005) stated that increasing sludge concentration results in an exponential increase in membrane fouling resistance during supra-critical operation [61], [71]. For instance as reported by Yamamoto et al. (1989), when the MLSS concentration exceeds 40 000 mg l<sup>-1</sup>, the flux decreases abruptly [68]. Indeed, since the MLSS concentration of the sludge suspension typically is several times greater than the concentration of dissolved species [53], it may impact fouling by increasing the dynamic viscosity of the mixed liquor [31]. Also high amounts of biopolymers (i.e., proteins, carbohydrates) increase the viscosity of the sludge suspension so that the permeate flux through the membrane is reduced and fouling is enhanced [72].

Process design can be optimized by adding non-ionic detergents and fouling reducers (adsorbents, metal salts coagulants or flocculants) which may alter both the flocs and the mixed liquor supernatant [38], [52], [62], [107]. Huyskens et al. (2012) reviewed literature about the effects of fouling reducers [107]. The use of fouling reducers showed promising results in short-term experiments, but because of their high cost [4], the uncertainty about the effect they have on the microbiology and their environmental impact [48], it is uncertain they would show the same degree of success in long-term applications.

Meng et al. (2006) stated that the particle size of sludge flocs, colloids and solutes present in the mixed liquor has an influence on fouling [53]. When large sized particles (like flocs) attach to the membrane, they tend to form a cake layer on the membrane surface. On the contrary, foulants which are smaller (e.g., solutes) or of comparable size (e.g., colloids) than the membrane pores, will tend to enter the pores and cause pore closure and pore blocking respectively. Thus fouling is greatly influenced by the average sludge particle size distribution of the mixed liquor.

#### **Influence of operating conditions**

An important parameter to be considered in view of achieving long-term and sustainable operation is the volumetric flux. High fluxes tend to enhance fouling by increasing convective transport of bacterial cells and other particles to the membrane surface [3]. Thus, in order to decrease the migration of



bacterial cells and nutrients towards the membrane surface and to avoid compaction of the biofilm [16], it is crucial to operate at a low 'sustainable' flux near the critical flux as to pursue a slow and gradual TMP increase that can be maintained over a longer period [7], [52], [62], [107]. If high productivities must be achieved, the low flux must be compensated by larger membrane areas [38].

Grelier et al. (2006) found membrane fouling in laboratory-scale experiments to be more dependent on SRT than on MLSS concentration [2] and Huang et al. (2008) and Meng et al. (2009) designated the SRT as the most important operating parameter in fouling phenomena [3], [48]. Short SRTs (< 10 days) might result in an accumulation of biopolymers [4], [67] and a decrease of sludge filterability [2], thus leading to high fouling rates and permeability decrease [4]. On the contrary divergent views exist on the effect of high SRTs on membrane fouling. For instance Le-Clech (2010) and Massé et al. (2006) stated that high SRTs generate higher MLSS concentrations in the form of smaller flocs and denser floc aggregates, thus impeding oxygen transfer due to increased mixed liquor viscosity [5], [70]. Moreover membrane fouling is enhanced by excessive development of filamentous bacteria [70]. On the other hand some authors found that the biopolymer concentration tend to decrease at longer SRT (from 10 to 60 days) [2], [61], [67], thus leading to lower sub-critical fouling and increased wastewater treatment efficiency [13]. Finally Judd (2008) evoked the advantage of promotion of slow-growers and reduction of excess sludge production [4]. Based on Grelier et al. (2006) a SRT of 40 days shows optimal membrane performance [2], but since full-scale plants are space-limited, a SRT between 15 and 40 days seems more appropriate, depending on the HRT and the feed solution [48].

Meng et al. (2007) investigated the effect of HRT on membrane fouling and stated that the HRT has an indirect rather than a direct influence on fouling [31]. Decreasing HRTs result in lower DO concentration due to the high biodegradation and thus oxygen utilization rate. Low HRTs moreover result in a high F:M ratio, larger floc sizes, higher MLSS concentration and a higher sludge viscosity, all of them influencing the oxygen transfer rate and the metabolic activity of the microorganisms.

Jeong et al. (2007) investigated the effect of the loading rate on bio-fouling and biopolymer production rate and found that high loading rates resulted in a larger amount of attached substances on the membrane surface [25] and higher fouling rates [120] caused by an increased sludge viscosity and MLSS concentration [31].

Low temperatures produce a more viscous suspension thus slowing down diffusion of particles away from the membrane surface and reducing the shear by air bubbles along the surface [60]. Low temperatures also require higher driving forces in order to achieve the same flux [40]. Finally when charged membranes are used in MBRs, their interaction with the charges on colloids or macromolecules (e.g., proteins) is affected by *pH*-changes of the mixed liquor. The *pH* can also alter inorganic precipitation of salts [48].



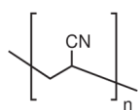
# Chapter 3: Research methodology

The effect of the membrane morphology and more specifically the effect of membrane surface charge on biofilm community structure and diversity, was assessed by means of two approaches:

- Performance determination of the membranes based on physico-chemical related measurements (ATR-FTIR, SEM, AFM, CAM, volume porosity measurement, electrokinetic characterization) and permeability related measurements (CWP, critical flux);
- Biofouling characterization based on molecular techniques (PCR-DGGE) and physico-chemical techniques (ATR-FTIR, SEM, CLSM).

## 1. MEMBRANE AND MODULE PREPARATION

### 1.1. Membrane material



Polyacrylonitrile  
(PAN)

The homopolymer polyacrylonitrile (PAN) was chosen to synthesize hand-made membranes to conduct the research on. The reasons are manifold. For instance PAN is known to be thermally stable [121] and to have a high degree of resistance against chemical cleaning agents (e.g., citric acid,  $\text{CH}_3\text{COOH}$ ,  $\text{NaClO}$ ,  $\text{H}_2\text{O}_2$  and weak alkaline solutions such as  $\text{NaOH}$ ) [45], [122]. Secondly Zhang et al. (2008) reported that compared to other membrane materials, like PVDF, PSf or PES, the more hydrophilic PAN membranes are more fouling-resistant [100]. Thirdly stable surface modifications are much easier to achieve compared to e.g., PSf membranes [123]. Finally PAN can be used in a wide range of full scale applications such as municipal and industrial wastewater treatment, biomedical applications and concentration of proteins or oil/water mixtures [122], [123].

### 1.2. Membrane casting

16 flat-sheet membranes were prepared for the experiments, all having PAN as base structure:

- Four neutral membranes containing no surface charges;
- Four negatively charged membranes (hydrolysis);
- Four positively charged membranes (hydrolysis followed by coating of 1 polymer layer);
- Four negatively charged membranes (hydrolysis followed by coating of 2 different polymer layers).



Dimethyl sulfoxide  
(DMSO)

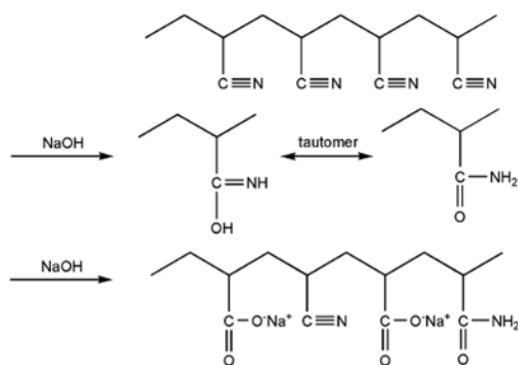
The PAN flat-sheet membranes were prepared via phase-inversion from a well-mixed and viscous casting solution at an air temperature of 21.6 °C and an air humidity of 22 %. The yellowish casting solution was prepared by dissolving the PAN polymer in dimethyl sulfoxide (DMSO), as 11 wt% and 13 wt% solution, during 24 hours, since DMSO is known to be a better solvent for PAN than e.g., DMF (dimethylformamide) [124]. The choice of 11 wt% and 13 wt% solutions is based on the requirement to finally obtain neutral membranes and charged membranes (after hydrolysis and layer-by-layer-deposition, see later) for which the fouling behaviour is solely determined by charge difference and not by differences in pore size (distribution), clean water permeability or surface roughness. Four 13 wt% solutions and twelve 11 wt% solutions were prepared. Each solution was casted (Automatic Film Applicator, Braive Instruments) on a polypropylene/polyethylene (PP/PE) non-woven support (Novatexx 2471, kindly supplied by Freudenberg, Germany) with a 250 μm wet thickness and at a casting velocity of 2.25 cm sec<sup>-1</sup>. The solvent was allowed to evaporate during 60 sec from the deposited nascent membrane, followed by immersion during 3 min of the polymer film in a coagulation bath composed of demineralised water (d-H<sub>2</sub>O) as non-solvent. The thus obtained asymmetric pristine 13 wt% and 11 wt% PAN membranes were stored in d-H<sub>2</sub>O for further use (*pH* = 7.02).

### 1.3. Preparation of the hydrolyzed PAN membranes

Hydrolysis of PAN membranes is a widely applied technique to render the membrane surface more hydrophilic and charged, eventually allowing for further modification [123]. First negative charges were introduced by hydrolysis of the twelve obtained 11 wt% PAN membranes based on the procedure described by Li et al. (2008) [125]. The membranes were immersed for 40 min at 50 °C in a stirred solution containing 10 wt% NaOH. The pristine membranes initially turned into a yellowish-red colour, indicating the formation of (-C=N-)<sub>n</sub> conjugated sequences [45], which faded with time during storage. The obtained hydrolyzed PAN membranes (PAN-H) were washed extensively with tap water in order to remove the remaining NaOH. They were kept under stirring in MilliQ water (mQ-H<sub>2</sub>O) (Millipore, Merck, 18.2 MΩ.cm) for some more time and finally stored in mQ-H<sub>2</sub>O for further use (*pH* = 8.96).

During hydrolysis of PAN with NaOH, part of the nitrile groups (C≡N) (dissociation constant *pK*<sub>a</sub> > 14) on the membrane surface were converted into carboxyl groups (-COOH) (*pK*<sub>a</sub> ~ 5) which can be readily ionized by the surrounding water (at *pH* > *pK*<sub>a</sub>) [125]. Possible mechanisms for the hydrolysis of PAN are given in **Figure 15**. Wang et al. (2009) reported that PAN-H membranes are resistant to several common organic solvents at room temperature and are well suited to play the role of supporting layer for composite membranes [45].





**Figure 15** Possible mechanism for the hydrolysis of PAN with NaOH (reproduced from [123]).

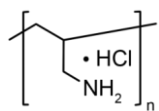
In this research 11 wt% PAN membranes are hydrolysed instead of 13 wt% PAN membranes because:

- 11 wt% PAN yields a high porosity membrane after phase inversion compared to 13 wt% PAN;
- membrane functionalization by hydrolysis results in a pore size reduction due to stretching of the carboxylic groups under basic conditions, as reported previously [126].

Thus the non-modified (or neutral) 13 wt% PAN membranes and the hydrolysed (or negatively charged) 11 wt% PAN-H membranes were expected to exhibit approximately the same pore size, what will be confirmed further on during the experiments (**Chapter 4, Section 2.1.2**).

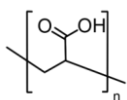
#### 1.4. Layer-by-layer deposition: membrane functionalization

Eight out of the twelve PAN-H membranes did undergo surface modification by dipcoating in aqueous solution of weak polyelectrolytes by means of manual layer-by-layer deposition.



Poly(allylamine  
hydrochloride)  
(PAH)

The membranes were first immersed in a rinsing solution containing 0.05 M NaNO<sub>3</sub> in mQ-H<sub>2</sub>O (*pH* = 6) for 10 min, in order to wash the pores before the polymer layer deposition. The wash step was followed by 30 min of dipping in an aqueous solution of the polycation poly(allylamine hydrochloride) (PAH) (*pKa* = 8.7 [127]) with a concentration of 0.1 g in 1 l rinsing solution. The thus obtained composite positively charged membranes (at *pH* < *pKa*) were then immersed again in the rinsing solution for 2x 10 min in order to stabilize the adsorbed layer and to remove unadsorbed PAH and thus preventing complexation of PAH and PAA in the next step [128]. The salt concentration has been reported to have no significant effect on the assembly outcome [128]. Four out of the eight membranes were stored in mQ-H<sub>2</sub>O for further use (*pH* = 8.45).



Poly(acrylic acid)  
(PAA)

The other four positively charged membranes continued the coating train with the polyanion. After an additional 10 min immersion in the rinsing solution, they were dipped for 30 min in a solution of 0.1 g poly(acrylic acid) (PAA) (pKa = 4.5 [129]) in 1 l rinsing solution. The thus obtained composite negatively charged membranes (at  $pH > pKa$ ) were then immersed again in the rinsing solution for 2x 10 min and finally stored in mQ-H<sub>2</sub>O for further use ( $pH = 8.41$ ).

### 1.5. Module potting

The obtained flat sheet membranes were potted into envelope-size modules (Figure 16). Each membrane sheet was cut at the appropriate size and folded double to form an envelope surrounding two sheets of spacer (3510 Corex, Agfa) and a permeate channel (silicon tube), meant to connect the module interior to the peristaltic pump of the reactor. Each folded membrane was fixed to a PVC frame (Bonte Ateliers, Leuven) by glueing the edges together using a 50/50 mixture of binder and hardener (UHU plus, endfest 300, Germany). The glued edges were allowed to dry overnight while keeping the membranes wet.

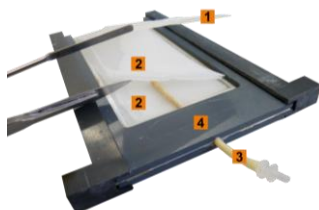


Figure 16 Structure of the envelope-sized modules. (1) double folded membrane sheet, (2) spacer sheets, (3) permeate channel, (4) PVC frame.

The final modules (Figure 17) had an effective filtration area of 2x 75 cm<sup>2</sup> and were stored in d-H<sub>2</sub>O for further use.

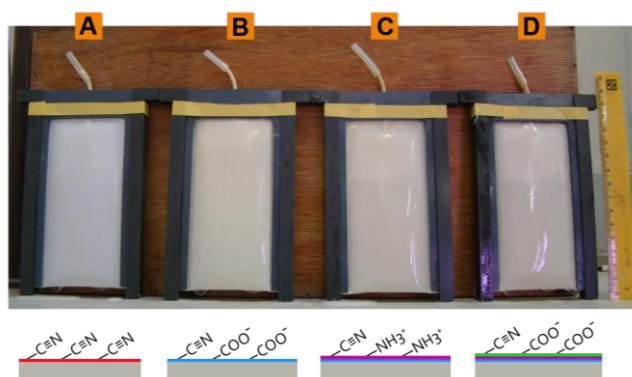


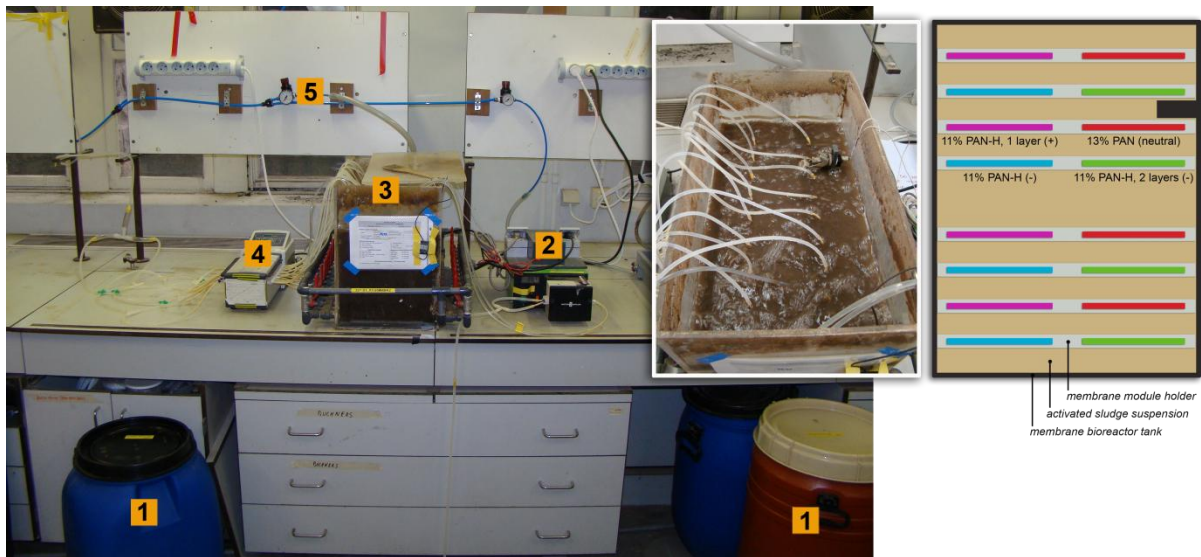
Figure 17 Final modules and their respective surface charges. (A) 13% PAN – neutral, (B) 11% PAN (-) – hydrolyzed, (C) 11% PAN (+) – 1 deposited layer PAH, (D) 11% PAN (-) – 2 deposited layers PAH & PAA.

## 2. OPERATING CONDITIONS OF THE LAB-SCALE MBR SYSTEM

### 2.1. Membrane bioreactor design

#### 2.1.1. Laboratory-scale high-throughput membrane bioreactor

Fouling experiments were conducted using a laboratory-scale high-throughput membrane bioreactor (HT-MBR) (**Figure 18**) composed of an aerated bioreactor tank with a volume of 37.8 l which contained the 4x four replicate membrane modules immersed in clusters of 4 different membrane types in 20 l activated sludge.



**Figure 18** Schematic of the HT-MBR. (1) feed tanks, (2) feed pump and level controller, (3) bioreactor containing the 4x 4 replicate membrane modules immersed in activated sludge, (4) permeate pump, (5) air supply. The upper right figure represents the clustered arrangement of the membrane replicates inside the bioreactor.

The permeate was sucked through a multichannel peristaltic pump (Watson Marlow, 205U) connected to the 4x four replicate modules and at an average total constant cross-flow rate of  $(25.6 \pm 3.1) \text{ l day}^{-1}$ , corresponding to  $\sim 6.5$  LMH per membrane, using cycles of 8 min filtration and 2 min relaxation without back-flush, as done by e.g., Piasecka et al. (2012) [6]. The use of moderate permeation and relaxation times allows for control of local instantaneous fluxes across the membrane thus mitigating fouling [27]. The MBR was fed (Watson Marlow, 503S) with a protamylasse solution as to keep the sludge suspension volume constant by means of a level controller. 1.4 l sludge suspension was withdrawn manually from the reactor weekly to control the sludge retention time (SRT) and total solids concentration (TS). The MBR was operated at a SRT of 100 days and an average hydraulic retention time (HRT) of 18.75 hours. The SRT is defined as:

$$\text{SRT} = \frac{V}{Q_{\text{sludge}}}$$

**Equation 9**



Where  $V$  ( $\text{m}^3$ ) is the working volume of the reactor and  $Q_{\text{sludge}}$  ( $\text{m}^3 \text{ day}^{-1}$ ) is the rate at which sludge is removed from the reactor [11]. The longer the SRT, the longer the contact time between bacteria and organic molecules, thus the higher the biodegradation [11], [70]. A SRT of 100 days is higher than generally reported in literature for the treatment of municipal wastewater, i.e., typically between 5 days [13] and 60 days [76], but since the HT-MBR here was operated on protamylasse wastewater (industrial origin), a SRT of 100 days is most common. For instance, Piasecka et al. (2012) reported to work with molasses wastewater (from alcohol distilleries) at a non-limiting SRT (i.e., no sludge withdrawal except for sampling) [6]. The HRT is defined as:

$$\text{HRT} = \frac{V}{Q_{\text{feed}}} \quad \text{Equation 10}$$

Where  $V$  ( $\text{m}^3$ ) is the volume of the reactor and  $Q_{\text{feed}}$  ( $\text{m}^3 \text{ h}^{-1}$ ) is the rate at which the reactor is fed. The HRT thus is a measure for the time needed by the liquid phase to migrate through the reactor [4]. A HRT of 18.75 hours is relatively high compared to HRTs previously reported for the treatment of municipal wastewater, e.g., varying between 5 hours [13] and 12 hours [2], [76]. Since the HT-MBR here was operated on protamylasse wastewater, a HRT of 18.75 hours is most common, like reported by Piasecka et al. (2012) or Bilad et al. (2011) who operated their MBR on molasses wastewater with a HRT of 18-20 hours [6], [130].

The MBR was aerated at a constant rate of 10 LPM ( $\text{l min}^{-1}$ ) (i.e.,  $0.6 \text{ m}^3 \text{ h}^{-1}$ ) unfiltered compressed air at a pressure of 3.25 bar (Variable Area Flow Meter EK-4BR, Kytola Instruments), which is in the range of reported aeration rate values, e.g. values as low as  $0.2 \text{ m}^3 \text{ h}^{-1}$  [2], [53], [76] and as high as  $1.2 \text{ m}^3 \text{ h}^{-1}$  [3], [27]. The air was introduced in the reactor by means of coarse bubbles rising from perforated pipes underneath the membrane modules to provide oxygen and turbulent mixing.

Finally the temperature was monitored four times a week and fluctuated between  $10.5 \text{ }^\circ\text{C}$  and  $16.2 \text{ }^\circ\text{C}$  according to variations in room temperature since no heat control was applied.

### 2.1.2. Origin of activated sludge and feed

The bioreactor was inoculated with 20 l aerobic activated sludge collected from the sedimentation tank of the local wastewater treatment plant of Leuven, Aquafin.

During the first 17 days, the HT-MBR was operated on  $1.5 \text{ ml l}^{-1}$  protamylasse feed (AVEBE, Veendam, The Netherlands) diluted in tap water. From day 18 on, the concentration was increased up to  $2.3 \text{ ml l}^{-1}$  as to control sludge bulking. The concentration was comparable to the one used by Bilad et al. (2010)

and Bilad et al. (2011) for the operation of a HT-MBR on molasses wastewater (i.e., 2.25 ml l<sup>-1</sup>) [130], [131]. Protamylasse can be defined as a protein-free potato-juice, a brownish and viscous residue of the industrial starch industry, containing a range of compounds necessary for microbial growth (Table 9). As seen from the table, the feed solution contains a pH-buffer (KH<sub>2</sub>PO<sub>4</sub>) thus influent pH was adjusted to neutral pH and had a value of (6.90 ± 0.25) throughout the experiments.

**Table 9** Average composition of the protamylasse residue (54% dry weight) (adapted from [132]).

Composition	Concentration (g l <sup>-1</sup> )				
<b>Amino acids</b>					<b>Total: 183.0</b>
Mainly:	Asparagine	65.1	Glutamine	39.7	
<b>Organic acids</b>					<b>Total: 135.2</b>
Citric acid	76.3	Oxalic acid	6.1	Lactic acid	13.2
Malic acid	35.6	Acetic acid	4.1		
<b>Sugars</b>					<b>Total: 142.3</b>
Glucose	35.6	Fructose	35.6	Saccharose	71.2
<b>Salts and minerals</b>					<b>Total: 225.7</b>
K <sup>+</sup>	97.6	Na <sup>+</sup>	0.8	Cu <sup>2+</sup>	0.04
PO <sub>4</sub> <sup>3-</sup>	25.4	NH <sub>4</sub> <sup>+</sup>	4.0	Cl <sup>-</sup>	8.1
Mg <sup>2+</sup>	4.5	Mn <sup>2+</sup>	0.03	NO <sub>3</sub> <sup>-</sup>	2.2
Ca <sup>2+</sup>	0.6	Zn <sup>2+</sup>	0.08	SO <sub>4</sub> <sup>2-</sup>	22.4

### 2.1.3. Maintenance of the HT-MBR

The reactor was inoculated with sludge on the 15<sup>th</sup> of September 2014 (Day 1) (Figure 19). First the sludge suspension was acclimated to the MBR system using random PVDF membranes for 72 days as to obtain stable operation before starting the fouling experiments, hereafter called 'Transient Period 1'. During this transient period, the feed pump did stop working several times thus perturbing stability.

The 4x four replicate modules were immersed in the reactor on the 25<sup>th</sup> of November 2014 (Day 72), hereafter called 'pristine membranes (P-membranes)'. On the 3<sup>rd</sup> of January 2015 (Day 111), after 39 days stable operation, hereafter called 'Fouling Period 1', the fouling experiment ended abruptly due to feed pump malfunctions. The membrane modules were removed from the reactor and cleaned thoroughly using a three-step protocol in order to remove the hardened and dried fouling cake on their surfaces: (i) washing with tap water during 5 min to remove loosely attached material, (ii) submerging intermittently in 2 ‰ NaClO (pH 10.55) in d-H<sub>2</sub>O during a total of 3.5 days, (iii) rinsing with d-H<sub>2</sub>O during 5 min to remove the cake residues and the residual NaClO. The NaClO solution was changed every day in order to maintain a constant chlorine concentration. The modules were filtered with mQ-H<sub>2</sub>O (as explained in Section 3.3.2) and stored in d-H<sub>2</sub>O for further use.

The reactor was run for 40 days using random PVDF and PVC/silica membranes as to obtain stable operation again before restarting the fouling experiments, hereafter called 'Transient Period 2'. During this transient period, the feed pump did stop working several times.

The cleaned replicate modules were immersed back in the reactor on the 12<sup>th</sup> of February 2015 (Day 151), hereafter called 'cleaned membranes (C-membranes)'. On the 23<sup>rd</sup> of March 2015 (Day 190), after 39 days stable operation, hereafter called 'Fouling Period 2', the fouling experiment was ended.

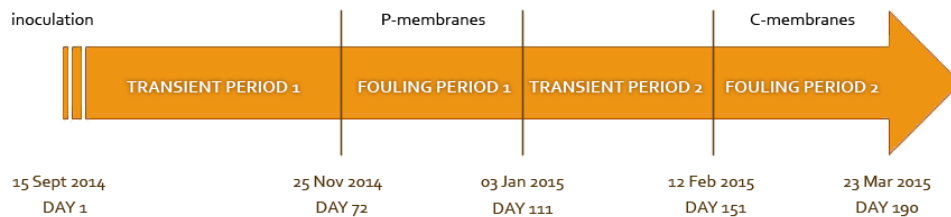


Figure 19 Timeline of the fouling experiments.

None of the equipment was sterile or autoclaved during use. The modules were not cleaned chemically or mechanically during the fouling periods. Only the protamylasse feed containers and the PVC tubes transporting the feed solution to the bioreactor vessel were thoroughly cleaned with 1 % NaClO (15° chlorine) during 30 min and rinsed with tap water during 5 min every week during both transient periods and fouling periods. The period between two cleaning moments, hereafter called 'maintenance period', thus lasted 8 days.

## 2.2. Quality measurements

### 2.2.1. Operational parameters

During both the transient periods and the fouling periods, the total solids (TS), the mixed liquor (volatile) suspended solids (ML(V)SS), the sludge volume index (SVI) and *pH* were monitored (*pH*-Meter 330, WTW) two times a week by taking uniform sludge samples from the middle zone of the bioreactor. The dissolved oxygen concentration (DO) (*pH*/Oxi 340i, WTW) was recorded only at the end of Fouling Period 2 since the measurement equipment was not available earlier.

The TS concept ( $\text{g l}^{-1}$ ) (expressed in dry weight) has already been introduced before as the concentration of suspended and dissolved solids present in the wastewater (Chapter 2, Section 1.1.1). It was measured by drying 3 ml activated sludge suspension in the oven (Mettler) during 2 h at 105 °C to constant weight and calculating the difference between wet and dry sample [11]. Measurements were performed in triplicates.

The total suspended solids (TSS) or MLSS concentration ( $\text{g l}^{-1}$ ) (expressed in dry weight) is defined as the concentration of suspended solids present in the wastewater. Its evolution with time is an indication of biomass growth [6]. It is obtained after filtration of the sludge suspension through a  $0.22 \mu\text{m}$  or  $0.45 \mu\text{m}$  filter paper and subsequently drying the filter residue in the oven at  $105 \text{ }^\circ\text{C}$  during 2 h to constant weight [11], [108]. The MLSS is obtained by calculating the difference between wet and dry sample. Here the TS concentration is used as approximation for the MLSS concentration.

The volatile suspended solids (VSS) or MLVSS concentration ( $\text{g l}^{-1}$ ) (expressed in dry weight) represents the organic fraction of the suspended solids in the wastewater. It is an approximation for the concentration of active biomass. It was measured by drying 3 ml activated sludge in the oven (Memmert) during 2 h at  $105 \text{ }^\circ\text{C}$  to constant weight, followed by ashing the residue in the muffle oven (B 180, Nabertherm) at  $550 \text{ }^\circ\text{C}$  during 3 h. The MLVSS was then calculated as:  $\text{MLVSS} = \text{MLSS} - \text{ash}$  [11], [108]. Measurements were performed in triplicates.

The SVI ( $\text{ml g}^{-1}$ ) is an empirical measure for the settleability and flocculation state of activated sludge [49]. It is defined as the total volume (ml) occupied by 1 g of MLSS after 30 minutes of sedimentation. Good settling sludge has a SVI equal to or less than  $100 \text{ ml g}^{-1}$  (expressed as dry weight), while bulking sludge (**Chapter 2, Section 1.2.2**) occurs at a SVI exceeding  $150 \text{ ml g}^{-1}$  (expressed as dry weight) [28]. In the latter case the diluted sludge volume index (DSVI) ( $\text{ml g}^{-1}$ ) is a better measure [11]. The settled volume was measured in twofold replicates in 100 ml graduated cylinders. The SVI was calculated according to:

$$\text{SVI} = \frac{\text{average settled volume (ml l}^{-1}\text{)}}{\text{average MLSS (g l}^{-1}\text{)}} \quad \text{Equation 11}$$

### 2.2.2. Physico-chemical analysis

During both the transient periods and the fouling periods, parameters for the measurement of organic pollution (COD) and parameters for the measurement of nutrient concentrations (TN, phosphate) were monitored once every two weeks by taking uniform sludge samples from the middle zone of the bioreactor, as well as feed wastewater samples and permeate samples from the outlet of the peristaltic tubes.

The concepts of Chemical Oxygen Demand (COD), total nitrogen (TN) and phosphate have already been introduced before (**Chapter 2, Section 1.1.1**). The concentrations were measured using Hach-Lange kits on the appropriate dilutions in tap water (**Table 10**) (LCK 314:  $\pm 2.5 \text{ mg l}^{-1}$ , LCK 138:  $\pm 0.26 \text{ mg l}^{-1}$  and LCK 349:  $\pm 0.03 \text{ mg l}^{-1}$  respectively) supported by Hach-Lange equipment (LT 200 Dry

thermostat and DR 1900 Portable spectrophotometer). No distinction was made between nitrogen species during the measurements ( $\text{NO}_3^-$ -N,  $\text{NO}_2^-$ -N,  $\text{NH}_4^+$ -N). Also the soluble COD (sCOD) of the sludge suspension were determined by filtering the liquid through a 0.45  $\mu\text{m}$  polyester-filter (Chromafil® PET-45/15 MS, Macherey-Nagel), as adapted from [70]. No replicates were used.

**Table 10** Hach-Lange measurements performed on permeate, sludge and protamylasse feed solution samples.

Sample	Dilution	COD <sup>29</sup>	TN <sup>30</sup>	phosphate <sup>31</sup>
Permeate	/	X		
	10x			X
	20x		X	
Feed solution	25x	X	X	X
Sludge suspension, filtered	3x	X		

The measured concentrations were used to calculate the COD:N:P ratio of the protamylasse feed solution and permeate as well as removal efficiencies. The removal efficiency (%), representing the relative concentration difference between reactor influent and effluent, was calculated as:

$$\text{RE} = \frac{C_i - C_e}{C_i} * 100 \quad \text{Equation 12}$$

Where  $C_i$  is the concentration in the influent and  $C_e$  is the concentration in the effluent [11].

Finally the average COD concentration of the feed was used to determine the sludge loading rate and the volumetric loading rate. The sludge loading rate ( $B_x$ ) ( $\text{kg COD kg}^{-1} \text{MLSS d}^{-1}$ ), also designated as the food-to-microorganism ratio (F:M), represents the amount of substrate given daily to the microorganisms. The volumetric or organic loading rate ( $B_v$ ) ( $\text{kg COD m}^{-3} \text{d}^{-1}$ ) was already introduced before (Chapter 2, Section 1.3.2). The volumetric loading rate is expressed per reactor volume ( $\text{m}^3$ ) and is calculated according to [11]:

$$B_v = \text{MLSS} * B_x \quad \text{Equation 13}$$

### 2.2.3. Microscopic analysis

The sludge composition and floc structure and size were analyzed microscopically (BX51, Olympus) with a 10x zoom magnification and by means of the objectives UPlanFI 100x/1.30 oil Ph3  $\infty/0.17$  (magnification 100x), UPlanFI 40x/0.75 Ph2  $\infty/0.17$  (magnification 40x) and UPlanFI 10x/0.30 JAPAN (magnification 10x) every two weeks in order to assess the quality and state of the sludge biomass and

<sup>29</sup> measurement range: 15-150  $\text{mg l}^{-1}$

<sup>30</sup> measurement range: 1-16  $\text{mg l}^{-1}$

<sup>31</sup> measurement range: 0.05-1.50  $\text{mg l}^{-1}$



the presence of microorganisms other than bacteria in view of rapid process optimization (e.g., organic loading, aeration). The microscope images (analySIS®, Soft Imaging System GmbH, Germany) at a magnification 100x were used to quantify the number of filamentous bacteria by means of the arbitrary Filament Index (FI). The FI has a scale between 0 and 5, representing none to very many filaments, and is determined based on a series of reference images as explained by Eikelboom (2000) [28]. Microscopic analysis was also performed every two weeks on the permeate and during three maintenance periods of 8 days on the protamylasse feed solution in order to assess the presence of bacteria or other micro-organisms.

### 3. MEMBRANE PERFORMANCE MEASUREMENT

Since the structural properties of membranes used in the MBR influence the membrane separation process and the (bio)fouling phenomena, it is essential to collect information on the membrane characteristics (e. g., surface groups, top layer thickness, pore size, surface charge, surface roughness, degree of hydrophilicity/hydrophobicity, permeability, etc.). Two types of characterization methods can be distinguished, the latter being considered as a validation method for the former [37]:

- Physico-chemical related measurements
- Permeability related measurements

#### 3.1. Membrane sampling

Physico-chemical related measurements were performed on membrane disks or coupons with an area of 1.77 cm<sup>2</sup> cut out of the membrane sheets. Permeability related measurements were performed (i) on membrane disks or coupons with an area of 1.77 cm<sup>2</sup> cut out of the membrane sheets or (ii) on the membrane modules. Unless specified otherwise, all measurements were performed on P-membranes (Section 2.1.3).

#### 3.2. Physico-chemical related measurements

##### 3.2.1. Attenuated Total Reflectance Fourier Transform Infrared Spectroscopy

Attenuated Total Reflectance Fourier Transform Infrared Spectroscopy (ATR-FTIR) allows determination of the functional groups present at the membrane surface, by collecting an infrared spectrum in the range 4000-370 cm<sup>-1</sup> and assigning chemical bonds to typical vibration typologies.

Two coupon replicates per membrane type were air-dried during 24 h to remove the majority of the water, followed by drying in a vacuum oven (Sheldon Manufacturing 1410, VWR International) at 29 Hg.vac (i.e., 50 mbar) (Mad.Duo2, Pfeiffer Vacuum) at room temperature during 6 h prior to analysis,



in order to minimize IR absorbance due to water present in the sample which could occur other peaks. After drying, the coupons were stored in closed recipients partly filled with cobalt chloride desiccants pending the measurements. The IR spectra were collected by measurements at room temperature on 2 to 4 points per coupon replicate using a FTIR spectrometer (Alpha-P, Bruker Corporation) and baseline corrected with optical spectroscopy software (OPUS, Bruker Corporation). ATR-FTIR measurements were performed on both the P- and the C-membranes in order to investigate the effect of long-term cleaning with NaClO. The IR spectra of the C-membranes are presented in [Section 2.1.1 of Appendix 1](#).

### 3.2.2. Scanning Electron Microscopy

Scanning Electron Microscopy (SEM) allows determination of the surface structure and membrane morphology (top layer thickness, cross-section, porosity [37]) by means of electrons accelerated towards the membrane sample and backscattered to a detector, which records depth and surface information, thus yielding a two- or three-dimensional image of the sample [133].

A coupon of each membrane type was air-dried for 24 h and cut (surface analysis) or fractured manually (cross-sectional analysis). No liquid nitrogen was required since PAN is naturally very brittle in its dry state. The membrane samples were mounted on a SEM-holder by means of double-sided adhesive tape. Samples meant for surface analysis were coated with a thin layer of a mixture of gold and palladium (Sputtering Device 07120/172, Balzers Union) prior to analysis. Samples meant for cross-sectional analysis were coated with a thin layer of gold (Auto Fine Coater JFC-1300, JEOL USA). The membrane surface structures were analyzed using a scanning electron microscope (SEM XL30 FEG, Philips) and imaging software (XL30 Microscope Control) at an accelerating voltage of 10 kV and magnifications 1500x and 10 000x as well as at 12 kV and magnification 50 000x. The membrane cross-sections were analyzed using a scanning electron microscope (JSM-6010 LV, JEOL USA) and imaging software (InTouch, JEOL USA) at an accelerating voltage of 10 kV and magnifications 300x, 330x or 350x and 3000x or 3500x. SEM measurements were performed on both the P- and the C-membranes in order to investigate the effect of long-term cleaning with NaClO. The SEM images of the C-membranes are presented in [Section 2.1.2 of Appendix 1](#).

### 3.2.3. Atomic Force Microscopy

Atomic Force Microscopy (AFM) allows determination of the three-dimensional micro-topography of the membrane surface (to atomic resolution [134], [135]) based on attractive forces (hydrogen bonding, van der Waals) and repulsive forces (electrostatic) between the scanning probe and the membrane surface [24], [133] It is often used as complementary technique to SEM [44], [78].

Measurements were performed in collaboration with Prof. Dhr. Alexander Volodin for the Department of Physics and Astronomy of the KUL. One coupon of each membrane type was air-dried during 24 h prior to analysis. Measurements were performed in dry state at three different locations per coupon as to take into account local heterogeneities of the membrane surface. Scans were performed at tapping mode using a scanning probe microscope (PicoPlus – AFM, Series 5500, Agilent Technologies Inc., USA) and thus allowing minimal deformation of the surface topography of the dried membranes [44]. Silicon tips (Pointprobe-Plus® Silicon-SPM-Sensor, Nanosensors, Germany) hold by a cantilever with a thickness of  $(2.0 \pm 1) \mu\text{m}$ , a resonance frequency of 6-21 kHz and a force constant of 0.02-0.77  $\text{N m}^{-1}$  were used at a tip height of 10-15  $\mu\text{m}$ . The images were flattened (1<sup>st</sup> order) in order to exclude the long-wave variations related to the substrate. The membrane surface roughness was determined from 1x1  $\mu\text{m}$  and 10x10  $\mu\text{m}$  areas at each location and reported in terms of the root mean square height,  $R_{\text{ms}}$  (nm) [121], [125]:

$$R_{\text{ms}} = \sqrt{\frac{1}{n} \sum_{i=1}^n |Z_i - \bar{Z}|^2} \quad \text{Equation 14}$$

With  $n$  the locations per coupon,  $Z_i$  (nm) the height at location  $i$  and  $\bar{Z}$  (nm) the average height of the  $n$  data points.

#### 3.2.4. Contact Angle Measurement

Contact Angle Measurements (CAM) allow determination of the degree of hydrophilicity/hydrophobicity of chemical groups attached to the outer layer of a membrane surface by measurement of the wetting or contact angle formed between the solid surface and the line tangent to the surface of the droplet used for the analysis. A contact angle of less than 90 degrees represents a hydrophilic surface, while a contact angle between 90 and 180 degrees represents a hydrophobic surface [98].

Two coupon replicates of each membrane type were air-dried for 24 h prior to analysis. Contact angles were measured by placing one drop of  $\text{d-H}_2\text{O}$  with a volume of 2  $\mu\text{l}$  at 3 locations per coupon replicate with a dropper at room temperature. Directly after placing the droplet on the membrane surface, a camera recorded the time-evolution of the drop from the side view, followed by on-line measurements of the contact angle on both sides of the drop (left and right angle, as measure for the droplet uniformity) by a goniometer (DSA 10-MK2, Krüss). These measurements were averaged out to yield the average contact angle ( $\vartheta$ -value).



### 3.2.5. Volume porosity measurement

Water uptake measurements based on the method described by Panda et al. (2015) were performed to determine the swelling potential and volume porosity of the P-membranes [121]. Two coupon replicates per membrane type were immersed in d-H<sub>2</sub>O immediately after synthesis during a non-limiting amount of days (> 72 h) followed by oven-drying at 60°C during 24 h. The oven temperature would not alter the chemical structure of the membranes since the glass transition temperature of PAN is 85 °C [45], 106 °C for PAA and around 90 °C for PAH [136]. The water uptake results, calculated as a water mass loss after drying, were used to determine the volume porosity of the membranes ( $\epsilon$ ), using following relationship [121]:

$$\epsilon (\%) = \frac{V_{\text{voids}}}{V_{\text{total}}} = \frac{(m_{\text{wet}} - m_{\text{dry}})}{\rho_w * A * \Delta x} * 100 \quad \text{Equation 15}$$

With  $V_{\text{voids}}$  (m<sup>3</sup>) the pore volume of the membrane,  $V_{\text{total}}$  (m<sup>3</sup>) the total volume of the membrane,  $\rho_w = 1\,000\,000$  g m<sup>-3</sup> the water density at room temperature,  $A = 0.000314$  m<sup>2</sup> the membrane surface area and  $\Delta x = 0.0005$  m the membrane thickness (non-woven support + porous membrane).  $m_{\text{wet}}$  (g) and  $m_{\text{dry}}$  (g) are the mass of the wet and air-dried membrane coupon respectively. The wet membrane mass was obtained by removing the excess water from the surface of the membrane coupons with filter paper. The effect of the Novatexx non-woven support was taken into account by subtracting its water mass uptake from the measurements.

### 3.2.6. Electrokinetic characterization

Zeta ( $\zeta$ ) potential or surface electric potential measurements [137] allow for the determination of the surface charge density of membranes [115] and is calculated based on the relative migration of a colloidal suspension with varying  $pH$  along the membrane surface [133]. The  $\zeta$ -potential values are highly dependent on surface characteristics of the membranes (e.g., functional groups, wettability, roughness), on the properties of the electrolyte solution used for the measurements (e.g., concentration,  $pH$ , valence of ions) and measurement conditions (e.g., temperature) [137]–[139].

Measurements were performed in collaboration with Prof. Dhr. Anthony Szymczyk from the *Institut des Sciences Chimiques de Rennes* (France). The apparent  $\zeta$ -potential can be determined based on measurements of the tangential streaming current, induced by a hydrostatic gradient, and which represents the amount of charged particles that flow along the membrane surface and their subsequent accumulation downstream of the membrane [133], [137]. One pair of coupon replicates per membrane type, stored in d-H<sub>2</sub>O prior to analysis, was mounted as a channel in a streaming potential cell (SurPASS Electrokinetic Analyzer, Anton Paar) at a channel height or inter-membrane

distance of  $(95 \pm 5)$   $\mu\text{m}$ . An electrolyte solution of 0.001 M KCl was pumped through the cell at room temperature based on hydrostatic pressure increments from 0 to 300 mbar. The  $pH$  of the electrolyte solution was adjusted between 3 and 8 by means of 0.1 M HCl and 0.1 M KOH solutions. The electrokinetic behaviour of the membrane samples was analyzed under  $N_2$  inert atmosphere and the streaming current was monitored by Ag electrodes coated with AgCl. Data acquisition took place by means of the Visiolab software. The relationship between the streaming current,  $I_s$  (A), and the  $\zeta$  – potential (V) is given by the Helmholtz-Smoluchowski equation [115], [137], [140]:

$$I_s = - \frac{W * h_{ch} * \epsilon_0 * \epsilon_r * \Delta P * \zeta}{\eta * L} \quad \text{Equation 16}$$

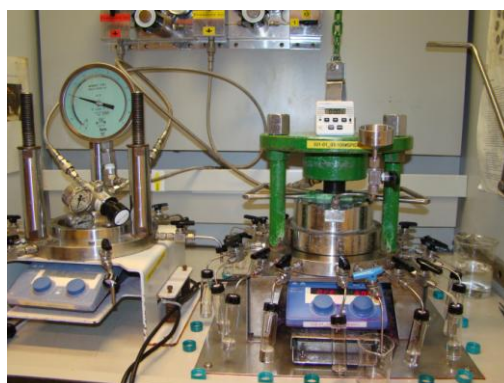
With  $W$  (m) the channel width,  $h_{ch}$  (m) the channel height,  $\epsilon_0$  the vacuum permittivity ( $8.854E-12$  F  $m^{-1}$ ),  $\epsilon_r$  (-) the dielectric constant of the electrolyte solution,  $\Delta P$  ( $N\ m^{-2}$ ) the hydrostatic pressure,  $\eta$  ( $kg\ m^{-1}\ s^{-1}$ ) the viscosity of the electrolyte solution and  $L$  (m) the channel length. The determination of the surface charge density based on  $\zeta$ -potential values is done as explained by Schaep et al. (2001) [115].

### 3.3. Permeability related measurements

#### 3.3.1. Clean water permeance of membrane coupons

The clean water permeance (CWP) ( $LMH\ bar^{-1}$ ) is defined as the maximum flux per unit TMP that the membrane can achieve in the absence of (bio)fouling [37].

The CWP of three membrane coupon replicates per membrane type was assessed at room temperature by means of a stainless steel high throughput device (HT pressure driven liquid separation, in collaboration with Agila) running 16 dead-end filtrations in parallel at a constant pressure of 1.3 bar (Nuova Fima) using mQ- $H_2O$  (Figure 20).



**Figure 20** High-throughput device for the CWP measurement of membrane coupons.

The feed water was stirred at 500 rpm during filtration. After a compression period of 15 min the permeate of each coupon was collected in vials in triplicate. The CWP of each membrane type

( $CWP_{coupon}$ ) was determined from the TMP (bar) and the pure water flux ( $J_{w, coupon}$ ) (LMH) using following relationship:

$$CWP_{coupon} = \frac{J_{w,coupon}}{\Delta P} \quad \text{Equation 17}$$

Where  $J_{w,coupon}$  was obtained from the mass difference between the empty and the full vial. Finally the average hydraulic resistance ( $R_m$ ) ( $m^{-1}$ ) of each membrane type was determined by calculating the hydraulic resistance of each coupon ( $R_{m, coupon}$ ) using the relationship:

$$J_{w, coupon} = \frac{\Delta P}{\eta_{water} * R_{m,coupon}} \quad \text{Equation 18}$$

With  $\eta_{water} = 2.78E-12$  bar h the dynamic viscosity of water at 20 °C.

### 3.3.2. Clean water permeance of membrane modules

The CWP of all 16 modules was assessed at room temperature by connecting the modules, mounted vertically in a container filled with mQ-H<sub>2</sub>O, to a multi-channel peristaltic pump (Watson Marlow, 205U) performing cross-flow filtration by sucking mQ-H<sub>2</sub>O out of the module interior (**Figure 21**). The CWP was performed on both the P- and the C-membranes in order to determine fouling recovery.



**Figure 21** Set-up of the CWP measurement of the membrane modules.

The modules were first washed and compacted during 1 h at 90 rpm (~68.8 LMH), followed by filtration at 60 rpm (~48.2 LMH) during 30 min, then 30 rpm (~25.5 LMH) during 30 min and finally 10 rpm (~8.6 LMH) during 30 min. The feed water was not stirred during filtration. At the end of each filtration period the TMP (bar) was recorded (DG-10-S, WIKA pressure gauges, USA) and the permeate of each module was collected in vials in duplicate. The CWP of each membrane type ( $CWP_{module}$ ) was determined from the TMP (bar) and the pure water flux ( $J_{w, module}$ ) (LMH) using following relationship:

$$CWP_{module} = \frac{J_{w,module}}{\Delta P} \quad \text{Equation 19}$$

Where  $J_{w,module}$  was obtained from the mass difference between the empty and the full vial. TMPs with values of zero were excluded from the calculations.

Finally the average hydraulic resistance ( $R_{m,P\text{-module}}$ ) ( $m^{-1}$ ) for P-membranes and the average resistance after cleaning  $R_{m,C\text{-module}}$  ( $m^{-1}$ ) for C-membranes was determined for each membrane type by calculating the hydraulic resistance of each module using the relationships:

$$J_{w, \text{module}} = \frac{\Delta P}{\eta_{\text{water}} * R_{m,P\text{-module}}} \text{ or } J_{w, \text{module}} = \frac{\Delta P}{\eta_{\text{water}} * R_{m,C\text{-module}}} \quad \text{Equation 20}$$

With  $\eta_{\text{water}} = 2.78E-12$  bar h the dynamic viscosity of water at 20 °C.

### 3.3.3. Critical flux determination

The theory of critical flux was already extensively explained previously (**Chapter 2, Section 2.2.7**). The most widely used methodology to assess the critical flux value and the short-term fouling rate, is the TMP measurement in flux-stepping experiments during constant-flux filtration on membrane modules with activated sludge, performed in the MBR. Due to a personal error, the critical flux measurement was performed on the C-membranes instead of the P-membranes. Thus the critical flux values of the pristine membranes were extrapolated from the results obtained based on the cleaned membranes.

Based on an adaptation of the methodology used by Le Clech et al. (2003), van der Marel et al. (2009), Pollice et al. (2005) and Cho et al. (2002), the flux-stepping experiment was performed with flux steps of 30 min, involving 20 min filtration (Watson Marlow, 205U) and 10 min relaxation [59]–[61], [99]. An arbitrary maximum flux scale of 50 rpm ( $\sim 35.0$  LMH) was reached starting from an initial flux scale of 5 rpm ( $\sim 3.5$  LMH) and with a flux step height of 5 rpm ( $\sim 3.5$  LMH). The corresponding TMP was recorded every 5 min (DG-10-S, WIKA pressure gauges, USA).

Two different figures were obtained based on the collected results. Firstly a graph, summarizing the experimental data, was plotted to represent the TMP (mbar), averaged over the modules of the same membrane type, and the flux (LMH) against time (min). Secondly, the average fouling rate  $d\Delta P/dt$  ( $mbar\ h^{-1}$ ) was plotted against the flux (LMH). From the figure, the (apparent) critical flux ( $J_c$ ) could be determined.  $J_c$  is defined as the maximum flux above which deviation from the linear trend occurs by

calculation of  $\frac{d^2\Delta P}{dJ^2}$  [59]. Alternatively the determination of  $J_c$  could be based on arbitrary threshold

values like a threshold fouling rate of  $0.1\ mbar\ min^{-1}$  [59] or a threshold permeance change  $K > 0.9\ K_0$ , with  $K_0$  the permeance during the first flux step [55]. Threshold values are necessary to determine  $J_c$  since fouling does always occur during MBR operation with activated sludge [59] [60]. The effect of temperature on the critical flux value was minimized by correction of  $J_c$  based on following empirical formula from [141]:



$$J_c^T = J_c^{20} * 1.025^{(T-20)}$$

Equation 21

Where  $J_c^T$  and  $J_c^{20}$  are the critical flux values at a sludge temperature  $T = 14.2$  °C during the measurements and at 20°C respectively.

#### 4. BIOFOULING (COMMUNITY) CHARACTERIZATION

Meng et al. (2010) considered MBR fouling as a Black Box, despite the many efforts to correlate the fouling mechanism to influences of membrane materials, sludge characteristics and operating conditions [24]. They identified three approaches to unravel the mysteries around fouling:

- Microbiological identification
- Morphological visualization of the fouling layer
- Chemical characterization of the foulants

These approaches will be employed in order to explore the physical structure and microbial diversity of the biofilm formed during the fouling experiments and to correlate the findings with the system specifications.

##### 4.1. Preliminary observations

###### 4.1.1. Bacterial enumeration

An approximation of vial cell numbers present in the protamylase feed solution ( $\Delta t =$  day 4 of the maintenance period), the permeate, the sludge and in the biofilm of two randomly chosen modules ( $\Delta t =$  day 30 of the fouling experiment) was obtained by means of serial dilutions.

Feed wastewater and permeate samples were taken from the outlet of the peristaltic tubes and inoculated without pretreatment. The sludge samples were taken from the middle of the reactor and sonicated (Vibra-Cell VCX 130, Sonics & Material) in an ice-water bath during 10 min at an amplitude of 20% and a pulse cyclus of 30 sec on/30 sec off in order to reduce the surface tension between filamentous bacteria and floc-formers [29] and to dissociate floc-formers from particles [8]. The effect of sonication on the integrity of the bacterial structures was evaluated by microscopic analysis (BX51, Olympus) with a 10x zoom magnification and by means of the objective UPlanFI 100x/1.30 oil Ph3  $\infty/0.17$  (magnification 100x). Before sampling of the biofilm, each module was taken out of the bioreactor and rinsed with d-H<sub>2</sub>O during 1 min in order to remove all loosely attached sludge material. Biofilm samples were obtained by carefully scraping cell material from the two identical membrane surfaces of the module over the full length of the membrane with a sterile stainless steel scraper and



transferred and resuspended in 65  $\mu\text{l}$  10 mM  $\text{MgSO}_4 \cdot 7\text{H}_2\text{O}$  in mQ- $\text{H}_2\text{O}$ . After sampling the modules were immersed back in the reactor.

200  $\mu\text{l}$  of inoculum were used to construct a dilution series in liquid Tryptone Soy Agar (TSA) ( $\text{pH}$  7.02) from  $10^{-1}$  to  $10^{-12}$ . The dilution series were performed in microtiterplates and incubated during 96 h on a shaking platform at 23.5  $^\circ\text{C}$ . Each sample was evaluated in triplicate series. The last well in the series exhibiting turbidity was considered to have originated from ten or fewer cells [8]. The average density of viable cells in each sample was expressed as Most Probable Number (MPN)  $\text{ml}^{-1}$  sample and was determined by means of MPN tables as published and explained by Blodget (2010) [142].

#### 4.1.2. Membrane fouling rate

The evolution of the transmembrane pressure (TMP) with time of each membrane module replicate, an indicator of the fouling rate, was monitored (DG-10-S, WIKA pressure gauges, USA) twice a week during Fouling Period 1. Before measurement, each module was taken out of the bioreactor and rinsed with d- $\text{H}_2\text{O}$  during 1 min in order to remove all loosely attached sludge material. The modules were immersed back in the reactor and the TMP was recorded after 15 min stabilization. The overall fouling rate was calculated as:

$$\frac{d\Delta P}{dt} = \frac{\text{TMP}_{t_{39}} - \text{TMP}_{t_1}}{39} \quad \text{Equation 22}$$

With  $t_1$  and  $t_{72}$  (day) the time moment the pressure was monitored.

## 4.2. Microbiological identification

### 4.2.1. Membrane sampling and sample storage

During Fouling Period 1 the bacterial diversity and composition of the protamylasse feed solution, the sludge suspension and the membrane biofilm developing on the modules were analysed.

Feed samples were collected in a sterile microcentrifuge tube from the outlet of the peristaltic tubes on day 1, day 2, day 3, day 4 and day 8 of two maintenance periods of 8 days. The samples were centrifuged (Centrifuge 5424, Eppendorf or Mikro 200R, Hettich Zentrifugen) at room temperature during 15 min at 12 000 rcf. The supernatant was discarded and the pellet was resuspended in 450  $\mu\text{l}$  GTE buffer (25 mM Tris.Cl, 10 mM EDTA, 50 mM glucose,  $\text{pH}$  8.31) by vortexing at intermediate speed (< 1600 rpm). The samples were stored at -21  $^\circ\text{C}$  for DNA extraction.

A sample of the pellet at the bottom of the feed container was collected in a sterile microcentrifuge tube on day 8 of the maintenance period by resuspending an aliquot of the pellet in 450  $\mu$ l GTE buffer by vortexing at intermediate speed (< 1600 rpm). The sample was stored at -21 °C for DNA extraction.

Sludge samples of 1 ml were taken from the middle of the reactor on the 25<sup>th</sup> of November 2014 (Day 72), on the 1<sup>st</sup> of December 2014 (Day 78), on the 8<sup>th</sup> of December 2014 (Day 85), on the 15<sup>th</sup> of December 2014 (Day 92), on the 19<sup>th</sup> of December 2014 (Day 96) and on the 2<sup>nd</sup> of January 2015 (Day 110) and collected in a sterile microcentrifuge tube. The samples were centrifuged at room temperature during 15 min at 3000 rcf. The supernatant was discarded and the pellet was resuspended in 450  $\mu$ l GTE buffer by vortexing at intermediate speed (< 1600 rpm). The samples were stored at -21 °C for DNA extraction.

Biofilm samples of each of the 4x four replicate modules were taken on the 25<sup>th</sup> of November 2014 (Day 72), on the 1<sup>st</sup> of December 2014 (Day 78), on the 8<sup>th</sup> of December 2014 (Day 85), on the 15<sup>th</sup> of December 2014 (Day 92), on the 19<sup>th</sup> of December 2014 (Day 96) and on the 2<sup>nd</sup> of January 2015 (Day 110). Before sampling of the biofilm, each module was taken out of the bioreactor and rinsed with d-H<sub>2</sub>O during 1 min in order to remove all loosely attached sludge material. Biofilm samples were obtained by carefully scraping cell material from the two identical membrane surfaces of the module over the full length of the membrane with a sterile stainless steel scraper (**Figure 22**). The sample was transferred and resuspended in a sterile microcentrifuge tube containing 450  $\mu$ l GTE buffer by vortexing at intermediate speed (< 1600 rpm). The samples were stored at -21 °C for DNA extraction. After sampling the modules were immersed back in the reactor.

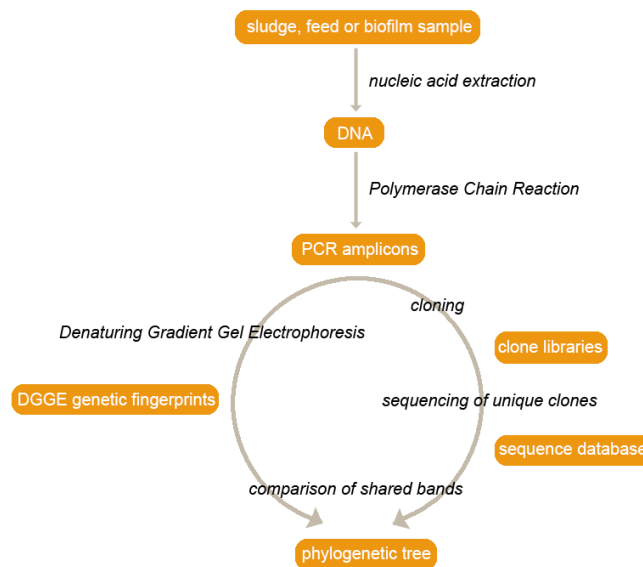


**Figure 22** Membrane sampling. Each vertical line corresponds to a sampling moment. The same pattern is present at the back side of the module.

#### 4.2.2. Culture-independent analysis of microbial communities

**Figure 23**, adapted from Muyzer et al. (1998), depicts the different steps undergone in view of determination of the microbial community composition and diversity of the protamylasse feed, sludge and membrane biofilm samples [143]. Culture-independent analysis was preferred here since culture-dependent analysis (i.e., cultivation, isolation) are rather time-consuming and may lead to an

underestimation of the real community diversity [13]. Indeed, it has been reported that only between 1% and 15% of all bacteria present in activated sludge and introduced on laboratory media, grow effectively, i.e. they exhibit a low cultivability [144], [145].



**Figure 23** Flowdiagram applied for the culture-independent analysis of microbial communities (adapted from [143]).

### DNA extraction and purification

Genomic DNA was extracted using the cetyltrimethylammonium bromide (CTAB)-lysozyme method [146] with some modifications (Appendix 4). This method yields DNA-fragments of length < 50 kb.

### Detection through Polymerase Chain Reaction

Polymerase Chain Reaction (PCR) allows for amplification of the extracted DNA samples in view of assessment of the diversity of microorganisms present in the protamylasse feed solution, the sludge suspension and responsible for biofilm formation in MBRs, by Denaturing Gradient Gel Electrophoresis (DGGE).

A mastermix with a volume of [2x number of samples + negative control (NC) + 2] was prepared and distributed over the individual PCR tubes. PCR reactions were performed in duplicate on each DNA sample in order to obtain large amounts of PCR products. Each PCR mix (25 µl) contained 7.5 µl PCR water (DNase and RNase free mQ-H<sub>2</sub>O), 0.5 µl GelTrack Loading Dye, 12.5 µl AccuStart II PCR Toughmix (Quanta Sciences inc.) and 1.25 µl of each primer (10 µM). 2 µl extracted template DNA was added to each PCR mix, originated from the four module replicates. Indeed, the purpose is not to investigate microbial differences between module replicates, but between different membrane types. The NC consisted of 2 µl PCR water. The Eubacterial primers GC-63F forward primer and 518R reverse

primer (Table 11) were used to amplify a gene fragment of 496 bp from the 16S rRNA gene. Thermocycling conditions (serial n° 5333 00004, Eppendorf Mastercycler) were 95 °C for 5 min (initial denaturation), followed by 25 amplification cycles, each consisting of three steps: 94 °C for 30 sec (denaturation), 60 °C for 30 sec (annealing) and 72 °C for 1 min (elongation). Thermocycling was ended with a final extension at 72 °C for 8 min. The PCR amplicons were cooled to 10 °C and stored at -21 °C for further use.

**Table 11** Sequence and annealing temperature of the forward primer GC-63F and the reverse primer 518R [147]

Primer	Primer sequence (5' → 3')	Annealing temperature, T <sub>m</sub> (°C)
Forward, GC-63F	CGC CCG CCG CGC GCG GCG GGC GGG GCG GGG	82.6
	GCA CGG GGG GCA GGC CTA ACA CAT GCA AGT C	
Reverse, 518R	ATT ACC GCG GCT GCT GG	58.7

The DNA quantity (ng  $\mu\text{l}^{-1}$ ) of the PCR amplicons were determined by 'broad range (BR)' Qubit measurements (Qubit® 3.0 Fluorometer, Life Technologies, Invitrogen) following manufacturer's instructions. 5  $\mu\text{l}$  of the PCR products were also examined on a 1.5% agarose gel stained with GelRed against a 2  $\mu\text{l}$  GeneRuler 100 bp plus DNA-ladder. Electrophoresis was performed at 6 V  $\text{cm}^{-1}$  for 60 min (PS 3003, Gibco BRL) in 1x TAE running buffer (40 mM Tris, 20 mM acetic acid, 1 mM EDTA, pH 8.3). After electrophoresis, the gel was visualized (GeneSnap, Syngene) on an UV transilluminator (Bio Imaging, Syngene) at an intensity of 500 ms.

### Denaturing Gradient Gel Electrophoresis fingerprinting

DGGE of GC-63F/518R PCR products was performed in order to determine the microbial diversity (evolution) of the samples by separation of the PCR amplicons with a different base sequence [148], which results in different denaturing characteristics and migration speed of the DNA. It is assumed that each band thus represents a different Operational Taxonomic Unit (OTU), corresponding to a predominant bacteria within the community [149].

The DGGE experiment was conducted according to Cheyns (2010) [148]. Approximately 300 ng PCR product of each sample were loaded on an 8% acrylamide gel containing a linear gradient (INGENY gradient maker) of 35-60% denaturant (a mixture of urea and formamide). A DGGE ladder, consisting of a mixture of 10 different 16S rRNA gene fragments obtained from *E. coli* clones and prepared according to Ruyters (2010), was distributed evenly over the gel [150]. Seven to ten water lanes were loaded at each side of the gel. After completing electrophoresis (INGENY phorU), the gel was stained with a GelRed-TAE solution (20  $\mu\text{l}$  GelRed, 100 ml 1x TAE buffer) for 30 min, and visualized (GeneSnap,

Syngene) on an UV-transilluminator (Bio Imaging, Syngene) at an intensity of 400 ms. Community fingerprint images were processed and analyzed with GelCompar II software (Applied Maths) and a dendrogram, calculated with the Dice coefficient taking into account the number of shared bands, was constructed from clustering of all data from the gels based on the UPGMA<sup>32</sup> algorithm. The structural diversity of the samples was compared based on the Shannon diversity index evaluation of the normalized band patterns of the specific groups, H, based on the underlying formula [149], [151]:

$$H = \sum_{i=1}^S P_i \log P_i \quad \text{Equation 23}$$

With S the number of species and  $P_i$  the relative frequency of the observations.

### 4.3. Physico-chemical analysis of the biofilm

At the end of Fouling Period 2, the fouled C-membranes were taken out of the bioreactor and the biofilm structure (thickness, composition, density) was investigated by means of (microscopic) fouling measurement techniques: ATR-FTIR, SEM and CLSM.

#### 4.3.1. Attenuated Total Reflectance Fourier Transform Infrared Spectroscopy

ATR-FTIR allows determination of the functional groups of organic membrane foulants [24]. Two coupon replicates were carefully cut out of the fouled membranes taking care not to disturb or destroy the biofilm. The coupons underwent the same procedure as described previously in this chapter in [Section 3.2.1](#).

#### 4.3.2. Scanning Electron Microscopy

Scanning Electron Microscopy (SEM) allows for qualitative description of the morphology of the foulants [76]. Two coupon replicates were carefully cut out of the fouled membranes taking care not to disturb or destroy the biofilm. The coupons did undergo a stringent pretreatment adapted from the procedure described by Miura (2006) and Meng (2007) [76], [90]. The samples were first fixed by immersion in 25 ml 3% (v/v) glutaraldehyde solution in 0.1 M phosphate buffer (*pH* 7.2) for 2 h. The samples were then washed twice for 10 min followed by 1 h in 0.1 M phosphate buffer (*pH* 7.2). Finally the samples were dehydrated in a seven-step ethanol series in mQ-H<sub>2</sub>O (25%, 50%, 75%, 85%, 95%, 100%, 100%) for 15 min each dehydration step. The dehydrated samples were mounted on a SEM-holder by means of double-sided adhesive tape and coated prior to surface-analysis as described

---

<sup>32</sup> Unweighted Pair Group Method of Arithmetic means



previously (Section 3.2.2). They were examined at an accelerating voltage of 25 kV and magnifications 250x, 1500x and 10 000x.

### 4.3.3. Confocal Laser Scanning Microscopy

Confocal Laser Scanning Microscopy (CLSM) is an optical microscope technique [152] which allows for 3D and depth visualization of the biofilm structure as well as determination of the biofilm thickness. The biofilm is stained with dyes targeting the biopolymers of interest and the fluorescence light is visualized. Moreover it may allow for discrimination of the membrane foulants (proteins, bacteria, polysaccharides) and determination of their spatial distribution within the biofilm [24].

One coupon was carefully cut out of the fouled membranes taking care not to disturb or destroy the biofilm. The coupon was immersed in 25 ml 0.1 M phosphate buffer and stored in the fridge during 24 h prior to staining and without additional fixation. The biofilm was stained based on the procedure adapted from Lee et al. (2007) [106]. The samples were incubated at room temperature in the dark during 30 min after immersion in a 10 ml mixture of 5  $\mu$ M of two non-selective nucleic acid fluorescence dyes in 10 mM  $\text{MgSO}_4 \cdot 7\text{H}_2\text{O}$ , being SYTO 9 and SYTO 62, which are specific to prokaryotes but may also stain eukaryotic microorganisms (cytoplasmatic, mitochondrial or nuclear staining) [153]. Proteins and polysaccharides were not stained. The stained biofilm was fixed on a microscope cover glass. The images were immediately acquired (Olympus Fluoview Viewer software, Ver.4.1) with a laser-scanning microscope (FV1000-IX81, Olympus Fluoview) by means of the objectives UPLanSAPO 40x/0.90  $\infty$ /0.17/FN26.5 (magnification 40x) and UPLanSAPO 100x/1.40oil  $\infty$ /0.17/FN26.5 (magnification 100x). At magnification 40x, depth images were acquired by optical sectioning using steps of 1  $\mu$ m, while at magnification 100x the step sizes were set at 0.5 or 0.25  $\mu$ m. Biofilm thicknesses were calculated by multiplying the number of slices taken by the size of each step. The image size was adjusted to 512 x 512 pixels, 1x zoom and an aspect ratio 1:1. Signals were recorded sequentially in the green channel (SYTO 9, excitation at 488 nm, emission at 500-524 nm) and in the red channel (SYTO 62, excitation at 635 nm, emission at 655-755 nm). Finally the three dimensional structure of the biofilm was reconstructed and images were processed (evaluation version, Imaris Bitplane, Zurich, Switzerland).

## 5. STATISTICAL ANALYSIS

It is assumed that the variables follow a normal distribution ( $\mu$ ,  $\sigma^2$ ) with variance  $\sigma^2$ . The only exception is the Shannon diversity index which is assumed to follow a lognormal distribution, since it is

calculated based on environmental samples [154]. Thus it is converted to log-values prior to analysis. All data are expressed as (mean  $\bar{X} \pm$  standard deviation  $s$ ) with  $n$  the sample size or replicates.

Although statistical hypothesis testing between two small populations is not a very powerful tool, independent two-tailed Student's t-tests were applied to determine if two sets of data are significantly different from each other based on a mutual comparison of all possible pairs of means  $\mu_i$  [155].

Null hypothesis  $H_0: \mu_1 = \mu_2$  **Equation 24**  
 Alternative hypothesis  $H_a: \mu_1 \neq \mu_2$  **Equation 25**

t-statistic 
$$T = \frac{\bar{X}_1 - \bar{X}_2}{s_{x_1 x_2} * \sqrt{\frac{2}{n}}}$$
 **Equation 26**

With the pooled standard deviation  $s_{x_1 x_2} = \sqrt{0.5 * (s_{x_1}^2 + s_{x_2}^2)}$  **Equation 27**


With  $s_{xi}^2$  the unbiased estimator of the variance of sample  $i$ . Reject  $H_0$  if  $|T| > t_{1-\frac{\alpha}{2},v}$  with  $\alpha = 0.05$  the statistical significance,  $v = 2n-2$  the degrees of freedom and  $t_{1-\frac{\alpha}{2},v}$  from tables. Probability values (p-values), indicating statistical significance, are also given. Sample means were considered significantly different at a 95% confidence interval ( $p < 0.05$ ).







## Chapter 4: Results & discussion

The results obtained from the membrane physico-chemical related measurements (ATR-FTIR, SEM, AFM, CAM, volume porosity measurement, electrokinetic characterization) and permeability related measurements (CWP, critical flux) on the pure and functionalized PAN membranes, as well as biofouling characterization measurements of the biofilm based on molecular techniques (PCR-DGGE) and physico-chemical techniques (ATR-FTIR, SEM, CLSM), are presented here. Each section is concluded with a brief summary, marked by , meant for busy people. But first the stability of operation of the HT-MBR is assessed.

### 1. MEMBRANE BIOREACTOR AND QUALITY MEASUREMENTS


The HT-MBR, which was operated at intermittent mode (8 min filtration – 2 min relaxation) and which contained four replicates of each membrane type (i.e., the neutral membranes 13% PAN (neutral), the negatively charged membranes 11% PAN-H (-) and 11% PAN-H, 2 layers (-) and the positively charged membranes 11% PAN-H, 1 layer (+)), was monitored during both Transient Periods 1 and 2 and Fouling Periods 1 and 2, which were defined in [Section 2.1.3 of Chapter 3](#). [Table 12](#) and [Table 13](#) give an overview of the operating conditions and physico-chemical properties of the HT-MBR respectively. For an extensive discussion on the values presented here as well as microscopic investigation of the sludge suspension, protamylasse feed solution and permeate, please refer to [Section 1 of Appendix 1](#).

**Table 12** Summary of the characteristics and operating parameters of the HT-MBR over both Transient Periods 1 and 2 and Fouling Periods 1 and 2. Values are given as (mean  $\pm$  standard deviation).

Parameter	Value	Parameter	Value
Reactor volume (l)	37.8	Total cross-flow rate (l day <sup>-1</sup> )	25.6 $\pm$ 3.1
Activated sludge volume (l)	20	Aeration rate (LPM)	10
Protamylasse feed solution concentration (ml l <sup>-1</sup> )	1.5 $\rightarrow$ 2.3	Dissolved oxygen concentration (mg O <sub>2</sub> l <sup>-1</sup> )	4.6 $\pm$ 0.6
HRT (hours)	18.75	SVI (ml g <sup>-1</sup> )	153 $\pm$ 37
SRT (days)	100	pH	7.81 $\pm$ 0.24
TSS (g l <sup>-1</sup> )	6.05 $\pm$ 1.74	VSS (g l <sup>-1</sup> )	5.31 $\pm$ 1.79
Average volumetric loading rate (kg COD m <sup>-3</sup> d <sup>-1</sup> )	1.05	Average sludge loading rate (kg COD kg <sup>-1</sup> TSS d <sup>-1</sup> )	0.17
Temperature (°C)	13.6 $\pm$ 1.2		

**Table 13** COD, TN and phosphate concentrations in the feed solution, the sludge supernatant and/or the permeate as well as their nutrient ratio and the removal efficiencies (%). Values are given as (mean  $\pm$  standard deviation). sCOD = soluble COD.

Parameter	Feed solution	Sludge	Permeate	Removal efficiency (%)
COD (mg O <sub>2</sub> l <sup>-1</sup> )	823.1 $\pm$ 202.3		71.2 $\pm$ 10.2	90.9 $\pm$ 2.9
sCOD (mg O <sub>2</sub> l <sup>-1</sup> )		98.2 $\pm$ 20.9		
TN (mg TN l <sup>-1</sup> )	132.8 $\pm$ 39.5		70.7 $\pm$ 33.1	49.3 $\pm$ 22.9
P (mg PO <sub>4</sub> <sup>3-</sup> -P l <sup>-1</sup> )	9.9 $\pm$ 3.7		8.4 $\pm$ 2.0	25.5 $\pm$ 11.8
COD:N:P	100:17:1		100:138:18	

 Summarized, the HT-MBR started to show steady-state behaviour at the end of Fouling Period 2. The activated sludge pH provided the required membrane surface charges. The bioreactor exhibited normal biomass concentrations with irregularly shaped flocs and good carbon, nitrogen and phosphate removal efficiencies over the complete experimental period, but the activated sludge settled poorly due to proliferation of filamentous bacteria. This might among others be due to an unevenly distributed oxygen supply within the bioreactor. Moreover the sludge was inhabited by a series of non-bacterial microorganisms. Thus overall the sludge was of good to moderate quality and the membranes seemed to fully retain microorganisms from the sludge suspension.

## 2. MEMBRANE PERFORMANCE MEASUREMENT

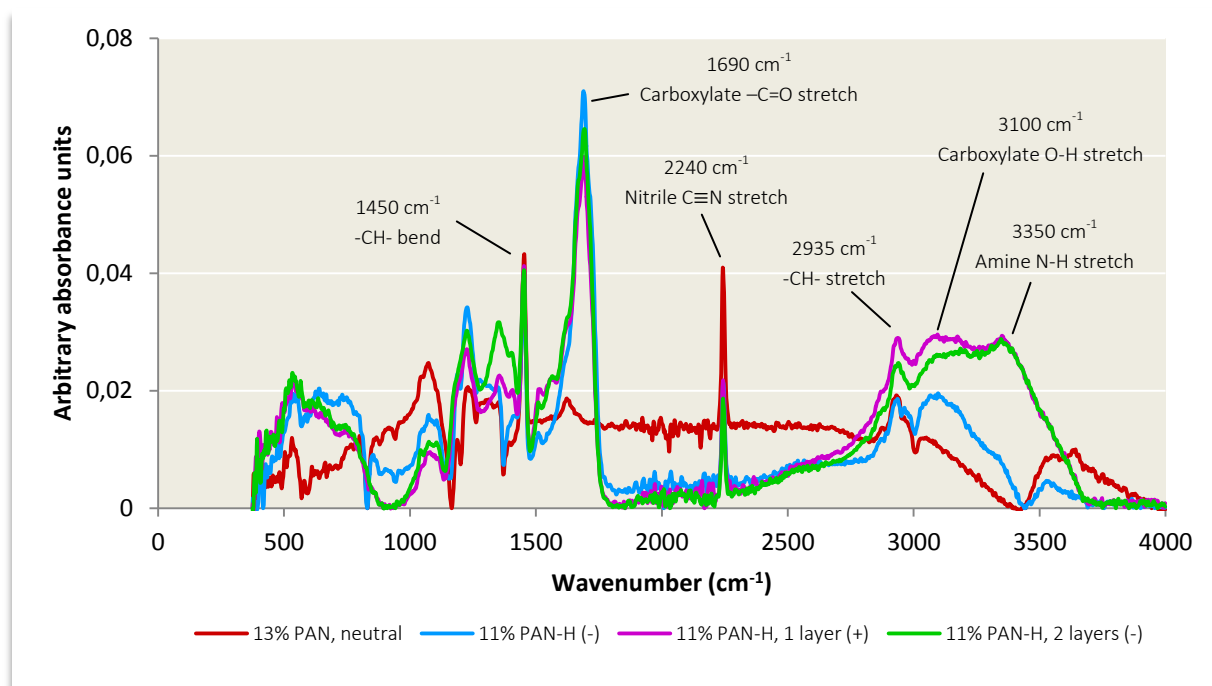
### 2.1. Physico-chemical related measurements

#### 2.1.1. Attenuated Total Reflectance Fourier Transform Infrared Spectroscopy

**Figure 24** gives the ATR-FTIR spectra of the P-membranes. The ATR-FTIR spectra of the C-membranes are given in **Section 2.1.1** of **Appendix 1**, together with the discussion. The absorbance values correspond to typical literature values (from below 0.010 to 0.35), although most authors do not indicate absorbance values or units on their graphs. The 13% PAN (neutral) membranes show three important peaks at 1450 cm<sup>-1</sup>, 2240 cm<sup>-1</sup> and 2935 cm<sup>-1</sup>, corresponding to the (-CH-) bend of PAN backbone, the nitrile (C $\equiv$ N) stretching vibration of the membrane surface groups and the asymmetric (-CH-) stretching vibration of the PAN backbone, respectively [121], [126], [156].

The spectrum of the 11% PAN-H (-) membranes show the three same important peaks as the neutral membrane type. The hydrolysis procedure did not transform all surface nitrile groups into carboxylate groups since the peak at 2240 cm<sup>-1</sup> did not change significantly. Additionally, a prominent peak at 1690 cm<sup>-1</sup> can be noticed, corresponding to the carbonyl (-C=O) stretch vibration of the carboxylate surface groups, as well as a peak at 3100 cm<sup>-1</sup> corresponding to the carboxylate (O-H) stretch vibration. For instance Moya et al. (2001), Moharram et al. (2002) and Kirwan et al. (2003) assigned the carbonyl (-C=O) stretching vibration to FTIR-peaks in the range 1685-1725 cm<sup>-1</sup> [156]–[158]. The

shifting to lower wavenumbers could be attributed to an interaction between the ( $\text{-C=O}$ ) groups and the nitrile ( $\text{C}\equiv\text{N}$ ) groups remaining at the membrane surface after hydrolysis. As shown in **Figure 15** (**Chapter 3**) amide groups ( $\text{-CONH}_2$ ) could be produced during the first hydrolysis step and be subsequently transformed into carboxylate groups. However no amide group peak ( $1570\text{ cm}^{-1}$ ) [126] was present on the FTIR spectra, thus indicating the predominance of the carboxylate groups and complete hydrolysis.



**Figure 24** ATR-FTIR spectra of the four membrane types (P-membranes).

The 11% PAN-H, 1 layer (+) and 11% PAN-H, 2 layers (-) membranes exhibit the same peaks as the 13% PAN (neutral) and the 11% PAN-H (-) membranes. Indeed the application of one and two polyelectrolyte layers respectively on the 11% PAN-H membrane, interrupted with rinsing steps, may result in an incomplete coating of the membrane surface thus carboxylate and nitrile surface groups can protrude into the external environment. Moreover the polymers are believed to undergo interpenetration and rearrangement at the membrane surface in function of the  $pH$  of the solution, thus being present at an equal volume fraction, independent on which polymer was deposited first [159]. Additionally, the membranes exhibit a peak at  $3350\text{ cm}^{-1}$ , corresponding to the asymmetric amine (N-H) stretch [158].

✨ Summarized, the ATR-FTIR results show the presence of the required functional groups on the membrane surfaces which provide them with neutral ( $\text{C}\equiv\text{N}$ ) or charged properties ( $\text{-COO}^-$ ,  $\text{-NH}_3^+$ ) in aqueous solutions or in the sludge suspension when these are characterized by a  $pH$  ranging between the  $pK_a$  values of the respective functional groups.

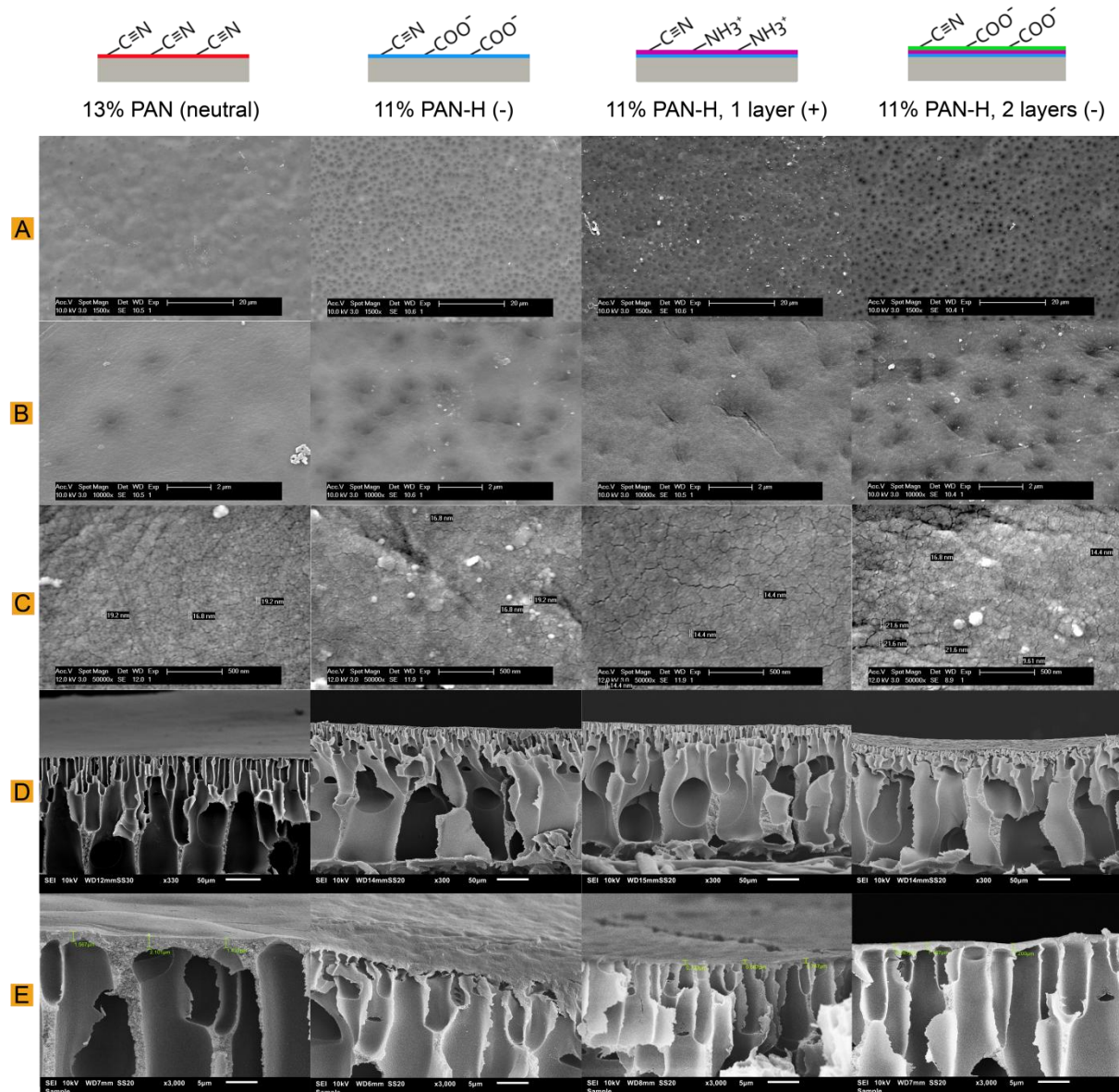
### 2.1.2. Scanning Electron Microscopy

**Figure 25** shows the surface and cross-sectional images of the four membrane types (P-membranes) at different magnifications. The SEM cross-sectional and surface images of the C-membranes are given in **Section 2.1.2** of **Appendix 1**, together with the discussion.

The cross-sectional images (D) of **Figure 25** show asymmetric integrally skinned membranes consisting of finger-like pores or macrovoids extending from just below the membrane surface to the Novatexx support over a distance of approximately 250  $\mu\text{m}$ , corresponding to the wet casting thickness during membrane manufacturing. This open porous structure developed after phase-inversion provides physical support for the selective top layer at the membrane surface, which can be hardly distinguished. The distance between the top layer and the top of the macrovoids, the so-called sub layer, ranges between 1.4 and 2.1  $\mu\text{m}$  for the 13% PAN (neutral) membrane and between 0.6 and 1.2  $\mu\text{m}$  for the 11% PAN-H (-) as well as for the 11% PAN-H, 1 layer (+) and 11% PAN-H, 2 layers (-) membranes (images (E) of **Figure 25**). As seen from the images (D) and (E), surface modification of the PAN membrane (hydrolysis or/and coating) may adjust membrane properties but do not alter the macroporous structure. The deposited PAH and PAA layers at the membrane surface cannot be distinguished on the cross-sectional images (E) since their individual thickness must range between 3 and 5  $\text{\AA}$  at  $pH$  6 (i.e., the  $pH$  of the rinsing solution during membrane synthesis) [159], [160]. Since membrane preparation for SEM is a meticulous work, some errors can occur during membrane fracturing, as has been the case for 11% PAN-H (-) (image (E) of **Figure 25**) where no clear cut was obtained. It had been better to dip the membrane in liquid nitrogen before fracturation.

Next, the surface images (A) and (B) exhibit a relatively rough structure consisting of depressions of approximately 600 nm diameter, which are apparently amplified as polyelectrolyte layers are coated upon the membrane surface (compare 13% PAN (neutral) to 11% PAN-H, 2 layers (-), images (A), (B) and (D) of **Figure 25**). Apparent increasing surface roughness with increasing number of deposited layers has already been reported [125]. The depression-like structures may be confused with pores, however these are not, nor artefacts due to sample preparation or to the SEM electron beam, as has been confirmed by AFM measurements (**Section 2.1.3**). Fritzsche et al. (1993) reported these depression-like structures to be caused by small macrovoid structures residing between 90 and 200 nm below the membrane surface above the larger macrovoids and originating from the phase inversion process (PAN concentration not mentioned) [44]. They may extend to the surface and cause ruptures around which the membrane surface is depressed due to rapid water intrusion into the fluid-like nascent membrane. However no such small macrovoids can be detected here on the cross-sectional images (E). Yet most authors mostly do report smooth surfaces of the PAN and PAN-H

membranes instead of structural depressions (e.g., [123], [125], [126]), but the final membrane morphology always is dependent on the coagulation bath temperature and the polymer concentration: lower temperatures and higher polymer concentrations (and thus higher viscosity of the casting solution) result in more dense and smooth surfaces [121], [122], [124].



**Figure 25** SEM surface and cross-sectional visualization of the four membrane types (P-membranes). (A) 10 kV, magnification 1500x, (B) 10 kV, magnification 10 000x, (C) 12 kV, magnification 50 000x, (D) 10 kV, magnification 300x or 330x, (E) 10 kV, magnification 3000x.

Ding et al. (2015) investigated the surface structure of PAN membranes made of different PAN concentrations and reported to distinguish pores at a 500x magnification for 8 wt% PAN membranes in DMSO, but not at higher PAN concentrations (12 wt%, 16 wt%, 20 wt%, 24 wt%) [124]. However here it is assumed that their designated pores might be artefacts of their membrane surface because of their large size. The real pores are actually only visible at magnifications 50 000x or higher and are



positioned between densely packed nodule or grainy like aggregates. Here the four membrane types seem to exhibit pore sizes in the range 9-21 nm (images (C) of **Figure 25**) and thus are designated as UF membranes. The small pore sizes explain the apparent absence of bacteria in the permeate (**Section 1.3** of **Appendix 1**) since most can be fully retained by the membranes. It has been reported that hydrolysis of PAN would decrease the pore size due to swelling [123], however this phenomenon was not observed here. Nevertheless exact pore size values are difficult to determine and magnification 150 000x would yield a better resolution; though no such performant equipment was available. Such small pores may also be partly obscured by the surface topography. For instance, Fritzsche et al. (1993) distinguished pores with diameter in the 12-20 nm range and reported their size to stay unchanged upon drying [44], and Panda et al. (2015) reported pore sizes between 11 and 18 nm [121]. The white spherical elements visible on the membrane surface at high magnification (images (C)) may be attributed to dust or other particles interfering during sample preparation.

*✨ Summarized, the pure and functionalized PAN membranes exhibited the typical finger-like macroporous structure obtained via the phase inversion technique with a very thin skin layer probably in the Å range and responsible for the overall membrane performance. Although literature reports mostly designate PAN and derived PAN membranes as smooth membranes, the surface depressions and valleys observed here, and which showed amplification as the number of coated layers increased, tell a different story. Thus the reason for their existence is still unclear, but they are certainly no artefact products of membrane preparation for SEM measurements, as confirmed by AFM measurements. The surface structure of all membranes at nm scale consisted of nodular aggregates with nm pores in between; the synthesised membranes are thus UF membranes.*

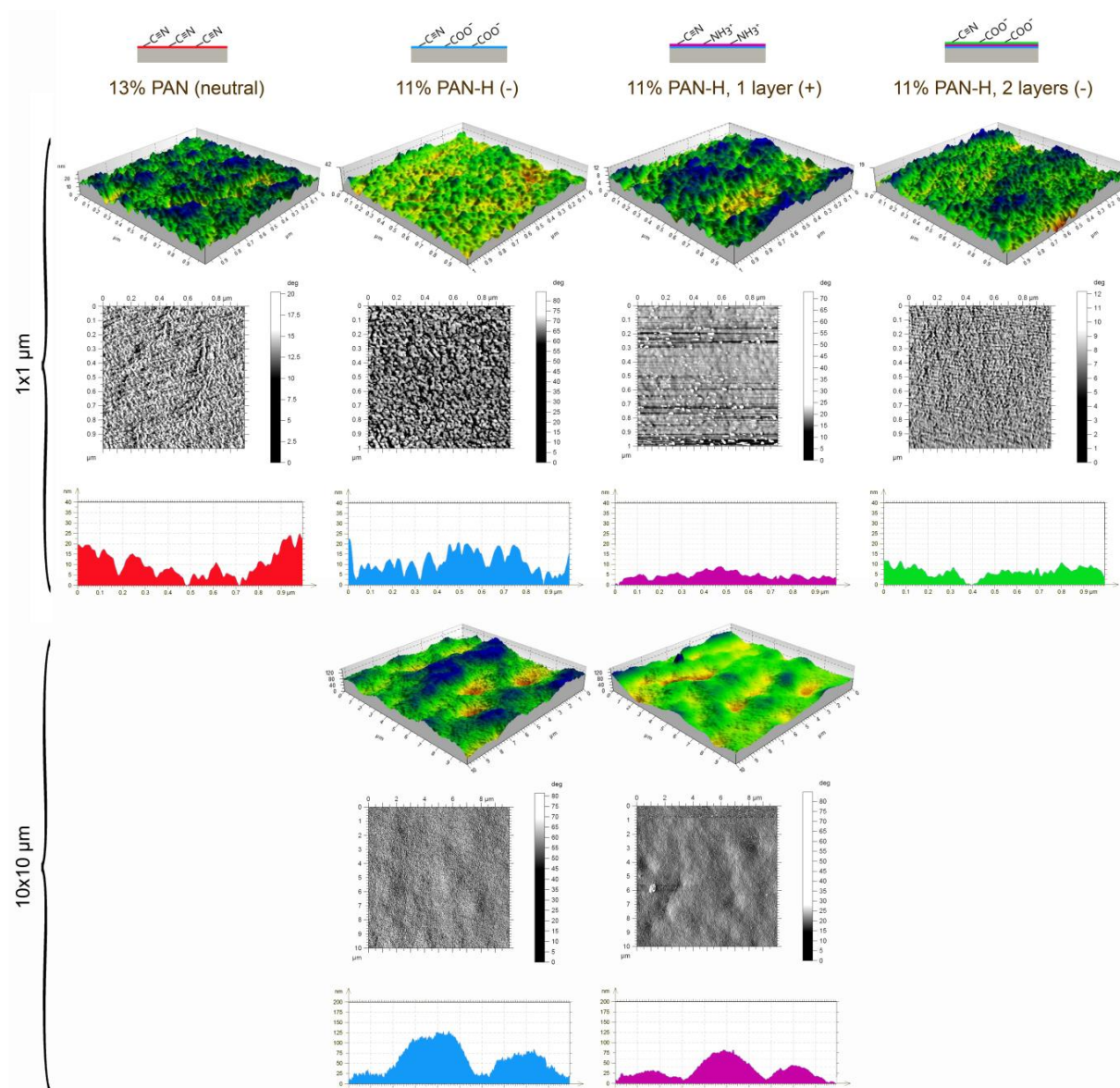
### 2.1.3. Atomic Force Microscopy

**Figure 26** represents surface images (3D and 2D respectively) as well as a profile of the upper surface region of the four membrane types (P-membranes) obtained via scanning of the surface at 1x1  $\mu\text{m}$  and 10x10  $\mu\text{m}$ . The images of the first and second row within each series (1x1  $\mu\text{m}$  or 10x10  $\mu\text{m}$ ) do not have the same scale bar. The 10x10  $\mu\text{m}$  images of the membranes 13% PAN (neutral) and 11% PAN-H, 2 layers (-) are missing due to an unfortunate mishap.

The AFM observations at 10x10  $\mu\text{m}$  (3D and 2D surface images) clearly indicate depression-like structures at the membrane surfaces, represented by colour (intensity) variations (blue regions being the highest regions, orange regions the lowest). These were already observed during SEM (**Section 2.1.2**). The observations thus indicate that they are no artefacts related to sample preparation for SEM measurements. Moreover these depressions do not reach the zero value of the z-axis on the profile images represented on the third row nor exhibit dark areas on the 3D images. This indicates that they



are no pores, as already concluded earlier. These conclusions are assumed to be equally valid for the 13% PAN (neutral) and 11% PAN-H, 2 layers (-) membranes.

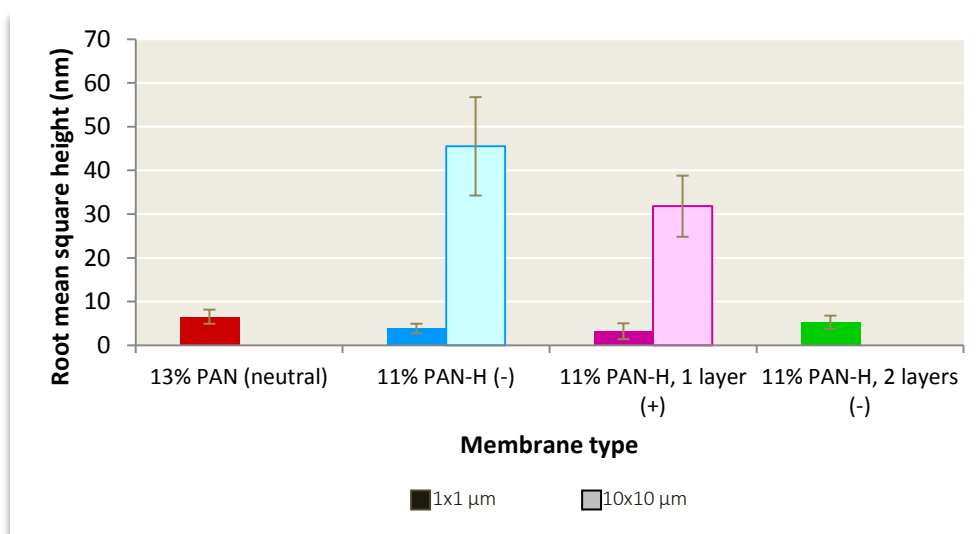


**Figure 26** Atomic Force Microscopy observations (2D and 3D) of the four membrane types at 1x1  $\mu\text{m}$  and of only two membrane types at 10x10  $\mu\text{m}$  surface areas (P-membranes). The first and second row of images within each series (1x1  $\mu\text{m}$  or 10x10  $\mu\text{m}$ ) represent the three dimensional and the two dimensional surface structure respectively. The third row of images within each series represents the profile structure of the upper surface region of the membranes.

The AFM images at 1x1  $\mu\text{m}$  scale indicate the presence of assemblies of nodule-like structures on the membrane surface and thus confirm the SEM observations. The actual pores are to be found between these nodules and are represented as small dark areas. Since they are assumed to have a diameter around 10-20 nm that does not shrink upon drying [44] they cannot be observed on the profile images of the 1x1  $\mu\text{m}$  images either. Though, the small profile segments extending to the zero-value of the z-axis might possibly be considered as pores that are not fully detected due to forces interacting

between the membrane surface and the AFM tip [44] or due to a lack of sensibility of the measurements (e.g., AFM tip too large or not sharp enough).

**Figure 27** gives the membrane roughness expressed as root mean square height. The 13% PAN (neutral) membrane had a  $R_{ms}$  of  $(6.5 \pm 1.6)$  nm at  $1 \times 1 \mu\text{m}$  scale. The 11% PAN-H (-) is characterized by a  $R_{ms}$  of  $(3.8 \pm 1.1)$  nm at  $1 \times 1 \mu\text{m}$  scale and  $(45.5 \pm 11.2)$  nm at  $10 \times 10 \mu\text{m}$  scale. 11% PAN-H, 1 layer (+) exhibited a  $R_{ms}$  of  $(3.2 \pm 1.8)$  nm at  $1 \times 1 \mu\text{m}$  scale and  $(31.8 \pm 7.0)$  nm at  $10 \times 10 \mu\text{m}$  scale. Finally the 11% PAN-H, 2 layers (-) membrane showed a  $R_{ms}$  value of  $(5.3 \pm 1.5)$  nm at  $1 \times 1 \mu\text{m}$  scale. Comparison between these values indicated no statistical difference in roughness between membrane types at  $1 \times 1 \mu\text{m}$  scale (Student's  $t$ ,  $0.05 < p < 0.80$ ). Thus the microstructure of the membranes stays unchanged after surface modification. For instance, Li et al. (2008), who coated PAN-H with bilayers of poly(diallyldimethylammonium chloride) and poly(ether ether ketone), reported the thickness of the aggregates and the surface roughness to increase as more than five bilayers were coated upon the membrane surface [125]. However, since here only 1 bilayer (PAH-PAA) was coated the surface roughness was not expected to increase. One of the reasons may be that the PAH and PAA polymer adopt a flat or train-like conformational arrangement upon coating, positioned closely to the surface [159]. Also at  $10 \times 10 \mu\text{m}$  scale no significant difference was observed between the 11% PAN-H (-) and 11% PAN-H, 1 layer (+) membranes (Student's  $t$ ,  $0.10 < p < 0.20$ ). However this observation cannot be extrapolated to the missing data and additional AFM measurements should be performed. Moreover SEM observations suggested an increase in surface roughness as the number of coated layers increased (**Section 2.1.2**). Nevertheless, if all membranes exhibit the same surface roughness, it will thus not be the cause of possible differences in bacterial attachment [96].



**Figure 27** Membrane surface roughness expressed as root mean square height (nm) for the four membrane types at  $1 \times 1 \mu\text{m}$  and for two membrane types  $10 \times 10 \mu\text{m}$  surface areas (P-membranes). Error bars represent standard deviations from the mean value ( $n = 3$ ).



☀ Summarized, AFM observations complement and confirm the SEM observations: the valleys observed at the membrane surfaces are inherent structures of the membranes, while the effective pores lie between nodular structures covering the surface at the nm scale. The membranes exhibited the same roughness at  $1 \times 1 \mu\text{m}$  scale indicating that the microtopography of the pure PAN membrane was not influenced upon modification and due to specific conformational arrangement of the coated polymers. The observations at  $10 \times 10 \mu\text{m}$  scale cannot be extrapolated to the missing data, but there might be an indication that the surface roughness is not significantly different either between membranes at this scale.

#### 2.1.4. Contact Angle Measurement

Figure 28 gives the contact angles  $\vartheta$  of the four membrane types (P-membranes) measured with d- $\text{H}_2\text{O}$ . The water drops were absorbed extremely fast by the dried membranes, indicating their hydrophilic character and wettability (i.e., wetting angles values below 90 degrees).

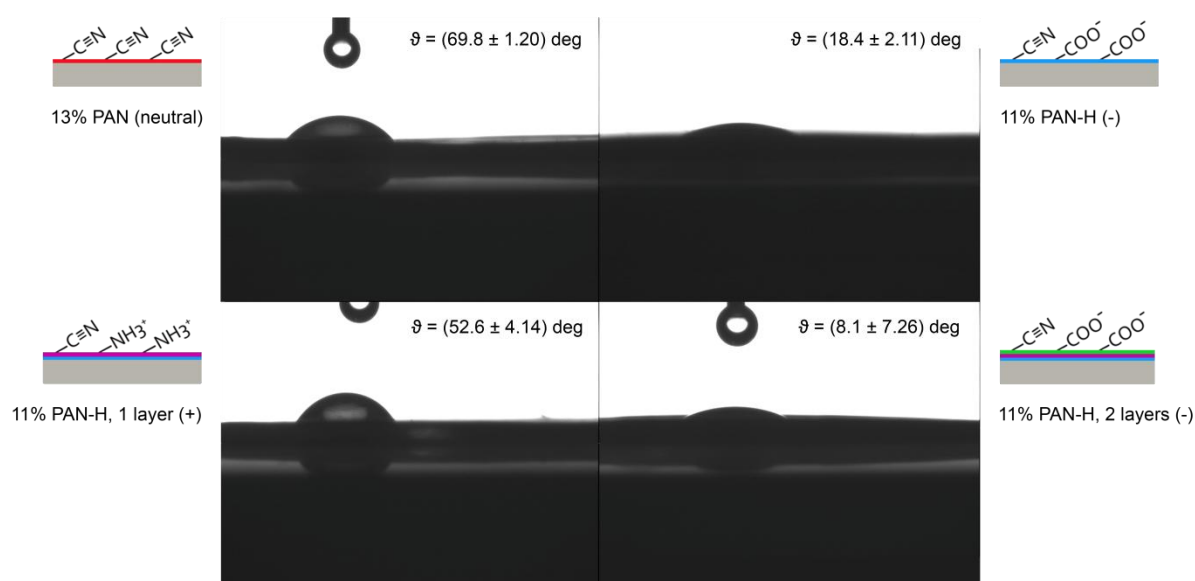


Figure 28 Contact angle images of the four membrane types (P-membranes) performed with d- $\text{H}_2\text{O}$ , and their respective contact angle  $\vartheta$ . Values are given as (mean  $\pm$  standard deviation) ( $n = 2 \times 3$ ).

As expected the pure PAN membrane (13% PAN (neutral)) showed to be more hydrophobic than the charged membranes with an average contact angle of 69.8 degrees. Values in literature are reported to vary between e.g., 47 degrees for 12 wt% PAN [124] to 76 degrees for 20 wt% PAN [121]. Ding et al. (2015) reported the degree of hydrophilicity of PAN membranes to be dependent on polymer concentration and phase inversion conditions [124]. They found that increasing polymer concentrations and higher coagulation bath temperatures render a more polar membrane surface, thus enhancing hydrophilicity.


The hydrolyzed PAN membrane (11% PAN-H (-)) showed increasing membrane wettability with an average  $\theta$  value of 18.4 degrees, due to the polar character of the carboxylate ( $-\text{COO}^-$ ) surface groups, thus facilitating hydrogen bonding with the water molecules [110]. The  $pH$  of the d- $\text{H}_2\text{O}$  drop used during the experiment was not measured, but it is assumed to be in the range 4.5-5.8 [161]. Indeed freshly produced d- $\text{H}_2\text{O}$  should have a  $pH$  of 7 due to the lack of ions, but during use it comes into contact with atmospheric carbon dioxide, thus reducing the  $pH$  to slightly acidic values. In this  $pH$  range, the carboxylic surface groups were ionized for 80-90 % [159].

The difference in degree of hydrophilicity between the positively and negatively charged coated membranes must be explained by a difference in charge of the PAN-H surface on the one hand and the charge density of the polyelectrolytes on the other hand. It has been reported that the surface wettability and thickness of weakly charged polyelectrolyte multilayers is strongly dependent on the  $pH$  of the rinsing solution used during layer-by-layer deposition, since it controls the charge density of the adsorbing polymers as well as the charge density of the previously adsorbed polymers [159]. However at  $pH$  6 (i.e., the  $pH$  of the rinsing solution used here during the layer assembly), PAH is fully protonated while PAA and the 11% PAH-H (-) membrane are almost fully protonated (80-90 %). In this  $pH$  region, both PAH and PAA polymers are reported to be deposited as very thin layers of approximately the same thickness (3-5 Å) due to spreading of the polymer chains over the surface instead of stacking upon one another [159]. Moreover the polymers are believed to undergo interpenetration and rearrangement at the membrane surface in function of the  $pH$  of the solution, thus being present at an equal volume fraction, independent on which polymer was deposited first [159]. Thus, although CAM theoretically only gives information on the degree of hydrophilicity of the outer layer of the membrane surface [78], it may be assumed here that the results are slightly influenced by the underlying charges (11% PAN-H (-) and/or 11% PAN-H, 1 layer (+)). These conclusions are further strengthened by the observations made during the electrokinetic characterization, explained later ([Section 2.1.6](#)).

In the  $pH$  range of the d- $\text{H}_2\text{O}$  drop used for the experiment ( $pH$  4.5-5.8), the degree of ionization of the carboxylic groups decreases ( $-\text{COO}^- \rightarrow -\text{COOH}$ ). This phenomenon is less pronounced for 11% PAN-H, 2 layers (-) than for 11% PAN-H (-). For instance, a statistical comparison of the wetting angles of both negatively charged membranes showed that the  $\theta$  value of 11% PAN-H (-) is significantly different from the  $\theta$  value of 11% PAN-H, 2 layers (-) (Student's  $t$ ,  $p < 0.01$ ), indicating that 11% PAN-H, 2 layers (-) is more hydrophilic than 11% PAN-H (-). Indeed, it has been reported that assembly of polyelectrolytes into a multilayered structure alters the dissociation constant ( $pK_a$ ) of the individual polyelectrolytes compared to their value in aqueous solution due to the influence of local electrostatic

forces after coating [128]. Burke et al. (2003) explained this phenomenon by assuming that the charged surface upon which the polyelectrolyte is coated, promotes protonation or dissociation of the deposited layer to neutralize the residual negative or positive charges respectively, and does this more strongly than repulsive forces between neighbouring groups resulting from this protonation or dissociation [128]. For instance PAA would experience a shift to lower pKa values (pKa 4.5 → 4.1), i.e., an increase in acidic strength [128], while 11% PAN-H (-) does not, explaining the difference in contact angle due to differences in degree of ionization of the surface charges.

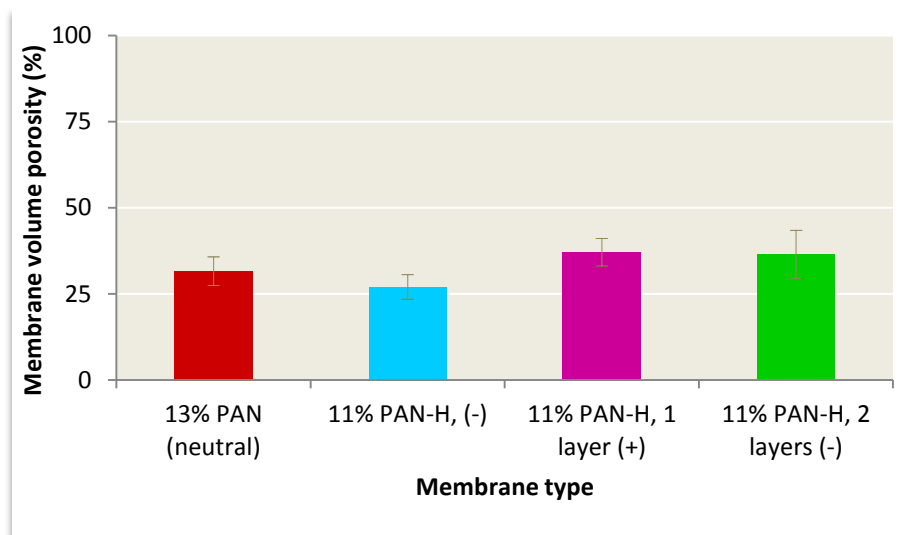
In contrast to PAA, the amino groups of PAH stay fully protonated in the *pH* range of the d-H<sub>2</sub>O drop used for the experiment (*pH* 4.5-5.8). But although the amount of PAA surface charges decreases slightly at *pH* 4.5-5.8 compared to PAH, this change is assumed to be almost insignificant. Therefore 11% PAN-H, 2 layer (-) is assumed to have a larger charge density than 11% PAN-H, 1 layer (+) due to its smaller atomic mass unit (compare 1.55E-25 Da for the monomer allylamine hydrochloride to 1.20E-25 Da for the monomer acrylic acid), thus explaining its more hydrophilic character. Indeed, both polymers bear one charge per monomer.

 Summarized, the neutral pure 13% PAN membrane, characterized by chemically inert nitrile (C≡N) surface groups, showed a higher degree of hydrophobicity than the functionalized charged PAN membranes, of which the polar character was provided by the carboxylate (-COO<sup>-</sup>) and amine (-NH<sub>3</sub><sup>+</sup>) surface groups at the *pH* of the test-water. The negatively charged 11% PAN-H, 2 layers (-) seemed to be the most hydrophilic membrane due to a shift in the dissociation constant of its surface carboxylate groups upon coating on the one hand, as well as a charge density difference on the other hand. These phenomena explain its larger hydrophilic character compared to hydrolyzed PAN and positively charged PAN membrane, respectively. Overall, due to interpenetration phenomena of the coated polymer layers, the CAM results are assumed to be slightly influenced by the charges of the underlying structures, and these observations are strengthened by electrokinetic characterization of the membranes. Thus based on the results presented here, it could be expected that the negatively charged membranes, which show the largest hydrophilicity, would foul more slowly than the positively charged membrane, and itself more slowly than the neutral PAN membrane, as explained previously in **Chapter 3, Section 3.4.2**. However, hydrophobicity is not the major parameter affecting fouling behaviour, as seen in **Section 2.2.2**.


### 2.1.5. Volume porosity measurement

**Figure 29** represents the volume porosity of the four membrane types (P-membranes). 13% PAN (neutral) exhibits a volume porosity of (31.5 ± 4.1) %. 11% PAN-H (-) exhibits a volume porosity of

( $27.0 \pm 3.6$ ) %. Finally 11% PAN-H, 1 layer (+) and 11% PAN-H, 2 layers (-) have a volume porosity of ( $37.1 \pm 4.0$ ) % and ( $36.5 \pm 7.0$ ) % respectively. Statistical comparison of the measurements shows no significant difference between the porosities of the membrane types (Student's t,  $0.10 < p < 0.80$ ), indicating that the surface modifications (hydrolysis, layer-by-layer deposition) did not alter the porosity. However it has already been reported that higher polymer concentrations result in membranes with a lower porosity [122], [124]. Thus it could have been expected that the 11 wt% PAN membranes would have been more porous than the 13 wt% PAN membrane. The porosities are higher than generally reported in literature for UF membranes (0.1-5% [38]). However Panda et al. (2015) reported a porosity of 25% for a membrane made of 20% PAN [121]. Since high polymer concentrations yield denser membranes, it can be assumed that the porosity values obtained here for 13 wt% and 11 wt% PAN membranes are accordingly reliable. High porosities yield high permeabilities, as has been observed indeed (Section 2.2.1 of this chapter).



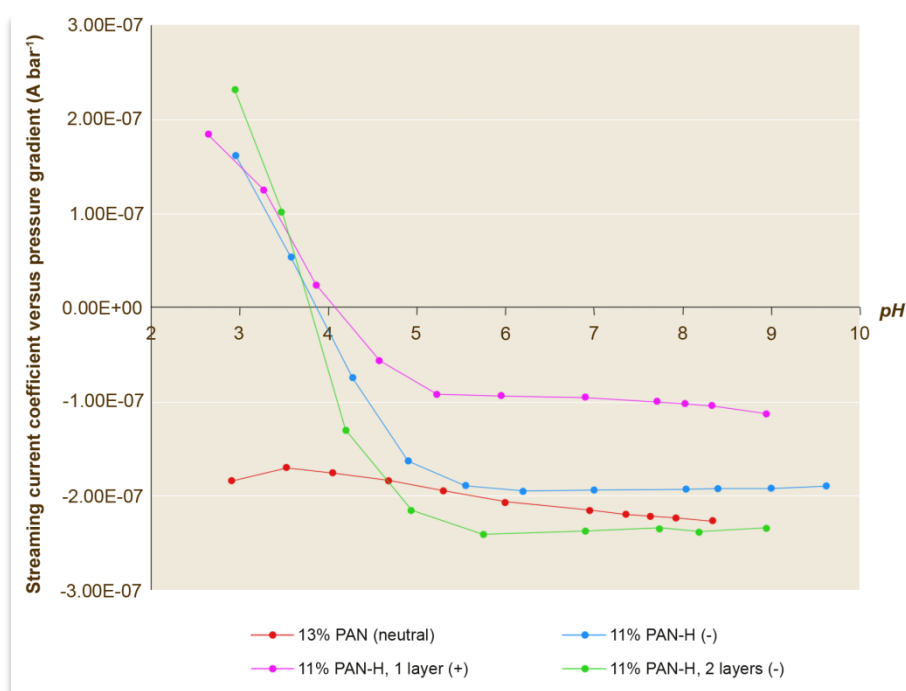
**Figure 29** Membrane volume porosity measurements (-) of the four membrane types (P-membranes) based on water uptake measurements. Error bars represent standard deviations from the mean value ( $n = 2$ ).

 Summarized, all membranes exhibited the same high volume porosity of around 30%, indicating that surface modification by hydrolysis and layer-by-layer deposition did not alter the membrane structure.

### 2.1.6. Electrokinetic characterization

**Figure 30** represents the streaming current coefficient in function of the  $pH$  of the electrolyte solution pumped tangential to the membrane surface of the four membrane types (P-membranes). The membrane samples as well as the non-woven support did swell considerably during the measurements and exhibited inconsistent results compared to expectations, as will be presented

below. Two explanations may be put forward. Firstly, according to Prof. Dhr. Szymczyk from the *Institut des Sciences Chimiques de Rennes* (France), who performed the electrokinetic measurements, it may be attributed to the pure PAN membrane itself which exhibits a relatively large finger-like structure, as observed during SEM (Section 2.1.2). The macroporous structure might be accessible to part of the streaming current, thus influencing the electrokinetic data. Secondly, it has already been reported previously that polymeric membranes swell in water when they have undergone surface modifications aiming at increasing their polar character [138]. However the non-woven support, which is made of hydrophobic polypropylene and polyethylene polymer fibres, should not swell in water and should exhibit a different electrokinetic response compared to the one obtained during the measurements. After a brief investigation, the producer indeed affirmed that the non-woven support has been treated with tension-active and antistatic agents as protection of the fibres from external damage. Trace amounts of these reagentia present at the surface of the non-woven support may alter the electrokinetic measurements.



**Figure 30** Streaming current coefficient ( $A \text{ bar}^{-1}$ ) versus  $pH$  for the four membrane types (P-membranes). The intersection of the curves with the x-axis corresponds to the isoelectric point.

Thus the swelling behaviour of the samples imply that a calculation of the  $\zeta$ -potential and charge density of the membranes based on the measurements may be unreliable since it would only give overall values for the porous composite membranes instead of information on the individual membrane surface characteristics [140]. However, assuming, but without proof, that the overall contribution of the non-woven support and the pure PAN membrane is identical for all membranes, the measurements do allow a relative comparison between the membrane types. The shape of the so-

called 'acid-base titration curve' [128] (i.e., plot of streaming current potential against  $pH$ ) and the position of the isoelectric point stay unchanged when plotting the  $\zeta$ -potential, calculated from the streaming current potential via the Helmholtz-Smoluchowski equation, against  $pH$ . If the non-woven support has a large contribution to the streaming current data, it will also have a large contribution to the derived  $\zeta$ -potential values. Though, Prof. Dhr. Szymczyk is considering performing electrokinetic measurements on the bare non-woven support as well as on free-standing membrane films in the near future in order to clear up the research question. The remainder of this section thus attempts to interpret the data collected so far.

As seen from **Figure 30** the charged membranes (11% PAN-H (-) as well as 11% PAN-H, 1 layer (+) and 11%-PAN-H, 2 layers (-)) do exhibit a different behaviour compared to the neutral 13% PAN membrane over the  $pH$  range considered, although all membranes show acidic behaviour [162].

The 13% PAN (neutral) membrane shows a stable negative charge independent on the  $pH$  of the electrolyte solution and does not have an isoelectric point, i.e., the data points do not cross the x-axis thus there is no  $pH$  where the  $\zeta$ -potential is equal to zero [133]. Among other studies [126], [139], Cho et al. (2012), who investigated the  $\zeta$ -potential of nanofibres made of 11 wt% PAN in DMF as solvent at a  $pH$  ranging between 5 and 8 and based on streaming current measurements, indicated almost exactly the same behaviour but without providing substantial explanation [137]. According to Prof. Dhr. Szymczyk, the observation made for the 13% PAN (neutral) membrane suggests the presence of strong acid functions onto its surface and may be the result of interference with the non-woven PP/PE support, since pure polyacrylonitrile is stable in aqueous solutions. However the studies mentioned above do not report the use of such kind of non-woven support, thus the explanation might be incomplete. A possible complementary explanation for the negative surface charges may also come from Kolská et al. (2013). They stated that water molecules might undergo intensified autolysis ( $2 H_2O \rightarrow H_3O^+ + OH^-$ ) at the surface of (highly) hydrophobic membranes and the  $OH^-$  molecules may adsorb preferably to hydrophobic, non-polar or chemically inert surfaces compared to the  $H_3O^+$  molecules. On the contrary, the  $K^+$  and  $Cl^-$  ions from the electrolyte solution are indifferent to these surfaces [138]. Moreover, rough surfaces, like of the PAN membranes (**Section 2.1.2**), have been reported to exhibit a strong influence on the  $\zeta$ -potential since the flow of the electrolyte solution over the membrane surface is not evenly distributed and may result in higher surface charges [138].

In contradiction to 13% PAN (neutral), all charged membranes exhibited the same behaviour with an isoelectric point around  $pH = 4$  and thus indicating that they bear a positive net charge at a  $pH < 4$  and a negative net charge at a  $pH > 4$ . Here the charge mechanism is dominated by the ionization or

dissociation of the surface groups ('intrinsic charges' [126]) instead of preferential adsorption of ions from the electrolyte solution [138]. According to Prof. Dhr. Szymczyk, the horizontal trend in the data points from around  $pH = 5.5$  suggests the presence of weak acid functions onto their surfaces, and indeed, the surface carboxylic are reported to be weak acids [128]. On the contrary the surface amine groups are weak bases, thus should exhibit a reversed S-shaped curve with a plateau at positive streaming current potential. Several observations can be made.

Firstly, the inflection point of the curves has been reported to be the point where the  $pH$  equals the dissociation constant ( $pK_a$ ) of the functional groups [128]. The trend represented by 11% PAN-H (-) has already been observed by Bao et al. (2009), who investigated the electrokinetic behaviour of hollow fibre hydrolyzed PAN membranes over the  $pH$  range 3-9 and in different electrolyte solutions [126]. As expected, most of the carboxylic surface groups (dissociation constant  $pK_a \sim 5$ ) are negatively charged at a  $pH > pK_a$ . However at low  $pH$  the membrane exhibits positive surface charges. The  $K^+$  ions from the electrolyte solution probably do not adsorb on the membrane surface [138] thus it cannot explain this increase in streaming current in acidic conditions. Bao et al. (2009) explain this phenomenon by a shrinking of the carboxylic groups at low  $pH$  [126]. Moreover the electrokinetic properties of 11% PAN-H (-) might possibly be explained by the contribution of residues from tension-active and antistatic agents on the underlying hydrophilized non-woven support, which were possibly not observable for the hydrophobic 13% PAN (neutral) membrane, thus leading to an overestimation of the real electrokinetic values [140].

Secondly, the  $pK_a$  value of the polymers PAH and PAA in solution are 8.7 and 4.5 respectively. Since the results shown in **Figure 30** indicate that their  $pK_a$  in the multilayer structure is around  $pH = 4$ , it seems to indicate a shift to lower apparent  $pK_a$  values. The observation corresponds partly with the ones made during the contact angle measurements (**Section 2.1.4**) and already reported by Burke et al. (2003) [128]. The trend shown by 11% PAN-H, 1 layer (+) membrane, coated with PAH as polymer layer, exhibits a reverse S-shaped curve compared to what has been reported in literature, as already mentioned above [128]. However the overall trend still is as expected since the membrane is positively charged at a  $pH$  below the apparent  $pK_a$  value of the coated polymer. The negative values at high  $pH$  might indicate the contribution of the hydrolyzed non-woven support and the PAN-H underlying membrane structure to the overall surface charge: once all amine groups are deionised (i.e., back to neutral state), the membrane becomes negatively charged due to deprotonation of the carboxylate groups of the PAN-H structure [162]. Finally the  $pH$ -dependency of the 11% PAN-H, 2 layers (-) membrane is as expected [128] since these membranes bear carboxylate surface groups and are thus negatively charged at a  $pH$  above the apparent  $pK_a$ . The positive charges at low  $pH$  may

indicate a substantial contribution of the underlying PAH layer to the overall surface charge, based on the same principle as mentioned above.

*✦ Summarized, the extensive swelling of the macroporous structures of the synthesized composite membranes (i.e., the chemically modified non-woven support as well as the pure PAN membrane), indicating their accessibility to part of the streaming current, did alter the electrokinetic measurements by providing data values only valid for the overall composite membranes. Subsequent derivation of the zeta potential and surface charge densities was not possible. Nevertheless the raw streaming current measurements suggest the presence of strong acid functions onto the surface of the neutral pure PAN membrane, and of weak acid functions onto the surface of the charged membranes. Conclusions on the pKa shift of coated layers drawn from the CAM measurements, might be confirmed here. However the underlying structures may have a substantial contribution to these observations. Future electrokinetic measurements on the bare non-woven support and the free-standing membrane films are planned in order to complete the data and explain the measurements.*

## 2.2. Permeability related measurements

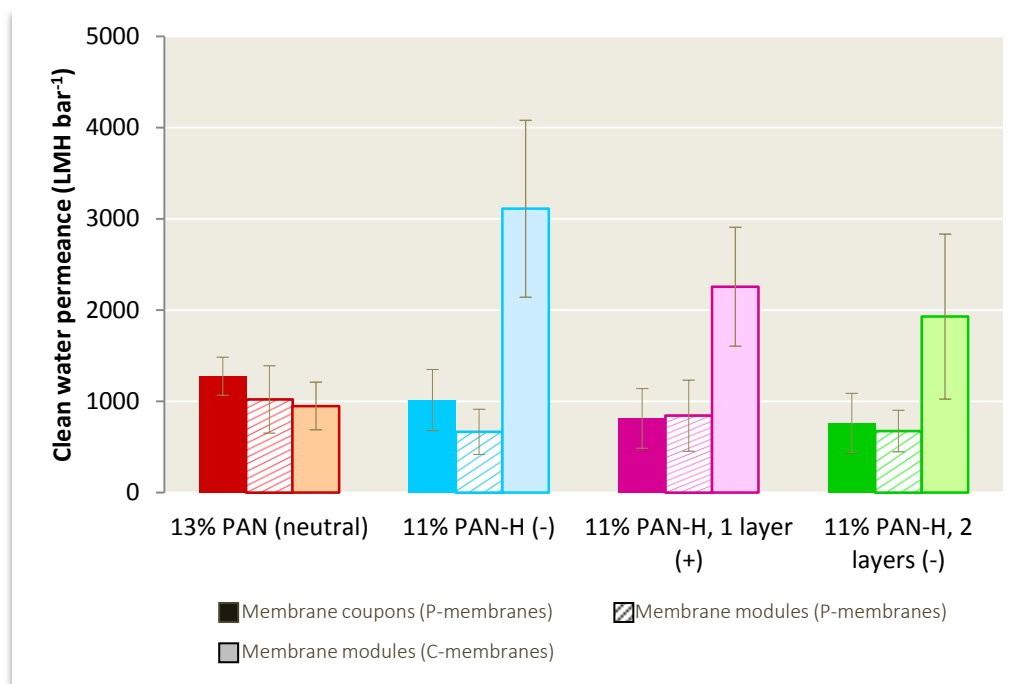
### 2.2.1. Clean water permeance

**Figure 31** gives the clean water permeability of the four membrane types, for both the P- as well as the C-membranes. The discussion on the permeability results of the C-membranes, as well as the calculated hydraulic resistances ( $R_m$ ) of the membranes are given in **Section 2.2.1** of **Appendix 1**. The permeabilities were not corrected to a standard temperature of 20 °C, but were all obtained by filtration at room temperature (fluctuating around 21.6 °C).


Statistical comparison of the permeabilities obtained by filtration of the coupons and filtration of the respective P-modules demonstrated that the CWP values of the coupons were not different from the modules, as expected, except for the membrane 11% PAN-H (-), where a statistical difference was obtained (Student's t,  $0.02 < p < 0.03$ ). However the choice of the threshold significance limit is arbitrary (here set at 95%). If a 99% confidence interval was chosen instead, no statistical difference would have been noted. The permeability values of the P-membranes fluctuate around an overall CWP value of 890 LMH bar<sup>-1</sup>. However most authors report pure water permeability values of around 210 LMH bar<sup>-1</sup> for 16 wt% PAN [124] and 250 LMH bar<sup>-1</sup> for 13 wt% PAN [122]. Thus the synthesised membranes are characterised by high permeabilities decreasing the need for severe pumping and reducing overall operational costs. Mutual statistical comparison of the coupons and the modules indicated a significant difference between the CWP values of the 13% PAN (neutral) and 11% PAN-H, 2



layers (-) coupons and modules (Student's  $t$ ,  $0.001 < p < 0.005$  and  $0.03 < p < 0.04$  respectively). This could be explained by the slight increase in membrane thickness upon layer-by-layer deposition, thus slightly decreasing the clean water permeability [37]. Moreover the swelling behaviour of PAA in contact with a solvent at  $pH$  5-7 (here : mQ-H<sub>2</sub>O) has been reported to decrease the membrane permeability [163].



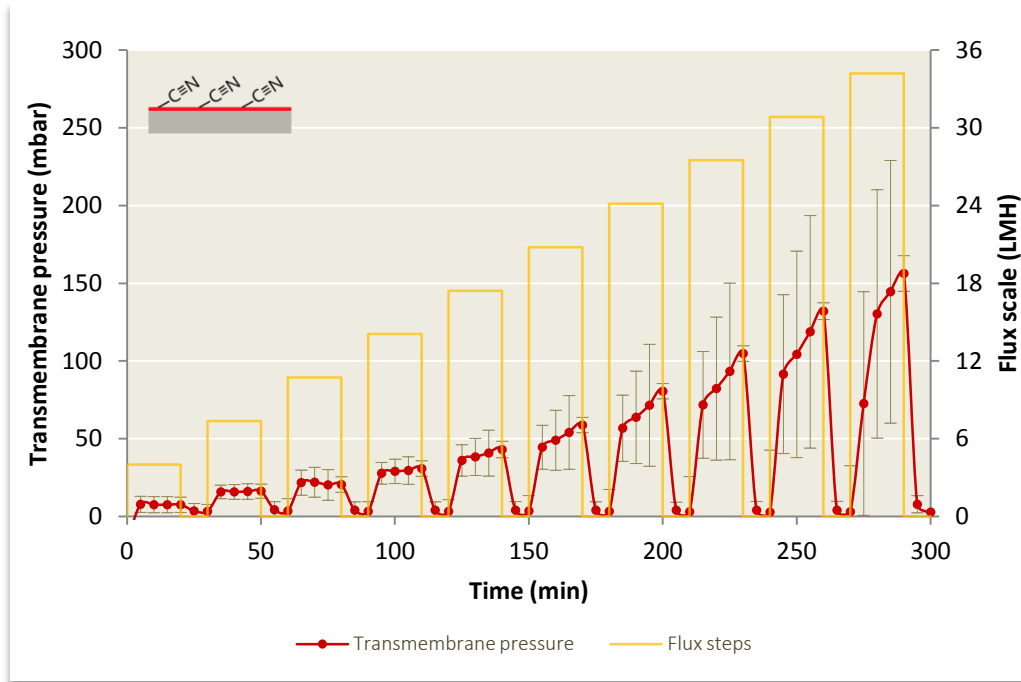
**Figure 31** Clean water permeance (LMH bar<sup>-1</sup>) of coupons (pristine) ( $n = 3 \times 3$ ) and modules (P- and C-membranes) ( $n = 4 \times 2$ ) of the four membrane types, performed with mQ-H<sub>2</sub>O. Error bars represent standard deviations from the mean value.

 Summarized, the membrane coupons and the respective membrane modules were characterized by the same high clean water permeance of around 890 LMH bar<sup>-1</sup>. Thus together with the observations and conclusions drawn from the physico-chemical related measurements (ATR-FTIR, SEM, AFM, CAM, volume porosity measurement, electrokinetic characterization), the initial requirement is fulfilled, namely to obtain neutral and charged membranes for which the fouling behaviour would be solely determined by charge difference or membrane material and not by differences in pore size (distribution), clean water permeability or surface roughness.

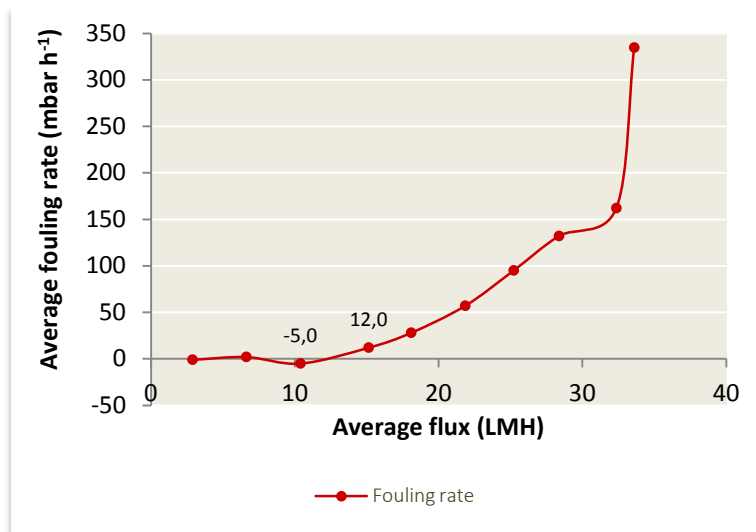
### 2.2.2. Critical flux

**Figure 32** shows the flux-stepping experiment performed on the 13% PAN (neutral) modules (C-membranes). **Figure 33** shows the evolution of the mean fouling rate in function of the applied flux, based on the measurements obtained during the flux-stepping experiment of the 13% PAN (neutral) modules. As seen from the graph, the fouling rate increased exponentially during the flux-stepping

experiment. The corresponding graphs for the cleaned 11% PAN-H (-), 11% PAN-H, 1 layer (+) and 11% PAN-H, 2 layers (-) membranes are presented in [Section 2.2.2 of Appendix 1](#). As the flux-stepping experiment advanced, the TMP of the membranes did not decrease immediately back to 0 bar when the permeate pump was interrupted at each flux-step, thus indicating that foulants gradually attached to the membrane surface and could not be removed simply by flux stoppage but the aeration shear forces had to interfere.



**Figure 32** Flux-stepping measurements on 13% PAN (neutral) modules (C-membranes). Error bars represent standard deviations from the mean value ( $n = 4$ ).



**Figure 33** Mean fouling rate ( $\text{mbar h}^{-1}$ ) versus average flux (LMH) as determined in the flux-stepping experiment on 13% PAN (neutral) modules (C-membranes) ( $n = 4$ ). The labels indicate the threshold limits for the critical flux determination.

As already mentioned in **Chapter 3 (Section 3.3.3)**, the critical flux value  $J_c$  can be determined based on a variety of approaches. The obtained  $J_c$  value was then extrapolated to the P-membranes, taking into account the observations made via SEM and the CWP measurements (**Sections 2.1.2 and 2.2.1 of Appendix 1**). Here it has been chosen to use a fouling rate threshold value to define the critical flux:  $J_c$  is the flux at which the fouling rate exceeds  $6 \text{ mbar h}^{-1}$ . The choice of threshold value corresponds to the one made by Le Clech et al. (2003). Although they used municipal wastewater to conduct their experiments and their TSS value was  $3 \text{ g l}^{-1}$  (i.e., two times lower than the values obtained here), they applied a HRT ranging between 16 and 24 and an infinite SRT, thus corresponding to the retention times applied here to the HT-MBR [59]. For instance for the cleaned 13% PAN (neutral) membrane,  $J_c$  lies between 10.4 and 15.1 LMH (**Figure 33**). Since this membrane type did not seem to undergo major modifications upon cleaning with NaClO, the  $J_c$  value of the pristine membranes is also assumed to lie between 10.4 and 15.1 LMH.

**Table 14** gives the critical flux values of the different membrane types, as well as the corresponding value corrected at a standard temperature of  $20 \text{ }^\circ\text{C}$ . Since all charged membranes exhibited an apparent increased surface smoothness (SEM), unchanged pore sizes (SEM) and an increased permeability or apparent porosity (SEM, CWP) upon cleaning with NaClO, and since these changes respectively increase, do not influence and decrease the critical flux value, it is assumed here that the critical flux values determined for the C-membranes are equally applicable on the P-membranes, since the relative contribution of the structural and morphological changes mentioned above remain uncertain.


**Table 14** Critical flux values at the operating condition of the HT-MBR as well as corrected to a standard temperature of  $20 \text{ }^\circ\text{C}$ , for the four membrane types. The values for the C-membranes were obtained via the flux-stepping experiments and based on a threshold fouling rate value of  $6 \text{ mbar h}^{-1}$ , and used for extrapolation of the critical flux values of the P-membranes.

Membrane type	Critical flux value at the operation temperature of the HT-MBR (LMH)	Correction of the critical flux value to a standard temperature of $20 \text{ }^\circ\text{C}$ (LMH)
13% PAN (neutral)	$10.4 < J_c < 15.1$	$12.0 < J_c < 17.4$
11% PAN-H (-)	$15.1 < J_c < 18.1$	$17.4 < J_c < 20.9$
11% PAN-H, 1 layer (+)	$10.4 < J_c < 15.1$	$12.0 < J_c < 17.4$
11% PAN-H, 2 layers (-)	$6.6 < J_c < 10.4$	$7.6 < J_c < 12.0$

Initial fluctuations in fouling rate at low fluxes, caused at the start-up of the flux-stepping experiment, were not taken into account when assessing the critical flux value. Thus only when the fouling rate started to show a consistent increase, suggesting fouling to occur, the values were considered. The differences in critical flux values may not be attributed to differences in porosity or pore size, since they are assumed to be the same (see previously, **Sections 2.1.2 and 2.1.5**), but to differences in



degree of hydrophilicity of the membranes. Madaeni et al. (1999) suggested that the  $J_c$  is larger for more hydrophilic membranes [39]. It can be observed here that the more hydrophobic membranes 13% PAN (neutral) and 11% PAN-H, 1 layer (+) have low  $J_c$  values compared to the more hydrophilic 11% PAN-H membrane, as determined by contact angle measurements (see previously, [Section 2.1.4](#)). However, as it was stated that 11% PAN-H, 2 layers (-) is the most hydrophilic membrane, it should exhibit the larger critical flux. Since it is not the case here, it could be stated that although efforts have been made to position the membrane replicates in the HT-MBR in such a way that they all experience the same conditions, the 11% PAN-H, 2 layers (-) modules may have been subjected to lower aeration shear forces than the other modules, thus increasing its initial fouling rate by rapid deposition of sludge particles onto the membrane surface. However, eventually all membrane types exhibited the same fouling rate, except 13% PAN (neutral) which seemed to have a larger fouling rate at high fluxes (compare [Figure 33](#) and [A-Figure 11](#), [A-Figure 13](#) and [A-Figure 15](#) in [Appendix 1](#)).

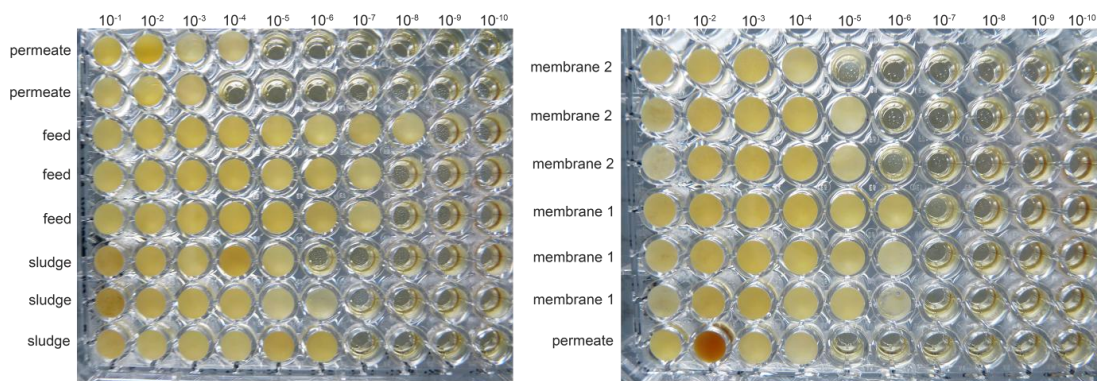
 Summarized, the critical flux values of the membranes were influenced by the degree of hydrophilicity of the membranes as well as positional aspects in the HT-MBR (uniformity of the oxygen supply). Since the bioreactor was operated at  $\sim 6.5$  LMH, i.e., in sub-critical region for all membranes, during both the Transient Periods and Fouling Periods, it thus can be concluded that no severe fouling was expected to occur during long-term operation. Thus the gradual and slow fouling experiments could be conducted without the need to clean the membranes chemically or to apply additional fouling control strategies other than intermittent cross-flow operation with relaxation.

### 3. BIOFOULING (COMMUNITY) CHARACTERIZATION

#### 3.1. Preliminary observations

##### 3.1.1. Bacterial enumeration

[Figure 34](#) represents the dilution series in TSA performed on the sludge, protamylasse feed, permeate and randomly chosen membrane samples. The sludge samples showed bacterial growth until dilution  $10^{-5}$  (1 replicate) and  $10^{-6}$  (2 replicates). The protamylasse feed samples taken at day 4 of the maintenance period, exhibited growth until dilution  $10^{-7}$  (2 replicates) and  $10^{-8}$  (1 replicate). The permeate samples showed growth until dilution  $10^{-3}$  (1 replicate) and  $10^{-4}$  (2 replicates). Finally the randomly chosen membrane samples, which were actually two replicate modules of 13% PAN (neutral) on Day 30 of the Fouling Period 2, showed growth until dilution  $10^{-5}$  (2 replicate),  $10^{-6}$  (3 replicates) and  $10^{-7}$  (1 replicate).



**Figure 34** Dilution series in Tryptone Soy Agar of the sludge, protamylasse feed (maintenance day 4), permeate and random two randomly chosen membranes (Day 30 of the Fouling Period 2) ( $n = 3$ ).

**Table 15** gives an estimate of the mean density of bacteria in the samples, expressed as Most Probable Number (MPN) value per ml sample. The membrane samples were not expressed this way since the sample was taken by scraping the membrane surface followed by resuspension in solution, thus the original bacterial density cannot be expressed per ml or converted per surface area of the membrane. In any case the membrane surfaces (i.e., pore channel fouling not taken into account) seemed to exhibit a bacterial density as high as the sludge. For instance, Ivnitsky et al. (2007) reported that the bacterial density on membranes are of the magnitude  $10^6$  colony-forming units (CFUs)  $\text{cm}^{-2}$ , regardless of the operating or hydrodynamic conditions of the MBR, the membrane type or the type of effluents it treats [164].

**Table 15** Approximate amount of bacteria in the sludge suspension, protamylasse feed solution from day 4 of the maintenance period, membrane surface and permeate, expressed as Most Probable Number (MPN)  $\text{ml}^{-1}$  sample.

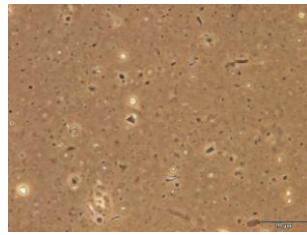
Sample	MPN $\text{ml}^{-1}$
Sludge	$4.65 \cdot 10^7$
Protamylasse feed solution	$2.15 \cdot 10^9$
Permeate	$4.65 \cdot 10^5$

The sludge seemed to house fewer bacteria than the protamylasse feed solution by a factor 100. However three remarks can be made.

Firstly, the feed sample tested here is from day 4 of the maintenance period. As mentioned previously, bacteria did develop in the feed tanks from the moment fresh feed was used until the moment the feed was replaced. Thus the bacterial density found here is only a snapshot at a certain time point: between day 1 and day 3, the density was less, between day 5 and day 8, the density was larger.


Secondly, the sludge was sonicated before inoculation in order to break the sludge flocs and disperse bacteria as much as possible in the medium (compare the sludge structure in **A-Figure 5** of **Appendix 1**

and in **Figure 35** after sonication). Microscopic analysis performed after the treatment showed well-dispersed cells and a decrease or even disappearance of filaments. There was no guarantee the bacteria did not die during sonication or were fully dispersed and randomly distributed within the sample after treatment. For instance it has been reported that the cell viability after sonication reaches 55% [165]. If a certain amount of bacteria was still clumped or if a numerable amount of bacteria died, the MPN value underestimates the actual bacterial density of the sludge. In this case, it is probably better to speak of an estimation of the CFUs instead of the amount of individual bacteria [142].



**Figure 35** Microscopic image of the sludge sample after sonication (magnification 1000x, oil objective).

Finally, as has already been mentioned previously in **Chapter 3**, only 1-15% of all bacteria present in activated sludge and introduced on laboratory media, are estimated to be cultivable [144], [145]. For instance, since TSA is a very rich medium, slow growing bacteria are outcompeted by rapid growers. Thus it could be estimated that the MPN value given here for the sludge must be multiplied by a factor up to 100 in order to obtain the real amount of cells in the samples. No such derivation has to be made for the permeate and the protamylasse feed samples, though. Indeed, it would be highly unlikely that enormous amounts of bacteria are present in the permeate. Indeed, the bacteria are retained by the membranes in the HT-MBR, as explained previously from the microscopic analysis (**Section 1.3 of Appendix 1**), and although no special attention has been drawn to keep the permeation tubes sterile (explaining the presence of bacteria), such high amounts of bacteria are not believed to be able to grow in nutrient deficient conditions (i.e., the bacteria in the bioreactor process the nutrients into new biomass). As for the synthetic feed solution, which is supposed to be free of bacterial contamination upon inoculation, it can be viewed as a sort of laboratory medium left under non-sterile conditions during the maintenance period. The high nutrient concentrations thus will enhance rapid bacterial development.

 *Summarized, based on the MPN technique, the activated sludge suspension seemed to house fewer bacteria than the protamylasse feed solution by a factor 100. Among others, the effect of sonication pretreatment on the cell viability as well as the low cultivability of bacterial members of natural*

samples may be possible explanations. The high number of bacteria detected in the protamylasse feed solution and the permeate are attributed to the non-sterile working conditions.

### 3.1.2. Membrane fouling rate

Figure 36 represents the evolution of the TMP of the replicate modules of 13% PAN (neutral) immersed in the HT-MBR during Fouling Period 1. The equivalent graphs for the other membrane types are presented in Section 3.1.1 of Appendix 1. As seen from Figure 36, the four membrane replicates did not foul at the same rate. The main explanation for this phenomenon is the badly distributed aeration of the HT-MBR, although a previous study [131] stated that positional effects for this particular reactor are minimal. While the replicates 3 and 4 experienced shear forces along their surfaces, replicates 1 and 2 were positioned in less turbulent zones thus the fouling layer could build up. However the replicates show large variations in their TMP trend. Thus it is assumed that the aeration conditions were quite variable even within the low-turbulence zone of the reactor. Also the effect of membrane sampling and subsequent removal of a small amount of biofilm material may explain the large variations within the TMP trend. The same trend can be observed in A-Figure 16, A-Figure 17 and A-Figure 18 in Appendix 1. Thus the two module replicates of each membrane type exhibiting the slowest fouling rate (e.g., module replicates 3 and 4 for 13% PAN (neutral) in Figure 36) were used for culture-independent biofouling community characterization (see later, Section 3.2.1). The other replicates were only used to keep the HT-MBR operated. The remainder of the discussion deals with the slow fouling membrane replicates.

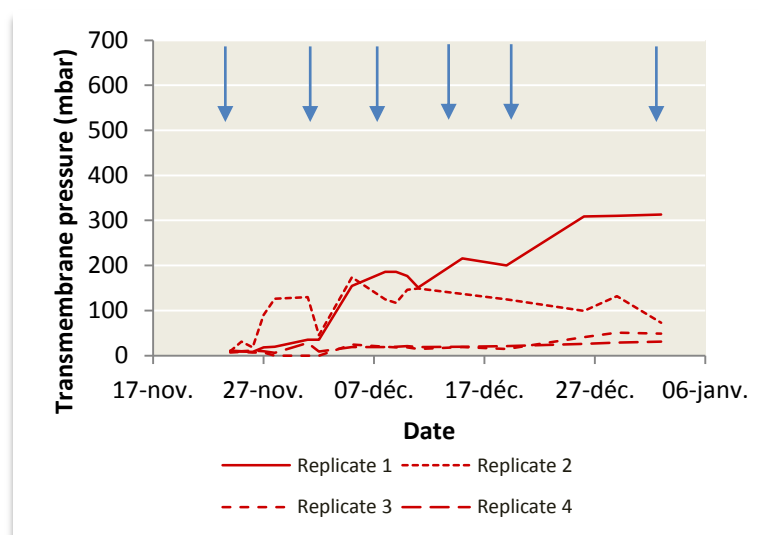


Figure 36 Evolution of the transmembrane pressure (mbar) of the module replicates of 13% PAN (neutral) during Fouling Period 1. Arrows indicate time points of biofilm sampling.


As seen on the Figures, the short-term ‘conditioning stage’ (Section 3.3 of Chapter 3) cannot be distinguished since the TMPs were recorded on a daily basis instead of every hour of the first day of





immersion. The time-evolution of the TMP was characterized by a slow and linear rise (the 'sustainable stage'), instead of a two-stage TMP profile often reported in literature, characterised by a sudden TMP rise [99] [7]. Indeed, this sudden TMP rise occurs when membranes are already highly fouled or in supra-critical conditions, but here the HT-MBR was operated at a flux below the critical flux of the sludge suspension (**Section 2.2.2**), explaining the low TMP increment with time. All pairs of membrane replicates seemed to foul at the same rate ( $0.32 \text{ mbar day}^{-1}$  on average), with the exception of 11% PAN-H, 2 layers (-) which exhibited a larger fouling rate ( $1.5 \text{ mbar day}^{-1}$  on average). Since the membrane modules were positioned the same way during the critical flux experiment (**Section 2.2.2**) as during the whole Fouling Periods, the conclusion drawn from the critical flux experiment can be extended here: although efforts have been made to position the membrane replicates in the HT-MBR in such a way that they all experience the same conditions, the 11% PAN-H, 2 layers (-) modules may have been subjected to lower aeration shear forces than the other modules.

Visual inspection of the biofilm layer in development on the membrane surfaces did not reveal major differences in structure, colour (brownish and relatively slimy) or coverage. However in the last week of Fouling Period 1, before the pump malfunctions did occur, several dark brown and disperse pustule or mushroom like structures developed on the membrane surface in a non-ordered way. Unfortunately no picture or sample has been taken of these structures, thus it can only be speculated that they may be of bacterial origin and may have originated from an intensively developing colony present in the surface biofilm or newly attached to the membrane surface.

 *Summarized, because of lack of uniformity in the aeration system of the HT-MBR, only two of the four module replicates per membrane type were used to characterize the biofilm structure and community composition. The chosen module replicates did foul linearly at an average fouling rate of  $0.32 \text{ mbar day}^{-1}$  and visually exhibited identical biofilms.*

## 3.2. Microbiological identification

### 3.2.1. DGGE fingerprinting of PCR-amplified 16S rRNA gene fragments

The DNA quantity of the sludge, membrane and feed samples obtained by means of Qubit measurements after PCR is presented in **A-Table 2** and **A-Table 3** of **Appendix 1**. The AGE gel obtained after electrophoresis of the PCR products is presented in **A-Figure 19** of **Appendix 1**, together with the designation of the lanes in **A-Table 4** and **A-Table 5**.

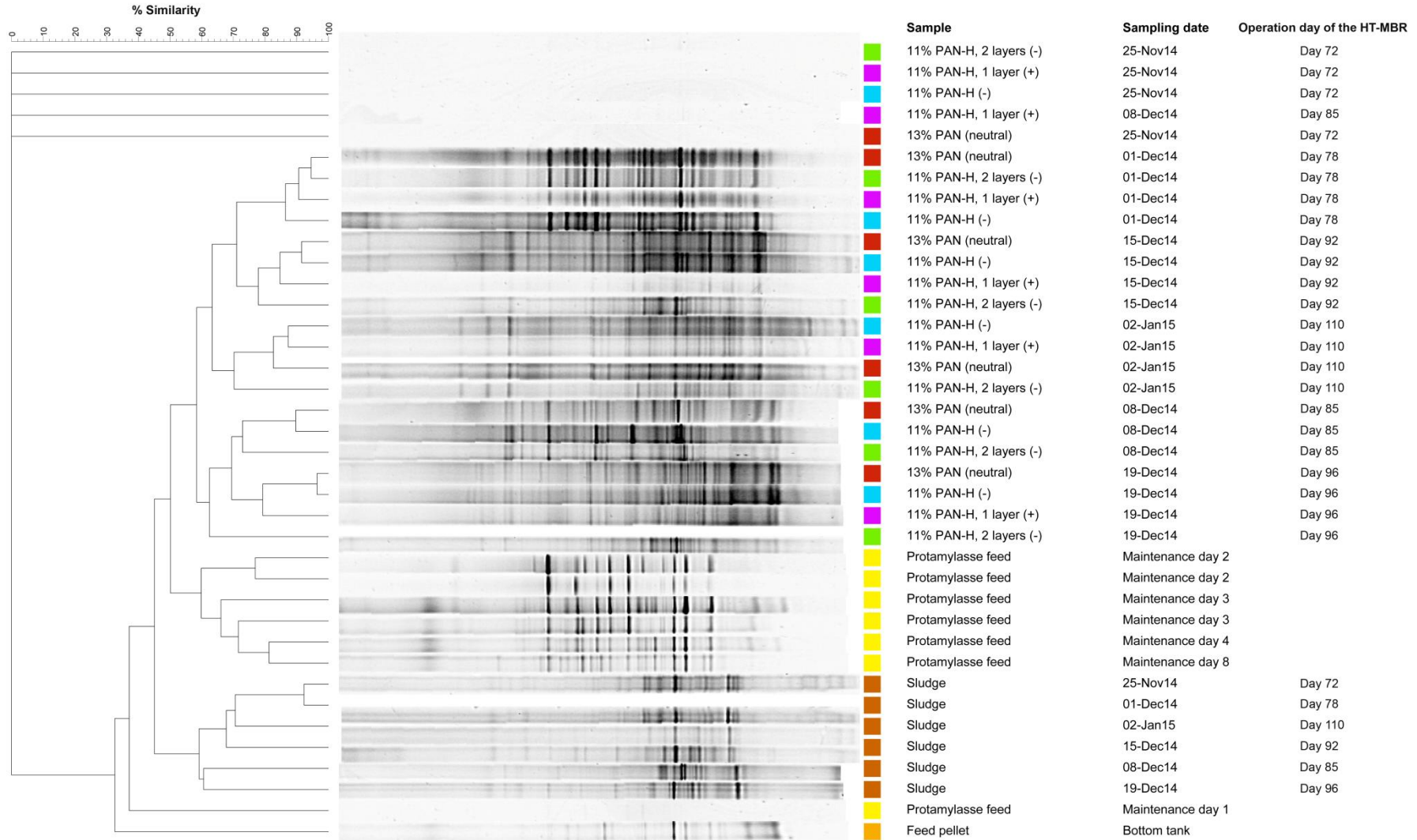
**Figure 37** represents the dendrogram constructed from the 16S rRNA gene community fingerprint of the membrane biofilms, the activated sludge and the protamylasse feed samples. Although numerous



intensive bands are distinguishable, representing the most dominant bacteria in the samples, some weak bands result in a smear unfit for analysis. Most of the sequences exhibited a similarity at the nodes of less than 90% (i.e., less than 90% of shared bands). **Figure 38** gives the number of Operational Taxonomic Units (OTUs) computed from the fingerprints of the four membrane types at every sample time point. Although it is assumed that each band in the fingerprint corresponds to a different OTU, some bacterial species could have the same G+C DNA content but a different base sequence, thus a single band could represent different species [148], [151]. Moreover one bacterial species could be represented by different fingerprints G+C sequence micro-heterogeneity and thus produce multiple bands [143], [151], [166]. Thus the number of OTUs only gives an approximation of the number and abundance of bacterial species within the community. Finally it must be said that PCR-DGGE is reported to only detect bacterial populations that make up at least 1% of the total community, thus bacterial populations present in very low abundance within the community are mostly excluded from the analysis [143], [149], [151].

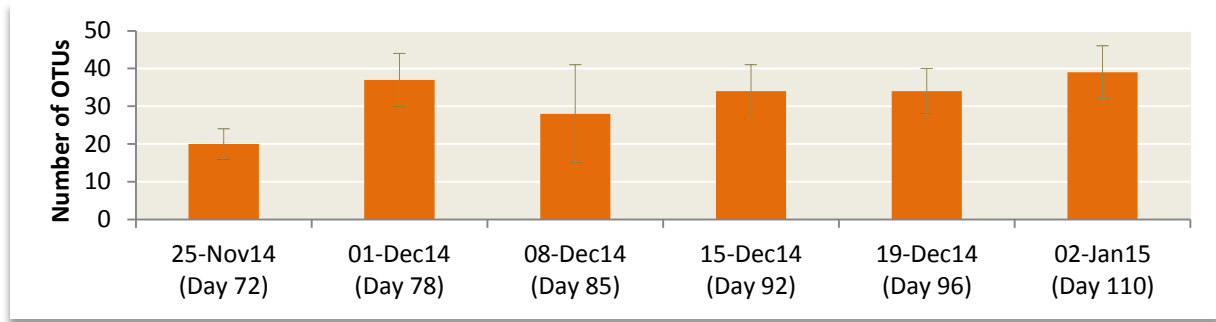
Firstly, based on **Figure 37** it may be stated that the planktonic community of activated sludge differs significantly from that of the protamylasse feed, and both differ significantly from the sessile community of the membrane biofilms, independently on the sampling time point or on the membrane type. Among other publications [89], [91], Huang et al. (2008) and Piasecka et al. (2012) already observed that most of the OTUs detected in planktonic biomass were not detected in the biofilm fingerprints [3], [6], or at least not in the same relative abundance [90]. While the  $\alpha$ -,  $\beta$ -,  $\gamma$ - and  $\delta$ -*Proteobacteria* are the dominant species found in biofilms, as mentioned previously in **Chapter 2 (Section 3.2.3)**, the activated sludge communities of both aerobic and anaerobic MBRs were reported to be dominated by  $\alpha$ -,  $\beta$ - or  $\gamma$ -*Proteobacteria* [6], [13], [64], [144], [145], [151] (e.g., *Pseudomonas* sp. which is reported to always be present in activated sludge [13], [14]), *Bacteroidetes* [6], [64] and Gram-positive bacteria characterized by a high G+C DNA content (generally > 50%) [145] (although some members have found to be low G+C [167]). The latter include the class of the *Actinobacteria* and more specifically the filamentous actinomycetes [8], [151], [168], to which *M. parvicella*, a filamentous bacteria predominant in sludge and already presented previously in **Section 1.3 of Appendix 1**, is related [28], [169]. However, since most of these bacteria have not been reported to colonize membrane surfaces, it explains the band clustering of the dendrogram. Moreover the sludge profiles exhibit small fluctuations over time during the fouling experiment (e.g., variation in relative abundance of common bands). It has already been reported that planktonic bacterial community function and structure in the sludge suspension are highly diverse but do fluctuate over time according the changes in conditions of the HT-MBR [3], [6], [64]. On the contrary the protamylasse feed solutions did not

**Figure 37** Bacterial 16S rRNA gene community fingerprints (DGGE profile showing differences in community structure and respective dendrogram) derived from membrane biofilms, activated sludge and protamylasse feed solution at different sampling time points of the Fouling Period 1 performed in the HT-MBR. The scale bar represents the percentage similarity at the nodes. The standard markers were removed from the DGGE profile for the sake of clarity.



undergo physical or chemical changes between day 1 and day 8 of each of the maintenance periods, allowing for a stable community to develop from day 1. As seen from **Figure 37**, the protamylasse feed sample of day 1 of the maintenance period differs significantly from the feed samples of the other days of the maintenance period, indicating it did not contain enough biomass as already supported by microscopic investigation (**Section 1.3 in Appendix 1**). Finally the feed pellet developing at the bottom of the feed tank exhibited a lower microbial abundance and diversity than the feed samples taken from the solution.

Secondly the results reveal that the bacterial community of the membranes sampled on the first sampling time point (25<sup>th</sup> of November 2014, Day 72) differs significantly from the bacterial community of the membranes sampled at the other time points. The main reason might be that membrane sampling did not yield enough bacterial DNA product for analysis since the pristine membranes were only freshly immersed in the HT-MBR. Low DNA concentrations thus make it difficult to perform fingerprint comparison analysis. For instance, the number of OTUs of the samples from 25-Nov14 differed significantly from the number of OTUs of the other membrane sample time points (Student's t,  $0.001 < p < 0.015$ ) (**Figure 38**). On the other hand, since fingerprint analysis did indicate the presence of a few fingerprint bands, it may indicate the development of a specific pioneer flora of on average 20 pioneering OTUs during the very first hours and days of biofilm development on the membrane surfaces that was eventually replaced by a different community later on. Piasecka et al. (2012) already reported the presence of 25 OTUs responsible for pioneering biofilm development in a MBR operated on molasses wastewater [6]. Only a specific set of species are known to be able to initiate biofouling and to eventually modify the surface characteristics of the membrane resulting in subsequent uniform fouling [6]. To cite two example studies, Zhang et al. (2006) found among others the *α-Proteobacteria* to be the major bacterial populations present in biofilms of just a few hours old [89], while Zhang et al. (2007) designated *Acinetobacter calcoaceticus* from the  $\gamma$ -subgroup of the *Proteobacteria* to be a good biofouling initiator [170]. Since these bacterial populations also are assumed to be some of the major populations in the sludge community (see above), it may be stated that the dominant bacteria from the sludge initiate biofouling, but are eventually competed out in mature biofilms, as already reported previously [6], [16], [171]. Indeed, the activated sludge suspension may favour some dominant bacterial species, while bacteria present in low abundances within the solution may grow preferably in nascent biofilms on the membranes due to e.g., protection from fluctuations in living conditions [171], thus becoming selectively enriched in biofilms [171]. However according to Zhang et al. (2006) specific bacteria rather than the bulk biomass of the sludge suspension are responsible for biofilm initiation [89].

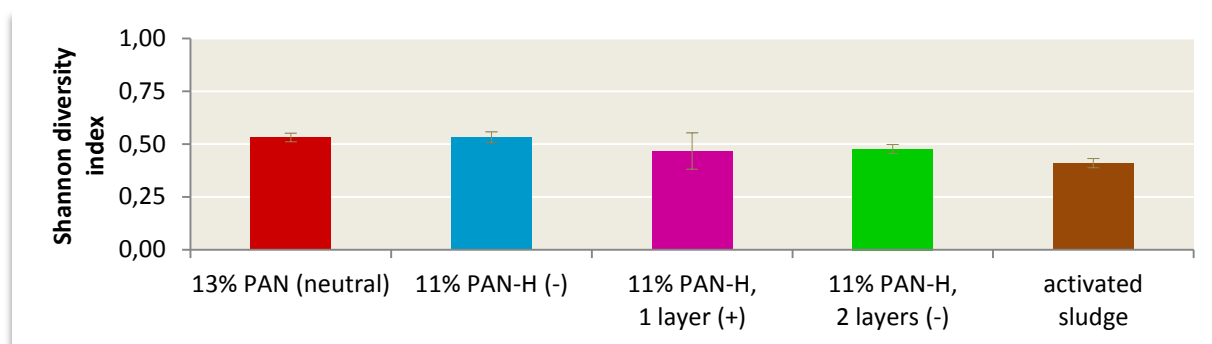


**Figure 38** Number of Operational Taxonomic Units derived from the number of bands in the fingerprints of the membrane samples taken at different time points. Error bars represent standard deviations from the mean value based on the band number of the four membrane types ( $n = 4$ ).

Next, the lack of branch similarity between membrane types on the 25<sup>th</sup> of November 2014 (since they do not cluster together) may indicate the influence of positional effects in the HT-MBR. For instance, oxygen deficiency that was likely to occur in the sludge suspension surrounding membrane 11% PAN-H, 2 layers (-) as already mentioned previously, could have modified the adhesion tendency of the microbial species [24]. The lack of branch similarity may indicate membrane surface effects (here: charge) as well in the selection of appropriate foulants. As explained previously in **Chapter 2 (Section 3.4.2)** 13% PAN (neutral) could have exhibited a lower fouling degree and biofilm diversity than 11% PAN, 1 layer (+) [96], and itself could have had a lower fouling tendency than the 11% PAN-H (-) and 11% PAN-H, 2 layers (-) membranes [117], due to the influence of the surface charge. However the surface effect would eventually fade out as the initial stages of fouling are surpassed due to deposition and accumulation of material which covers the membrane surface. Overall, it would have been interesting to perform a DGGE analysis on the two different membrane module replicates of the 25<sup>th</sup> of November 2014 instead of merging the replicate DNA samples before PCR. Additionally alternative fingerprinting techniques could be applied. A frequently used molecular technique is Terminal Restriction Length Polymorphism (T-RFLP) fingerprinting [6], [13], [14], [64], [171], [172], which is based on enzymatic digestion of fluorescently labelled PCR amplicons [173]. In combination with real-time quantitative Polymerase Chain Reaction (qPCR), which allows for enumeration of the amplified DNA extracted from the samples from both viable and death cells, and 16S rRNA gene-clone library construction and sequencing, it would allow for visualization of the OTUs responsible for biofouling initiation as well as for determination of the diversity and composition of the sludge and biofilm communities. This might have allowed visualization of differences in pioneering bacterial communities during the initial fouling stages, as to confirm above mentioned hypothesis statistically.

Finally, the results reveal that the bacterial community developing on the membranes differ between sampling time points but not between membrane types. This suggests that the relative abundance and structure of bacterial population changes with time due to interactions between members of the

biofilm as well as with the external environment (e.g., fluctuating operating conditions and hydrodynamics). These interactions modify the local biofilm environment with time by creating ecological protective niches within the biofilm based on physical gradients, leading to exclusion or favouring of existing members within the community [171]. *β-Proteobacteria*, or more specifically *Rhodocyclus*- or *Ralstonia*-related bacteria, were reported to be the dominant phylogenetic group in mature biofilms, although the relative dominance of the  $\alpha$ -,  $\beta$ -,  $\gamma$ - and  $\delta$ -*Proteobacteria* in biofilms may vary with time due to e.g., variations in mixed liquor viscosity or aeration rate [90]. For instance it has been reported that nutrient rich environments favour the  $\gamma$ -*Proteobacteria* against the  $\beta$ -subgroup [90]. Martiny (2003), who examined the development of biofilms in a drinking water system during three years, found that the biofilm communities did stabilize only after two years of operation [171]. However the fingerprints did not indicate an increase in bacterial species since no significant increase in OTUs was observed throughout the sample time points (Student's t,  $0.10 < p < 0.80$ ) (Figure 38). Moreover the observation suggests that although there might be a selective attachment of bacteria during the initial stages of fouling, the local characteristics of the membrane (here: charge) do not play a decisive role on the long term in selecting the key foulants. Nevertheless one could consider repeating the fouling experiment and using several HT-MBRs, each containing one membrane under the same operating conditions, instead of using a single HT-MBR containing all 16 modules. This would give guarantee that the MBR environment itself and the proximity of and thus possible mutual interaction between the modules did not play a significant role in the long-term selection of key foulants.




**Figure 39** Log-values of the Shannon diversity index for the membrane and activated sludge samples. Error bars represent standard deviations from the mean value calculated from the values homogenized over the different time points ( $n = 6$ ).

A comparison of the log-values of the Shannon diversity indices of the membrane, feed and sludge samples in Figure 39 indicate a statistical difference between the diversity of the membranes 13% PAN (neutral) and 11% PAN-H (-) compared to membrane 11% PAN-H, 2 layers (-) (Student's t,  $0.001 < p < 0.005$ ), while no statistical difference was found between 11% PAN-H, 1 layer (+) and 11% PAN-H, 2 layers (-) (Student's t,  $0.30 < p < 0.80$ ). As already mentioned previously in Sections 2.2.2 and 3.1.2, the



modules 11% PAN-H, 2 layers (-) may have been subjected to different aeration and turbulence conditions in the HT-MBR, resulting in a shift in the microbial community structure and diversity compared to other membrane types. According to expectations, the diversity of 11% PAN-H, 1 layer (+) should also differ significantly from the diversity of 11% PAN-H, 2 layers (-). However, probably because of the lack of bacterial DNA product yield from sampling, the banding patterns of 11% PAN-H, 1 layer (+) exhibited large differences in intensity compared to other membrane types (see the bands on the 8<sup>th</sup> and 15<sup>th</sup> of December 2014 in [Figure 37](#)), thus rendering fingerprint analysis relatively unreliable. Finally a comparison between the log-values of the Shannon diversity indices of the membranes and the sludge samples revealed a significant higher diversity for the membrane samples (Student's  $t$ ,  $p < 0.001$ ), except for 11% PAN-H, 1 layer (+) (Student's  $t$ ,  $0.1 < p < 0.2$ ). This inconsistency may be explained as done above. The observation is in contradiction with studies reported earlier [89] where the planktonic biomass exhibited a higher diversity than the biofilm community, but may be explained by a selective enrichment of specific bacterial species in the biofilm compared to the bulk biomass. Moreover these bacterial populations may make up less than 1% of the sludge community, thus remaining undetected by PCR-DGGE fingerprinting techniques. However, since all publications used here to support the observations, report the application of different operating conditions and the use of different membrane materials and wastewater types, generalizations are very difficult to make. As reported by Boon et al. (2002), the Shannon diversity index is only an indication of the diversity within a community rather than an absolute value [151].

 Summarized, since the planktonic communities of the activated sludge did exhibit differentiated branching in the dendrogram from the sessile communities of the biofilm, independently on the sampling time point or on the membrane type, it may be concluded that bacterial populations from the sludge suspension were selectively enriched within the biofilms. Dominant bacteria from the sludge may initiate biofouling, but are assumed to be eventually competed out in mature biofilms due to physical and chemical changes of the local biofilm environment. Moreover, the membrane samples exhibited a higher microbial diversity than the sludge samples at every time. Secondly variations in biofilm community structure and composition were monitored over time, suggesting that local variations in the biofilm and the gradual development of ecological protective niches favour or exclude specific bacterial populations. The largest time-dependent difference in amount of OTUs was observed between the samples from the first sampling time point (25-Nov14, Day 72) and the samples taken at the other time points, most probably explained by a lack of bacterial product suitable for analysis. Finally, the bacterial communities did not differ between membrane types at a certain sampling time point, suggesting that the membrane surface charges do not affect biofilm community composition. Although results tended to indicate small membrane surface effects on pioneering communities on the



*first day of immersion, the major explanation probably has to be found in the influence of positional effects within the HT-MBR, such as aeration issues. Thus, the local characteristics of the membrane (here: charge) do not play a decisive role on the long term in selecting the key foulants. However the experiment should be repeated with several HT-MBRs, each containing one membrane under the same operating conditions, instead of using a single HT-MBR containing all 16 modules, in order to confirm this hypothesis indisputably by excluding proximity effects. Moreover alternative and widely used molecular techniques, such as a combination of T-RFLP, qPCR and 16S rRNA clone library construction and sequencing, could be tested against PCR-DGGE fingerprint outcomes.*

### 3.3. Physico-chemical analysis of the biofilm

As already explained in [Section 2.2.1](#) of [Appendix 1](#), the fouling experiment during Fouling Period 2 was only performed on the cleaned 13% PAN (neutral) modules, since the other membrane types lost their structural and chemical properties due to extended cleaning with NaClO. At the end of Fouling Period 2 (Day 190) the fouled modules were removed from the HT-MBR and the biofilm structure was analysed using ATR-FTIR, SEM, AFM and CLSM.

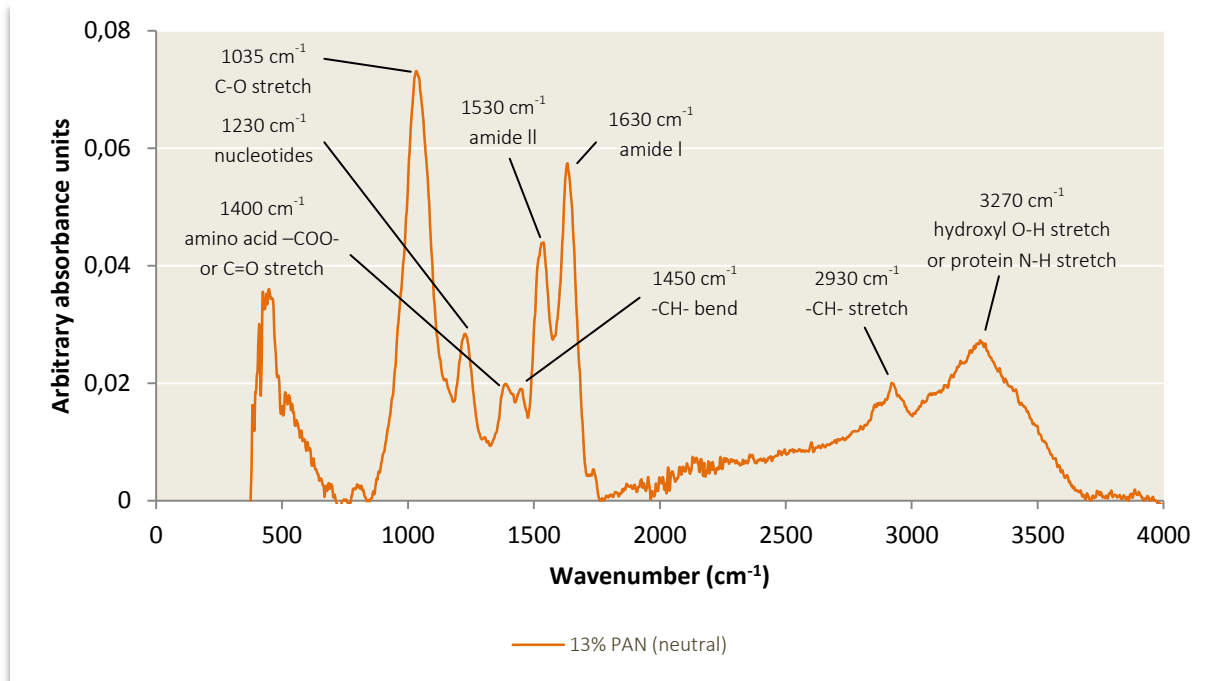
#### 3.3.1. Attenuated Total Reflectance Fourier Transform Infrared Spectroscopy

ATR-FTIR was performed in order to identify the main components of the biomass developing on the membrane surface. [Figure 40](#) represents the ATR-FTIR spectrum of the membrane foulants of 13% PAN (neutral) after a fouling period of 39 days, which differs considerably from the spectrum obtained of the pristine membrane ([Figure 24](#)).

The only two peaks that are still visible from [Figure 24](#) are the (-CH-) bend and stretch vibrations, at wavenumbers  $1450\text{ cm}^{-1}$  and  $2930\text{ cm}^{-1}$  respectively [76], [130], which could be attributed to the PAN backbone as well as to the carbon backbone of the biopolymers. The nitrile ( $\text{C}\equiv\text{N}$ ) functional group of the membrane material cannot be discerned anymore, suggesting the biofilm did cover the membrane surface well. However, since only a small surface area of the membrane was screened, it cannot be generalized to the whole surface coverage.


Proteins can be discerned from the peaks around  $1530\text{ cm}^{-1}$  and  $1630\text{ cm}^{-1}$  which are specific for the secondary conformation of proteins, called Amide II (N-H bend and C-N stretch) and Amide I (C=O stretch) respectively [24], [76], [130], [174]–[176]. Meng et al. (2010) reported that the peak at  $1630\text{ cm}^{-1}$  could also be attributed to aromatic compounds or humic-like substances [24]. Additionally the peak around  $1400\text{ cm}^{-1}$  corresponds to the asymmetric stretch of carboxyl (-COO-) or carbonyl (C=O) groups of amino acids [24], [176]. The hydroxyl (O-H) stretch is represented by the broad peak at  $3270$

$\text{cm}^{-1}$  [76]. However  $3270 \text{ cm}^{-1}$  could also be attributed to the (N-H) stretch vibration of proteins [174]. The peak around  $1035 \text{ cm}^{-1}$  may represent (C-O) stretch vibration of polysaccharides or polysaccharide-like substances [76], [175], [176]. Finally the peak around  $1230 \text{ cm}^{-1}$  can be assigned to the phosphate vibrations in nucleotides [175].



**Figure 40** ATR-FTIR graph of the fouling layer of membrane 13% PAN (neutral).

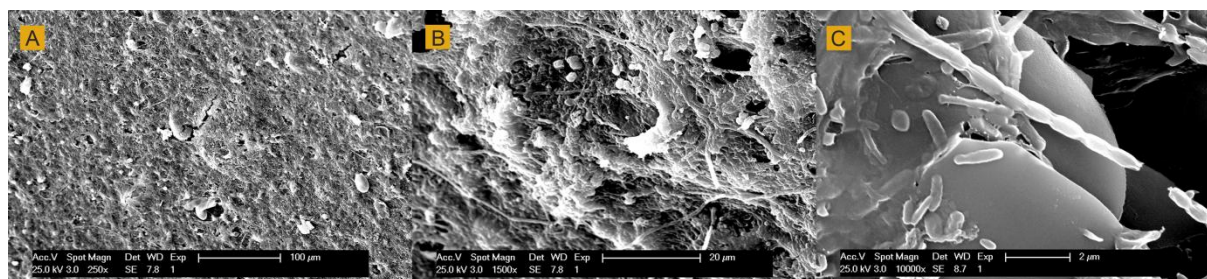
Small shifts in wavenumber values or band intensities compared to those reported in literature may be caused by differences in  $pH$  and ionic strength of the sludge, leading to conformational changes of the biopolymers [24] or by the presence of other substituents on the biomolecules [176]. All functional groups distinguished here suggest the presence of bacteria, protein and polysaccharide like substances (biopolymers, humic substances) in the cake layer, mostly originating directly from deposition of activated sludge material [130], and increase the degree of hydrophilicity of the biofilm, as already have been reported by Tansel et al. (2008) [98]. However Jinhua et al. (2006) reported that the degree of hydrophobicity of bacteria may even increase when attached onto the membrane, thus counterbalancing the relative increase in hydrophilicity of the biofilm and enhancing further bacterial attachment [24], [91].

 Summarized, the spectrum of the fouled membrane differs considerably from the spectrum of the pristine membrane and exhibits IR peaks mainly associated with bacteria (phosphate in nucleotides) and biopolymers (proteins, polysaccharides).




### 3.3.2. Scanning Electron Microscopy

SEM was performed in order to visualize the morphology of the biofilm and determine the composition of the biofilm. **Figure 41** shows the rough three dimensional structure of the biofilm developing on the surface of the 13% PAN (neutral) membrane after 39 days of fouling. A comparison of image (B) of **Figure 41** with image (A) of **Figure 25** indicates that the biofilm and deposited particles covers the membrane surface well since the surface features of the pristine membrane cannot be discerned anymore. Moreover the images show a clear size difference between the components of the biofilm ( $\mu\text{m}$  range) and the depressions and pores (nm range) of the pristine membrane, illustrating why the membranes were capable of retaining particulate matter and bacterial species from the sludge suspension and the biofilm. A number of spherical and rod-shaped bioparticles (e.g., *Bacillus* sp.) as well as a network of filaments could be distinguished, embedded in a matrix of what it is assumed to be biopolymers (EPS) or an artefact of SEM preparation (see for instance the viscous-like structure surrounding the chains of rods in image (C) of **Figure 41**). Although SEM gives information on the biofilm structure and allows for discrimination based on size and shape of the particles, it only gives little information on the nature of the foulants (organic, inorganic) or on the specific bacterial species. Moreover the rather stringent SEM pretreatment may alter the original structure of the fouling layer [24]. Nevertheless SEM provides enjoyable images of the biofilm.



**Figure 41** SEM surface images of the fouling layer of membrane 13% PAN (neutral) at magnifications 250x (A), 1500x (B) and 10 000x (C) and 25 kV.

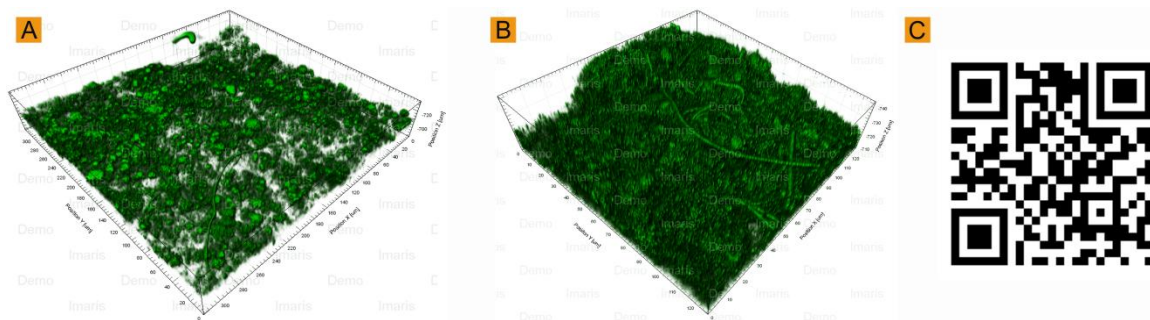
 Summarized, the SEM images of the fouled membrane differ considerably from the SEM images of the pristine membrane. The three-dimensional rough structure of the biofilm, consisting of organic and inorganic material and embedded in a polymeric matrix, covers the membrane surface completely.

### 3.3.3. Confocal Laser Scanning Microscopy

**Figure 42** represents the three dimensional architecture of the biofilm developing on the membrane surface of 13% PAN (neutral) after 39 days of operation and at different magnifications. It also gives access to a Youtube video highlighting the three dimensional composition of the fouling layer by migration of the fluorescence signal over the cake depth, apparently without signal distortions or loss

of fluorescence with depth. The images are represented in green, since for any undetermined reason staining and visualisation with SYTO 62 failed. The apparent loose coverage of the biofilm at magnification 40x (image A) may be due to background subtraction in order to eliminate background noise. Background subtraction was also applied on image B, but since the image was taken at another location of the biofilm, the effect seems to be less pronounced.

The biofilm was approximately 45  $\mu\text{m}$  in height dependent on the location on the membrane surface. It has been reported that the biofilm thickness does not depend on the operating conditions of the MBR, but tend to converge to the same order of magnitude, influenced by the balance between nutrient level, shear forces and transmembrane pressure [3], [164]. The bottom of the biofilm is uneven since the membrane surface was not smooth either (Sections 2.1.2 and 2.1.3) (the membrane surface is not visible since it was not stained).



**Figure 42** CLSM images of the biofouling layer of membrane 13% PAN (neutral) at magnifications 40x and 320x320  $\mu\text{m}$  surface area (A) and magnification 100x and 125x125  $\mu\text{m}$  surface area (B). The QR code<sup>33</sup> (C) gives access to a Youtube video highlighting the three dimensional structure of the biofilm (100x) by migration of the fluorescence signal over the cake depth. The images and the video were processed by means of the software evaluation version of Imaris Bitplane.


The biofilm was dense and mainly composed of discrete clusters of apparently a few dominant bacteria on different locations and at different heights spread across the membrane surface, as can be clearly seen in the video (QR code in Figure 42). The apparent low diversity may be in contradiction with the fingerprinting results which suggested a highly diverse biofilm. Since the samples were not fixated prior the CLSM analysis, a considerable amount of biofilm material may have been lost. However, the discrete bacterial clusters may be characteristic to biofilms in development since mature biofilms have been reported to consist of an even and smooth community structure without patches of independent populations [171]. Thus it suggests that each cluster or colony developed from one bacteria initially attaching onto the membrane surface or that bacteria seek each other and preferably assemble instead of living as simple individual elsewhere in the biofilm. Indeed, microorganisms can

---

<sup>33</sup> <http://youtu.be/96bUH84PlmM>

congregate by mutual detection and self-coordination based on the transfer of quorum sensing molecules, a small signal molecule called an autoinducer [24]. This molecule accumulates in the external environment when several bacterial members of the same species are present. When a certain threshold value is reached, which is proportional to a certain cell density, the autoinducer activates the transcription of specific genes, e.g., expressing surface adhesion proteins or excretion of EPS [6], [104], resulting in species with sessile phenotypes that are strongly different from their planktonic phenotypes [95]. For instance, it has been reported that the biofilm former *Pseudomonas aeruginosa*, a member of the  $\gamma$ -Proteobacteria, is strongly capable of cell density dependent gene regulation (e.g., in view of protection, transport, metabolism) [8], [95].

Image A (320x320  $\mu\text{m}$ ) and B (125x125  $\mu\text{m}$ ) of **Figure 42** depict the presence of an extended network of filamentous structures penetrating the biofilm with clearly visible septa between separate cells, possibly being filamentous fungi while the more tiny filaments somewhat detectable on image B and in the video might be of bacterial origin. Filamentous fungi, such as *Aspergillus* sp., have been reported to be capable of biofilm formation, as well as EPS production [177] and quorum sensing (e.g., related to sporulation) [178], although their biofilm formation mechanism differs slightly from biofilm initiation and development by bacteria [178]. But since they were only observed very sporadically in the activated sludge suspension by microscopic analysis (**Section 1.3 of Appendix 1**) it is rather unexpected to observe them in the biofilm. On the contrary, to my knowledge filamentous bacteria have not been reported to grow on membranes operated in an activated sludge suspension. The presence of bacterial filaments in biofilms has only been reported in applications where no membranes are used. For instance articles dealing with e.g., microbial fuel cells [179] and ultracompact biofilm reactors [180], used for the generation of electric power from organic matter and the treatment of wastewater respectively. They mentioned that the local conditions near the biofilm, such as low *pH* values, low DO concentration or low surface loading rates initiate filamentous overgrowth, and that once the filaments attach to the biofilm, further biofilm development is inhibited. Thus, although these observations do not apply to MBR membranes, there is no direct reason not to extend them to this specific environment.

 Summarized, the biofilm formed on the surface of the neutral pure PAN membrane had an average thickness of 45  $\mu\text{m}$  and was mainly composed of discrete clusters of bacteria, probably established via quorum sensing mechanisms and evolving towards a smooth mature biofilm community. Moreover an interpenetrating network of filamentous fungi and bacteria was observed, probably indicating some *pH* or other deviations from normal operation near the biofilm surface.



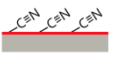

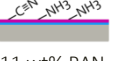
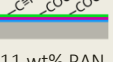


# Chapter 5: Conclusion & future prospects

## 1. CONCLUSION

The purpose of this study was to elucidate the relation between the specific surface charge (neutral, positive, negative) of polyacrylonitrile (PAN) membranes and the development and composition of the microbial community in the biofouling layer developed during 40 days in a submerged laboratory-scale aerobic membrane bioreactor (HT-MBR) operated on protamylasse feed. Four pure and functionalized PAN membrane types were used, each in four replicates, of which the principal characteristics determined in this work are summarized in **Table 16**. The membrane performances were determined based on physico-chemical related measurements (via ATR-FTIR, SEM, AFM, CAM, volume porosity measurement, electrokinetic characterization) and permeability related measurements (CWP, critical flux). The membrane biofouling was characterized based on molecular fingerprinting techniques (PCR-DGGE) and physico-chemical techniques (via ATR-FTIR, SEM, CLSM).

**Table 16** Overview of the membrane types synthesized and used in this work together with their physical properties determined via membrane performance measurements.

Membrane type	Surface charge	Surface modification	Module design	Pore size (nm)	Surface roughness (nm) at 1x1 $\mu\text{m}$ scale	Contact angle (degrees)	Volume porosity (%)	Clean water permeance (LMH bar <sup>-1</sup> )	Critical flux at 20°C (LMH)	Average fouling rate (mbar day <sup>-1</sup> )
 13 wt% PAN <sup>a</sup> in DMSO <sup>b</sup>	Neutral	/	FS <sup>c</sup>	9-21	6.5 $\pm$ 1.6	69.8 $\pm$ 1.20	31.5 $\pm$ 4.1	1169.0 $\pm$ 310.6	12.0-17.4	0.43
 11 wt% PAN in DMSO	Negatively charged	Hydrolysis	FS	9-21	3.8 $\pm$ 1.1	18.4 $\pm$ 2.11	27.0 $\pm$ 3.6	861.6 $\pm$ 345.4	17.4-20.9	0.29
 11 wt% PAN in DMSO	Positively charged	Hydrolysis + 1 deposited layer (PAH <sup>d</sup> )	FS	9-21	3.2 $\pm$ 1.8	52.6 $\pm$ 4.14	37.1 $\pm$ 4.0	826.7 $\pm$ 353.1	12.0-17.4	0.17
 11 wt% PAN in DMSO	Negatively charged	Hydrolysis + 2 deposited layers (PAH and PAA <sup>e</sup> )	FS	9-21	5.3 $\pm$ 1.5	8.1 $\pm$ 7.26	36.5 $\pm$ 7.0	721.9 $\pm$ 287.9	7.6-12.0	1.54

<sup>a</sup> PAN = polyacrylonitrile, <sup>b</sup> DMSO = dimethyl sulfoxide, <sup>c</sup> FS = flat sheet, <sup>d</sup> PAH = poly(allyl amine hydrochloride), <sup>e</sup> PAA = poly(acrylic acid)

The HT-MBR started to show steady-state behaviour at the end of the overall experimental period. The bioreactor exhibited normal biomass concentrations with irregularly shaped flocs and good carbon, nitrogen and phosphate removal efficiencies over the complete experimental period, but the activated sludge settled poorly due to proliferation of filamentous bacteria. This might among others be due to an unevenly distributed oxygen supply within the bioreactor. Moreover the sludge was inhabited by a series of non-bacterial microorganisms. Thus overall the sludge was of good to moderate quality and the membranes seemed to fully retain microorganisms from the sludge suspension.

**Membrane physico-chemical related measurements** revealed the presence of the required functional groups on the membrane surfaces (ATR-FTIR). They provided the membranes with neutral ( $C\equiv N$ ) or charged properties ( $-COO^-$ ,  $-NH_3^+$ ) at the  $pH$  of the activated sludge suspension. SEM measurements revealed typical finger-like macroporous structure with a very thin skin layer probably in the Å range and responsible for the overall membrane performance. The surface depressions and valleys observed at the surface of the membranes are certainly no artefact products of membrane preparation for SEM measurements, as confirmed by AFM measurements. The surface structure of all membranes at nm scale consisted of nodular aggregates with nm pores in between; the synthesised membranes are thus UF membranes. No apparent difference in surface roughness was observed between membrane types. CAM measurements indicated that the neutral pure 13% PAN showed a higher degree of hydrophobicity than the functionalized charged PAN membranes. The negatively charged 11% PAN-H, 2 layers (-) seemed to be the most hydrophilic membrane due to a shift in the dissociation constant of its surface carboxylate groups upon coating on the one hand, as well as a charge density difference on the other hand. Interpenetration phenomena of the coated polymer layers resulted in an influence of the charges of the underlying structures on the CAM and streaming current measurements. All membranes exhibited the same high volume porosity of around 30%, indicating that surface modification by hydrolysis and layer-by-layer deposition did not alter the membrane structure.

**Permeability related measurements** indicated that the membranes were characterized by a high clean water permeance of around  $890 \text{ LMH bar}^{-1}$ . Thus together with the observations and conclusions drawn from the physico-chemical related measurements (ATR-FTIR, SEM, AFM, CAM, volume porosity measurement, electrokinetic characterization), the initial requirement has been fulfilled, namely to obtain neutral and charged membranes for which the fouling behaviour would be solely determined by charge difference and membrane material and not by differences in pore size (distribution), clean water permeability or surface roughness. Since the HT-MBR was operated at a flux below the critical flux of the sludge suspension, the gradual and slow fouling experiments (average fouling rate 0.32

mbar day<sup>-1</sup>) could be conducted without the need to clean the membranes chemically or to apply additional fouling control strategies other than intermittent cross-flow operation with relaxation.

**PCR-DGGE fingerprinting** revealed that the planktonic communities of the activated sludge did exhibit differentiated branching in the dendrogram from the sessile communities of the biofilm, independently on the sampling time point or on the membrane type. Thus it may be concluded that bacterial populations from the sludge suspension were selectively enriched within the biofilms. Moreover, the membrane samples exhibited a higher microbial diversity than the sludge samples at every time. Secondly variations in biofilm community structure and composition were monitored over time, suggesting that local variations in the biofilm and the gradual development of ecological protective niches favour or exclude specific bacterial populations. The largest time-dependent difference in amount of OTUs was observed between the samples from the first sampling time point (25-Nov14, Day 72) and the samples taken at the other time points, most probably explained by a lack of bacterial product suitable for analysis. Finally, the bacterial communities did not differ between membrane types at a certain sampling time point, suggesting that the membrane surface charges do not affect biofilm community composition. Although results tended to indicate small membrane surface effects on pioneering communities on the first day of immersion, the major explanation probably has to be found in the influence of positional effects within the HT-MBR, such as aeration issues. Thus, the local characteristics of the membrane (here: charge) do not play a decisive role on the long term selection of the key foulants.

**Morphological visualization and chemical analysis** of the 40 days old biofilm grown on the 13% PAN (neutral) membranes revealed the presence of bacteria (phosphate in nucleotides) and biopolymers (proteins, polysaccharides) (ATR-FTIR) and the 45 µm thick biofouling coverage consisted of discrete bacterial clusters embedded in a polymeric matrix and interpenetrating by filamentous fungi and bacteria (SEM, CLSM).

## 2. FUTURE PROSPECTS

Overall, following guideline may be taken into consideration in view of future work and data validation. Enhanced knowledge of the specific relation between membrane and microorganisms as well as inter-microbial relations, would allow for development of more targeted anti-fouling strategies.

- The experiment should be repeated with one HT-MBR for each membrane under the same operating conditions, instead of using one single reactor containing all clusters, in order to exclude

proximity effects. Testing different feed solutions (of municipal, industrial origin), application of alternative operating conditions (including sterile equipment) and synthesis of membranes with different polymers and solvents might allow further process optimization in view of undisputable validation of the observations over a wide range of applications. However the step further to extrapolation to full-scale applications may still be a matter of uncertainty.

- Membrane characterization of PAN membranes could be brought one step further by detailed investigation of the surface microtopography and surface chemistry via optimization of techniques that were not able to deliver reliable results here or not easily accessible, namely electrokinetic measurements (for: surface charge density), porosimetry measurements (for: pore size distribution, surface porosity and average pore size), Transmission Electron Microscopy (for: pore size and surface topography), elemental analysis (for: chemical constituents), titration (for: ion-exchange capacity).
- Identification of the pioneering species as well as the relative contribution of the bacteria from the activated sludge to biofilm formation, could complete the data. Three approaches could be used. Firstly, the use of alternative and widely used molecular techniques such as a combination of T-RFLP, qPCR and 16S rRNA clone library construction followed by Sanger sequencing, could be tested against PCR-DGGE fingerprint outcomes and serve this purpose. Next, optimized use of the CLSM techniques and Fluorescence In Situ Hybridization would allow for time-dependent morphological characterization of the biofilm formers. Finally the application of cultivation-dependent techniques including isolation from the sludge and biofilm samples on adequate laboratory media followed by spiking of the activated sludge with selected and labelled members of the pure cultures, would allow for further morphological and physiological characterization and determination of the proportion of that specific member in the whole biofilm community.



## References

- [1] N. Abdel-Raouf, a a Al-Homaidan, and I. B. M. Ibraheem, "Microalgae and wastewater treatment.," *Saudi J. Biol. Sci.*, vol. 19, pp. 257–275, Jul. 2012.
- [2] P. Grelier, S. Rosenberger, and A. Tazi-Pain, "Influence of sludge retention time on membrane bioreactor hydraulic performance.," *Desalination*, vol. 192, pp. 10–17, May 2006.
- [3] L.-N. Huang, H. De Wever, and L. Diels, "Diverse and Distinct Bacterial Communities Induced Biofilm Fouling in Membrane Bioreactors Operated under Different Conditions.," *Environ. Sci. Technol.*, vol. 42, pp. 8360–8366, Nov. 2008.
- [4] S. Judd, "The status of membrane bioreactor technology.," *Trends Biotechnol.*, vol. 26, pp. 109–116, Feb. 2008.
- [5] P. Le-Clech, "Membrane bioreactors and their uses in wastewater treatments.," *Appl. Microbiol. Biotechnol.*, vol. 88, pp. 1253–1260, 2010.
- [6] A. Piasecka, C. Souffreau, K. Vandepitte, L. Vanysacker, R. M. Bilad, T. De Bie, B. Hellemans, L. De Meester, X. Yan, P. Declerck, and I. F. J. Vankelecom, "Analysis of the microbial community structure in a membrane bioreactor during initial stages of filtration.," *Biofouling*, vol. 28, pp. 225–38, Jan. 2012.
- [7] J. Zhang, H. C. Chua, J. Zhou, and A. G. Fane, "Factors affecting the membrane performance in submerged membrane bioreactors.," *J. Memb. Sci.*, vol. 284, pp. 54–66, Nov. 2006.
- [8] M. Madigan, J. Martinko, D. Stahl, and D. Clark, *Brock. Biology of Microorganisms.*, 13th ed. San Francisco: Pearson Education, p. 1150.
- [9] B. Van der Bruggen, "Cursustekst - IOS80A Waste Water Treatment Technology. Part 1: Legislation in Flanders and Primary Waste Water Technology.," Acco, Acco - Leuven. 3rd edition., 2012.
- [10] P. M. Armenante, "Characterization of Industrial Wastewaters."
- [11] I. Smets, "Cursustekst - IOS80A Waterzuivering en -hergebruik. Deel 2: Secundaire afvalwaterzuiveringstechnieken.," Acco, Acco Leuven. 4th edition., 2012.
- [12] D. Springael, "Cursustekst - ION96A Milieutechnische Microbiologie.," Katholieke Universiteit Leuven, Leuven, 2012.
- [13] H. Waheed, I. Hashmi, A. K. Naveed, and S. J. Khan, "Molecular detection of microbial community in a nitrifying–denitrifying activated sludge system.," *Int. Biodeterior. Biodegradation*, vol. 85, pp. 527–532, Nov. 2013.
- [14] S. J. Khan, F. Parveen, A. Ahmad, I. Hashmi, and N. Hankins, "Performance evaluation and bacterial characterization of membrane bioreactors.," *Bioresour. Technol.*, vol. 141, pp. 2–7, Aug. 2013.
- [15] "Titel II van het VLAREM Bijlagen. Bijlagen bij het besluit van de Vlaamse Regering van 1 juni 1995 houdende algemene en sectorale bepalingen inzake milieuhygiëne.," *Departement Leefmilieu, Natuur en Energie*, 1998. [Online]. Available: <http://www.lne.be/themas/vergunningen/bestand/regelgeving/titel-ii-van-het-vlarem-bijlagen-pdf/view?searchterm=milieuhygiëne>. [Accessed: 03-Jan-2015].
- [16] L. Vanysacker, B. Boerjan, P. Declerck, and I. F. J. Vankelecom, "Biofouling ecology as a means to better understand membrane biofouling.," *Appl. Microbiol. Biotechnol.*, vol. 98, pp. 8047–72, Oct. 2014.
- [17] E. Vaiopoulou, P. Melidis, and A. Aivasidis, "An activated sludge treatment plant for integrated removal of carbon, nitrogen and phosphorus.," *Desalination*, vol. 211, pp. 192–199, Jun. 2007.
- [18] S. Milia, G. Cappai, M. Perra, and A. Carucci, "Biological treatment of nitrogen-rich refinery wastewater by partial nitritation (SHARON) process.," *Environ. Technol.*, vol. 33, no. 13, pp. 1477–1483, 2012.
- [19] Y. Peng and G. Zhu, "Biological nitrogen removal with nitrification and denitrification via nitrite pathway.," *Appl. Microbiol. Biotechnol.*, vol. 73, pp. 15–26, Nov. 2006.
- [20] B. Kartal, J. G. Kuenen, and M. C. M. van Loosdrecht, "Sewage Treatment with Anammox.," *Science (80-)*, vol. 328, pp. 702–703, 2010.

- [21] L. Zhang, P. Zheng, C. Tang, and R. Jin, "Anaerobic ammonium oxidation for treatment of ammonium-rich wastewaters.," *J. Zhejiang Univ. Sci. B*, vol. 9, no. 5, pp. 416–426, May 2008.
- [22] P. Xinhong, Y. Hongbing, W. Libo, A. Lina, and F. Lixia, "CANON Process for Nitrogen Removal from Effluents of Municipal Sewage Treatment Plants.," *Trans. Tianjin Univ.*, vol. 19, no. 4, pp. 255–259, 2013.
- [23] K. A. Third, A. O. Sliemers, J. G. Kuenen, and M. S. M. Jetten, "The CANON System ( Completely Autotrophic Nitrogen-removal Over Nitrite ) under Ammonium Limitation : Interaction and Competition between three groups of Bacteria.," *Syst. Appl. Microbiol.*, vol. 24, pp. 588–596, 2001.
- [24] F. Meng, B. Liao, S. Liang, F. Yang, H. Zhang, and L. Song, "Morphological visualization, componential characterization and microbiological identification of membrane fouling in membrane bioreactors (MBRs).," *J. Memb. Sci.*, vol. 361, pp. 1–14, Sep. 2010.
- [25] T.-Y. Jeong, G.-C. Cha, I.-K. Yoo, and D.-J. Kim, "Characteristics of bio-fouling in a submerged MBR.," *Desalination*, vol. 207, pp. 107–113, Mar. 2007.
- [26] D. L. Seman, "Activated Sludge Microbiology.," *City of Youngstown*, 2013. [Online]. Available: [http://www.ohioewa.org/docs/Activated\\_Sludge\\_Microbiology\\_Seman.pdf](http://www.ohioewa.org/docs/Activated_Sludge_Microbiology_Seman.pdf). [Accessed: 26-Dec-2014].
- [27] J. Wu, P. Le-Clech, R. M. Stuetz, A. G. Fane, and V. Chen, "Effects of relaxation and backwashing conditions on fouling in membrane bioreactor.," *J. Memb. Sci.*, vol. 324, pp. 26–32, Oct. 2008.
- [28] D. H. Eikelboom, *Process Control of Activated Sludge Plants by Microscopic Investigation.*, 1st ed. Zutphen: IWA Publishing, 2000, p. 170.
- [29] T. R. Ramothokang, G. D. Drysdale, and F. Bux, "Isolation and cultivation of filamentous bacteria implicated in activated sludge bulking.," *Water SA*, vol. 29, pp. 405–410, 2003.
- [30] L. Metcalf and H. P. Eddy, *Wastewater engineering: collection, treatment, disposal*. New-York: McGraw-Hill Book Company, 1972.
- [31] F. Meng, B. Shi, F. Yang, and H. Zhang, "Effect of hydraulic retention time on membrane fouling and biomass characteristics in submerged membrane bioreactors.," *Bioprocess Biosyst. Eng.*, vol. 30, pp. 359–367, Sep. 2007.
- [32] G. Gaval and J.-J. Pernelle, "Impact of the repetition of oxygen deficiencies on the filamentous bacteria proliferation in activated sludge.," *Water Res.*, vol. 37, pp. 1991–2000, May 2003.
- [33] H. Lin, W. Peng, M. Zhang, J. Chen, H. Hong, and Y. Zhang, "A review on anaerobic membrane bioreactors: Applications, membrane fouling and future perspectives.," *Desalination*, vol. 314, pp. 169–188, Apr. 2013.
- [34] B.-Q. Liao, J. T. Kraemer, and D. M. Bagley, "Anaerobic Membrane Bioreactors: Applications and Research Directions.," *Crit. Rev. Environ. Sci. Technol.*, vol. 36, pp. 489–530, Dec. 2006.
- [35] K. C. Perez, "General overview. Anaerobic Wastewater Treatment.," Katholieke Universiteit Leuven, Leuven, 2013.
- [36] B. Van der Bruggen, "Cursustekst - IOS80A Waste Water Treatment Technology. Part 3: Tertiary Waste Water Treatment.," Acco, Acco - Leuven. 3rd edition., 2012.
- [37] I. F. J. Vankelecom, "Cursustekst - IOP35A Membraantechnologie.," Katholieke Universiteit Leuven, Leuven, 2013.
- [38] M. Mulder, *Basic principles of membrane technology.*, 2nd ed. Dordrecht: Kluwer Academic Publishers, 2003, p. 564.
- [39] S. S. Madaeni, A. G. Fane, and D. E. Wiley, "Factors influencing critical flux in membrane filtration of activated sludge.," *J. Chem. Technol. Biotechnol.*, vol. 74, pp. 539–543, 1999.
- [40] M. A. Kader, "A review of membrane bioreactor (MBR) technology and their applications in the wastewater treatment systems.," in *Eleventh International Water Technology Conference, IWTC11*, 2007, pp. 269–279.
- [41] K. A. Mason, J. B. Losos, S. R. Singer, P. H. Raven, and G. B. Johnson, *Biology.*, 9th ed. New-York: McGraw-Hill Book Company, p. 1279.

- [42] D. C. Stuckey, "Recent developments in anaerobic membrane reactors.," *Bioresour. Technol.*, vol. 122, pp. 137–148, Oct. 2012.
- [43] A. Ramesh, D. J. Lee, M. L. Wang, J. P. Hsu, R. S. Juang, K. J. Hwang, J. C. Liu, and S. J. Tseng, "Biofouling in Membrane Bioreactor.," *Sep. Sci. Technol.*, vol. 41, no. 7, pp. 1345–1370, Jun. 2006.
- [44] A. K. Fritzsche, A. R. Arevalo, M. D. Moore, and C. O'Hara, "The surface structure and morphology of polyacrylonitrile membranes by atomic force microscopy.," *J. Memb. Sci.*, vol. 81, pp. 109–120, 1993.
- [45] J. Wang, Z. Yue, and J. Economy, "Solvent Resistant Hydrolyzed Polyacrylonitrile Membranes.," *Sep. Sci. Technol.*, vol. 44, pp. 2827–2839, Aug. 2009.
- [46] L. Defrance and M. Y. Jaffrin, "Reversibility of fouling formed in activated sludge filtration.," *J. Memb. Sci.*, vol. 157, pp. 73–84, 1999.
- [47] S. Zhang, Y. Qu, Y. Liu, F. Yang, X. Zhang, K. Furukawa, and Y. Yamada, "Experimental study of domestic sewage treatment with a metal membrane bioreactor.," *Desalination*, vol. 177, pp. 83–93, Jun. 2005.
- [48] F. Meng, S.-R. Chae, A. Drews, M. Kraume, H.-S. Shin, and F. Yang, "Recent advances in membrane bioreactors (MBRs): membrane fouling and membrane material.," *Water Res.*, vol. 43, pp. 1489–1512, Apr. 2009.
- [49] P. K. Krzeminski, "Activated sludge filterability and full-scale membrane bioreactor operation.," Technische Universiteit Delft, 2013.
- [50] B. Gunder and K. Krauth, "Replacement of secondary clarification by membrane separation - results with plate and hollow fibre modules.," *Water Sci. Technol.*, vol. 38, no. 4–5, pp. 383–393, 1998.
- [51] S. Judd, "Submerged Membrane Bioreactors : Flat Plate or Hollow Fibre ?," *Filtr. Sep.*, vol. 39, no. 5, pp. 30–31, 2002.
- [52] M. L. Ferreira, "Wastewater Treatment.," *Delft University of Technology*, 2012. [Online]. Available: [http://ocw.tudelft.nl/en/courses/watermanagement/wastewater-treatment/lectures/4-membrane-bioreactors/?jumpurl=uploads%2Fmedia%2F4a.\\_Membrane\\_BioReactors.pdf&juSecure=1&mimeType=application%2Fpdf&locationData=11314%3Att\\_content%3A60364&juHash=2ee03e1ba5207455f465ddab983cc2d4335a0d05](http://ocw.tudelft.nl/en/courses/watermanagement/wastewater-treatment/lectures/4-membrane-bioreactors/?jumpurl=uploads%2Fmedia%2F4a._Membrane_BioReactors.pdf&juSecure=1&mimeType=application%2Fpdf&locationData=11314%3Att_content%3A60364&juHash=2ee03e1ba5207455f465ddab983cc2d4335a0d05). [Accessed: 16-Jan-2015].
- [53] F. Meng, H. Zhang, F. Yang, S. Zhang, Y. Li, and X. Zhang, "Identification of activated sludge properties affecting membrane fouling in submerged membrane bioreactors.," *Sep. Purif. Technol.*, vol. 51, pp. 95–103, Aug. 2006.
- [54] R. W. Field, D. Wu, J. A. Howell, and B. B. Gupta, "Critical flux concept for microfiltration fouling.," *J. Memb. Sci.*, vol. 100, pp. 259–272, Apr. 1995.
- [55] Y. Ye, P. Le-Clech, V. Chen, and A. G. Fane, "Evolution of fouling during crossflow filtration of model EPS solutions.," *J. Memb. Sci.*, vol. 264, pp. 190–199, Nov. 2005.
- [56] L. Defrance and M. Y. Jaffrin, "Comparison between filtrations at fixed transmembrane pressure and fixed permeate flux: application to a membrane bioreactor used for wastewater treatment.," *J. Memb. Sci.*, vol. 152, pp. 203–210, 1999.
- [57] F. Martínez, A. Martín, P. Prádanos, J. Calvo, L. Palacio, and A. Hernández, "Protein Adsorption and Deposition onto Microfiltration Membranes: The Role of Solute-Solid Interactions.," *J. Colloid Interface Sci.*, vol. 221, pp. 254–261, Jan. 2000.
- [58] S. Ognier, C. Wisniewski, and A. Grasmick, "Influence of macromolecule adsorption during filtration of a membrane bioreactor mixed liquor suspension.," *J. Memb. Sci.*, vol. 209, pp. 27–37, Nov. 2002.
- [59] P. Le Clech, B. Jefferson, I.-S. Chang, and S. Judd, "Critical flux determination by the flux-step method in a submerged membrane bioreactor.," *J. Memb. Sci.*, vol. 227, pp. 81–93, Dec. 2003.
- [60] P. van der Marel, A. Zwijnenburg, A. Kemperman, M. Wessling, H. Temmink, and W. van der Meer, "An improved flux-step method to determine the critical flux and the critical flux for irreversibility in a membrane bioreactor.," *J. Memb. Sci.*, vol. 332, pp. 24–29, Apr. 2009.
- [61] A. Pollice, A. Brookes, B. Jefferson, and S. Judd, "Sub-critical flux fouling in membrane bioreactors — a review of recent literature.," *Desalination*, vol. 174, pp. 221–230, Apr. 2005.

- [62] W. Yang, N. Cicek, and J. Ilg, "State-of-the-art of membrane bioreactors: Worldwide research and commercial applications in North America.," *J. Memb. Sci.*, vol. 270, pp. 201–211, Feb. 2006.
- [63] B. Lesjean and E. H. Huisjes, "Survey of the European MBR market: trends and perspectives.," *Desalination*, vol. 231, pp. 71–81, Oct. 2008.
- [64] C.-Y. Wan, H. De Wever, L. Diels, C. Thoeye, J.-B. Liang, and L.-N. Huang, "Biodiversity and population dynamics of microorganisms in a full-scale membrane bioreactor for municipal wastewater treatment.," *Water Res.*, vol. 45, pp. 1129–1138, Jan. 2011.
- [65] Frost&Sullivan, "Global Membrane Bioreactor (MBR) Market. Soaring Demand in Developing Markets Fuels Growth Momentum .," 2013. [Online]. Available: <http://www.frost.com/sublib/display-report.do?id=M7E2-01-00-00-00&bdata=aHR0cDovL3d3dy5nb29nbGUuYmUvdXJsP3NhPXQmcmN0PWomcT0mZXNyYz1zJnNvdXJzT13ZWlmY2Q9MSZ2ZWQ9MENDb1FGakFBjnVybd1odHRwJTNBjTjGjTjGd3d3LmZyb3NOlMnNvbSUyRnByb2QlMkZzZXJ2bGV0JTJGcmVwb3J0LXRvYy5wYWclM0ZyZXBpZCUzRE03RTItMDEtMDAtMDAtMDAmZWk9SEpXM1ZNnWxBOEjN0Fhd3FZQ1FDQSZ1c2c9QUZRakNOR0dlWE9GbHRaTjFqZ3hUWTBXTIM3MzFmGRUdyZidm09YnYuODM2NDAYmZksZC5aR1VAFkBCYWNrQH5AMTQyMTMxNzQwNzMOmg%3D%3D>. [Accessed: 15-Jan-2015].
- [66] F. Royan, "Membrane Multiplier: MBR set for Global Growth.," 2014. [Online]. Available: <http://www.waterworld.com/articles/wwi/print/volume-27/issue-2/regulars/creative-finance/membrane-multiplier-mbr.html>. [Accessed: 15-Jan-2015].
- [67] J. R. Pan, Y. Su, and C. Huang, "Characteristics of soluble microbial products in membrane bioreactor and its effect on membrane fouling.," *Desalination*, vol. 250, pp. 778–780, Jan. 2010.
- [68] K. Yamamoto, M. Hiasa, T. Mahmood, and T. Matsuo, "Direct solid liquid separations using hollow fiber membranes in activated sludge aeration tank.," *Water Sci. Technol.*, vol. 21, no. 4–5, pp. 43–54, 1989.
- [69] "Membraanbioreactor.," *Energie- en Milieu-informatiesysteem voor het Vlaamse Gewest (EMIS)*, 2010. [Online]. Available: <http://emis.vito.be/techniekfiche/membraanbioreactor>. [Accessed: 17-Jan-2015].
- [70] A. Massé, M. Spérandio, and C. Cabassud, "Comparison of sludge characteristics and performance of a submerged membrane bioreactor and an activated sludge process at high solids retention time.," *Water Res.*, vol. 40, pp. 2405–2415, Jul. 2006.
- [71] S. Liang, L. Song, G. Tao, K. A. Kekre, and H. Seah, "A Modeling Study of Fouling Development in Membrane Bioreactors for Wastewater Treatment.," *Water Environ. Res.*, vol. 78, pp. 857–863, 2005.
- [72] S. Rosenberger and M. Kraume, "Filterability of activated sludge in membrane bioreactors.," *Desalination*, vol. 151, pp. 195–200, Sep. 2002.
- [73] X. Huang, R. Liu, and Y. Qian, "Behaviour of soluble microbial products in a membrane bioreactor.," *Process Biochem.*, vol. 36, pp. 401–406, Dec. 2000.
- [74] "Actief slib systemen.," *Energie- en Milieu-informatiesysteem voor het Vlaamse Gewest (EMIS)*, 2010. [Online]. Available: <http://emis.vito.be/techniekfiche/actief-slib-systemen>. [Accessed: 17-Jan-2015].
- [75] V. Jacquemet, G. Gaval, S. Rosenberger, B. Lesjean, and J.-C. Schrotter, "Towards a better characterisation and understanding of membrane fouling in water treatment.," *Desalination*, vol. 178, pp. 13–20, Jul. 2005.
- [76] F. Meng, H. Zhang, F. Yang, and L. Liu, "Characterization of Cake Layer in Submerged Membrane Bioreactor.," *Environ. Sci. Technol.*, vol. 41, pp. 4065–4070, Jun. 2007.
- [77] L. Vanysacker, P. Declerck, R. M. Bilad, and I. F. J. Vankelecom, "Biofouling on microfiltration membranes in MBRs: Role of membrane type and microbial community.," *J. Memb. Sci.*, vol. 453, pp. 394–401, Mar. 2014.
- [78] G. N. B. Baroña, B. J. Cha, and B. Jung, "Negatively charged poly(vinylidene fluoride) microfiltration membranes by sulfonation.," *J. Memb. Sci.*, vol. 290, pp. 46–54, Mar. 2007.

- [79] K. Akamatsu, M. Okuyama, K. Mitsumori, A. Yoshino, A. Nakao, and S. Nakao, "Effect of the composition of the copolymer of carboxybetaine and n-butylmethacrylate on low-fouling property of dynamically formed membrane.," *Sep. Purif. Technol.*, vol. 118, pp. 463–469, Oct. 2013.
- [80] X. Li, F. Gao, Z. Hua, G. Du, and J. Chen, "Treatment of synthetic wastewater by a novel MBR with granular sludge developed for controlling membrane fouling.," *Sep. Purif. Technol.*, vol. 46, pp. 19–25, Nov. 2005.
- [81] Z. Wang, J. Ma, C. Y. Tang, K. Kimura, Q. Wang, and X. Han, "Membrane cleaning in membrane bioreactors: A review.," *J. Memb. Sci.*, vol. 468, pp. 276–307, Oct. 2014.
- [82] U. Metzger, P. Le-Clech, R. M. Stuetz, F. H. Frimmel, and V. Chen, "Characterisation of polymeric fouling in membrane bioreactors and the effect of different filtration modes.," *J. Memb. Sci.*, vol. 301, pp. 180–189, Sep. 2007.
- [83] J. Lee, W.-Y. Ahn, and C.-H. Lee, "Comparison of the filtration characteristics between attached and suspended growth microorganisms in submerged membrane bioreactor.," *Water Res.*, vol. 35, pp. 2435–2445, Jul. 2001.
- [84] Y. Marselina, P. Le-Clech, R. M. Stuetz, V. Chen, and Lifa, "Characterisation of membrane fouling deposition and removal by direct observation technique.," *J. Memb. Sci.*, vol. 341, pp. 163–171, Sep. 2009.
- [85] D. Spettmann, S. Eppmann, H.-C. Flemming, and J. Wingender, "Visualization of membrane cleaning using confocal laser scanning microscopy.," *Desalination*, vol. 224, pp. 195–200, Apr. 2008.
- [86] H. Yamamura, K. Kimura, T. Okajima, H. Tokumoto, and Y. Watanabe, "Affinity of Functional Groups for Membrane Surfaces: Implications for Physically Irreversible Fouling.," *Environ. Sci. Technol.*, vol. 42, pp. 5310–5315, Jul. 2008.
- [87] S. Ognier, C. Wisniewski, and A. Grasmick, "Characterisation and modelling of fouling in membrane bioreactors.," *Desalination*, vol. 146, pp. 141–147, Sep. 2002.
- [88] D. Wu, J. A. Howell, and R. W. Field, "Critical flux measurement for model colloids.," *J. Memb. Sci.*, vol. 152, pp. 89–98, 1999.
- [89] K. Zhang, H. Choi, D. D. Dionysiou, G. A. Sorial, and D. B. Oerther, "Identifying pioneer bacterial species responsible for biofouling membrane bioreactors.," *Environ. Microbiol.*, vol. 8, no. 3, pp. 433–440, Mar. 2006.
- [90] Y. Miura, Y. Watanabe, and S. Okabe, "Membrane Biofouling in Pilot-Scale Membrane Bioreactors ( MBRs ) Treating Municipal Wastewater : Impact of Biofilm Formation.," *Environ. Sci. Technol.*, vol. 41, pp. 632–638, Jan. 2007.
- [91] P. Jinhua, K. Fukushi, and K. Yamamoto, "Bacterial Community Structure on Membrane Surface and Characteristics of Strains Isolated from Membrane Surface in Submerged Membrane Bioreactor.," *Sep. Sci. Technol.*, vol. 41, no. 7, pp. 1527–1549, Jun. 2006.
- [92] J. S. Baker and L. Y. Dudley, "Biofouling in membrane systems — A review.," *Desalination*, vol. 118, pp. 81–90, Sep. 1998.
- [93] C. L. Chen, W. T. Liu, M. L. Chong, M. T. Wong, S. L. Ong, H. Seah, and W. J. Ng, "Community structure of microbial biofilms associated with membrane-based water purification processes as revealed using a polyphasic approach.," *Appl. Microbiol. Biotechnol.*, vol. 63, pp. 466–473, Jan. 2004.
- [94] P. Hörsch, A. Gorenflo, C. Fuder, A. Deleage, and F. H. Frimmel, "Biofouling of ultra- and nanofiltration membranes for drinking water treatment characterized by fluorescence in situ hybridization (FISH).," *Desalination*, vol. 172, pp. 41–52, Feb. 2005.
- [95] P. Stoodley, K. Sauer, D. G. Davies, and J. W. Costerton, "Biofilms as complex differentiated communities.," *Annu. Rev. Microbiol.*, vol. 56, pp. 187–209, Jan. 2002.
- [96] M. Pasmore, P. Todd, S. Smith, D. Baker, J. Silverstein, D. Coons, and C. N. Bowman, "Effects of ultrafiltration membrane surface properties on *Pseudomonas aeruginosa* biofilm initiation for the purpose of reducing biofouling.," *J. Memb. Sci.*, vol. 194, pp. 15–32, Nov. 2001.

- [97] B. A. Jucker, H. Harms, and A. J. B. Zehnder, "Adhesion of the Positively Charged Bacterium *Stenotrophomonas* (*Xanthomonas*) *maltophilia* 70401 to Glass and Teflon.," *J. Bacteriol.*, vol. 178, no. 18, pp. 5472–5479, 1996.
- [98] B. Tansel, J. Sager, J. Garland, S. Xu, L. Levine, and P. Bisbee, "Biofouling affinity of membrane surfaces under quiescent conditions.," *Desalination*, vol. 227, pp. 264–273, Jul. 2008.
- [99] B. . Cho and A. G. Fane, "Fouling transients in nominally sub-critical flux operation of a membrane bioreactor.," *J. Memb. Sci.*, vol. 209, pp. 391–403, Nov. 2002.
- [100] G. Zhang, S. Ji, X. Gao, and Z. Liu, "Adsorptive fouling of extracellular polymeric substances with polymeric ultrafiltration membranes.," *J. Memb. Sci.*, vol. 309, pp. 28–35, Feb. 2008.
- [101] M. Chen, D. Lee, and J. H. Tay, "Extracellular Polymeric Substances in Fouling Layer.," *Sep. Sci. Technol.*, vol. 41, pp. 1467–1474, Jun. 2006.
- [102] K. Milferstedt, M.-N. Pons, and E. Morgenroth, "Textural fingerprints: a comprehensive descriptor for biofilm structure development.," *Biotechnol. Bioeng.*, vol. 100, pp. 889–901, Aug. 2008.
- [103] X. J. Fan, V. Urbain, Y. Qian, and J. Manem, "Ultrafiltration of activated sludge with ceramic membranes in a cross-flow membrane bioreactor process.," *Water Sci. Technol.*, vol. 41, pp. 243–250, 2000.
- [104] K.-M. Yeon, W.-S. Cheong, H.-S. Oh, W.-N. Lee, B.-K. Hwang, C.-H. Lee, H. Beyenal, and Z. Lewandowski, "Quorum Sensing: A New Biofouling Control Paradigm in a Membrane Bioreactor for Advanced Wastewater Treatment.," *Environ. Sci. Technol.*, vol. 43, pp. 380–385, Jan. 2009.
- [105] V. Naddeo, V. Belgiorno, L. Borea, M. F. N. Secondes, and F. Ballesteros, "Control of fouling formation in membrane ultrafiltration by ultrasound irradiation.," *Environ. Technol.*, Dec. 2014.
- [106] W.-N. Lee, I.-S. Chang, B.-K. Hwang, P.-K. Park, C.-H. Lee, and X. Huang, "Changes in biofilm architecture with addition of membrane fouling reducer in a membrane bioreactor.," *Process Biochem.*, vol. 42, pp. 655–661, Apr. 2007.
- [107] C. Huyskens, H. De Wever, Y. Fovet, U. Wegmann, L. Diels, and S. Lenaerts, "Screening of novel MBR fouling reducers: Benchmarking with known fouling reducers and evaluation of their mechanism of action.," *Sep. Purif. Technol.*, vol. 95, pp. 49–57, Jul. 2012.
- [108] K. Bernaerts, "Reactor Engineering. Part b: Bioreactor Engineering.," Katholieke Universiteit Leuven, Leuven, 2012.
- [109] C. X. Liu, D. R. Zhang, Y. He, X. S. Zhao, and R. Bai, "Modification of membrane surface for anti-biofouling performance: Effect of anti-adhesion and anti-bacteria approaches.," *J. Memb. Sci.*, vol. 346, pp. 121–130, Jan. 2010.
- [110] L. Zou, I. Vidalis, D. Steele, A. Micheltore, S. P. Low, and J. Q. J. C. Verberk, "Surface hydrophilic modification of RO membranes by plasma polymerization for low organic fouling.," *J. Memb. Sci.*, vol. 369, pp. 420–428, Mar. 2011.
- [111] F. Liu, B.-K. Zhu, and Y.-Y. Xu, "Improving the hydrophilicity of poly(vinylidene fluoride) porous membranes by electron beam initiated surface grafting of AA/SSS binary monomers.," *Appl. Surf. Sci.*, vol. 253, pp. 2096–2101, Dec. 2006.
- [112] G. Kang, M. Liu, B. Lin, Y. Cao, and Q. Yuan, "A novel method of surface modification on thin-film composite reverse osmosis membrane by grafting poly(ethylene glycol).," *Polymer (Guildf.)*, vol. 48, pp. 1165–1170, Feb. 2007.
- [113] H. Yu, Y. Xie, M. Hu, J. Wang, S. Wang, and Z. Xu, "Surface modification of polypropylene microporous membrane to improve its antifouling property in MBR: CO<sub>2</sub> plasma treatment.," *J. Memb. Sci.*, vol. 254, pp. 219–227, Jun. 2005.
- [114] H.-Y. Yu, L.-Q. Liu, Z.-Q. Tang, M.-G. Yan, J.-S. Gu, and X.-W. Wei, "Surface modification of polypropylene microporous membrane to improve its antifouling characteristics in an SMBR: Air plasma treatment.," *J. Memb. Sci.*, vol. 311, pp. 216–224, Mar. 2008.
- [115] J. Schaep and C. Vandecasteele, "Evaluating the charge of nanofiltration membranes.," *J. Memb. Sci.*, vol. 188, pp. 129–136, 2001.



- [116] A. Roosjen, W. Norde, H. C. van der Mei, and H. J. Busscher, "The Use of Positively Charged or Low Surface Free Energy Coatings versus Polymer Brushes in Controlling Biofilm Formation.," *Prog. Colloid Polym. Sci.*, vol. 132, pp. 138–144, 2006.
- [117] B. Gottenbos, D. W. Grijpma, H. C. van der Mei, J. Feijen, and H. J. Busscher, "Antimicrobial effects of positively charged surfaces on adhering Gram-positive and Gram-negative bacteria.," *J. Antimicrob. Chemother.*, vol. 48, pp. 7–13, 2001.
- [118] K. Bazaka, M. V. Jacob, R. J. Crawford, and E. P. Ivanova, "Efficient surface modification of biomaterial to prevent biofilm formation and the attachment of microorganisms.," *Appl. Microbiol. Biotechnol.*, vol. 95, pp. 299–311, Jul. 2012.
- [119] Q. Li, S. Mahendra, D. Y. Lyon, L. Brunet, M. V. Liga, D. Li, and P. J. J. Alvarez, "Antimicrobial nanomaterials for water disinfection and microbial control: potential applications and implications.," *Water Res.*, vol. 42, pp. 4591–4602, Nov. 2008.
- [120] R. S. Trussell, R. P. Merlo, S. W. Hermanowicz, and D. Jenkins, "The effect of organic loading on process performance and membrane fouling in a submerged membrane bioreactor treating municipal wastewater.," *Water Res.*, vol. 40, pp. 2675–2683, Aug. 2006.
- [121] S. R. Panda and S. De, "Preparation, characterization and antifouling properties of polyacrylonitrile/polyurethane blend membranes for water purification.," *R. Soc. Chem. Adv.*, vol. 5, pp. 23599–23612, 2015.
- [122] N. Scharnagl and H. Buschatz, "Polyacrylonitrile (PAN) membranes for ultra- and microfiltration.," *Desalination*, vol. 139, pp. 191–198, 2001.
- [123] Z.-G. Wang, L.-S. Wan, and Z.-K. Xu, "Surface engineering of polyacrylonitrile-based asymmetric membranes towards biomedical applications: An overview.," *J. Memb. Sci.*, vol. 304, pp. 8–23, Nov. 2007.
- [124] S. G. Ding, X. Q. Cheng, Z. X. Jiang, Y. P. Bai, and L. Shao, "Pore morphology control and hydrophilicity of polyacrylonitrile ultrafiltration membranes.," *J. Appl. Polym. Sci.*, vol. 132, no. 20, p. n/a–n/a, May 2015.
- [125] X. Li, S. De Feyter, D. Chen, S. Aldea, P. Vandezande, F. Du Prez, and I. F. J. Vankelecom, "Solvent-Resistant Nanofiltration Membranes Based on Multilayered Polyelectrolyte Complexes.," *Chem. Mater.*, vol. 20, pp. 3876–3883, Jun. 2008.
- [126] W. Bao, Z. Xu, and H. Yang, "Electrokinetic and permeation characterization of hydrolyzed polyacrylonitrile (PAN) hollow fiber ultrafiltration membrane.," *Sci. China Ser. B Chem.*, vol. 52, no. 5, pp. 683–689, May 2009.
- [127] M. Fang, C. H. Kim, G. B. Saupe, H.-N. Kim, C. C. Waraksa, T. Miwa, A. Fujishima, and T. E. Mallouk, "Layer-by-Layer Growth and Condensation Reactions of Niobate and Titanoniobate Thin Films.," *Chem. Mater.*, vol. 11, no. 6, pp. 1526–1532, Jun. 1999.
- [128] S. E. Burke and C. J. Barrett, "Acid - Base Equilibria of Weak Polyelectrolytes in Multilayer Thin Films.," *Langmuir*, vol. 19, no. 8, pp. 3297–3303, 2003.
- [129] K. F. Tjipangandjara and P. Somasundaran, "Effects of the conformation of poly acrylic acid on the dispersion-flocculation of alumina and kaolinite fines.," *Adv. Powder Technol.*, vol. 3, no. 2, pp. 119–127, 1992.
- [130] M. R. Bilad, P. Declerck, A. Piasecka, L. Vanysacker, X. Yan, and I. F. J. Vankelecom, "Treatment of molasses wastewater in a membrane bioreactor: Influence of membrane pore size.," *Sep. Purif. Technol.*, vol. 78, pp. 105–112, Dec. 2010.
- [131] M. R. Bilad, P. Declerck, A. Piasecka, L. Vanysacker, X. Yan, and I. F. J. Vankelecom, "Development and validation of a high-throughput membrane bioreactor (HT-MBR).," *J. Memb. Sci.*, vol. 379, pp. 146–153, Sep. 2011.
- [132] Y. Elbahloul, K. Frey, J. Sanders, and A. Steinbüchel, "Protamylasse, a Residual Compound of Industrial Starch Production, Provides a Suitable Medium for Large-Scale Cyanophycin Production.," *Appl. Environ. Microbiol.*, vol. 71, pp. 7759–7767, 2005.

## A - VIII

- [133] D. De Vos, "Cursustekst - I0002a Kolloïdchemie.," Katholieke Universiteit Leuven - Cursusdienst LBK vzw, Leuven, 2012.
- [134] W. Richard Bowen, N. Hilal, R. W. Lovitt, and C. . Wright, "Characterisation of membrane surfaces: direct measurement of biological adhesion using an atomic force microscope.," *J. Memb. Sci.*, vol. 154, pp. 205–212, Mar. 1999.
- [135] N. Hilal, W. R. Bowen, L. Alkhatib, and O. Ogunbiyi, "A Review of Atomic Force Microscopy Applied to Cell Interactions with Membranes.," *Chem. Eng. Res. Des.*, vol. 84, no. A4, pp. 282–292, Apr. 2006.
- [136] H. Zhao, X. Wu, W. Tian, and S. Ren, "Synthesis and Thermal Property of Poly(Allylamine Hydrochloride).," *Adv. Mater. Res.*, vol. 150–151, pp. 1480–1483, Oct. 2011.
- [137] D. Cho, S. Lee, and M. W. Frey, "Characterizing zeta potential of functional nanofibers in a microfluidic device.," *J. Colloid Interface Sci.*, vol. 372, pp. 252–260, Apr. 2012.
- [138] Z. Kolská, Z. Makajová, K. Kolářová, N. K. Slepíčková, S. Trostová, A. Řezníčková, J. Siegel, and V. Švorčík, "Electrokinetic Potential and Other Surface Properties of Polymer Foils and Their Modifications.," *Polym. Sci.*, pp. 203–228, 2013.
- [139] A. Lin and P. Liu, "Electrokinetic Property of Modified Polyacrylonitrile Membranes in the Haemodialysis.," in *2009 3rd International Conference on Bioinformatics and Biomedical Engineering*, 2009, pp. 1–5.
- [140] A. Szymczyk, Y. I. Dirir, M. Picot, I. Nicolas, and F. Barrière, "Advanced electrokinetic characterization of composite porous membranes.," *J. Memb. Sci.*, vol. 429, pp. 44–51, Feb. 2013.
- [141] F. Fan, H. Zhou, and H. Husain, "Identification of wastewater sludge characteristics to predict critical flux for membrane bioreactor processes.," *Water Res.*, vol. 40, pp. 205–212, Jan. 2006.
- [142] R. Blodgett, "BAM Appendix 2: Most Probable Number from Serial Dilutions," *U.S. Food and Drug Administration*, 2010. [Online]. Available: <http://www.fda.gov/Food/FoodScienceResearch/LaboratoryMethods/ucm109656.htm#tab1>. [Accessed: 30-Apr-2015].
- [143] G. Muyzer and K. Smalla, "Application of denaturing gradient gel electrophoresis ( DGGE ) and temperature gradient gel electrophoresis ( TGGE ) in microbial ecology.," *Antonie Van Leeuwenhoek*, vol. 73, pp. 127–141, 1998.
- [144] M. Wagner, R. Amann, and H. Lemmer, "Probing Activated Sludge with Oligonucleotides Specific for Proteobacteria : Inadequacy of Culture-Dependent Methods for Describing Microbial Community Structure.," *Appl. Environ. Microbiol.*, vol. 59, no. 5, pp. 1520–1525, 1993.
- [145] M. Wagner, R. Erhart, W. Manz, R. Amann, H. Lemmer, D. Wedi, and K. Schleifer, "Development of an rRNA-Targeted Oligonucleotide Probe Specific for the Genus *Acinetobacter* and Its Application for In Situ Monitoring in Activated Sludge.," *Appl. Environ. Microbiol.*, vol. 60, no. 3, pp. 792–800, 1994.
- [146] M. H. Larsen, K. Biermann, S. Tandberg, T. Hsu, and W. R. Jacobs, "Genetic Manipulation of *Mycobacterium tuberculosis*.," in *Current Protocols in Microbiology*, John Wiley & Sons, Inc., 2007, p. Unit 10A.2.
- [147] P. Breugelmans, M. Uytbroek, J. Dijk, and K. Bers, "Protocol for Polymerase Chain Reaction (PCR).," Leuven, 2009.
- [148] K. Cheyns, J. Mertens, and P. Breugelmans, "Protocol for Denaturing Gradient Gel Electrophoresis (DGGE).," Leuven, 2010.
- [149] A. K. Goodhead, I. M. Head, J. R. Snape, and R. J. Davenport, "Standard inocula preparations reduce the bacterial diversity and reliability of regulatory biodegradation tests.," *Environ. Sci. Pollut. Res.*, vol. 21, pp. 9511–9521, Aug. 2014.
- [150] S. Ruyters, "Protocol for Making a DGGE ladder.," 2010.
- [151] N. Boon, W. De Windt, W. Verstraete, and E. M. Top, "Evaluation of nested PCR-DGGE (denaturing gradient gel electrophoresis ) with group-specific 16S rRNA primers for the analysis of bacterial



- communities from different wastewater treatment plants.," *FEMS Microbiol. Ecol.*, vol. 39, pp. 101–112, 2002.
- [152] M. Ferrando, A. Rozek, M. Zator, F. Lopez, and C. Guell, "An approach to membrane fouling characterization by confocal scanning laser microscopy.," *J. Memb. Sci.*, vol. 250, pp. 283–293, Mar. 2005.
- [153] "SYTO Red Fluorescent Nucleic Acid Stains," 2001.
- [154] APHA, "Standard Methods for the Examination of Water and Wastewater. Part 9000 Microbiological Examination.," 1999.
- [155] M. H. Kutner, C. J. Nachtsheim, J. Neter, and W. Li, *Applied Linear Statistical Models.*, Fifth. McGraw-Hill Book Company, 2005, p. 1396.
- [156] L. J. Kirwan, P. D. Fawell, and W. van Bronswijk, "In Situ FTIR-ATR Examination of Poly(acrylic acid) Adsorbed onto Hematite at Low pH.," *Langmuir*, vol. 19, pp. 5802–5807, Jul. 2003.
- [157] S. Moya, L. Dähne, A. Voigt, S. Leporatti, E. Donath, and H. Möhwald, "Polyelectrolyte multilayer capsules templated on biological cells: core oxidation influences layer chemistry.," *Colloids Surfaces A Physicochem. Eng. Asp.*, vol. 183–185, pp. 27–40, 2001.
- [158] M. A. Moharram, S. M. Rabie, and H. M. El-Gendy, "Infrared Spectra of gamma-Irradiated Poly(acrylic acid)-Polyacrylamide Complex.," *J. Appl. Polym. Sci.*, vol. 85, pp. 1619–1623, Aug. 2002.
- [159] S. S. Shiratori and M. F. Rubner, "pH-Dependent Thickness Behavior of Sequentially Adsorbed Layers of Weak Polyelectrolytes.," *Macromolecules*, vol. 33, no. 11, pp. 4213–4219, May 2000.
- [160] O. Mermut and C. J. Barrett, "Effects of Charge Density and Counterions on the Assembly of Polyelectrolyte Multilayers.," *J. Phys. Chem. B*, vol. 107, no. 11, pp. 2525–2530, Mar. 2003.
- [161] Lenntech, "Deionized/Demineralized Water." [Online]. Available: <http://www.lenntech.com/applications/process/demineralised/deionised-demineralised-water.htm>. [Accessed: 29-Apr-2015].
- [162] A. Schulze, M. F. Maitz, R. Zimmermann, B. Marquardt, M. Fischer, C. Werner, M. Went, and I. Thomas, "Permanent surface modification by electron-beam-induced grafting of hydrophilic polymers to PVDF membranes.," *RSC Adv.*, vol. 3, pp. 22518–22526, 2013.
- [163] D. Bhattacharyya, T. Schäfer, S. R. Wickramasinghe, and S. Daunert, Eds., *Responsive Membranes and Materials*, First. John Wiley & Sons, Ltd, 2013, p. 432.
- [164] H. Ivnitsky, I. Katz, D. Minz, G. Volvovic, E. Shimoni, E. Kesselman, R. Semiat, and C. G. Dosoretz, "Bacterial community composition and structure of biofilms developing on nanofiltration membranes applied to wastewater treatment.," *Water Res.*, vol. 41, pp. 3924–3935, Sep. 2007.
- [165] T. Falcioni, A. Manti, P. Boi, B. Canonico, M. Balsamo, and S. Papa, "Comparison of Disruption Procedures for Enumeration of Activated Sludge Floc Bacteria by Flow Cytometry.," *Cytom. Part B (Clinical Cytom.)*, vol. 70B, pp. 149–153, 2006.
- [166] A. Bruns, H. Hoffelner, and J. Overmann, "A novel approach for high throughput cultivation assays and the isolation of planktonic bacteria.," *FEMS Microbiol. Ecol.*, vol. 45, pp. 161–171, Jul. 2003.
- [167] R. Ghai, K. D. McMahon, and F. Rodriguez-Valera, "Breaking a paradigm: cosmopolitan and abundant freshwater actinobacteria are low GC.," *Environ. Microbiol. Rep.*, vol. 4, no. 1, pp. 29–35, Feb. 2012.
- [168] M. Ventura, C. Canchaya, A. Tauch, G. Chandra, G. F. Fitzgerald, K. F. Chater, and D. van Sinderen, "Genomics of Actinobacteria: tracing the evolutionary history of an ancient phylum.," *Microbiol. Mol. Biol. Rev.*, vol. 71, no. 3, pp. 495–548, Sep. 2007.
- [169] S. J. McIlroy, R. Kristiansen, M. Albertsen, S. M. Karst, S. Rossetti, J. L. Nielsen, V. Tandoi, R. J. Seviour, and P. H. Nielsen, "Metabolic model for the filamentous 'Candidatus Microthrix parvicella' based on genomic and metagenomic analyses.," *ISME J.*, vol. 7, pp. 1161–1172, Jun. 2013.
- [170] K. Zhang, H. Choi, M. Wu, G. a. Sorial, D. Dionysiou, and D. B. Oerther, "An ecology-based analysis of irreversible biofouling in membrane bioreactors.," *Water Sci. Technol.*, vol. 55, no. 8–9, pp. 395–402, May 2007.

## A - X

- [171] A. C. Martiny, T. M. Jørgensen, H.-J. Albrechtsen, E. Arvin, and S. Molin, "Long-Term Succession of Structure and Diversity of a Biofilm Formed in a Model Drinking Water Distribution System.," *Appl. Environ. Microbiol.*, vol. 69, no. 11, pp. 6899–6907, 2003.
- [172] A. Piasecka, R. Bernstein, F. Ollevier, F. Meersman, C. Souffreau, R. M. Bilad, K. Cottenie, L. Vanysacker, C. Denis, and I. Vankelecom, "Study of biofilms on PVDF membranes after chemical cleaning by sodium hypochlorite.," *Sep. Purif. Technol.*, vol. 141, pp. 314–321, Feb. 2015.
- [173] D. Springael, "Cursustekst - ION90A Biochemische analysetechnieken.," Leuven, 2012.
- [174] A. Jabs, "Determination of Secondary Structure in Proteins by Fourier Transform Infrared Spectroscopy (FTIR).," *Jena Library of Biological Macromolecules*. [Online]. Available: [http://jenalib.fli-leibniz.de/ImgLibDoc/ftir/IMAGE\\_FTIR.html](http://jenalib.fli-leibniz.de/ImgLibDoc/ftir/IMAGE_FTIR.html). [Accessed: 01-May-2015].
- [175] A. S. Landa, H. C. Van Der Mei, and H. J. Busscher, "Detachment of Linking Film Bacteria From Enamel Surfaces by Oral Rinses and Penetration of Sodium Lauryl Sulphate Through an Artificial Oral Biofilm.," *Adv. Dent. Res.*, vol. 11, no. 4, pp. 528–538, Nov. 1997.
- [176] K. J. Howe, K. P. Ishida, and M. M. Clark, "Use of ATR/FTIR spectrometry to study fouling of microfiltration membranes by natural waters.," *Desalination*, vol. 147, pp. 251–255, Sep. 2002.
- [177] V. M. Siqueira and N. Lima, "Biofilm Formation by Filamentous Fungi Recovered from a Water System.," *J. Mycol.*, pp. 1–9, 2013.
- [178] M. W. Harding, L. L. R. Marques, R. J. Howard, and M. E. Olson, "Can filamentous fungi form biofilms?," *Trends Microbiol.*, vol. 17, no. 11, pp. 475–480, Nov. 2009.
- [179] S. Ishii, T. Shimoyama, Y. Hotta, and K. Watanabe, "Characterization of a filamentous biofilm community established in a cellulose-fed microbial fuel cell.," *BMC Microbiol.*, vol. 8, no. 6, Jan. 2008.
- [180] H. Lin, S. L. Ong, W. J. Ng, and E. Khan, "Monitoring of Bacterial Morphology for Controlling Filamentous Overgrowth in an Ultracompact Biofilm Reactor.," *Water Environ. Res.*, vol. 76, pp. 413–424, 2004.
- [181] Bernardo, E. C., Egashira, R., & Kawasaki, J. (1997). Decolorization of molasses' wastewater using activated carbon prepared from cane bagasse. *Carbon*, 35(9), 1217–1221.
- [182] Santal, A. R., & Singh, N. P. (2013). Biodegradation of Melanoidin from Distillery Effluent : Role of Microbes and Their Potential Enzymes. In R. Chamy & F. Rosenkranz (Eds.), *Biodegradation of Hazardous and Special Products* (pp. 71–104). doi:10.5772/56252
- [183] Puspitasari, V., Granville, A., Le-Clech, P., & Chen, V. (2010). Cleaning and ageing effect of sodium hypochlorite on polyvinylidene fluoride (PVDF) membrane. *Separation and Purification Technology*, 72, 301–308. doi:10.1016/j.seppur.2010.03.001
- [184] Rouaix, S., Causserand, C., & Aimar, P. (2006). Experimental study of the effects of hypochlorite on polysulfone membrane properties. *Journal of Membrane Science*, 277(1-2), 137–147. doi:10.1016/j.memsci.2005.10.040

# Appendix 1: Complementary results

This section firstly contains the detailed description and discussion of the operating conditions and physico-chemical properties of the HT-MBR. Secondly it encompasses the results and discussion of the data obtained from the cleaned (C) membranes in comparison with the pristine (P) membranes. Indeed, these data are rather a side-product of the research and thus not included in the main part of the work. Finally it presents figures and tables that are important for the interpretation of the results but are redundant and thus not presented in the main part of the work. Each explanatory section is concluded with a brief summary, marked by ✨, meant for busy people, except for **Section 1** below, of which the summary is given in **Section 1** of **Chapter 4**.

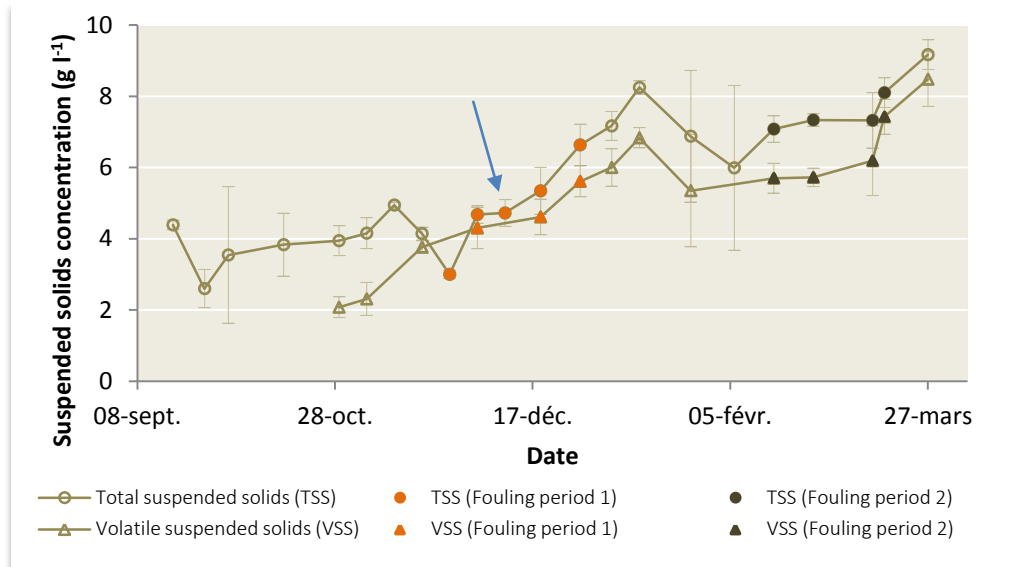
## 1. MEMBRANE BIOREACTOR AND QUALITY MEASUREMENTS

### 1.1. Operation of the HT-MBR

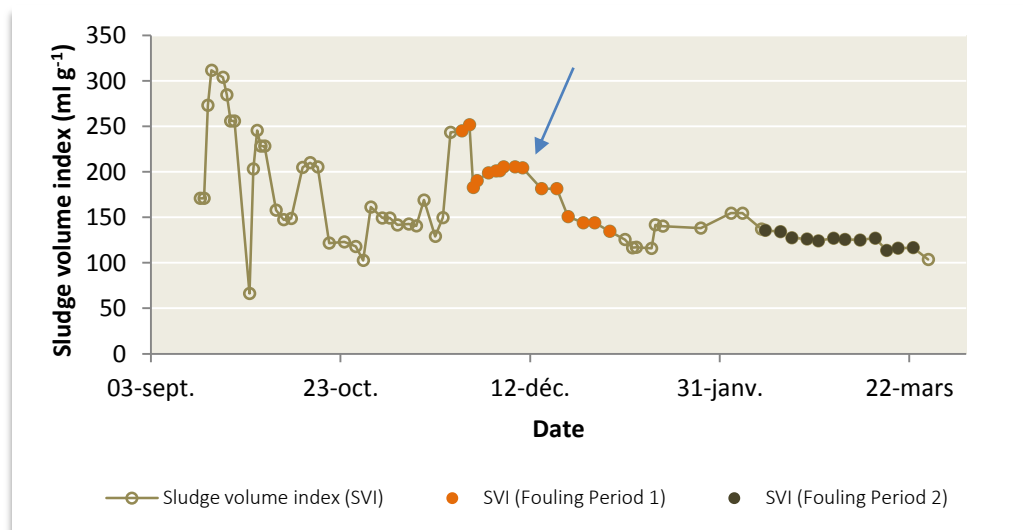
**A-Figure 1** represents the evolution of the sludge biomass concentration during both Transient Periods 1 and 2 and Fouling Periods 1 and 2, which were defined in **Section 2.1.3** of **Chapter 3**. The average TSS concentration increased slowly from  $2.60 \text{ g l}^{-1}$  to  $4.72 \text{ g l}^{-1}$  at the start of Fouling Period 1, and from the moment the protamylasse feed concentration was increased, the TSS showed a rapid increase to a final value of  $9.17 \text{ g l}^{-1}$  at the end of Fouling Period 2. Thus the increase in protamylasse feed concentration enhanced biomass growth in the mixed liquor, but no steady-state was observed during the monitoring period. The overall TSS concentration was in the range  $(6.05 \pm 1.74) \text{ g l}^{-1}$ , which corresponds to values reported in literature for operation on industrial wastewater, e.g., by Piasecka et al. (2012) (TSS increase from 8 to  $13 \text{ g l}^{-1}$  during their experiment), Bilad et al. (2010) ( $8\text{-}12 \text{ g l}^{-1}$ ) or Bilad et al. (2011) ( $10.2 \text{ g l}^{-1}$ ) [6], [130], [131], and guaranteed efficient removal of nutrients (see further, **Section 1.2**) [6]. The VSS concentration increased from  $2.08 \text{ g l}^{-1}$  to a final value of  $8.48 \text{ g l}^{-1}$  at the end of Fouling Period 2. The overall VSS concentration was in the range  $(5.31 \pm 1.79) \text{ g l}^{-1}$ , which is higher than the typical values reported in literature (i.e.,  $3 \text{ g l}^{-1}$  [11]).

**A-Figure 2** represents the evolution of the SVI during both Transient Periods and 40-day Fouling Periods. The SVI fluctuated between  $312 \text{ ml g}^{-1}$  and  $66 \text{ ml g}^{-1}$  during Transient Period 1, but tended to stabilize from Fouling Period 1 on when the protamylasse feed concentration was increased, to finally reach an apparent steady state with values between  $100$  and  $150 \text{ ml g}^{-1}$  at the end of Fouling Period 2, i.e., after a total operation period of 150 days. Indeed, it has already been reported that steady state conditions appear after a period lasting two to five times the SRT [70]. For instance Boon et al. (2002) worked with sludge from a wastewater treatment plant treating carbohydrate rich wastewater from

the potato processing industry and reported the long-term SVI to be  $100 \text{ ml g}^{-1}$  [151]. Unfortunately it was technically impossible to wait that long before starting the fouling experiment. The overall average SVI was  $(153 \pm 37) \text{ ml g}^{-1}$ , indicating bulking sludge, which was confirmed by microscopic analysis (see further, [Section 1.3](#)). Moreover Transient Periods 1 and 2 were characterized by excessive scum formation (not shown). Since membranes enhance biomass separation compared to conventional sedimentation technology, settleability is no longer a limiting factor to obtain an effluent of high quality ([Chapter 2](#)) [2].



**A-Figure 1** Evolution of the concentration of total suspended solids ( $\text{g l}^{-1}$ ) and volatile suspended solids ( $\text{g l}^{-1}$ ) during Transient Periods 1 and 2 and Fouling Periods 1 and 2. The blue arrow indicates the moment the concentration of the protamylasse feed solution was increased from  $1.5$  to  $2.3 \text{ ml l}^{-1}$ . Error bars represent standard deviations from the mean value ( $n = 3$ ).

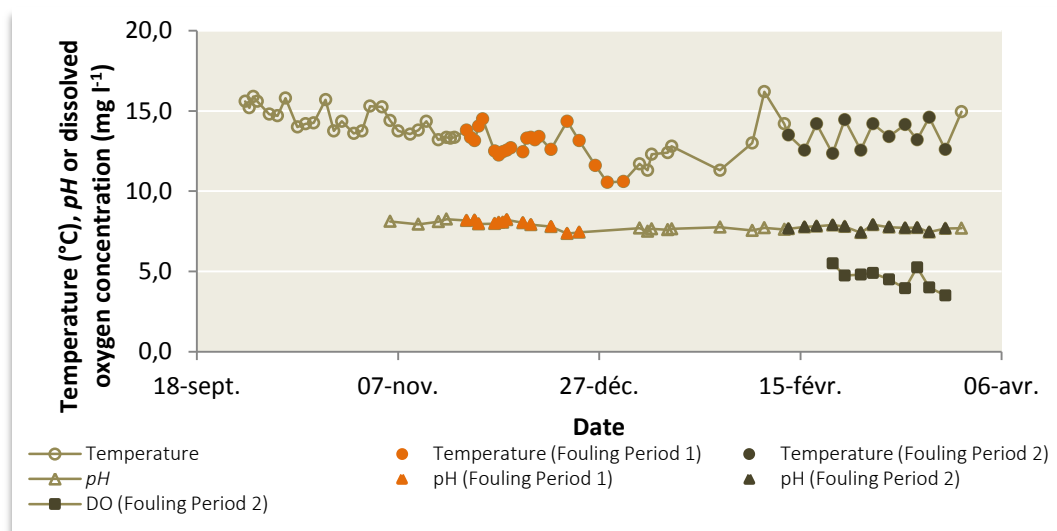


**A-Figure 2** Evolution of the sludge volume index ( $\text{ml g}^{-1}$ ) during Transient Periods 1 and 2 and Fouling Periods 1 and 2. The blue arrow indicates the moment the concentration of the protamylasse feed solution was increased from  $1.5$  to  $2.3 \text{ ml l}^{-1}$ .



QR code giving access to Youtube: bioreactor aeration video.

**A-Figure 3** represents the evolution of the temperature, the *pH* and the DO concentration of the sludge during both Transient Periods and Fouling Periods. As already mentioned earlier, the temperature fluctuated according to environment temperature since no heat control was applied (notice the temperature decrease during Fall). The overall average temperature was  $(13.6 \pm 1.2)$  °C. The *pH* of the sludge was stable at a value  $(7.81 \pm 0.24)$ , which corresponds to typical values reported by Khan et al. (2013) (*pH* 7-8) or by Piasecka et al. (*pH* 6-8) [6], [14]. Thus, based on a comparison between the *pKa* values of the surface groups and the *pH* of the sludge (**Chapter 3, Section 1**), it can be concluded that the synthesized membranes bore the required surface charge. The dissolved oxygen concentration was only recorded at the end of Fouling Period 2 since no equipment was available earlier, and showed values of  $(4.6 \pm 0.6)$  mg O<sub>2</sub> l<sup>-1</sup>. It is difficult to give an interpretation of the measurements in such a short period, but it may correspond to typical values reported in literature by Meng et al. (2007) ( $(4.76 \pm 1.27)$  mg O<sub>2</sub> l<sup>-1</sup>) or Piasecka et al. (2012) (6-8 mg O<sub>2</sub> l<sup>-1</sup>) [6], [31] or even be higher than reported values, e.g., Waheed et al. (2013) (2-2.5 mg O<sub>2</sub> l<sup>-1</sup>) or Grelier et al. (2006) (2 mg O<sub>2</sub> l<sup>-1</sup>) [2], [13]. It can be assumed that the measured DO values in the bioreactor vessel allowed for biodegradation by aerobic bacteria since the minimum concentration of DO required for this purpose is known to be 1-2 mg O<sub>2</sub> l<sup>-1</sup> [11]. However the bubble aeration in the reactor was not evenly distributed over the whole sludge suspension volume, thus creating zones of turbulence and zones of apparent sludge stationarity where anoxic conditions could develop and membrane surfaces were not sheared extensively (QR code<sup>1</sup>).



**A-Figure 3** Evolution of the temperature (°C), the *pH* and the dissolved oxygen concentration (mg O<sub>2</sub> l<sup>-1</sup>) of the sludge during Transient Periods 1 and 2 and Fouling Periods 1 and 2.

<sup>1</sup> <https://www.youtube.com/watch?v=8Lk7Ar3k6io>

## 1.2. Physico-chemical analysis

The HT-MBR was able to achieve good organic removal efficiencies, although the standard deviations on the measurements are rather high, mainly indicating fluctuations in the characteristics of feed and permeate samples as the measurements were performed on different days (Table 13 of Chapter 4). The calculated removal efficiencies take into account the effect of the membrane (i.e., retention of total suspended solids as well as biopolymers (proteins, polysaccharides) from the sludge supernatant) [70] as well as the effect of the sludge suspension (i.e., biodegradation of organic compounds).

The overall COD removal efficiency was  $(90.9 \pm 2.9)$  % and corresponds to typical values reported in literature [70]. A comparison of the COD of the sludge supernatant and the permeate, shows that the membrane retained up to  $(33.3 \pm 7.7)$  % of soluble COD. Massé et al. (2006) reported that these retained compounds are probably gradually degraded in the bioreactor [70]. The high COD values may be explained by relatively high concentrations of sugars (glucose, fructose, saccharose) in the protamylasse feed solution.

The overall TN removal efficiency was  $(49.3 \pm 22.9)$  %, which may be low compared to literature values (e.g., 59.8 % [14]), but which is still high knowing that the reactor was operated aerobically and an anoxic environment is needed for denitrification to occur. Nevertheless it can be assumed that some denitrification did occur by the activity of heterotrophic bacteria due to the unevenly distributed oxygen supply over the reactor volume, creating zones of oxygen deficiency, as mentioned earlier, as well as the occurrence of anoxic zones within the sludge flocs and with increasing biofilm depth [6], [28]. Khan et al. (2013) moreover reported the activity of various *Pseudomonas* sp., which are reported to grow in all different sludges, thus catalyzing the denitrification process of a MBR, even at high DO concentration [14]. The growth of nitrifying bacteria (slow-growers) was probably enhanced due to the long SRT and complete retention of the biomass by the membranes [13], [130]. Nitrogen assimilation in microbial cells as  $\text{NH}_2$  proteins is probably excluded since the average COD:N ratio of the protamylasse feed solution was 100:17 and thus smaller than the ratio 100:5 known as optimal for bacterial growth [164].

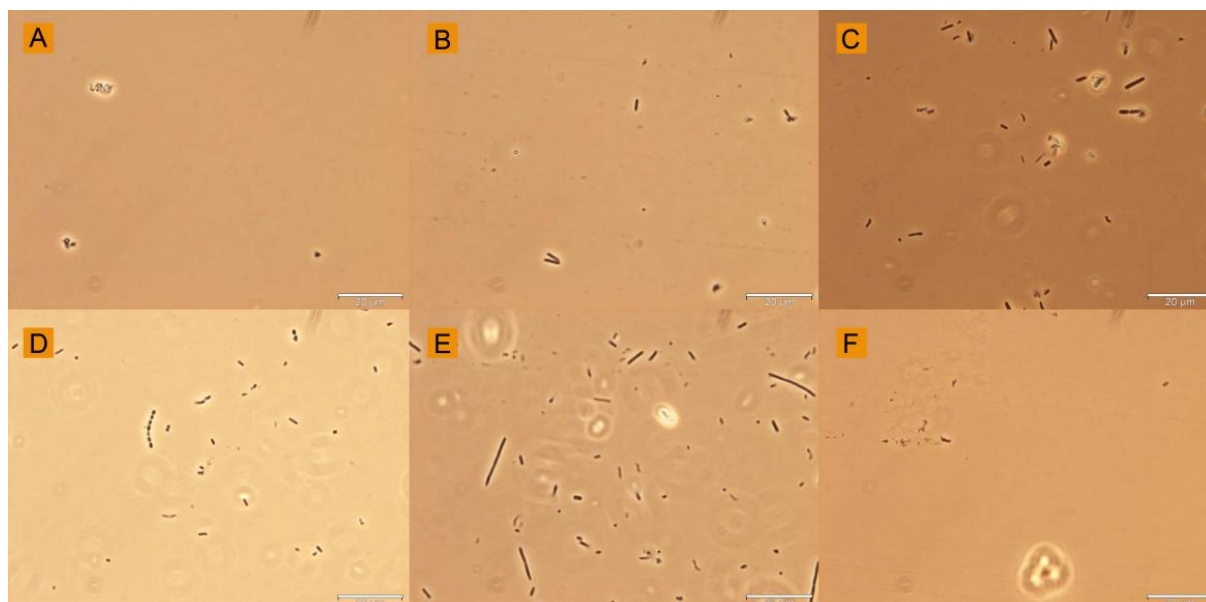
The overall phosphate removal efficiency was  $(25.5 \pm 11.8)$  %, which is relatively low compared to literature values (e.g., 46.5 % [8]). Anaerobic conditions necessary for phosphate removal were potentially created within the sludge flocs and with increasing biofilm depth [6], thus enabling phosphate release and subsequent phosphate accumulation in the aerobic zones of the flocs and the sludge suspension. Moreover phosphate accumulation within microbial cells was susceptible to occur since the average COD:P ratio of the protamylasse feed solution was 100:1, which corresponds to the

ratio known as optimal for bacterial growth [164]. Finally the proliferation of filamentous bacteria, among which possibly *Microthrix parvicella* (Section 1.3 below), may explain the phosphate removal since this bacteria is observed to store polyphosphate under anaerobic as well as under aerobic or anoxic conditions [169].

The average sludge loading rate of the HT-MBR was  $0.17 \text{ kg COD kg}^{-1} \text{ TSS d}^{-1}$  and the average volumetric loading rate was  $1.05 \text{ kg COD m}^{-3} \text{ d}^{-1}$ , corresponding to typical values reported in literature for the treatment of industrial wastewater [2], [14], [52].

### 1.3. Microscopic analysis

The protamylasse feed solution freshly inoculated in sterilised vessels on day 1 of the maintenance period contained almost no bacteria (image (A) of A-Figure 4). However, bacteria started to grow from day 2 on and on the last day of the maintenance period the free-living bacteria exhibited some nascent filaments among the community (image (E) of A-Figure 4). The sludge suspension community thus was influenced by these bacteria. Moreover they consumed part of the COD of the feed solution in the tank itself before it was delivered to the bacteria in the HT-MBR. Namely the COD of the feed decreased on average by 17.6% (data not shown) between day 1 and day 8 of the maintenance period, explaining the large standard deviation on the COD values of the feed presented above.



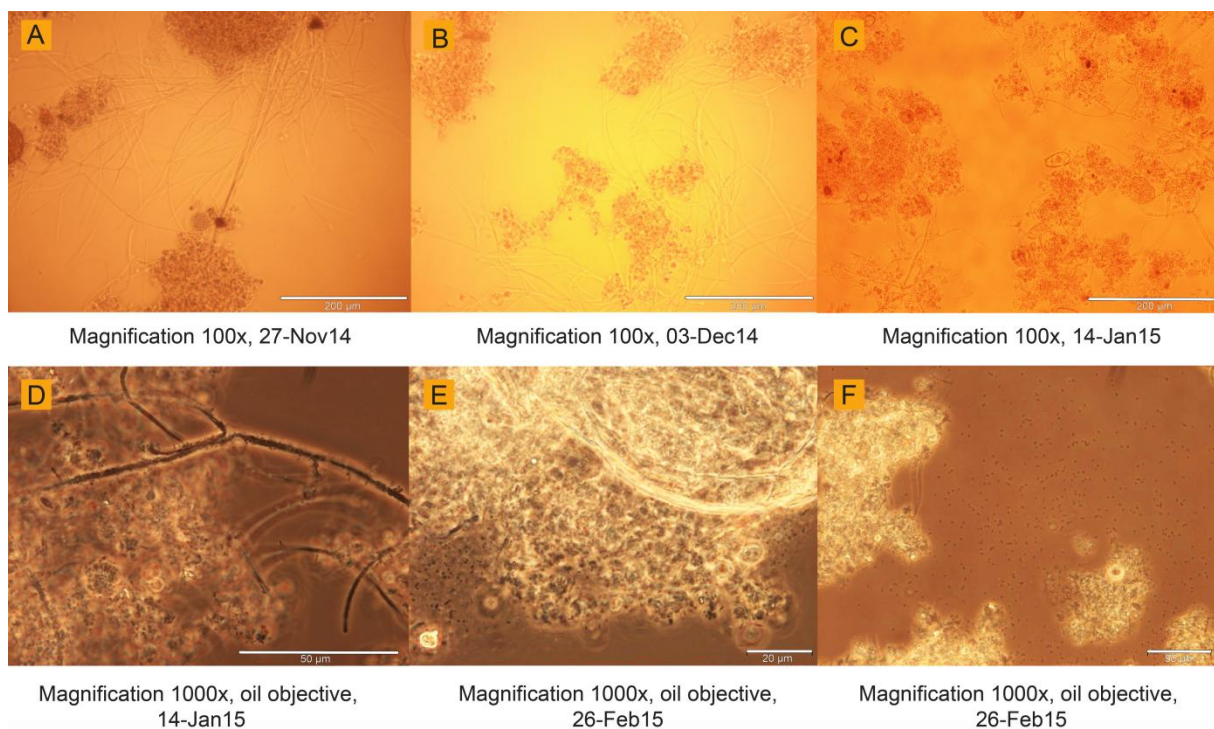
**A-Figure 4** Bacterial growth in the protamylasse feed solution during the maintenance period of 8 days and microscopic investigation of the permeate (magnification 1000x, oil objective). (A) feed day 1, (B) feed day 2, (C) feed day 3, (D) feed day 4, (E) feed day 8, (F) permeate.

During Transient Periods 1 and 2 and Fouling Periods 1 and 2 large numbers of filaments were observed microscopically growing through and at the edges of the sludge flocs, explaining the poor sludge settleability (A-Figure 5). Determination of the bacterial filamentous species based on



microscopic images requires an expert eye, but *M. parvicella* might be a potential member since it proliferates in sludges characterised by a sludge loading rate below  $0.2 \text{ kg BOD kg}^{-1} \text{ MLSS day}^{-1}$ , zones of oxygen deficiency and a high SRT [28]. Attached growth was often observed surrounding the filaments (image (D) of **A-Figure 5**). Based on Eikelboom (2000) and on images (A), (B) and (C) from **A-Figure 5**, the FI ranged between 3 and 4 during the whole monitoring period, indicating an excessive growth of filamentous bacteria [28]. The causes of bulking sludge are manifold. The proliferation of filamentous bacteria could be induced by e.g., too low dissolved oxygen concentrations [32], [76] due to the unevenly distributed oxygen supply or by a too low sludge loading rate [11]. Indeed, from the moment the protamylasse feed concentration was increased, the settleability of the sludge improved, but sludge bulking was still observable. It would have been judicious to apply step-feeding by feeding on discrete time moments instead of continuously, as to favour the growth of floc-forming bacteria [11]. Unfortunately the equipment was not available. Also an excessive SRT could cause bulking and foaming behaviour [26]. Although bulking sludge is not limiting in MBRs, an overgrowth of filamentous bacteria leads to an increase in sludge viscosity and hydrophobicity [31]. This in turns affects the filtration efficiency and fastens membrane fouling [48].

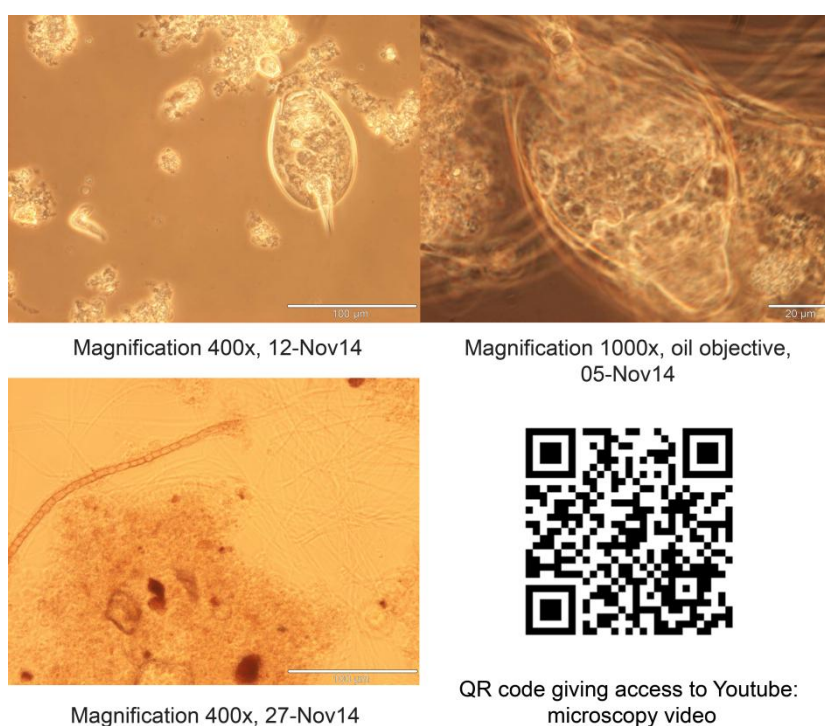
The morphology of the flocs did almost not change with time: the flocs were mostly irregularly shaped and robust, although at some time points free-living bacteria were found in the neighbourhood of the flocs (image (F) of **A-Figure 5**), as well as bacteria embedded in a slime matrix (image (E) of **A-Figure 5**). Floc dimensions varied between 50 and 500  $\mu\text{m}$ .



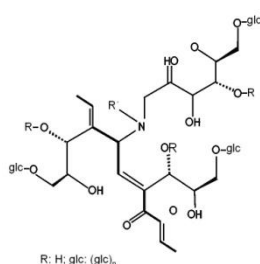
**A-Figure 5** Microscopic analysis of the sludge at different magnifications and time points.



Organisms other than free-living, filamentous or floc-forming bacteria were observed during the operation of the HT-MBR as well (A-Figure 6). For instance fungi could be sporadically seen (Image (C) of A-Figure 6) exhibiting clearly visible transverse septa and rectangular cells larger than bacterial filaments. Filamentous fungi do not cause bulking sludge [28] but may indicate abnormal conditions such as *pH* deviations [26], [29]. However, no such deviations were observed during the HT-MBR operation and the filamentous fungi were not predominantly present in the activated sludge suspension. Also protozoa and metazoan could be observed, for instance ciliates (image (A) and (B) of A-Figure 6, QR code to YouTube video) and nematodes (QR code to YouTube Video). This all indicated a sludge system of good to moderate quality.



**A-Figure 6** Microscopic analysis of the sludge at different magnifications and focusing on non-bacterial microorganisms. The QR code<sup>2</sup> gives access to a YouTube video showing the activity of ciliates and nematodes.



Basic structure of melanoidin

Microorganisms were not detected visually in the permeate during the operation of the HT-MBR, thus indicating that the membranes managed to fully retain microorganisms from the sludge suspension (A-Figure 4). On the contrary some particles were detected, but these may have originated from the set-up tubes. The brownish colour of the permeate may be attributed to melanoidin, a high molecular weight (> 5 kDa [2]) nitrogenous brown polymer present in wastewater originating from fermentation

<sup>2</sup> <https://www.youtube.com/watch?v=BBkvOE246Fw>

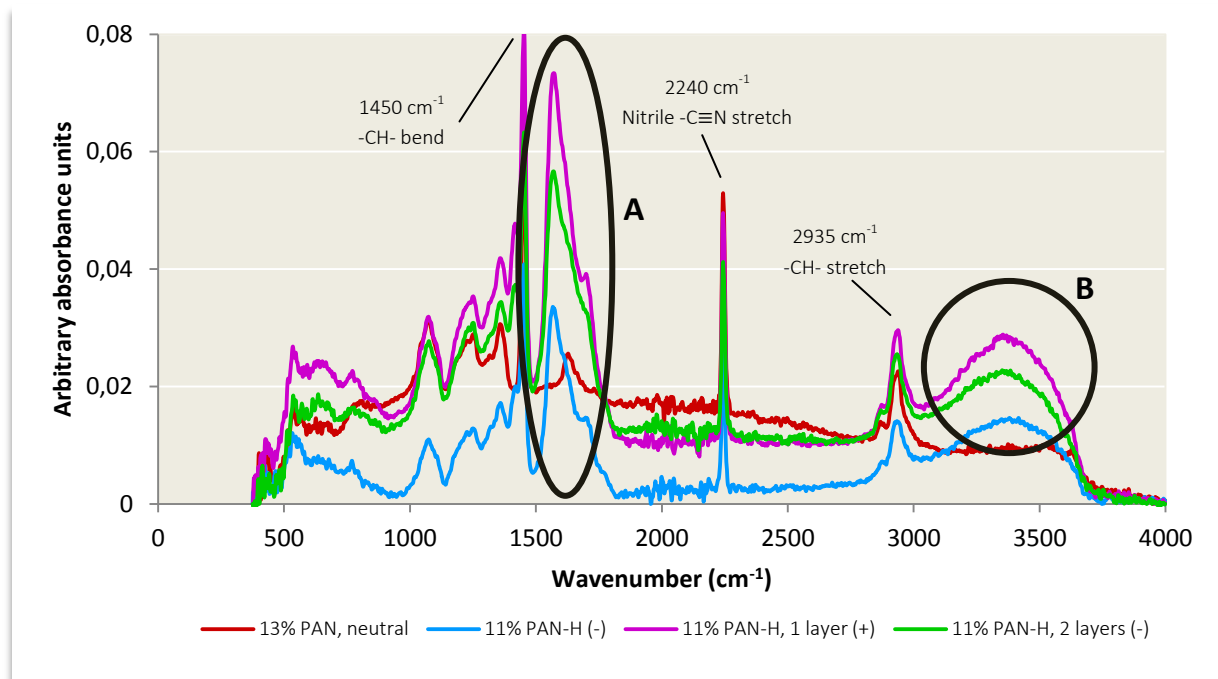
industries, as reported by Bernardo et al. (1997) [181]. Although it has been reported that melanoidin is highly resistant to biodegradation due to its structural complexity [182], its biodegradability may have been enhanced due to the long SRT the HT-MBR was operated at [130]. The non-degraded molecules may not have been retained by the membranes, and may thus explain the extremely low COD:N ratio of 100:138 of the permeate (Chapter 4, Section 3).

## 2. MEMBRANE PERFORMANCE MEASUREMENT

### 2.1. Physico-chemical related measurements

#### 2.1.1. Attenuated Total Reflectance Fourier Transform Infrared Spectroscopy

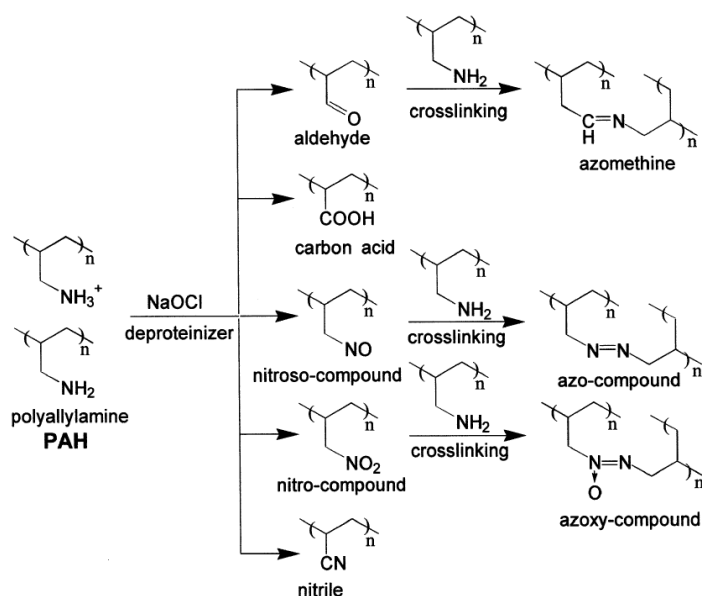
A-Figure 7 gives the ATR-FTIR spectra of the C-membranes. The typical peaks for the 13% PAN (neutral) membranes, i.e.,  $1450\text{ cm}^{-1}$ ,  $2240\text{ cm}^{-1}$  and  $2935\text{ cm}^{-1}$ , shown in Figure 24 of Chapter 4, are still present after intensive cleaning with NaClO. On the contrary the FTIR peaks associated with 11% PAN-H (-), as well as with 11% PAN-H, 1 layer (+) and 11% PAN-H, 2 layers (-) changed, indicating removal of the functionalized or deposited layers. Although PAN is known to show good resistance against NaClO as chemical cleaning agent (active chlorine < 15 ppm) [122], PAN-H is only known to show good solvent resistance (e.g., chloroform, acetone, hexane) [45]. Moreover cleaning with NaClO is generally applied for less than 24 h at low to moderate concentrations (0.1-1 %) [53], [59], [172]. Here cleaning was performed during 3.5 days with 2 % NaClO, thus altering the membrane surface chemistry.



A-Figure 7 ATR-FTIR spectra of the four membrane types (C-membranes). (A) intensification of the peak at  $1560\text{ cm}^{-1}$  and weakening of the peak at  $1690\text{ cm}^{-1}$ , (B) disappearance of the peak at  $3100\text{ cm}^{-1}$  and  $3350\text{ cm}^{-1}$ .

Firstly it could be assumed that NaClO did affect the negatively charged membranes by converting almost all carboxylic acid groups (-COOH) to negatively charged carboxylate groups (-COO<sup>-</sup>) due to its elevated *pH* (10.55), thus explaining the disappearance of the (O-H) stretch vibration at 3100 cm<sup>-1</sup>, the weakening of the carbonyl (-C=O) stretch vibration at 1690 cm<sup>-1</sup> and the intensification of the peak at 1560 cm<sup>-1</sup>, corresponding to the asymmetric carboxylate ion (-COO<sup>-</sup>) stretch vibration [156].

Secondly, it seems that the positively charged membrane is more influenced by the oxidation properties of NaClO than the negatively charged membranes. Moya et al. (2001) reported that oxidation of PAH destroys the positively charged amino groups and yields among others uncharged groups (e.g., mainly nitriles) and negatively charged groups (e.g., mainly carboxylic groups) [157]. The scheme of possible reactions of PAH reaction with NaClO is given in **A-Figure 8**, highlighting the complexity of ascribing FTIR peak shifts. Thus this may explain the disappearance of the amine (N-H) stretch vibration at 3350 cm<sup>-1</sup> together with the little intensification of the asymmetric carboxylate ion (-COO<sup>-</sup>) stretch vibration at 1560 cm<sup>-1</sup> and of the nitrile (C≡N) stretch at 2240 cm<sup>-1</sup> (compare its intensity with **Figure 24** of **Chapter 4**).



**A-Figure 8** Scheme of possible reactions taking place when incubating poly(allylamine hydrochloride) (PAH) in sodium hypochlorite (NaClO) (reproduced from [184]).

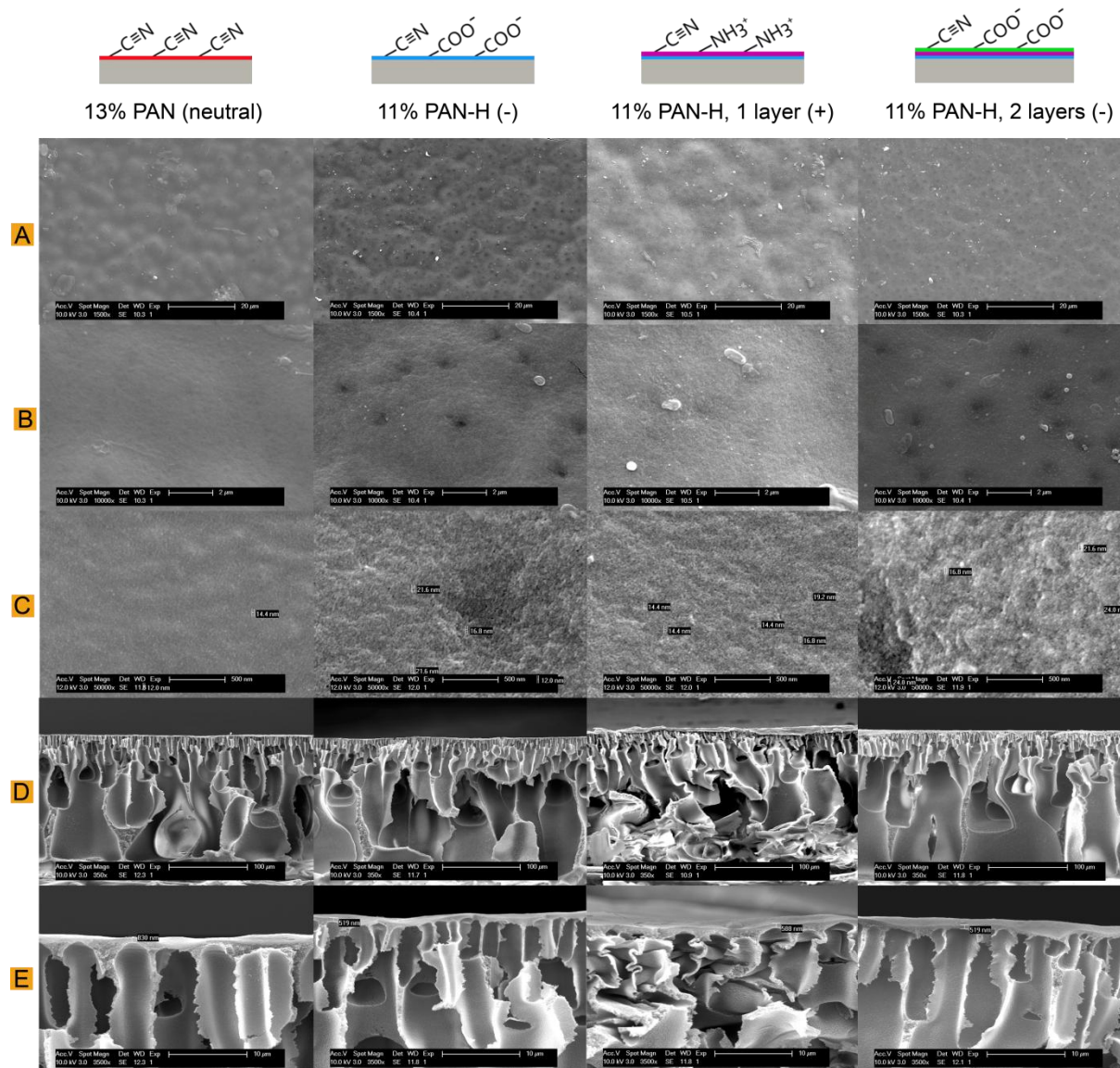
☀ Summarized, intensive membrane cleaning with NaClO influences the chemical structure of the functionalized charged PAN membranes at a higher degree than the neutral pure 13% PAN membrane, but the precise reaction mechanism is still unclear. It eventually leads to membrane ageing and its long-term application should be avoided in order to guarantee consistency and reliability of the membrane surface chemistry.

### 2.1.2. Scanning Electron Microscopy

**A-Figure 9** shows the surface and cross-sectional images of the four membrane types (C-membranes) at different magnifications. Like for the P-membranes, the cross-sectional images (D) show asymmetric integrally skinned membranes consisting of finger-like macrovoids extending along the membrane cross-section over a distance of approximately 250  $\mu\text{m}$ , corresponding to the wet casting thickness during membrane manufacturing. The sub layer thickness is approximately 1  $\mu\text{m}$  for the 13% PAN (neutral) membrane and ranges between 500 and 600 nm for the 11% PAN-H (-) as well as for the 11% PAN-H, 1 layer (+) and 11% PAN-H, 2 layers (-) membranes (images (E) of **A-Figure 9**). These values are lower than for the P-membranes and may possibly indicate the removal of (part of) the surface or deposited layer(s) due to extended chemical cleaning with NaClO. The sub layer thickness for 13% PAN (neutral) has decreased too compared to the P-membranes, but since it is known that pure PAN shows excellent resistance against NaClO [122], this decrease in thickness is attributed to the quality of the membrane preparation, fracturing and subsequent image quality. This conclusion can be extrapolated to the charged membranes too as second possible explanation for the decrease in sub layer thickness. As already mentioned previously, artefacts can occur during membrane preparation and fracturing, as is the case for 11% PAN-H, 1 layer (+), showing crushed pores (images (D) and (E) of **A-Figure 9**).

Next, the surface images (A) and (B) of the membranes 11% PAN-H (-) as well as 11% PAN-H, 1 layer (+) and 11% PAN-H, 2 layers (-) are significantly different from the images of the P-membranes and resemble 13% PAN (neutral) most (compare with **Figure 25, Chapter 4**). The depression-like surface structures that were present on the P-membranes apparently almost disappeared, exhibiting the underlying surface structure, which is the one of pure PAN. It seems that the positively charged membrane is more influenced by the oxidation reaction than the negatively charged membranes, as already mentioned previously during the discussion of the ATR-FTIR results above (compare images (B) of 11% PAN-H, 1 layer (+) on the one hand, and 11% PAN-H (-) and 11% PAN-H, 2 layers (-) on the other hand in **A-Figure 9**). This surface modification may be attributed to the long-term cleaning with NaClO, which did almost digest the deposited polymer layers as well as did alter the hydrolyzed membrane surface, as has been explained before [183], [184]. Moreover, as seen in images (C) of **A-Figure 9**, the density of pores at the surface of the charged membranes did increase considerably, without a change in apparent pore diameter, while the porosity of the neutral PAN membrane was not influenced. As a result, the permeability of the formerly charged membranes should increase drastically, and this was indeed observed (**Chapter 4, Section 6.2.1**). The spongy character after long-term cleaning of PVDF and PSf membranes with NaClO has already been reported by Puspitasari et al. (2010) and Rouaix et al. (2006) respectively [183], [184]. But in contrast to the observations made

here, they reported a decline in pore size followed by a subsequent pore size increase due to digestion or elimination of the coated layer. Since the resolution of the SEM images presented here did not allow for undisputable determination of the pore size, the same behaviour possibly applies.



**A-Figure 9** SEM surface and cross-sectional visualization of the four membrane types (C-membranes). (A) 10 kV, magnification 1500x, (B) 10 kV, magnification 10 000x, (C) 12 kV, magnification 50 000x, (D) 10 kV, magnification 350x, (E) 10 kV, magnification 3500x.

☀ Summarized, intensive cleaning with NaClO does not only influence the surface chemistry of the charged membranes, but also alters their physical structure. Membrane ageing is caused by digestion of the membrane modifier surfaces, while the underlying surface structure made of neutral pure 13% PAN membrane remains unaffected. Intensive oxidative cleaning of charged PAN membranes yields spongy structures characterized by an increase in apparent surface smoothness and no apparent pore size reduction, while the finger-like macroporous structure remains unchanged.




## 2.2. Permeability related measurements

### 2.2.1. Clean water permeance

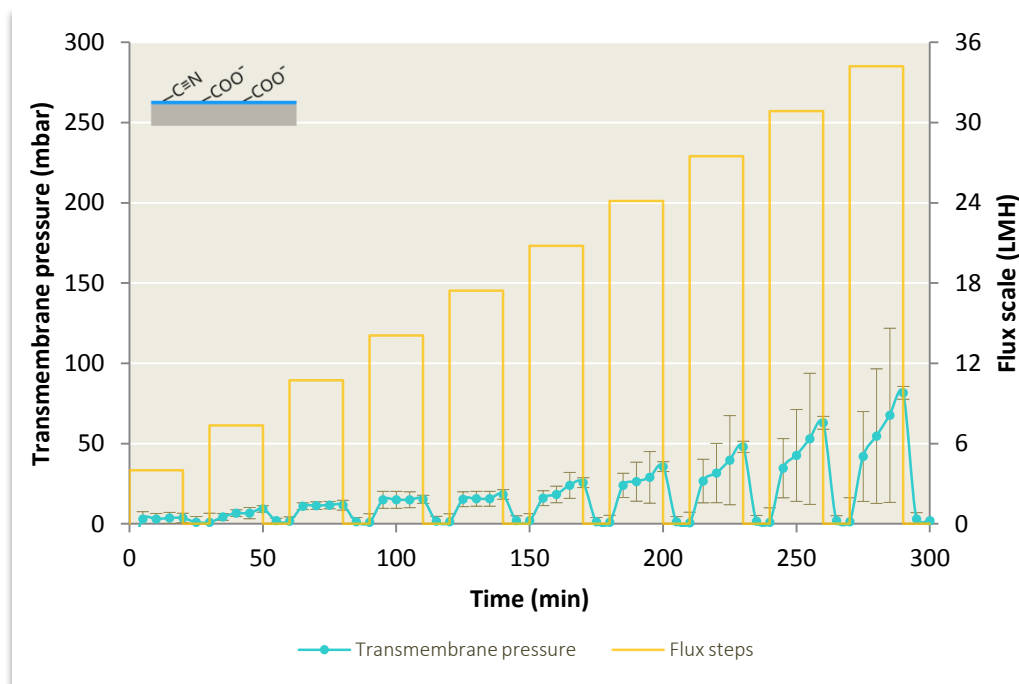
**Figure 31 (Chapter 4)** gives the clean water permeability of the four membrane types, both the P- as well as the C-membranes. The discussion on the permeability values of the P-membranes has already been conducted. Statistical comparison of the permeabilities obtained by the filtration of the P-modules and filtration of the respective C-modules after extended cleaning with NaClO, demonstrated the clean water permeability was not affected by the cleaning episode in the case of the 13% PAN (neutral) membrane, but drastically changed in the case of the charged membranes (Student's t,  $p < 0.001$  and  $0.001 < p < 0.005$ ). The permeability did increase significantly because of a significant decline in steady-state transmembrane pressure instead of a variation in flux (raw data not shown). Another explanation may be the increased hydrophilicity of the membranes upon cleaning thus supporting an enhanced clean water flux [184]. **A-Tabel 1** illustrates it clearly: while the intrinsic membrane resistance does not change upon cleaning for 13% PAN (neutral), it decreases between 60 and 80% for the charged membranes.

**A-Tabel 1** Hydraulic resistance ( $m^{-1}$ ) of coupons (pristine) ( $n = 3 \times 3$ ) and modules (P- and C-membranes) ( $n = 4 \times 2$ ) of the four membrane types.

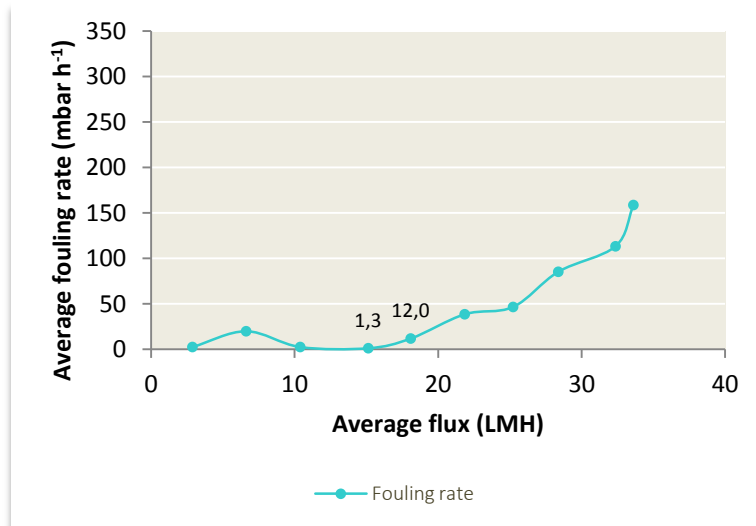
Membrane type	$R_{m,coupons} (m^{-1})$	$R_{m,P-modules} (m^{-1})$ A	$R_{m,C-modules} (m^{-1})$ B	Ratio B/A
13% PAN (neutral)	292 177.7	381 626.9	399 073.4	1.05
	$\pm$ 66 318.6	$\pm$ 92 527.9	$\pm$ 79 519.0	
11% PAN-H (-)	430 879.1	620 200.0	126 707.7	0.20
	$\pm$ 249 324.6	$\pm$ 244 897.9	$\pm$ 41 095.9	
11% PAN-H, 1 layer (+)	563 471.2	479 128.1	176 219.0	0.37
	$\pm$ 352 906.4	$\pm$ 132 614.1	$\pm$ 63 934.9	
11% PAN-H, 2 layers (-)	634 927.9	575 482.0	225 097.9	0.39
	$\pm$ 437 776.2	$\pm$ 137 743.6	$\pm$ 92 684.9	

 Summarized, intensive cleaning with NaClO does not only influence the surface chemistry and morphology of the charged membranes, but also alters the hydraulic performances of the membranes. However the neutral pure 13% PAN membranes are insensitive to these modifications. Since based on the ATR-FTIR, SEM, AFM and permeability measurements, the charged membranes did lose their structural and chemical properties due to long-term cleaning with NaClO, they were not reimmersed in the HT-MBR at the start of Fouling Period 2. Thus the fouling experiments during Fouling Period 2 were only performed on the 13% PAN (neutral) modules.

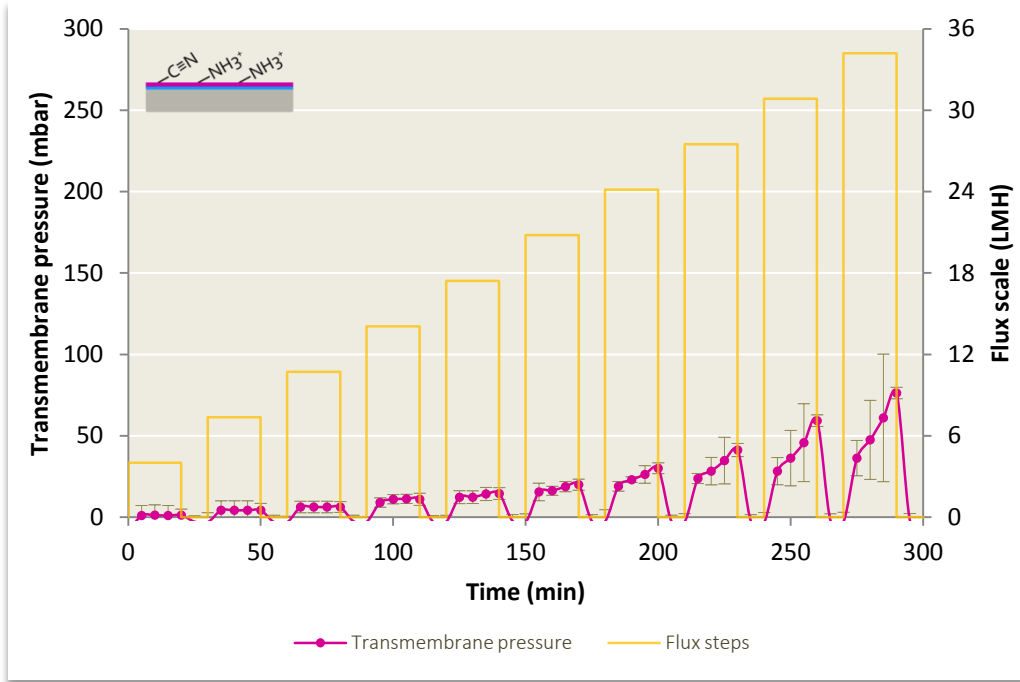
## 2.2.2. Critical flux



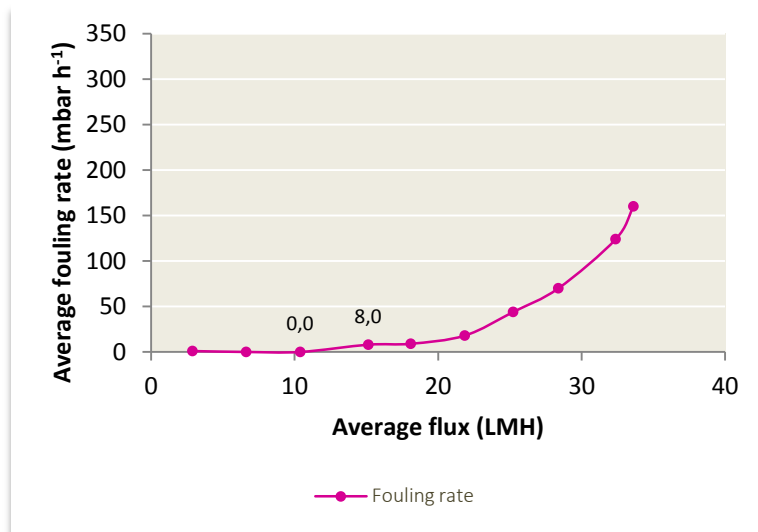
A-Figure 10 Flux-stepping measurements on 11% PAN-H (-) modules (C-membranes). Error bars represent standard deviations from the mean value ( $n = 4$ ).



A-Figure 11 Mean fouling rate (mbar h<sup>-1</sup>) versus average flux (LMH) as determined in the flux-stepping experiment on 11% PAN-H (-) modules (C-membranes) ( $n = 4$ ). The labels indicate the threshold limits for the critical flux determination.

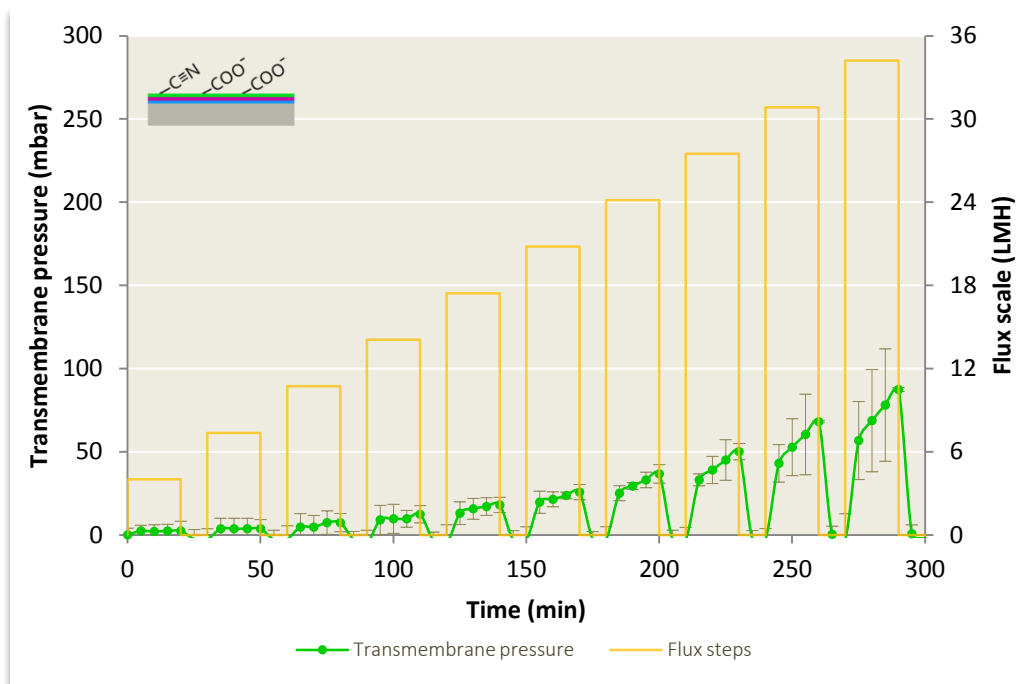


**A-Figure 12** Flux-stepping measurements on 11% PAN-H, 1 layer (+) modules (C-membranes). Error bars represent standard deviations from the mean value ( $n = 4$ ).

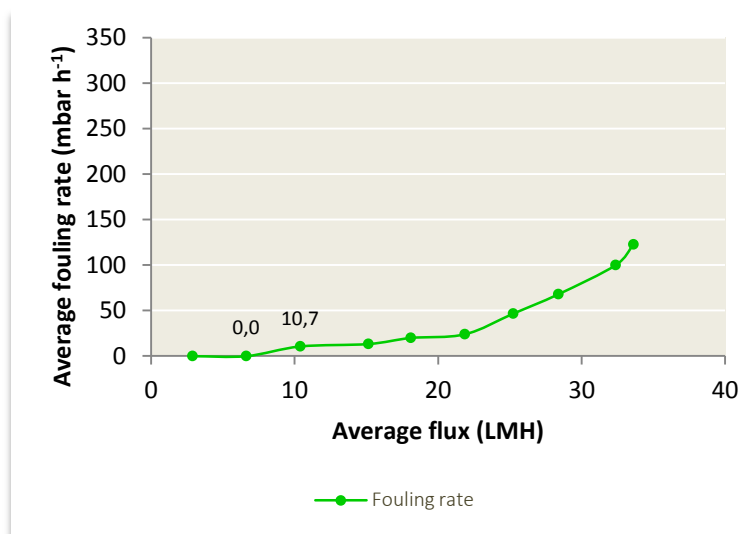


**A-Figure 13** Mean fouling rate ( $\text{mbar h}^{-1}$ ) versus average flux (LMH) as determined in the flux-stepping experiment on 11% PAN-H, 1 layer (+) modules (C-membranes) ( $n = 4$ ). The labels indicate the threshold limits for the critical flux determination.





**A-Figure 14** Flux-stepping measurements on 11% PAN-H, 2 layer (-) modules (C-membranes). Error bars represent standard deviations from the mean value ( $n = 4$ ).

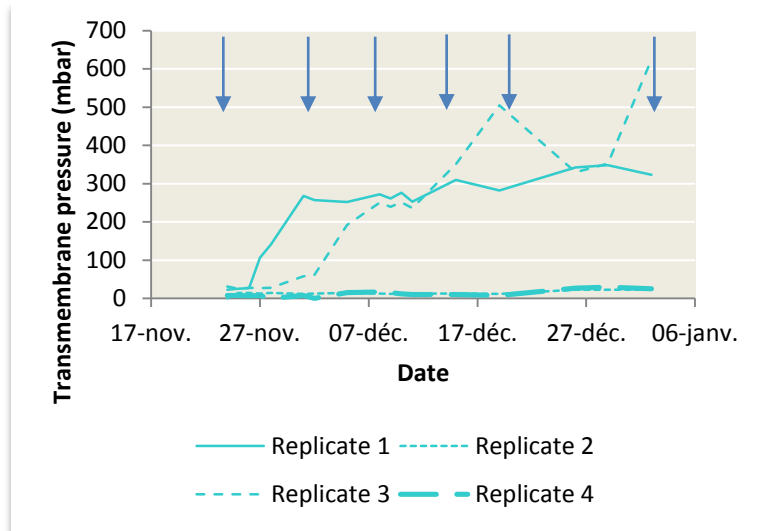


**A-Figure 15** Mean fouling rate (mbar h<sup>-1</sup>) versus average flux (LMH) as determined in the flux-stepping experiment on 11% PAN-H, 2 layers (-) modules (C-membranes) ( $n = 4$ ). The labels indicate the threshold limits for the critical flux determination.

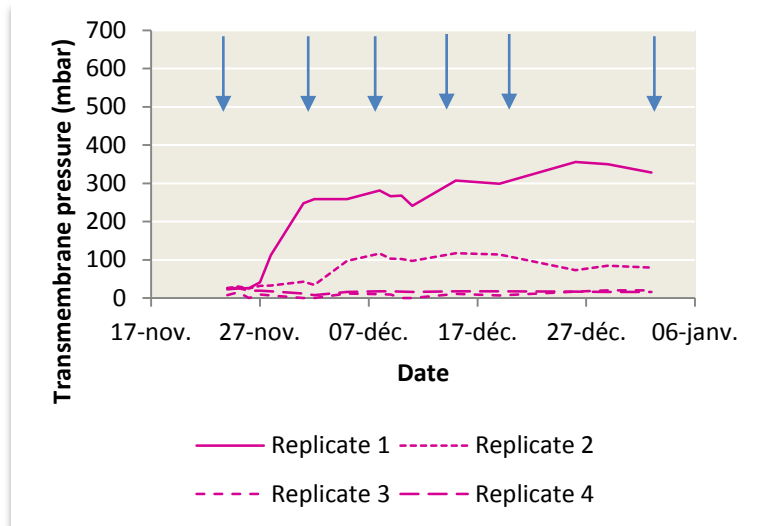
### 3. BIOFOULING (COMMUNITY) CHARACTERIZATION

#### 3.1. Preliminary observations

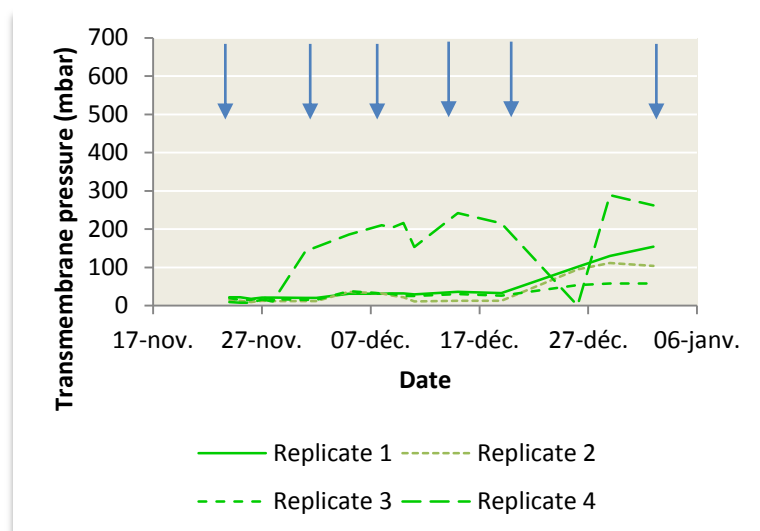
##### 3.1.1. Membrane fouling rate



A-Figure 16 Evolution of the transmembrane pressure (mbar) of the module replicates of 11% PAN-H (-) during Fouling Period 1. Arrows indicate time points of biofilm sampling.



A-Figure 17 Evolution of the transmembrane pressure (mbar) of the module replicates of 11% PAN-H, 1 layer (+) during Fouling Period 1. Arrows indicate time points of biofilm sampling.



**A-Figure 18** Evolution of the transmembrane pressure (mbar) of the module replicates of 11% PAN-H, 2 layers (-) during Fouling Period 1. Arrows indicate time points of biofilm sampling.

## 3.2. Microbiological identification

### 3.2.1. DGGE fingerprinting of PCR-amplified 16S rRNA gene fragments

As seen from **A-Table 2**, the genomic DNA concentration of the sludge and of the biomass developing at the membrane surfaces stayed approximately constant over time, except for 25-Nov14, which corresponds to the first day the pristine membranes were immersed in the HT-MBR (first contact moment between the membranes and the sludge biomass). The fluctuations in concentrations can be attributed to different amount of samples scraped off from the membrane surfaces meant for DNA extraction, or to some loss of material during processing of the samples. Since the concentration of PCR amplicons was not constant, different volumes were loaded on the DGGE gel in order to analyse approximately 300 ng per sample.

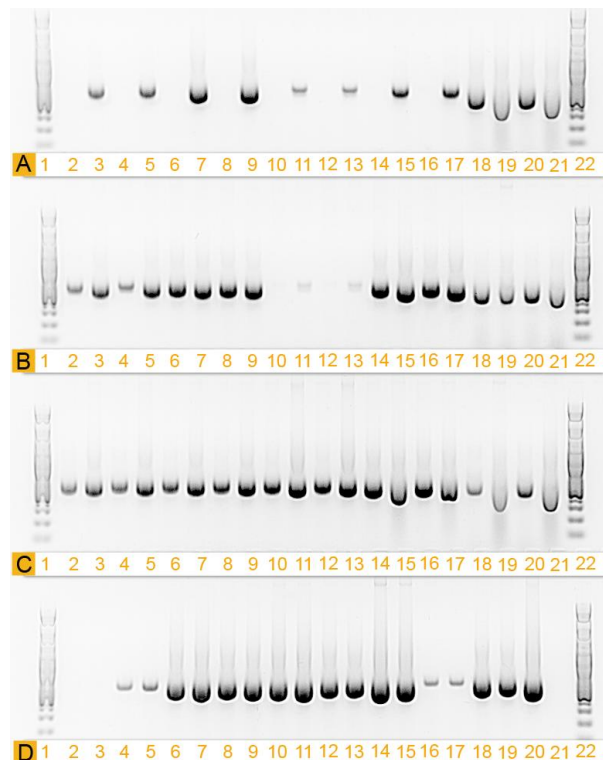
**A-Table 2** Genomic DNA quantity ( $\text{ng } \mu\text{l}^{-1}$ ) of the PCR amplicons of the sludge and the biofouling layer of the different membrane types sampled at different time points and determined based on Qubit measurements. Values are given as (mean  $\pm$  standard deviation) ( $n = 2$  membrane replicates).

Sample	Genomic DNA concentration ( $\text{ng } \mu\text{l}^{-1}$ ) at the sampling date					
	25-Nov14 (Day 72)	01-Dec14 (Day 78)	08-Dec14 (Day 85)	15-Dec14 (Day 92)	19-Dec14 (Day 96)	02-Jan15 (Day 110)
13% PAN (neutral)	/	$20.0 \pm 0.6$	$13.7 \pm 5.0$	$24.8 \pm 0.6$	$20.1 \pm 2.4$	$35.3 \pm 8.1$
11% PAN-H, (-)	/	$28.2 \pm 2.6$	$24.2 \pm 2.3$	$25.1 \pm 4.1$	$16.7 \pm 2.6$	$28.7 \pm 4.1$
11% PAN-H, 1 layer (+)	$5.1 \pm 1.6$	$13.9 \pm 1.1$	$4.5 \pm 0.2$	$6.3 \pm 0.1$	$46.2 \pm 2.3$	$72.6 \pm 2.0$
11% PAN-H, 2 layers (-)	$4.2 \pm 0.2$	$27.2 \pm 1.4$	$46.9 \pm 5.8$	$61.4 \pm 8.8$	$62.3 \pm 4.4$	$59.5 \pm 1.3$
Sludge	$49.1 \pm 3.5$	$51.8 \pm 9.3$	$32.0 \pm 0.3$	$31.5 \pm 3.6$	$32.1 \pm 2.4$	$49.5 \pm 5.2$

As seen from **A-Tabel 3**, the concentration of genomic DNA of the protamylasse feed samples increased with time from day 1 (feed freshly prepared in disinfected vessel) during the maintenance period, and eventually reached a final concentration of around  $100 \text{ ng } \mu\text{l}^{-1}$  on day 8, indicating bacterial development in the feed vessel. This observation was supported by the microscopic investigation of the feed solution (**Chapter 4, Section 1.3**) and attributed to the non-sterile working conditions enhancing bacterial growth in nutrient rich environments (**Chapter 4, Section 3.1.1**).

**A-Tabel 3** Genomic DNA quantity ( $\text{ng } \mu\text{l}^{-1}$ ) of the PCR amplicons of the protamylasse feed solution sampled at different time points during two maintenance periods and determined based on Qubit measurements. Values are given as (mean  $\pm$  standard deviation) ( $n = 2$ ). No replicate measurement was performed on the feed pellet developing at the bottom of the feed vessel.

Day of the maintenance period	Genomic DNA concentration ( $\text{ng } \mu\text{l}^{-1}$ )
Day 1	/
Day 2	$10.4 \pm 1.5$
	$10.8 \pm 0.8$
Day 3	$46.7 \pm 2.7$
	$61.9 \pm 4.1$
Day 4	$101.5 \pm 4.9$
Day 8	$98.1 \pm 2.7$
Feed pellet	95.6



**A-Figure 19** AGE gel of the PCR products obtained by electrophoresis on a 1.5% agarose gel and stained with GelRed, run against a GeneRuler 100 bp plus DNA-ladder.


**A-Figure 19** represents the AGE gel obtained by electrophoresis of the PCR amplicons of the sludge, membrane and protamylasse feed samples. The NC (lane n° 21 of row D) showed no signal, indicating absence of contamination during sample handling and processing. The majority of the bands hold a substantial amount of DNA and are not preceded by a smear of degraded RNA. Since the extracted DNA of all samples was amplified with the same forward and reverse primers, the position of the PCR amplicons is approximately on a horizontal line corresponding to the migration distance of the 400 to 500 bp sequence of the reference ladder (lane n° 1 and 22 of rows A, B, C and D), as expected. Small fluctuations from the horizontal line are due to differences in genomic DNA concentration, which makes high concentration bands appear more prominent and at a greater downward distance than low concentration bands.

**A-Table 4** Attribution of the lanes of the AGE gel presented in **A-Figure 19** (membrane and sludge samples).

Row	Sample	Sampling date					
		25-Nov14 (Day 72)	01-Dec14 (Day 78)	08-Dec14 (Day 85)	15-Dec14 (Day 92)	19-Dec14 (Day 96)	02-Jan15 (Day 110)
		Lane number					
A	13% PAN (neutral)	2, 4	3, 5				
	11% PAN-H (-)	6, 8	7, 9				
	11% PAN-H, 1 layer (+)	10, 12	11, 13				
	11% PAN-H, 2 layers (-)	14, 16	15, 17				
	Sludge	18, 20	19, 21				
B	13% PAN (neutral)			2, 4	3, 5		
	11% PAN-H (-)			6, 8	7, 9		
	11% PAN-H, 1 layer (+)			10, 12	11, 13		
	11% PAN-H, 2 layers (-)			14, 16	15, 17		
	Sludge			18, 20	19, 21		
C	13% PAN (neutral)					2, 4	3, 5
	11% PAN-H (-)					6, 8	7, 9
	11% PAN-H, 1 layer (+)					10, 12	11, 13
	11% PAN-H, 2 layers (-)					14, 16	15, 17
	Sludge					18, 20	19, 21

**A-Tabel 5** Attribution of the lanes of the AGE gel presented in **A-Figure 19** (protamylasse feed samples).

Row	Day of the maintenance period	Lane number <sup>3</sup>
D	Day 1	2, 3
	Day 2	4, 5, 16, 17
	Day 3	6, 7, 18, 19
	Day 4	10, 11
	Day 8	14, 15
	Feed pellet	20

 Summarized, Qubit measurement and AGE visualisation of the PCR products obtained from genomic DNA extracted from the activated sludge, protamylasse feed and membrane biofilm samples did indicate relatively stable DNA concentrations throughout the experimental period and DNA sequences of between 400 and 500 bp, and thus allowed for further use in DGGE fingerprinting analysis. The negative control showed no signal.

---

<sup>3</sup> Lane numbers 8, 9, 12 and 13 are of no meaning for this work.

## Appendix 2: Risk assessments

- PAN membrane preparation/characterization
- Membrane potting
- Continuous filtration experiment
- COD measurement
- TN measurement
- Phosphate measurement
- Biofouling characterization by SEM

The risk assessments were submitted to *COK-Safety@biw.kuleuven.be*.





## Appendix 3: List of products

Reagens	Bruto formula	CAS n°	Supplier references
<b>Membrane and module preparation</b>			
Binder, contains epoxy resin	/	/	UHU plus, endfest 300 90.5 gr/75 ml
Dimethyl sulfoxide, zur Analyse	C <sub>2</sub> H <sub>6</sub> O <sub>5</sub>	67-68-5	Acros Organics
Hardener, contains N,N-dimethyldipropylenetriamine	/	10563-29-8	UHU plus, endfest 300 72.5 gr/75 ml
Poly(acrylic acid, sodium salt) solution, 35 wt% in H <sub>2</sub> O	(C <sub>3</sub> H <sub>4</sub> O <sub>2</sub> ) <sub>x</sub> .(C <sub>3</sub> H <sub>3</sub> O <sub>2</sub> ) <sub>y</sub> .yNa	9003-04-7	Sigma-Aldrich 416037-100ML Average Mw = 15.000 g/mol
Poly(allylamine hydrochloride)	(C <sub>3</sub> H <sub>2</sub> N) <sub>n</sub> .HCl	71550-12-4	Sigma-Aldrich 283215-5G Average Mw = 15.000 g/mol
Polyacrylonitrile	(C <sub>3</sub> H <sub>3</sub> N) <sub>n</sub>	25014-41-9	Scientific Polymer Products Inc. Average Mw = 150.000 g/mol
Sodium hydroxide - pearl, analytical reagent grade	NaOH	1310-73-2	Fisher Chemical 1KG
Sodium nitrate a.r.	NaNO <sub>3</sub>	7631-99-4	Chem-Lab NV 1KG
<b>Operating conditions of the lab-scale MBR system</b>			
2-propanol	C <sub>3</sub> H <sub>8</sub> O	67-63-0	Hach Lange GMBH LCK 138
4-chloor-3,5-dimethylfenol = chloroxylenol	C <sub>8</sub> H <sub>9</sub> ClO	88-04-0	DettolMedical chloroxylenol 4.9%, antiseptum-desinfectans 1L
Dipotassium peroxodisulfate	K <sub>2</sub> S <sub>2</sub> O <sub>8</sub>	7727-21-1	Hach Lange GMBH LCK 138
Disodium tetraborate	Na <sub>2</sub> B <sub>4</sub> O <sub>7</sub>	1330-43-4	Hach Lange GMBH LCK 138
Mercury(II)sulfate	HgSO <sub>4</sub>	7783-35-9	Hach Lange GMBH LCK 314
Phosphoric acid, 33%	H <sub>3</sub> PO <sub>4</sub>	7664-38-2	Hach Lange GMBH LCK 138
Sodium hydroxide	NaOH	1310-73-2	Hach Lange GMBH LCK 138
Sodium hypochlorite	NaClO	7681-52-9	Aqueous solution containing 3.6% active chlorine, 15° Chl (Javel) Delhaize, 2L
Sodium hypochlorite solution, reagent grade	NaClO	7681-52-9	Sigma-Aldrich 425044-1L Available chlorine 10-15%
Sodium metaborate	NaBO <sub>3</sub> .4H <sub>2</sub> O	10486-00-7	Hach Lange GMBH LCK 349
Sodium peroxodisulfate	Na <sub>2</sub> S <sub>2</sub> O <sub>8</sub>	7775-27-1	Hach Lange GMBH LCK 349
Sodiumazide	NaN <sub>3</sub>	26628-22-8	Hach Lange GMBH LCK 138
Sulfuric acid, 11%	H <sub>2</sub> SO <sub>4</sub>	7664-93-9	Hach Lange GMBH LCK 349
Sulfuric acid, 16%	H <sub>2</sub> SO <sub>4</sub>	7664-93-9	Hach Lange GMBH LCK 349
Sulfuric acid, 60%	H <sub>2</sub> SO <sub>4</sub>	7664-93-9	Hach Lange GMBH LCK 138
Sulfuric acid, 90%	H <sub>2</sub> SO <sub>4</sub>	7664-93-9	Hach Lange GMBH LCK 314

Reagens	Bruto formula	CAS n°	Supplier references
<b>Membrane performance measurement</b>			
Methylene blue	C16H18N3S.Cl	61-73-4	/
<b>Biofouling (community) characterization</b>			
0.5M EDTA	C10H12FeN2NaO8	60-00-4	/
1M Tris.Cl, pH 8.0	(Trizma base: C4H11NO3)	(Trizma base: 77-86-1)	(Trizma-base: Sigma-Aldrich, T6066-1KG)
25:24:1 phenol-chloroform-isoamyl alcohol mixture; BioUltra, for molecular biology	/	136112-00-0	Sigma-Aldrich 77617-500ML
2-propanol molecular biology grade	C3H8O	67-63-0	AppliChem
50x TAE Tris/Acetic Acid/EDTA Buffer	/	Tris acetate: 6850-28-8; EDTA: 60-00-4	Bio-Rad Laboratories 1l
6x LD, 6x DNA Loading Dye	/	/	Thermo Scientific 1 ml
AccuStart II PCR ToughMix	/	/	Quanta Sciences inc. 1.25 ml
Acrylamide/N,N'-Methylenebisacrylamide 37.5:1; for biochemistry; 40% mix solution in water	(C7H10N2O2.C3H5NO)n	25034-58-6	Acros Organics 500 ml
Ammonium persulphate	/	7727-54-0	Bio-Rad Laboratories 10g
Cetrimide (=hexadecyltrimethyl ammonium bromide)	C19H42BrN	57-09-0	Sigma-Aldrich H9151-25G
Di-sodiumhydrogen phosphate PA	Na2HPO4	7558-79-4	/
DNAse and RNAse free water	/	/	The Epigenetics Company Zymo Research 10 ml
Ethanol absolute	C2H6O	64-17-5	AnalaR NORMAPUR VWR BDH Prolabo
Formamide, 99.5%; for analysis	CH3NO	75-12-7	Acros Organics 100 ml
Forward primer (GC-63F)	/	/	J.T'SYEN
GeneRuler 100 bp plus DNA Ladder, 0.5 µg/µl	/	/	Thermo Scientific 50 µg
Glutaraldehyde solution, Grade II, 25wt% in H2O	C5H8O2	111-30-8	Sigma-Aldrich G6257-1L
Lysozyme chloride form, from chicken egg white	47400 units/mg solid 54500 units/mg protein (UV)	9066-59-5	Sigma-Aldrich L2879-5G
Magnesium sulphate heptahydrate	MgSO4.7H2O	10034-99-8	Merck 1kg
Proteinase K	/	39450-01-6	AppliChem Pancrea MM = 27000 g/mol
Qubit dsDNA BR Buffer	/	/	Life Technologies Invitrogen 50 ml

Reagens	Bruto formula	CAS n°	Supplier references
<b>Biofouling (community) characterization (continued)</b>			
Qubit dsDNA BR Reagent, 200x concentrate in DMSO	/	/	Life Technologies Invitrogen 250 µl
RedGel Nucleic Acid Stain, 10000x in DMSO	/	/	Biotium 0.5 ml
Reverse primer (518R)	/	/	J.T'SYEN
RNAase A, 100 mg/ml	/	/	Qiagen 1.25 ml
Sodium dihydrogenphosphate.1H2O PA 99%	NaH2PO4.H2O	10049-21-5	Merck 500g
Sodium chloride	NaCl	7647-14-5	AnalaR NORMAPUR VWR BDH Proplabo
Sodium dodecyl sulfate	C12H25NaO4S	151-21-3	Sigma-Aldrich 71729-500G
SYTO® 62 Red Fluorescent Nucleic Acid Stain - 5 mM Solution in DMSO	/	/	Life Technologies Invitrogen
SYTO® 9 Green Fluorescent Nucleic Acid Stain	/	/	Life Technologies Invitrogen
TEMED, N,N,N',N'-tetramethylethylene-diamine	C6H16N2	110-18-9	Bio-Rad Laboratories 5 ml
Ultra Pure Agarose	/	9012-36-6	Invitrogen
Urea; powder, BioReagent, for molecular biology, suitable for cell culture	CH4N2O	57-13-6	Sigma-Aldrich U5378-1KG
α-D-glucose, 96% anhydrous	C6H12O6	492-62-6	Sigma-Aldrich 158968-500G



## Appendix 4: CTAB protocol

### Adapted CTAB-lysozyme method for genomic DNA extraction

Based on [32]

- A.** Transfer the sample suspension in 450  $\mu\text{l}$  GTE buffer to a sterile 2-ml microcentrifuge tube containing 50  $\mu\text{l}$  of a 10  $\text{mg ml}^{-1}$  lysozyme solution.

*EDTA binds heavy metals and forms complexes with bivalent cations, thus destabilizing the cell membrane. It inhibits deoxyribonuclease thus prevents DNA to be broken up. Glucose increases the osmotic pressure and enhances cell lysis. The lysozyme solution was prepared in MQ instead of 25 mM Tris.Cl. Lysozyme weakens the peptidoglycan cell wall and permits water to enter the cell, thus causing lysis.*

- B.** Mix gently and incubate 1 h at 37 °C at 900 rpm shaking speed (MB-102, ThermocCell Mixing Block, Bioer).

- C.** Make a 2:1 solution (v/v) of 10% SDS solution and 10  $\text{mg ml}^{-1}$  proteinase K in MQ. Add 150  $\mu\text{l}$  of this solution to the cells and mix gently. Incubate 40 min at 55 °C at 900 rpm shaking speed.

*SDS is an anionic detergent destroying the cytoplasmic membrane of the cells. Proteinase K destroys proteins. Plasmids and chromosomal DNA are released from the cells.*

- D.** Add 1  $\mu\text{l}$  RNAase A.

*Destruction of the RNA released from the cell.*

- E.** Add 200  $\mu\text{l}$  of 5 M NaCl and mix gently.

*NaCl blocks the binding of DNA to cetrimide.*

- F.** Preheat CTAB solution to 65 °C in a water bath (RTE-101, Neslab), add 160  $\mu\text{l}$ , and mix gently. Incubate 10 min at 65 °C in a water bath.

- G.** Add an equal volume (~1 ml) 25:24:1 (v/v) phenol/chloroform/isoamyl alcohol, shake vigorously to mix, and microcentrifuge for 5 min at 12 000 rcf and 4 °C (Centrifuge 5424, Eppendorf or Mikro 200R, Hettich Zentrifugen).

*The aqueous (upper) layer (isoamyl alcohol) contains the DNA. The apolar (bottom) layer (phenol/chloroform) contains the undesirable organic compounds (lipids, proteins, polysaccharides, etc.).*

- H.** Transfer 900  $\mu\text{l}$  aqueous layer to a fresh sterile 2-ml microcentrifuge tube.

- I.** Repeat extraction with 25:24:1 (v/v) phenol/chloroform/isoamyl alcohol, shake vigorously to mix, and spin in microcentrifuge for 5 min at 12 000 rcf and 4 °C.

- J.** Transfer 800  $\mu\text{l}$  to fresh sterile 1.5-ml microcentrifuge tube.

*CAUTION: For BSL3 organisms, dip tube in a disinfectant such as Vesphene Ilse to disinfect outer surface. From this point on, the supernatant can be processed in a BSL-2 laboratory (see Strategic Planning).*

- K.** To 800  $\mu\text{l}$  aqueous layer, add 560  $\mu\text{l}$  (0.7 vol) isopropanol, mix gently by inversion until the DNA has precipitated out of solution.

*Precipitation of DNA.*

## A - XXXVIII

- L. Incubate 30 min at room temperature. Microcentrifuge for 15 min at 12 000 rcf, room temperature.
- M. Aspirate supernatant and add 1 ml of 70% ethanol in MQ to wash DNA pellet. Mix gently by inversion and microcentrifuge 5 min at 12 000 rcf at room temperature.

*DNA is washed in order to remove precipitated salts.*

- N. Carefully aspirate supernatant, avoiding the pellet, and air-dry DNA pellet for 2 min. Do not overdry.
- O. Add 30, 50 or 100  $\mu$ l TE buffer (10 mM Tris.HCl, 0.1 mM EDTA in MQ, pH 8.23), depending on size of DNA pellet, to dried DNA pellet and store overnight at 4 °C to allow pellet to dissolve. Store up to 1 year at -20 °C.

*RNase A can be added to TE (1  $\mu$ g/ml) to reduce RNA contamination.*

## Appendix 5: Polarized summary

Traditional wastewater treatment installations, abbreviated as CASP, have the disadvantages of for instance not being capable of delivering high quality water at all times as well as requiring a lot of space. Therefore alternative technologies have been developed, including membrane bioreactors, abbreviated as MBRs, using membranes through which the wastewater is filtered in combination with so-called activated sludge containing microorganisms that perform the biodegradation of the pollutants. However this technology is not perfect either. It has high investment costs, but most importantly, the pores of the membranes can be filled up or covered by particles as well as microorganisms, thus blocking the water from passing through. This phenomenon is more commonly referred to as 'fouling' or biofilm formation. Fouling leads to high energy demands and related costs in order to prevent, to diminish or to remediate the phenomenon. Moreover it prevents the broader market development of the MBRs. A lot of researchers already have tried to find efficient anti-fouling strategies. However the underlying processes are still unclear as well as the knowledge of the relation between the microorganisms and the membranes, referred to as biofouling.

The main goal of this study was to gather knowledge about the relation between the microorganisms and the membrane surface. The used membranes were made of polyacrylonitrile (PAN), a synthetic molecule, and some of them were chemically modified as to bear either a positive or negative charge. The membranes were placed during 40 days inside a laboratory-scale MBR, which was fed with protamylase, a by-product of the potato industry. The physico-chemical properties of the membranes themselves were determined by means of several techniques (ATR-FTIR, SEM, AFM, CAM, volume porosity measurement, electrokinetic measurement), but also their performance was analyzed in terms of permeability (via CWP) and fouling tendency (via critical flux measurements). The microorganisms in the MBR which interacted with the membranes and developed upon their surfaces were characterized on a molecular level (referred to as PCR-DGGE fingerprinting) but also their chemical properties and morphology were determined (via ATR-FTIR, SEM, CLSM).

The results revealed that the membranes differed from each other only in terms of surface charge and membrane material (as a result of the chemical modifications applied), but that they were similar in terms of physical properties (including pore size, permeability and surface roughness). The molecular investigations indicated that the microorganisms growing in the biofilm at the membrane surface were different from the ones present in the activated sludge of the MBR. Next it seemed that the community of microorganisms in the biofilm evolved with time, but that all membranes housed the same community at a certain moment in time. These observations allow concluding that certain microorganisms are more prone to colonize membrane surfaces than others and that the surface charges of the membranes do not play a decisive role in the selection of these microorganisms. These observations might help the scientific community to develop more efficient anti-fouling strategies.

**Keywords:** membrane bioreactor, polyacrylonitrile, surface charge, biofouling, PCR-DGGE fingerprinting.